CHEMICAL CONSTITUENTS OF *PRISMATOMERIS MALAYANA* RIDLEY AND QUANTITATIVE STRUCTURE ACTIVITY RELATIONSHIP STUDY ON ANTI-INFLAMMATORY AGENTS AND THEIR ANALOGUES

NOR HAYATI ABDULLAH

DEPARTMENT OF CHEMISTRY
FACULTY OF SCIENCE
UNIVERSITI OF MALAYA
KUALA LUMPUR

2014

CHEMICAL CONSTITUENTS OF *PRISMATOMERIS MALAYANA* RIDLEY AND QUANTITATIVE STRUCTURE ACTIVITY RELATIONSHIP STUDY ON ANTI-INFLAMMATORY AGENTS AND THEIR ANALOGUES

NOR HAYATI ABDULLAH

**THESIS SUBMITTED IN FULFILMENT
OF THE REQUIREMENT FOR THE
DEGREE OF DOCTOR OF PHILOSOPHY**

**DEPARTMENT OF CHEMISTRY
FACULTY OF SCIENCE
UNIVERSITI OF MALAYA
KUALA LUMPUR**

2014

ABSTRACT

Prismatomeris malayana Ridley of Rubiaceae was investigated for its anti-inflammatory properties by evaluating their inhibition of the hyaluronidase and lipoxygenase activity and of TPA-induced inflammation in mice. The leaf was found to be the most active in the three selected assays. From bioassay guided fractionation and isolation, ursolic acid **60** was isolated and found to be the compound responsible for the hyaluronidase inhibitory activity. The isolation work on the leaves yielded five pentacylic triterpenoids (PTC) (3β-hydroxyurs-12-en-28-oic acid **60** [ursolic acid], 3β, 19, 24-trihydroxyurs-12-en-28-oic acid **61** [barbinervic acid], 3β,23-dihydroxyurs-12-en-28-oic acid **62**, 28-*O*-β-glucopyranosyl-3α,19α,23-trihydroxyurs-12-en-28-oic acid **63** and 3β-hydroxyurs-11-en-13,28-olide **65**); three iridoids (asperulosidic acid **68**, scandoside **70** and prismalayanoside **66**). Compound **66** (prismalayanoside) is novel with an unprecedented spiro-octa-lactone ring. The ten compounds isolated from the roots are; one PTC (3β-hydroxyolean-12-en-28-*O*-acetoate **64**); eight anthraquinones (lucidin-3-methyl ether **71**, rubiadin-1-methyl ether **11**, damnacanthol **72**, rubiadin **10**, 1-ethyl-3-hydroxymethyl-4-hydroxy-9,10-anthraquinone **73**, 2-methoxy-3-oxyhydroxymethyl -9,10-anthraquinone **74**, and lucidin-*ω*-methyl ether **21**) and one iridoid (asperulosidic acid **68**). Further investigation of the stems led to the isolation of lucidin-*ω*-methyl ether **21** (an anthraquinone) and asperuloside **69** (an iridoid)**.** Seven analogues (**75**-**81**) were prepared by structural modification of ursolic acid **60**. The quantitative structure activity relationship study (QSAR) was carried out to correlate the selected twenty two ursolic acid analogues with their hyaluronidase inhibitory activity. The statistical characteristic provided by the best multi linear model gave R^2 value of more than 0.9 thus indicating good predictive ability.

ABSTRAK

Prismatomeris malayana Ridley dari Rubiaceae telah di kaji untuk ciri-ciri anti-radangnya dengan mengenal pasti perencatannya terhadap aktiviti hialuronidas dan lipoksigenas dan juga terhadap keradangan ditingkatkan-TPA dalam tikus. Daun didapati adalah paling aktif dalam ketiga-tiga essei terpilih. Dari fraksinasi dan isolasi berpandukan essei, asid ursolik **60** telah diasingkan dan didapati adalah sebatian yang bertanggungjawab untuk perencatan aktiviti hialuronidas. Pengasingan keatas daun menghasilkan lima triterpenoids pentasiklik (PTC) (3β-urs-12-en-28-oic acid **60** (asid ursolik), 3β, 19, 24-trihidroksiurs-12-en-28-oic acid **61** [asid barbinervik], 3β,23-dihidroksiurs-12-en-28-oic acid 6**2**, 3β-hidroksiurs-11-en-13,28-olide **65** dan 28-*O*-β-glukopiranosil-3α,19α,23-trihidroksiurs-12-en-28-oic asid **63**) dan tiga iridoid [asid asperulosidik **68**, skandosida **70** dan prismalayanoside **66**). Sebatian **66** (prismalayanosida) adalah nobel dengan gelang "spiro-octa-lactone". Sepuluh sebatian dari akar adalah satu PTC [3β-hidroksiolean-12-en-28-*O*-acetoate **64**], lapan antrakuinon [lucidin-3-metil eter **71,** rubiadin-1-metil eter **11,** damnakantol **72,** rubiadin **10**, 1-etill-3-hidroksimetil-4-hidroksi-9,10-antrakuinon **73** dan 2-metoksi-3-oksohidroksimetil -9,10-antrakuinon **74**] dan satu iridoid [asid asperulosidik **68**]. Kajian lebih lanjut keatas batang berjaya mengasingkan dua sebatian antrakuinon [lucidin-ω-metil eter **21**] dan iridoid [asperulosida **69**]**.** Tujuh terbitan (**75-81**) telah disediakan dari struktur modifikasi ke atas asid ursolik **60.** Kajian perhubungan kuantitatif struktur activity (QSAR) telah dilakukan untuk menghubungkan dua puluh dua terbitan asid ursolik **60** terpilih dengan aktiviti perencatan hialuronidas mereka. Ciri-ciri statistik telah dihasilkan melalui model multi linear terbaik yang memberikan nilai R^2 lebih dari 0.9 seterusnya menunjukkan keupayaan ramalan yang memuaskan.

ACKNOWLEDGEMENT

Alhamdulillah, thanks to Allah the Almighty. I finally come to the end of this study. I would like to express my sincere thanks to my supervisor Prof Dr. Khalijah Awang, Associate Professor Dr. Ibrahim Ali Noorbatcha (UIAM) and Professor Dr. Noel F. Thomas for their supervision, valuable guidance, concern, understanding and support throughout this research study.

My deep acknowledgement goes to Dato' Dr. Abdul Latif Mohmod, Director General of Forest Research Institute Malaysia (FRIM) for granting a study leave. I also would like to acknowledge Dr. Rasadah Mat Ali, Director of Natural Product Division, FRIM, for her moral support and regular push to finish this study. I am also grateful to Dr. Ling Sui Kiong, Head of Phytochemistry Programme, FRIM who has given me great ideas, guidance and critical comments throughout the course of this study. Special thank also to Dr. Nor Azah Mohd. Ali who always being a good listener and gives me spirit from beginning towards the end of this study.

This work was made possible through the scholarship generously offered by the Ministry of Natural Resources Environment (NRE) Malaysia, for which is greatly acknowledge.

I also would like to dedicate my special thanks to many people who have helped to make this work completed. My special thanks goes to all staff in Phytochemistry laboratory (FRIM); Siti Aisha Abu Bakar, Mohamad Faisal Iskandar Sukhari and other members. Unforgettable, our late ethno botanist, Zainon Abu Samah who was identified and collected the sample for this research. To all members of Phytochemistry laboratory (UM), thanks for sharing a lots of information and great friendship.

Finally, to my family; my mother and late father, my husband and children (Saiful, Anuar, Naiem, Alissya and Faris) who gives me the strength to finish this piece of work. I love all of you.

CONTENTS **Page**

LIST OF FIGURES

LIST OF SCHEMES

LIST OF TABLES

ABBREVIATIONS

^{13}C	Carbon NMR
^{1}D-NMR	One dimension nuclear magnetic resonance
^{1}H	Proton NMR
2D-NMR	Two dimension nuclear magnetic resonance
AA	Arachidonic acid
ACE	Angiotensine converting enzyme
acetyl-CoA	Acetyl-coenzyme A
AM1	Austin model
BMLR	Best multi-linear regression
BSA	Bovine serum albumin
CC	Column chromatography
CD_3OD	Deuterated methanol
$CDCl_3$	Deuterated chloroform
CH_2Cl_2	Dichloromethane
CH_3	Methyl group
$CHCl_3$	Chloroform
cm^{-1}	Per centimeter
COSY	^{1}H-^{1}H Correlation spectroscopy
COX	cyclooxygenase
d	Doublet
DAHP	3-deoxy-D-arabino-heptulosonate-7-phosphate
dd	Doublet of doublet
DEPT	Distortioness enhancement by polarization transfer
DMEM	Dulbecco's modified eagle's medium

DMF	Dimethylformamide
DMSO	Dimethylsulphoxide
dt	Doublet of triplet
EA	Ethyl acetate
EFAs	Essential fatty acids,
ESI	Electron spray ionisation
eV	Electron Volt
$FeCl_3$	Ferric chloride
FPP	farnesyl pyrophosphate
FT-NMR	Fourier transform nuclear magnetic resonance
g	Gram
GlcNAc	N-acetyl-D-glucosamine
GlcUAc	D-glucuronic acid
HA	Hyaluronic acid
HCl	Hydrogen chloride
HMBC	Heteronuclear multiple bond correlation
HMQC	Heteronuclear multiple quantum correlation
HMW	high molecular weight
HOMO	highest occupied molecular orbital
HRESIMS	High resolution electrospray ionization mass spectroscopy
HSQC	Heteronuclear single quantum correlation
Hz	Hertz
IL-I	Interleukins-1
IPP	isopentenyl pyrophosphate
IR	Infrared
J	Coupling constant

kg	Kilogram
LC- MS/MS	Liquid chromatography-mass spectroscopy mass spectroscopy
LMW	Low molecular weight
LOX	Lipoxygenase
LUMO	Lowest unoccupied molecular orbital
M	Molar
m	Meter
m	Multiplet
m/z	Mass per charge
MeOH	Methanol
MEP	2-C- methyl-D-erithritol-4-phosphate
MHz	Mega Hertz
ml	Mililitre
mM	Milimolar
MVA	Mevalonic acid
NDGA	nordihydroguaiaretic acid
NH_3	Ammonia
NMR	Nuclear magnetic resonance
NOESY	Nuclear overhauser effect spectroscopy
NSAIDS	Non-steroidal anti-inflammatory drugs
OCH_2O	Methylenedioxy
OCH_3	Methoxyl group
OH	Hydroxyl group
PAF	Platelet activating factor
PEP	Phosphoenol pyruvate
PGE	Prostaglandins

pH	Power of hydrogen
ppm	Part per million
PPSA1	Partial positive surface area
PTLC	Preparative thin layer chromatography
PTC	Pentacyclic triterpenoids
PCC	Pyridinium chlorochromate
q	Quartet
QSAR	Quantitative structure activity relationship
RM1	Recife model 1
s	Singlet
SAR	Structure activity relationship study
SCF	Self consistent field
SRB	Sulforhodamine B
t	Triplet
TCA	Trichloroacetic acid
TLC	Thin layer chromatography
TPA	12-*O*-tetradecanoylphorbol-13-acetate
UV	Ultraviolet
α	Alpha
β	Beta
δ	Chemical shift
λ	Maximum wave length

CHAPTER 1:
INTRODUCTION

1.1 General

There are three different types of medicine: traditional, herbal and pharmaceutical (de Padua et al., 1999). The same plant may be consumed as a medicinal tea or it may be cultivated and processed into a herbal medicine alternatively formulation in different communities or countries. It may provide a lead compound for pharmaceutical development. These systems of medicine are complementary in health care and can in no way substitute for one another.

Since ancient times people have been exploring nature, and plants in particular have been one of the major foci in the search of new drugs (Verpoorte, 1999). As of today, plants have provided many novel natural compounds (Graham, 2005) with potent activities and biological properties such as taxol **1**, artemisinin **2**, vinblastin **3**, quinine **4**, morphine **5**. In order to find new leads from plants, random screening of plant species is presently widely used based on chemotaxonomy, traditional use or plant ecological observations. In 1995, Pimn et al. reported that there are about 250,000 different plant species of which 70% have not been investigated at all while the other 30% have only been partially investigated. This means that more than 70% of higher plants have not been adequately studied for potentially useful biological activity and the plant kingdom has not received sufficient attention as a resource for possible medicinal agents (Pimn et al., 1995).

In 1988, the database NAPRALERT was reported to contained more than 88,000 secondary metabolites, and every year some 4000 new ones are being reported (Verpoorte, 1999). In addition, over half of the world's 25 best selling pharmaceuticals for 1991 owed their origin to a natural source material (O'Neil & Lewis, 1993) and

120 plant-derived compounds are currently used as drugs (Farnsworth et al., 1985). In another extensive review of new drugs introduced between 1981 and 2002 (Newman et al., 2003), 28% of the 868 new chemical entities were natural products or derived from natural products, while another 28% of drugs were created around a pharmacophore from a natural product.

Several natural anti-inflammatory drugs were identified in plant extracts that have been used in traditional medicine for the relief of pain, fever and inflammation related diseases (Maria et al., 2010) such as curcumin **6**, resveratrol **7** and lupeol **8**. Inflammation has been recognized as a common mechanism of disease in neurological and neuropsychiatric diseases; therefore, interest in anti-inflammatory drugs has increased among investigators. Natural compounds are currently being considered for treatment of chronic inflammatory and neurodegenerative diseases due to the serious adverse effect of modern drugs used to treat inflammation.

The most frequently prescribed drugs in modern medicine were non-steroidal anti-inflammatory drugs (NSAIDS) which are very effective in the alleviation of pain, fever and inflammation (Inger et al., 2010). The term NSAID refers to structurally diverse chemical compounds that share the ability to inhibit the activity of the prostaglandin biosynthetic enzymes, the cyclooxygenase (COX) isoforms 1 and 2 (Maria et al., 2010). By 2010, about fifty different NSAIDS preparations were available in the market with main indications from mild to moderate pain of somatic origin (Inger et al., 2010). NSAIDS may be classified as salicylates, arylalkanoids acids (diclofenac, indomethacine, nabumethone, sulindac), 2-arylpropionic acids or profens (ibuprofen, flurbioprofen, ketoprofen, naproxen), N-arylanthranilic acids or fenamic acids (mafenamic acid, meclofenamic acid), pyrazolidine derivatives (phenylbutazone),

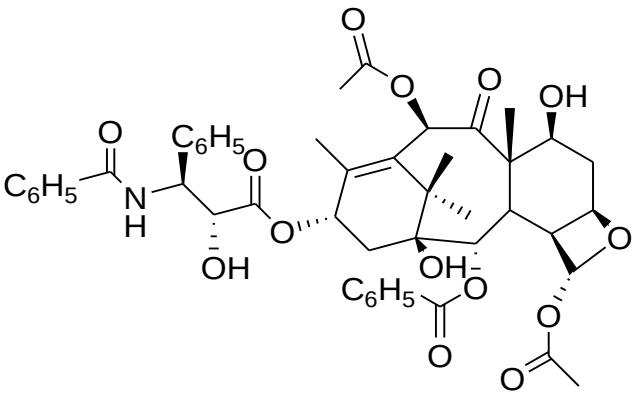

1

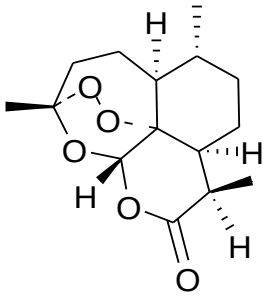

2

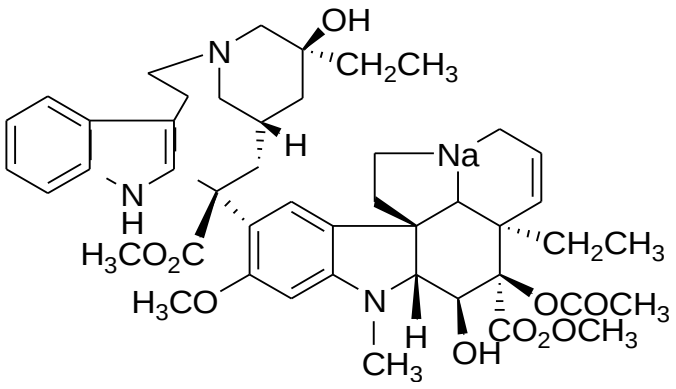

3

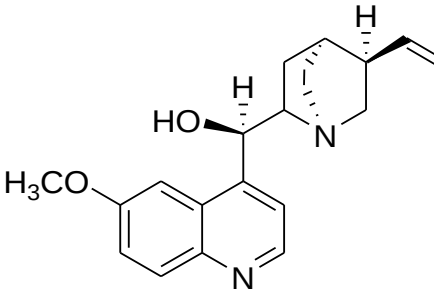

4

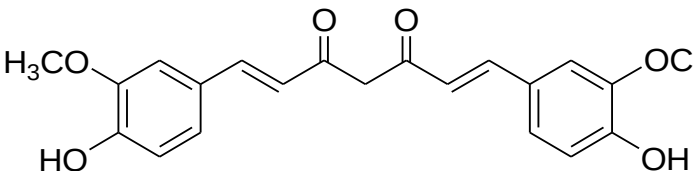

6

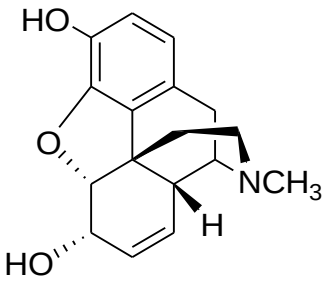

5

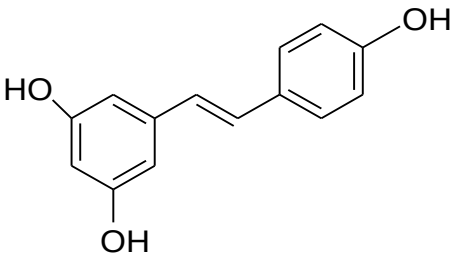

7

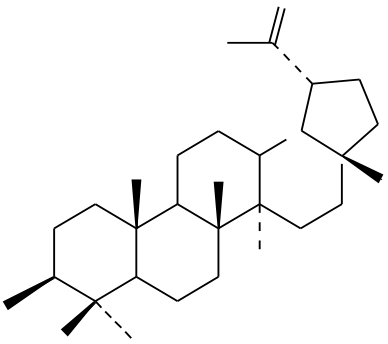

8

oxicams (piroxicam, meloxicam), sulfonilides (nimesulide) and others. However, the mechanisms underlying their beneficial effects remain largely unknown.

One important development was the discovery of selective COX-2 inhibitors (coxibs) which were introduced into clinical practice because of their reduced risk of gastrointestinal bleeding compared to non-selective COX inhibitors. Unfortunately, these compounds later shown to posses significant cardiovascular adverse effects, thus leading to the withdrawal from the market of one drug of this class, (rofecoxib) (Imbimbo et al., 2009). The selective NSAIDS also have the same adverse effect such as diclofenac, ibuprofen and piroxicam. NSAIDS also show gastrointestinal toxicity mediated by the inhibition of COX-1 effects on the gastric mucosa resulting in heartburn, dyspepsia, nausea, abdominal pain (subjective symptoms), erosions, asymptomatic ulcers (superficial gastro duodenal mucosal lesions) and perforation, symptomatic ulcers, bleeding (serious gastro duodenal ulcers) (Inger et al., 2010).

In Malaysia, the plant *Prismatomeris malayana* has not been extensively investigated for the chemical constituents even though it is widely used in traditional medicine, especially in relation to anti-inflammatory aspects. Therefore, the objectives of the study are:

1. To evaluate the anti-inflammatory activity of this plant using three assays; hyaluronidase, lipoxygenase and TPA mouse ear oedema inhibitory activity.
2. (a) To conduct bioassay guided fractionation and isolation on this plant in order to isolate and elucidate the structure of the active anti-inflammatory chemical compound/s

(b) To isolate and elucidate structure of the other chemical compounds from this plant and also evaluate them.

3. To synthesize analogous of the active compound from 2(a) for quantitative structure activity relationship (QSAR) study.
4. To construct a QSAR model that relates the structure with the bioactivity values on the active compound and the analogues.

1.2 Rubiaceae: Distribution and habitat

Rubiaceae is distributed worldwide but found mainly in tropical countries with about 500 genus and 6000 species (Ng, 1990). It was an important component of the lower strata of the rain forest. In terms of stem density, has great variation from 0.1 stem per acre to 14 stems per acre (Ng, 1990). Distribution of some known species are *Gardenia carinata* in northen part of Peninsular Malaysia while *Timonius wallichianus* in south of Peninsular Malaysia.

The plants of this family with the most economic use are coffee (*Coffea Arabica* L., *C. liberica bull*., *C. robusta* Linden) and quinine (*Cinchona ledgeriana* Moens, *C. succirubra* Pavon) which are natives to Peru (Keng, 1969). The gambier, a tanning material from *Uncaria gambier* Roxb. was at one time an important crop on Singapore Island.

The Rubiaceae family is used in traditional medicine as an exceptional source of anti-malarial herbs (Milkyas et al., 2013) such as *Pentas micrantha.* Decoctions of *Rennelia elliptica* are taken as aphrodisiac, body aches and as post natal tonic (Osman et al., 2010) whereas the famous *Morinda citrifolia* has been used for a broad range of

therapeuthic uses such as to treat diabetic (Kohei et al., 2010). Phytochemical investigation have shown that many Rubiaceous plants have been found to contain napthtohydroquinones and anthraquinones both free and as glycosides (Su-ching et al., 1995) such as *Galium verum* (Derek et al., 1995), *Rubia lanceolata* Hayata (Su-Chin et al., 1995), *Pentas micrantha* (Milkyas et al., 2013) and *Ophiorrhiza pumila* (Mariko et al., 1998). The anthraquinones, in particular the 9,10-anthraquinones, were reported to posses anti-plasmodial, anti-viral, anti bacterial, anti-fungal, protein cleaving, anti-cancer and anti-malarial properties (Endale et. al., 2012; Koyama et al ., 2008; Singh et al., 2006; Chan et al., 2011; Suzuki et al., 2005; Wang et al., 2008; Winter et al., 1995)

1.3 General appearance and morphology

The Rubiaceae are trees, shrubs, or infrequently herbs comprising about 450 genera and 6,500 species, including some lianous forms. Common plants included gardenia, cinchona, weet woodruff, partridgeberry, gambier, ixora, and noni (Keng, 1969). The leaves are simple and usually entire, opposite or sometimes whorled and stipules are present and interpetiolar (Keng, 1969, Ng, 1990, Corner, 1988). The flowers are nearly always bisexual and actinomorphic, often heterostylous, and usually are in cymose inflorescences. The calyx is mostly somewhat reduced four to five lobes. Sometimes the lobes are obsolete, rarely greatly expanded and brightly colored. The sympetalous corolla is mostly four to five lobed, occasionally with three or up to ten lobes. The androecium consists of as many stamens as corolla lobes and is adnate to the corolla tube or epigynous zone, alternate with the lobes. The gynoecium consists of a single compound pistil of two or seldom more carpels, a single style, and a nearly always inferior ovary with the number of locules equaling the number of carpels, each with

one many axile ovules. An epigynous nectary disk is usually present. The fruit is variable and sometimes forming multiples.

1.4 Taxonomy of Rubiaceae

The botanical classification of the family is most intricate, depending chiefly on the minute structure of the ovary, stamens and seeds (Corner, 1988). Hsuan Keng (1969) was divided the order rubiales into two families; rubiaceae and caprifoliaceae. The key to the rubiaceae family was opposite and stipulate leaves and regular flower. The family members are either herbs, shrubs or trees and some times climbers. The subfamilies Rubioideae and Cinchonoideae, are generally recognized mainly by the number of ovules in an ovary–locule.

Bremer et al. (2000), suggests the classification of the Rubioideae through their phylogenetic analyses based on molecular data *i.e* protein coding *rbc*L gene, the spacer sequence between *atp*Band and *rbc*L and the third, non-coding intron marker (rps16) from Andersson and Rova (1999). The classification is under the genus *Prismatomeris* under subtribe Prismatomerinae and tribe Morindeae. Scheme 1.4 summarized the classification of the Rubiaceae family. The list of *Prismatomeris* species, as retrieved on in http://iphy10.org/~rpage/theplantlist/A/rubiaceae/Prismatomeris, were listed in table 1.4 together with their reference. The list also included the varieties and subspecies of *Prismatomeris*.

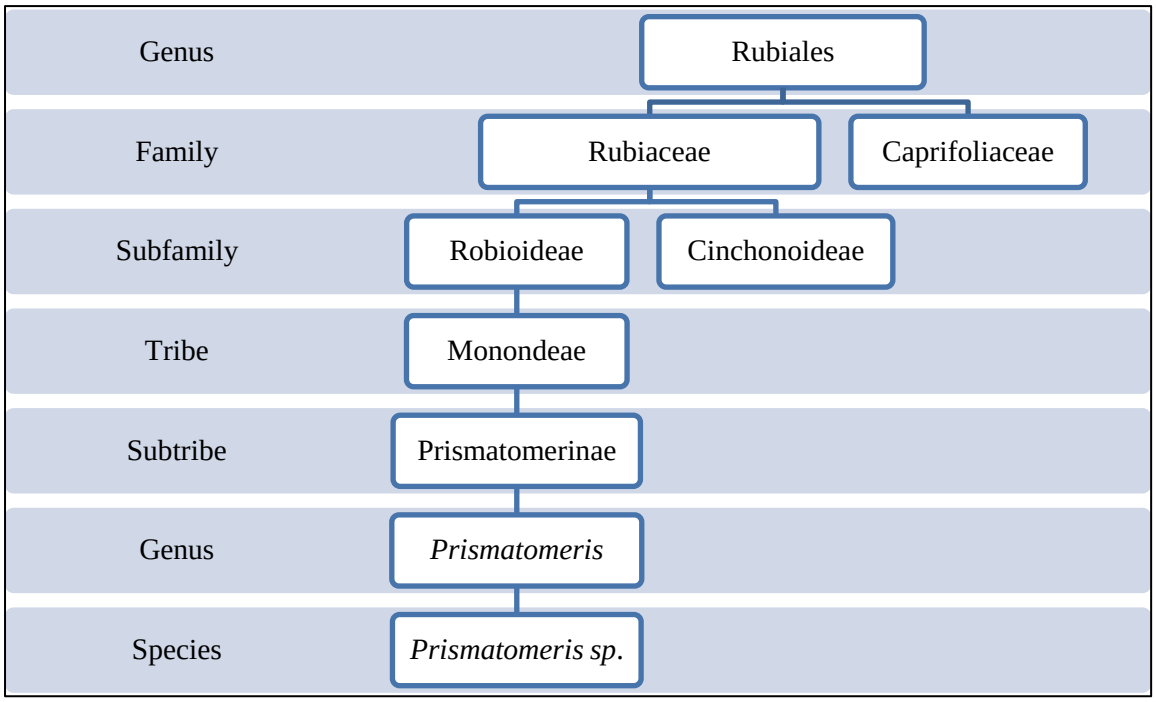

Scheme 1.4: Classification of Rubiaceae

Table 1.4: The list of *Prismatomeris* species and reference.

Species	**References**
P. albidiflora Thwaites	Hooker's J. Bot. Kew Gard. Misc. 8: 269 1856
P. albidiflora var. *fergusonii* (Thwaites ex Bedd.) Trimen	Handb. Fl. Ceylon 2: 356 1894
P. albidiflora var *javanica* Valeton	Bijdr. Boomsoort. Java 8: 199 1902
P. andamanica Ridl.	Bull. Misc. Inform. Kew 1939: 607 1940
P. beccariana (Baill. Ex K. Schum.) J.T. Johanss	Opera Bot. 94: 57 1987
P. brachypus Ridl.	Bull. Misc. Inform. Kew 1939: 602 1940
P. brevipes Hutch.	Pl. Wilson. 3: 413 1916
P. connata Y.Z. Ruan	Acta Phytotax. Sin. 26: 447 1988
P. euphlebia Merr.	Mitt. Inst. Allg. Bot. Hamburg 7:301 1937
P. Thwaites ex Bedd.	Fl. Sylv. S. India 134/10 1871
P. filamentosa Craib	Bull. Misc. Inform. Kew 1932: 436
P. fragrans Geddes	Bull. Misc. Inform. Kew 1927: 173
P. fragrans subsp. *andamanica* (Ridl.) J.T. Johanss.	Opera Bot. 94: 45 1987
P. glabra (Korth) Valeton	Bot. Jahrb. Syst. 44: 569 1910
P. grifthii Ridl.	J. Fed. Malay States Mus. 10: 96 1920
P.harmandii Pit.	Fl. Indo-Chine 3: 429 1924
P. henryi (H. Lév.) Rehder	J. Arnold Arbor. 16: 328 1935
P. javanica (Valeton) Ridl.	Bull. Misc. Inform. Kew 1939: 606 1940
P. kinabaluensis J.T. Johanss.	Opera Bot. 94: 40 1987
P. labordei (H. Lév.) Merr. Ex Rehder	J. Arnold Arbor. 18: 249 1937
P. lepidophloia (Miq.) Ridl.	Bull. Misc. Inform. Kew 1939: 601 1940
P. linearis Hutch.	Pl. Wilson. 3: 414 1916
P. malayana Ridl.	J. Fed. Malay States Us. 10: 142 1920
P. memecyloides Craib	Bull. Misc. Inform. Kew 1932: 437
P. mollis Craib	Bull. Misc. Inform. Kew 1932: 437
P. multiflora Ridl.	Bull. Misc. Inform. Kew 1939: 603
P. neurophylla (Miq.) Ridl.	Bull. Misc. Inform. Kew 1939: 606
P. obtusifolia Merr.	Philipp. J. Sci. 26: 492 1925
P. ovalifolia Ridl.	Bull. Misc. Inform. Kew 1939: 605
P. parkinsonii Ridl.	Bull. Misc. Inform. Kew 1939: 605
P. parviflora Ridl.	Bull. Misc. Inform. Kew 1939: 605
P. robusta J.T. Johanss.	Opera Bot. 94: 40 1987
P. sessiliflora Pierre ex Pit.	Fl. Indo-Chine 3: 429 1924
P. subsessilis King & Gamble	J. Asiat. Soc. Bengal, Pt. 2, Nat. Hst. 73: 91 1904
P. tetrandra (Roxb.) K. Schum.	Nat. Pflanzenfam. 4(4): 138 1891
P. tetrandra subsp. *malayana* (Ridl.) J.T. Johanss.	Opera Bot. 94: 40 1987
P. tetrandra subsp. *tetrandra*	unknown
P. tetrandra var. *multiflora* (Ridl.) Y.Z. Ruan	Acta Phytotax. Sin. 26: 447 1988
P. tetrandra var. *philippinensis* Ridl.	Bull. Misc. Inform. Kew 1939: 603

1.5 The genus: *Prismatomeris*

The genus *Prismatomeris* comprises twenty five species in the world, of which approximately grow in tropical Asia (Lemmens & Bunyapraphatsara, 2003). It is classified in the tribe *Morindeae*, together with *Morinda* and *Renellia*; it seems closely related to the latter genus. However some authors have placed it in a separate tribe *Prismatomerideae* (Lemmens & Bunyapraphatsara, 2003).

The genus *Prismatomeris* is a small shrub tree, glossy pale brown bark flaking off when dry, each inter node with a median longitudinal ridge ending between each pair of leaf stalks. The leaves are ovate to elliptic or slightly obovate. Secondary veins are known to inarch to form a series of marginal loops while tertiary veins are reticulate or obscure. The stipules of the leaves are triangular, bifid at the tip and the apices are either looks like two cusps or fine points (Ridley, 1967). Its flowers are stalked or sessile, in terminal and axillary clusters of two to ten bisexual and heterostylous. The calyx cup fringed by four to six teeth or sub truncate. The colour is white (Ridley, 1967). The ovary are two-celled while ovules one per cell. It attached to ovary cross wall with filiform style and two-lobed stigma. The fruit are globose to ellipsoid with one or two seeded. The seed are globose, with a narrow lateral groove at its point of attachment.

1.6 The species: *Prismatomeris malayana*

P. tetrandra (Roxb.) K. Schum (figure 1.6.1-1.6.4) is also synonym to *P. malayana Ridley* and *P. albidiflora King* (Lemmens & Bunyapraphatsara, 2003). Locally it is

known as tongkat aji samat. This species can be found in north-eastern India, Sri Lanka, Bangladesh, Burma, southern Laos, Vietnam, southern China, Thailand, Peninsular Malaysia, Singapore, Anamas Island (Indonesia) and Philipines (Luzon). The distribution mainly in lowlands regions up to 500m altitude, but sometimes in montane forest up to 1700 m altitude, in humid evergreen forest as well as dry forest, scrub vegetation, on dunes, also on shale and limestone .

P. malayana is a shrub or small tree up to 7 m tall; young branches with 2 prominent longitudinal ridges (Lemmens & Bunyapraphatsara, 2003). It will flowering at 5 ft. tall. (Corner, 1988). It has dark grey brown colored bark. The twigs are brittle. The leaves decussately opposite on vertical branches, distichously opposite on horizontal branches, simple and entire. The petiole are 2-25 mm long while the stipules are interpetiolar, narrowly triangular, up to 7.5 mm long and either caduceus or persistent (Lemmens & Bunyapraphatsara, 2003). Figure 1.2 illustrates the flower (Corner, 1988) and the flowering and fruiting branch of *P. malayana (*Lemmens & Bunyapraphatsara, 2003). The flowers are bisexual, heterodistylous, strongly scented. Its pedicel is up to 3.5m long while calyx is tubular with up to 2.5mm long and usually denticulate. Its corolla is hypocrateriform with tube up to 3cm long and lobes up to 2.5cm long. The colour of flower is white with stamens inserted above the middle of the corolla tube. The disk of flower is annular with two celled inferior ovary which is filiform style and it has 2-lobed stigma.

The fruits are sub globose drupe with 7-11 mm in diameter and the colour is blackish-purple to blackish-blue and it is 1-seeded. The seed is almost spherical, up to 9 mm in diameter with dark reddish-brown testa and endosperm corneous (Lemmens & Bunyapraphatsara, 2003).

1.7 Medicinal significance and known biological importance of *Prismatomeris species.*

In the traditional medicinal system, every part of *Prismatomeris malayana* is very useful. In Peninsular Malaysia and Thailand traditional medicinal system, the leaves have been applied as a poultice to fresh wounds (Burkill, 1966). In Cambodia, a decoction of the leaves, made by extended boiling with coconut palm and lawsonia roots, is used to treat bronchitis. In Thailand, the macerated roots in water are used to treat snakebites whereas in Indochina, the decoction has been used in a mixture with coconut and henna to treat bronchitis (Lemmens & Bunyapraphatsara, 2003).

The wood is considered a tonic and depurative in herbal tea drink after childbirth in Indochina. People in Thailand will use the decoction of the mixture of roots or stem with other herbal plant to treat bloody vomiting (Lemmens & Bunyapraphatsara, 2003). The author interviewed a few traditional medicinal practioners and found out that the root of *P. malayana* is one of the ingredients in a tonic containing also *Eurycoma longifolia* (tongkat ali) used as a preparation for improving blood circulation and providing energy.

Past reports have illustrated that there has been a few biological activity studies on *Prismatomeris sp*. An extract of *P. tetrandra* was found to be cytotoxic in brine shrimp lethality bioassay and on human tumor cell line (Dey et al., 2003). Kartsen et al. (2007) reported on the isolation and determination of absolute configuration of the

Figure 1.6.1: *Prismatomeris malayana* Ridley

Figure 1.6.2: The leaves and roots of *Prismatomeris malayana* Ridley

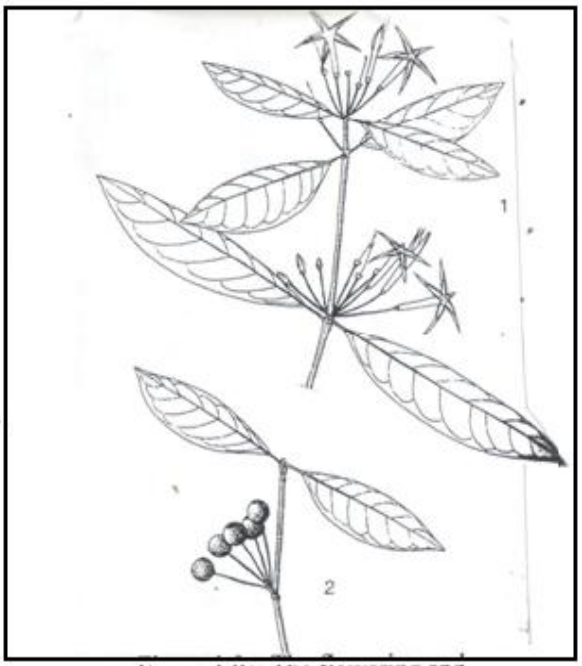

Figure 1.6.3: The flowering and fruiting branch of *Prismatomeris malayana* Ridley (Lemmens,R.H.M.J.& Bunyapraphatsara N., 2003)

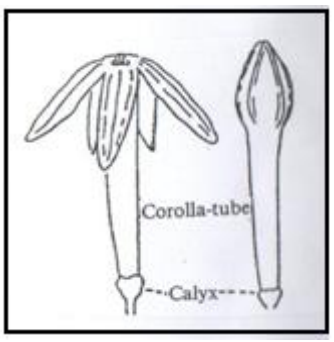

Figure 1.6.4: The flower of *Prismatomeris malayana* Ridley (Corner E.J.H, 1988)

new cytotoxic iridoids from *Prismatomeris tetrandra* namely as prismatomerine **9**. A number of anthraquinones, iridoids, triterpenoids and steroids were isolated from this species (Jiang et al., 2005; Zi-Ming et al., 2005). Kwanjai et al. (2005), reported on the biological activity such as anti-plasmodial, anti-tuberculosis, anti-fungal and cytotoxicity of the isolated anthraquinones and triterpenoids from *Prismatomeris fragrans*. Their preliminary study revealed that the hexane and dichloromethane extracts of the root and stem exhibited anti-plasmodial activity against *Plasmodium falciparum* (IC_{50} range 3.1- 3.7 μg/mL), anti-mycobacterial activity against *Mycobacterium tuberculosis* (MIC range 25-100 μg/mL), anti-fungal activity against *Candida albicans* (IC_{50} range 11-17 μg/mL) and cytotoxicity against BC and NCI-H187 cell lines (IC_{50} range 2-8 μg/mL).

The root methanol extracts of *Prismatomeris sessiflora* Pierre *ex* Pitard showed significant anti-malarial potential against $T_{9/94}$ *Plasmodium falciparum* (Kittisak et al., 1999). However, the isolated rubiadin **10** and rubiadin-1-methyl ether **11** (anthraquinones) revealed weak activity on the anti-malarial assay with IC_{50} range 13,000 ng/mL and 1,560 ng/mL respectively.

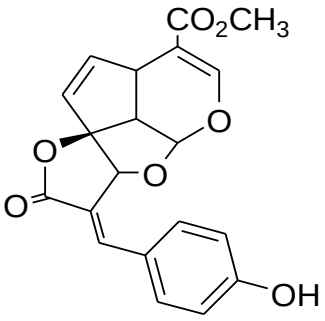

9

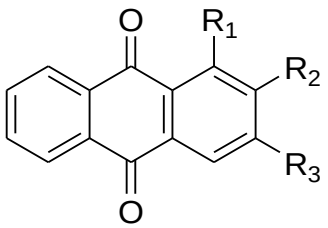

10 R_1=R_3= OH R_2=CH_3

11 R_1= OCH_3 R_2= CH_3 R_3= OH

CHAPTER 2:

GENERAL CHEMICAL ASPECTS

2.1 Introduction

Plants can be classified based on their physical characteristics and are hierarchically divided into kingdom, sub-kingdom, division, class, sub-class, order, family, genus and species. Besides that, through observations on reported findings, it may be expected that similar types of chemical constituents could be found in similar plant orders or family. This expectation is based on the assumption that similar plant orders or family contain similar types of enzymes, and that these enzymes can probably catalyse similar biotransformations ultimately leading to similar chemical structures (Vierhuis et al., 2001; Umezawa, 2003).

2.2 Chemical constituents of *Prismatomeris*

Examination of the literature has demonstrated that *Prismatomeris* species produces mainly anthraquinones, iridoids and triterpenoids (Lee, 1968, Kittisak et al., 1999, Zi-Ming et al., 2005, Kwanjai et al., 2005 and Kartsen et al., 2005). The iridoids and triterpenoids are classified under the terpenes groups while the anthraquinones are considered as phenolics. Further discussion will be carried out on these three groups of chemical constituents to understand their classification, structures, biogenetic pathways in plants and to list down their medicinal properties.

Lee (1968), Kittisak et al. (1999) and Zi-Ming et al. (2005) reported on the isolation of two anthraquinones i.e. rubiadin-1-methyl ether **11** and rubiadin **10** from *Prismatomeris malayana, P. sessiflora* and *P. tetrandra* respectively. The two anthraquinones were also isolated from *P. fragrans* (Kwanjai et al., 2005). Besides these two anthraquinones, Zi-Ming et al. (2005) also reported another six

anthraquinones from *P.tetrandra* as following: 1-hydroxy-2,3-dimethoxy-7-methyl-9,10-anthraquinone **12**, 1,3-dihydroxy-5,6-dimethoxy-2-methyl-9,10-anthraquinone **13**, 3-hydroxy-1,5,6-trimethoxy-20-methyl-9,10-anthraquinone **14**, 1-hydroxy-2-methyl-9,10-anthraquinone **15**, 1,3-dihydroxy-2-methoxy-9,10-anthraquinone **16** and 2-hydroxy-3-hydroxmethyl-9,10-anthraquinone **17**. Another six anthraquinones were identified from *P. fragrans* i.e. 1,3-dihyroxy-2-methyl-5,6-dimethoxyanthraquinone **18**, nordamnacanthal **19**, damnacanthal **20**, lucidin-ω-methyl ether **21** and 1-hydroxy-2-hydroxymethyl-3-methoxyanthraquinone **22 (**Kwanjai et al., 2005). A complex iridoid, prismatomerin 9 has been isolated from *P. tetrandra* together with gaertneroside **23** (Kartsen et al., 2005).

A biological activity investigation on *P. fragrans* by Kwanjai et al. (2005) reported on the isolation of two triterpenoids, β-acetylolean-12-en-28-olic acid **24** and 3β-*O*-acetyl-11α, 12α-epoxyolean-28, 13-olide **25** and β-sitosterol **26**.

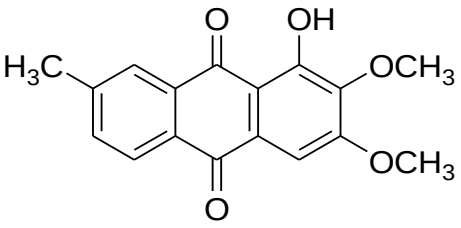

12

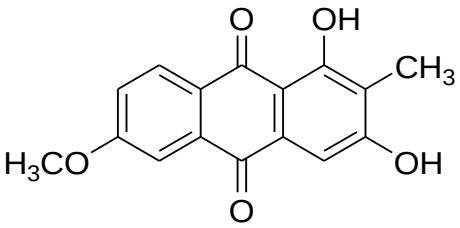

13

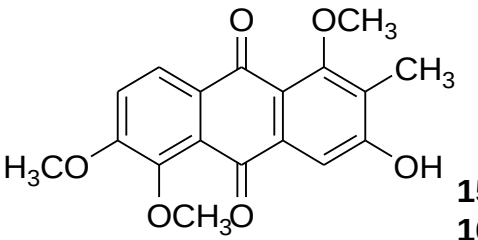

14

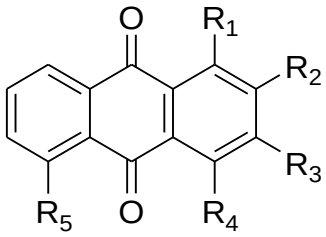

15 R_1= OH R_2= CH_3 R_3=R_4=R_5= H
16 R_1=R_3= OH R_2= OCH_3 R_4=R_5= H
17 R_1=R_4=R_5= H R_2= OH R_3= CH_2OH

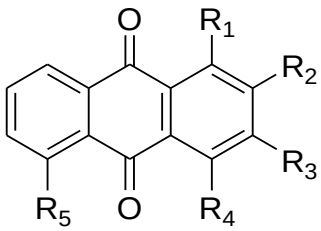

18 R_1= OH R_2= CH_3 R_3= OH
R_4=R_5= OCH_3
19 R_1= OH R_2= CHO R_3= OH
R_4=R_5= H
20 R_1= OCH_3 R_2= CHO R_3= OH
R_4=R_5= H
21 R_1= OH R_2= CH_2OCH_3 R_3= OH
R_4=R_5= H
22 R_1= OH R_2= CH_2OH R_3= OCH_3
R_4=R_5= H

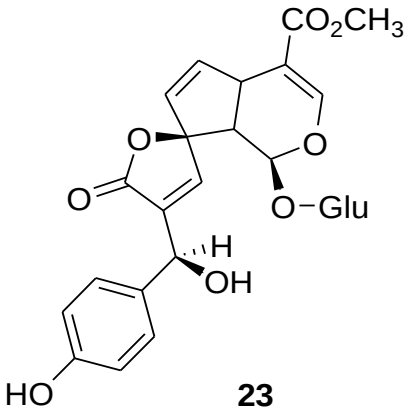

23

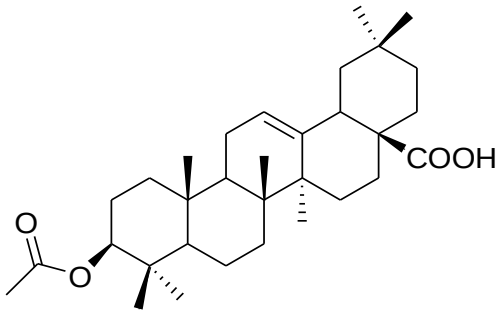

24

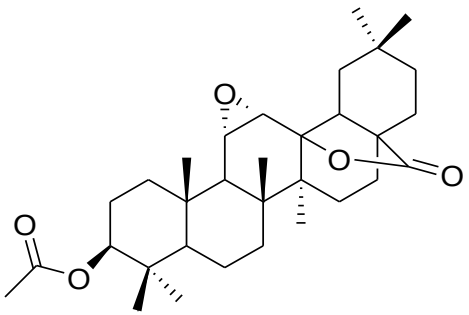

25

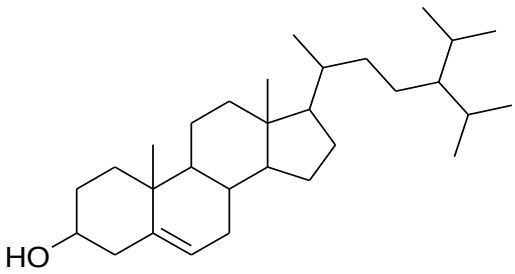

26

2.3 Terpenoids

Terpenes are one of the most important classes of natural products. These compounds are widely distributed in nature. Terpenes often possess a five carbon unit, known as isoprene unit **33** and is commonly represented by the symbol C_5 (Ruzicka, 1953). The number of isoprene units **33** incorporated in the particular terpenes, serves as basis for the classification of these group of compounds as listed in table 2.3 (Grisehach, 1965). Thus, monoterpenes are composed of two isoprene units and have the molecular formula $C_{10}H_{18}$, sesquiterpenes contains three isoprene units; $C_{15}H_{28}$, diterpenes have four isoprene units ; $C_{20}H_{34}$ and triterpenes are composed of six isoprene units; $C_{30}H_{50}$.

Table 2.3: Classification of terpenoids

No. of Carbon	Name	Parent	Subclass	Occurence
10	Monoterpenoids	GPP **27**	Iridoids	Oils
15	Sesquiterpenoids	FPP **28**	Abscesic	Oil, Resins
20	Diterpenoids	GGPP **29**	Gibberellins	Resin, Bitters, Heartwood
25	Sesterpenoids	GFPP **31**	-	Resin. Bitters, Heartwood
30	Triterpenoids	Squalene **30**	Phytosterols, Cardenolides, Saponins	Resin. Bitters, Heartwood, Latex
40	Carotenoids **34**	Phytones **32**	-	Gene tissues, Root and Fruit
10^{13}-10^{14}	Rubbers	GGPP **29**	-	Latex, root

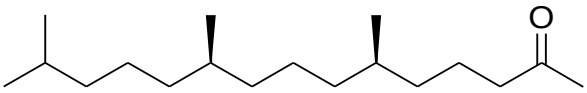

32

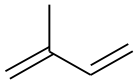

33

2.3.1 Biosynthesis of triterpenoids and iridoids

The mode of synthesis of compounds in plants will be discussed in this part. Two terms that usually used in this field are “biogenesis” and “biosynthesis. However, it is customary that the former term is used for a hypothesis, and the latter for an experimentally proven route (Nakanishi et al., 1974). The immense variety of structural types found in the terpenoids was rationalized by the isoprene rule of Ruzicka (Ruzicka, 1921). The biogenetic isoprene rule implies the involvement of an isoprene’s branched five carbon units in the biosynthesis of terpenoids. The isoprene units **33** could be linked together in a head-to-tail, tail-to-tail or head-to-head manner. During the biosynthesis, terpenoids could be formed by a linear arrangement of isoprene units **33** followed by various cylisations, rearrangements of the carbon

skeleton and by the loss or addition of carbon atoms. However, the isoprene is not a precursor of the triterpenoids

Triterpenoids constitute a large and diverse group of natural products. The biosynthesis proceeds via the formation of 15-C atom farnesyl pyrophosphate (FPP) **28** from the linkage of three isoprene **33** unit in a head-to-tail manner (scheme 2.3.1). Two FPP **28** linked in a tail-to-tail manner to give squalene **30**, a 30-C atoms (Holstein et al., 2004). Squalene **30** is oxidized to oxidosqualene **35** or squalene 2,3-epoxide (Abe et al., 1993, Haralampidis et al., 2002). Cyclization of oxidosqualene **35** to saponins can proceed in two ways, either *via* 'chair-chair-chair conformation' or *via* 'chair-boat-chair' conformation (Vincken et al., 2007). The stereochemistry clearly showed the configuration of the C8 and C14 atoms. Cyclisation *via* the 'chair-chair-chair' conformation resulted in the methyl group at the C8 atom pointing upwards while the one at C14 atom is pointing downwards, whereas the opposite is the case after cylization of the 'chair-boat-chair' conformation (Vincken et al., 2007). Oxidosqualene **35** is further converted to cyclic derivatives via protonation and epoxide ring opening, which creates a carbocation which can undergo several types of cyclization reactions. After these cyclizations, subsequent rearrangements can proceed in different ways by a series of hydride shifts and/or methyl migrations, which lead to the formation of new carbocations. Finally, the carbocations are neutralized by proton elimination to give a double bond or a cylopropanyl ring, or by reaction with water to give a hydroxyl group. Scheme 2.3.2 illustrates the cyclisation of oxidosqualene to the various triterpenes skeletons.

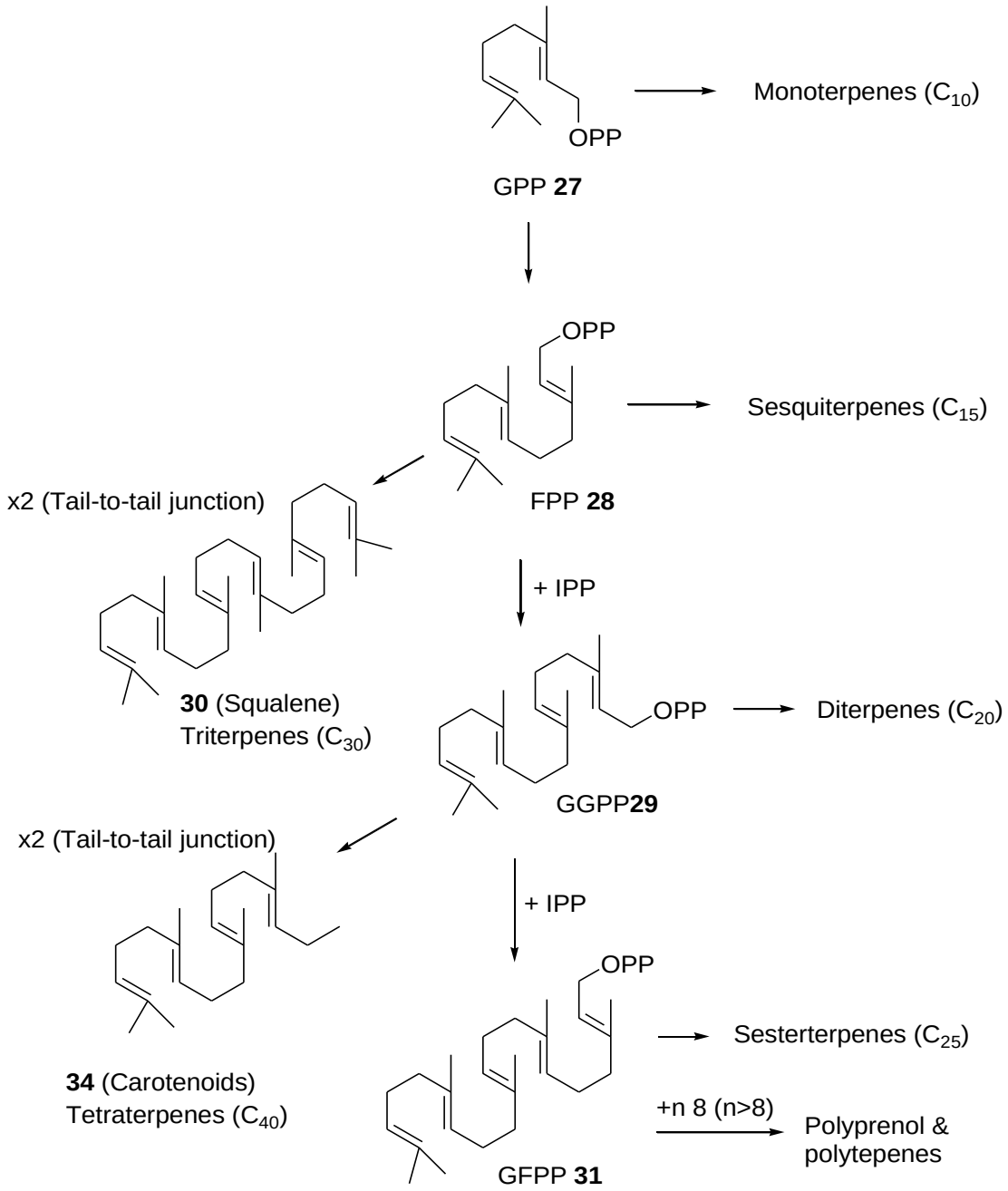

Scheme 2.3.1: General scheme of terpenoid biosynthesis

IPP-Isopenthenyl pyrophosphate

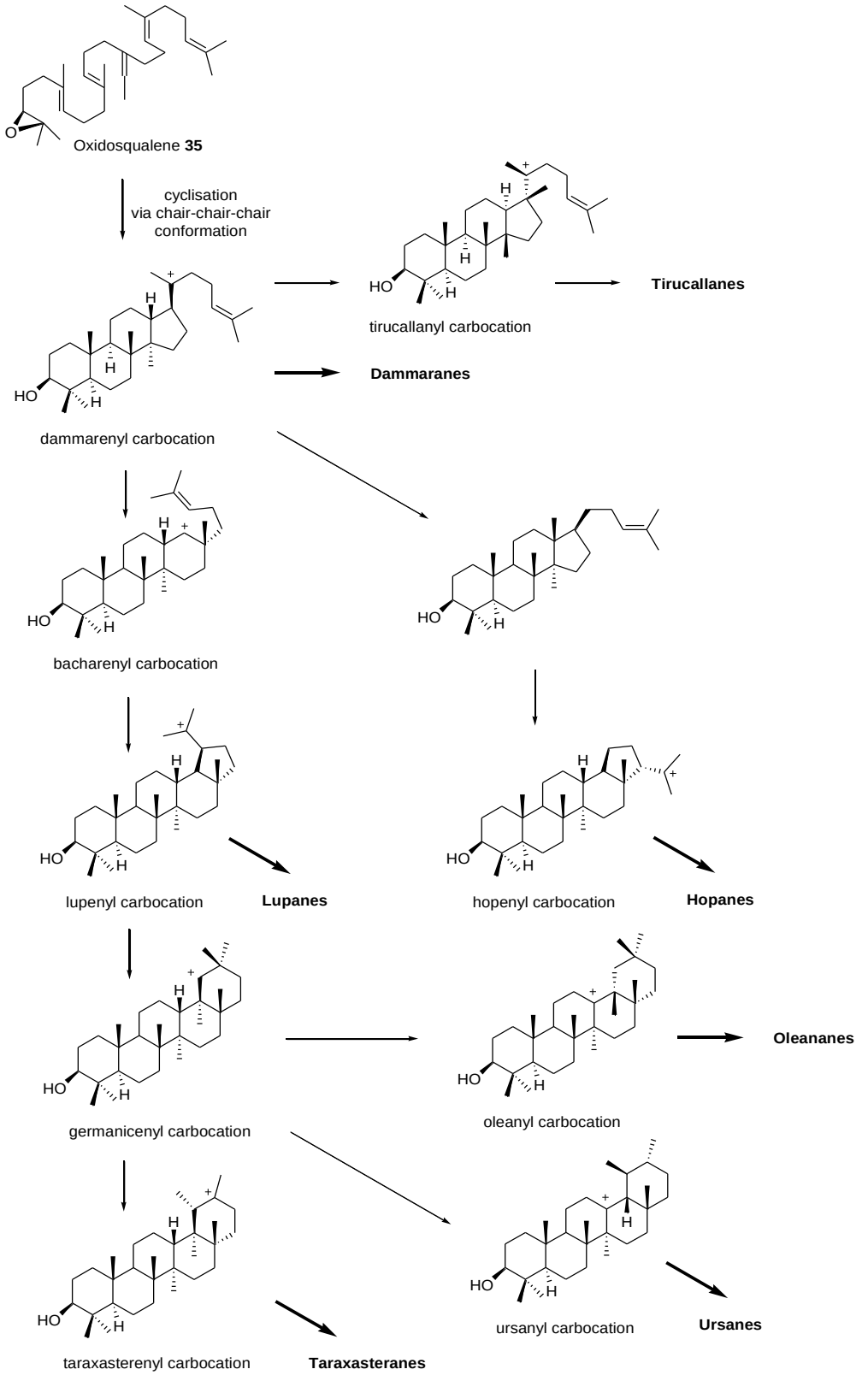

Scheme 2.3.2: The cyclization of oxidosqualene to the various saponins skeletons

Iridoids are usually found as glycosides (Biswanath et al., 2007). Structurally they are cylopentano [c] pyran monoterpenoids which is also known as the iridane **36** skeleton cis-2-oxa-bicyclo-[4,3,0]-nonane (Jean, 1995).

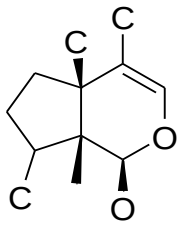

36

Iridoids generally have ten carbon atoms. The eleventh carbon is generally part of a carbomethoxyl group (loganin **37**, geniposide **38**) or part of carboxylic acid group (monotropein **39**) or by an aldehyde or methyl group (lamioside **40**). Sometimes the eleventh carbon is absent (aucubin **41**, catalpol **42**). Secoiridoids and plumeria iridoids is another group with a different skeleton (Jean, 1995; Biswananth et al., 2007). Secologanin **43**, gentiopicroside **44** and oleoside **45** are examples of secoiridoids while plumericin **46** is an example for plumeria.

Biogenetically and chemotaxonomically of iridoids provide a structural link between terpenes and alkaloids (Biswananth et al., 2007). The incorporation of labeled mevalonic acid and geraniol derivatives into iridoid-type structures demonstrated the terpenoid character of iridoids (Jean, 1995). One of the proposed mechanisms involves the cyclisation of 10-oxo-geranial **47** to iridodial **48** or to 8-epi-iridodial **49**. The glucosylation and oxidation of iridodial **48** leads to loganin **37,** the lead precursor of most iridoids. The same process also applies to 8-epi-iridodial **49** to lead, *via* 8-epiloganin, to antirrhinoside **50**, and gardenoside **51**. Loganin **37** will undergo a ring opening which leads to the secoiridoids *via* the secologanin **43**; the precursor of all the secoiridoids. Scheme 2.3.3 shows the proposed simplified biogenesis of iridoids.

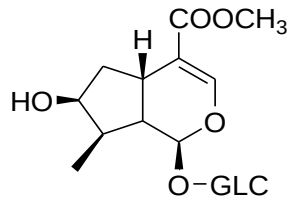

37

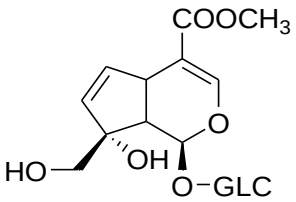

39

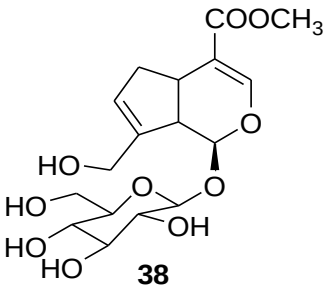

38

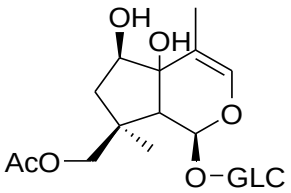

40

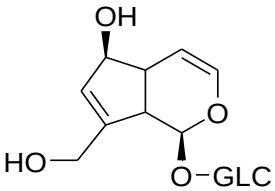

41

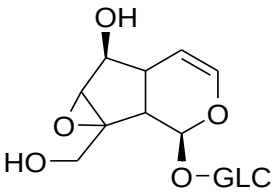

42

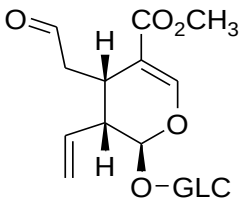

43

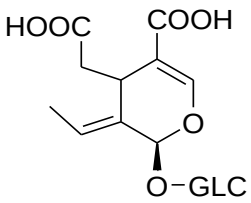

44

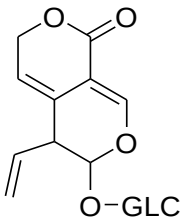

45

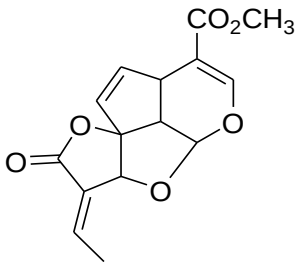

46

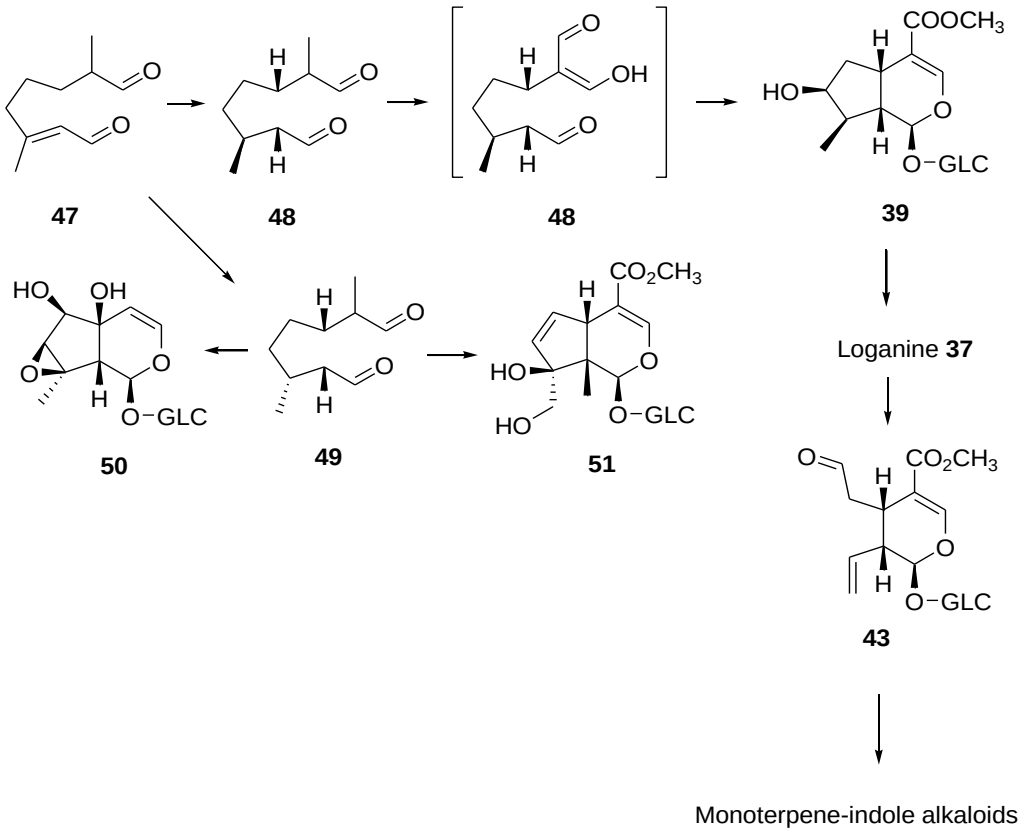

Scheme 2.3.3: Simplified biosynthesis of iridoids

2.4 Aromatic or benzenoid compound.

The fundamental structural element that characterizes phenolics is the presence of one or more aromatic rings substituted by at least one hydroxyl group, free or engaged in another function such as ether, ester or glycoside (Jean, 1995). Plant phenolic compounds are widely distributed in plant kingdom. Recently, polyphenols have gained an importance due to their potential use as prophylactic and therapeutic agents in many diseases, as well as their anti oxidant properties (Venketeshwer, 2012). Table 1.2.2 illustrates the classification of the phenolic constituents in plants which provided by Harbone & Simmons (1964).

Table 2.4: The classification of the phenolic constituents in plants

Carbon	**Families of phenols**
	Simple phenols
C6	Phenolic acids and related compounds
C6-C1	Acetophenones and phenylacetic acids
C6-C2	Cinnamic acids and related compounds
C6-C3	Coumarins, isocoumarins and chromones
C15	Flavones
C15	Isoflavones and Isoflavonoids
C15	Flavonols, dihydroflavonols and related compounds
C15	Anthocyanidins
C15	Chalcones, aurones and dihydrochalcones
C30	Biflavonyls
C6-C1-C6	Benzophenones, xanthones and stilbenes
C6-C2-C6	Quinones
C6-C10-C14	Betacyanins
C18	

2.4.1 Biosynthesis of anthraquinones

Anthraquinones **52** is a good example of a class of natural products incooporating a quinine moiety. It is naturally occurred when the dione **53** conjugated to two condensed polycyclic aromatic system (Jean, 1995). Generally, quinones arise from the oxidation of phenols.

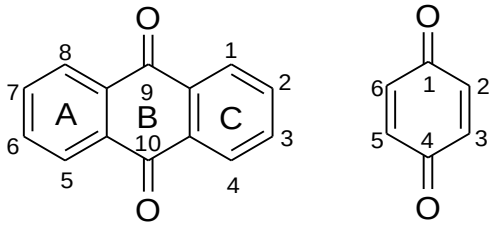

52 **53**

One of the remarkable features of anthraquinone biosynthesis in higher plants is that they are derived from a variety of different precursors and pathways (Leistner, 1981). The two main biosynthetic pathways leading to anthraquinones are the polyketide pathway (Van Den Berg & Labadie, 1989) and the chorismate pathway (Leistner, 1985). However, anthraquinones in the family Rubiaceae such as those from *Morinda*, *Rubia* and *Galium* species are considered to be biosynthesised *via* the chorismate acid pathway (Scheme 2.4.1). The shikimic acid and chorismic acid pathway shall be discussed in the next paragraph.

Thus, it was established that rings A and B of anthraquinones **52** in *Rubia* (Leistner, 1981), *Morinda* (Leistner, 1967) and *Galium* (Bauch & Leistner, 1978, Inoue et al., 1984) are derived from shikimic acid **54** (Leistner & Zenk, 1967), α-ketoglutarate **57** via o-succinylbenzoate **56** whereas ring C of *Rubia* type is derived from mevalonic acid (MVA) **58** (Leistner, 1981, 1985) or 2-C-methyl-D-erithritol-4-phosphate pathway (MEP) **59** in *Cinchona* (Ying-Shan et al., 2002).

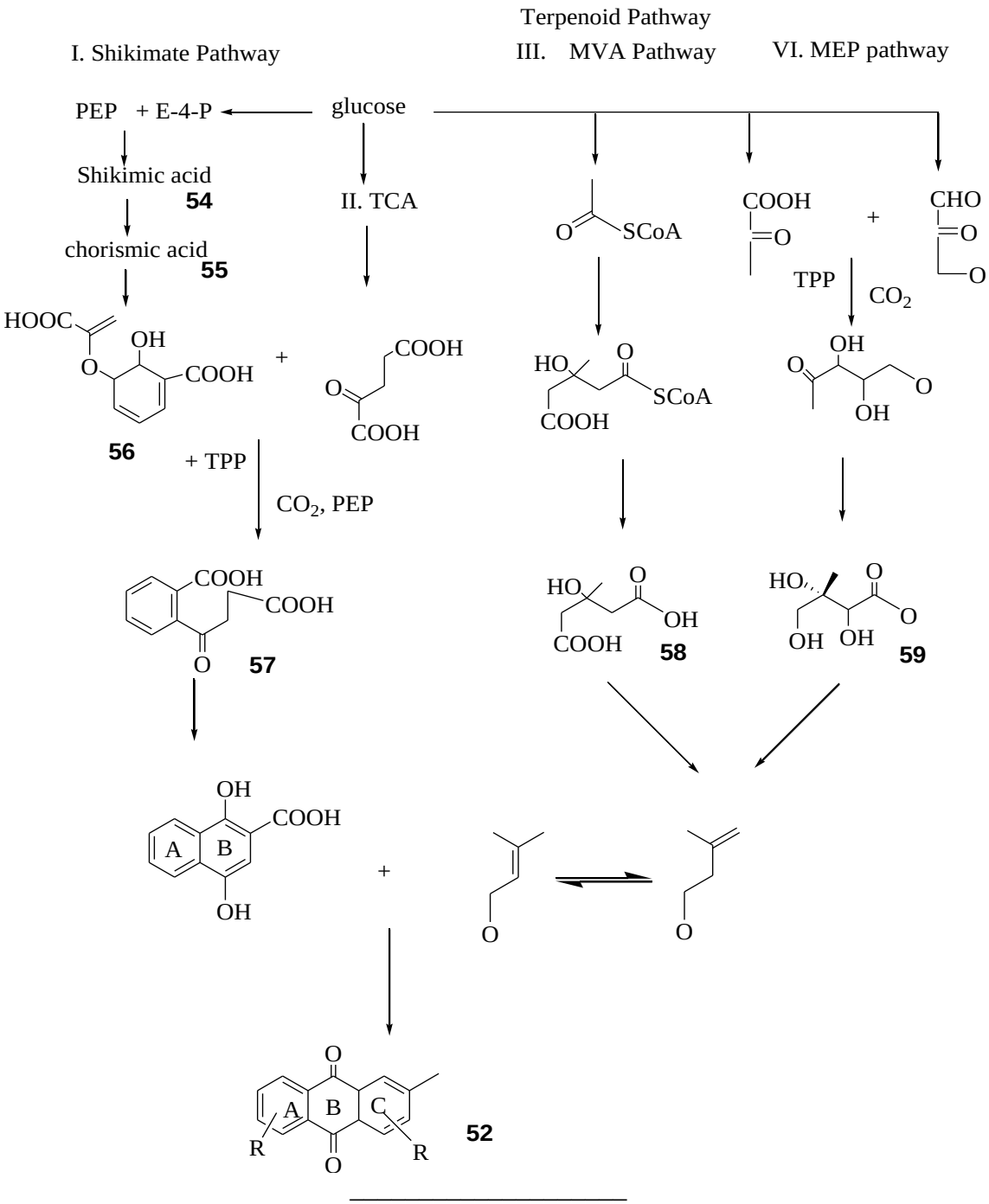

E-4-P=erythrose 4-phosphate, P=phosphate residue, PEP=phosphoenolpyruvate, TCA=tricarboxylic acid, TPP=thiamine diphosphate.

Scheme 2.4.1: Biosynthetic pathway leading to anthraquinones in the Rubiaceae

CHAPTER 3:

RESULTS AND DISCUSSION

3.1 Introduction

In this study, seventeen compounds were successfully isolated, purified and finally the structures were fully elucidated. The structures were determined by a combination of spectroscopic methods; 1D-NMR (^{1}H, ^{13}C, DEPT), 2D-NMR (COSY, HMQC and HMBC), IR, MS (LCMS/MS). The structures of the compounds were also elucidated by comparison with previous work.

3.2 Structural elucidation of isolated compounds from *Prismatomeris malayana* Ridley.

The isolated compounds from this plant species could be classified into three type; pentacylic triterpenoids (**60-65**), iridoids (**66, 68, 69, 70**) and anthraquinones (**71, 11,72, 10, 73, 74, 21**). Compound **73** and**74** are new while compound **66** was novel.

3.2.1 Compound A: *3β-hydroxyurs-12-en-28-oic acid* (*Ursolic acid*)

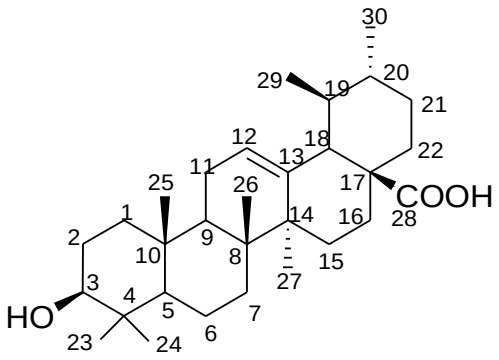

60

Ursolic acid (3β-hydroxyurs-12-en-28-oic acid) **60** (compound A) was obtained as a white amorphous powder and produced a pseudo-molecular ion peak $[M+Na]^+$ at m/z 479.35059 by ESI-MS which is consistent with the molecular formula of $C_{30}H_{48}O_3$. Its IR spectrum gives strong peaks at 1686cm^{-1} corresponding to the stretching of a C=O, a broad and sharp absorption band between 3866 and 3188 cm^{-1}, and 2860 cm^{-1} indicate the presence of a COOH functional group (Silverstein et al.,1991).

The ^{1}H NMR (figure 3.2.1.1) gives two sets of doublet (δ0.99, *J*=5.2 Hz, 3H, H-30 and δ1.03, *J*= 4.8 Hz, 3H, H-29) of two secondary methyl groups, five tertiary methyl groups (δ1.25, H-23; 1.08, H-26; 1.04, H-24; 1.28, H-27 ;0.90, H-25) and a tri substituted olefinic double bond (δ5.54, *brs*) for H-12. The presence of an oxymethine proton resonating at δ3.50 (*brt*, *J*=8.5) for H-3, was revealed in the ^{1}H-NMR of compound A. The configuration of 3β-secondary hydroxyl group was in agreement with the observed coupling constant, for 3β–urs-12-*e*n-28-oic acid (Chien-Ya et. al., 2001). The occurrence of doublet at δ2.68 (*J*=11.8Hz), for H-18 as well as a characteristic doublet of triplets signal (δ2.17, J_1=4.4, J_2=8.6 Hz, 1H) for H-16 suggested that compound A is an urs-12-en derivative (Chien-Ya et al., 2001).

Moreover, the chemical shifts of the carbon and proton were identical to those reported for 3β-urs-12-en-28-oic acid (table 3.2.1).

The ^{13}C NMR spectrum (figure 3.2.1.2) combined with analysis of the DEPT spectrum (figure 3.2.1.3) allowed to differentiate thirty resonances into seven methines, nine methylenes, seven methyls and seven quarternary carbons, of which were assigned to a pentacyclic triterpene skeleton. The presence of an olefinic group at δ139.0 and 125.4 (C-13 and C-12) in ^{13}C spectrum of compound A, were the characteristic of ursane type skeleton (Naidu et. al, 1988). A signal at δ180.0 (C-28) indicated the presence of carboxylic acid. Another significant signal was revealed at δ77.6 (C-3) which belongs to the hydroxylated carbon.

Figure 3.2.1.4 showed the HMQC spectrum of compound A which help to correlate the proton and carbon which are bonded together. The structure was further confirmed by the correlations detected in the HMBC spectrum (figure 3.2.1.5a and b) between H-18 (δ 2.68) and C-12 (δ 125.5), C-19 (δ 39.2), C-29 (δ17.3), C-17 (δ 47.9), C-16 (δ 24.7), C-13 (δ 139.1), C-14 (δ 42.3) and another set of correlations between H-12 (δ 5.54) and C-11 (δ 23.4), C-10 (δ 37.2), C-14 (δ 42.3) and C-18 (δ 53.3). These two sets of correlations giving and evidence that the double bond at C-12 and C-13 and carboxyl geoup at C-28. Another set of correlation between H-3 (δ 3.50) and C-4 (δ 39.3), C-23 (δ 28.6), C-24 (δ 16.4) support the assignment on the position of hydroxylated C-3. Figure 3.2.1.6 illustrates the selected HMBC correlation of compound A.

Hence the complete assignments of compound A was achieved. As a result, with comparison of the spectroscopic data obtained from compound A with the literature

values, the former was confirmed to be 3β-hydroxyurs-12-en-28-oic acid (ursolic acid) **60** (Werner et al., 2003, Simone et al., 2007).

Table 3.2.1: ^{1}H NMR [300 MHz, δ_H (*J*, Hz)] and ^{13}C NMR [75 MHz, δ_C] of **60** in C_5D_5N

Position	**^{13}C***	**^{13}C**	**^{1}H(*J*,H)***	**^{1}H(*J*,H)**
1	39.2	38.9	1.00	0.95
			1.58	1.30
2	28.2	28.4	1.81,	1.80
			1.81	1.80
3	78.2	77.7	3.44*dd*	3.50 (*brt*, *J*=8.5)
4	39.6	39.3	-	-
5	55.9	55.6	0.88*d*	1.10
6	18.8	18.5	1.58	1.50
7	33.7	33.3	1.59	1.60
			1.39	
8	40.1	39.8	-	-
9	48.1	47.9	1.65	1.55
10	37.5	37.2	-	-
11	23.7	23.4	1.96	1.90
12	125.7	125.5	5.49*s*	5.54*s*
13	139.3	139.1	-	-
14	42.6	42.3	-	-
15	28.8	27.8	1.22	1.15
			2.33*t*	2.30
16	25.0	24.7	2.14 *t*	δ 2.19 (*dt*, J_1= 4.4, J_2= 8.6)
17	48.1	47.9	-	-
18	53.6	53.3	2.63*d*	2.68 (*d*, *J*=11.8)
19	39.5	39.2	1.49	1.25
20	39.4	39.2	1.05	1.00
21	31.1	30.8	1.40	1.50
22	37.4	37.0	1.97	1.75
23	28.8	28.6	1.24*s*	1.25
24	16.5	16.4	1.02*s*	1.04
25	15.7	15.5	0.92	0.90
26	17.5	17.2	1.06 *s*	1.08
27	24.0	23.7	1.24s	1.28
28	179.7	180.0	-	-
29	17.5	17.3	1.02*d*	1.03 (*d*, J_1=4.8)
30	21.4	21.2	0.97*d*	0.99 (*d*, J_1=5.2)

***^{13}C NMR [150 MHz in C_5D_5N] Werner et al., 2003
*^{1}H NMR [600MHz in C_5D_5N] Werner et al., 2003

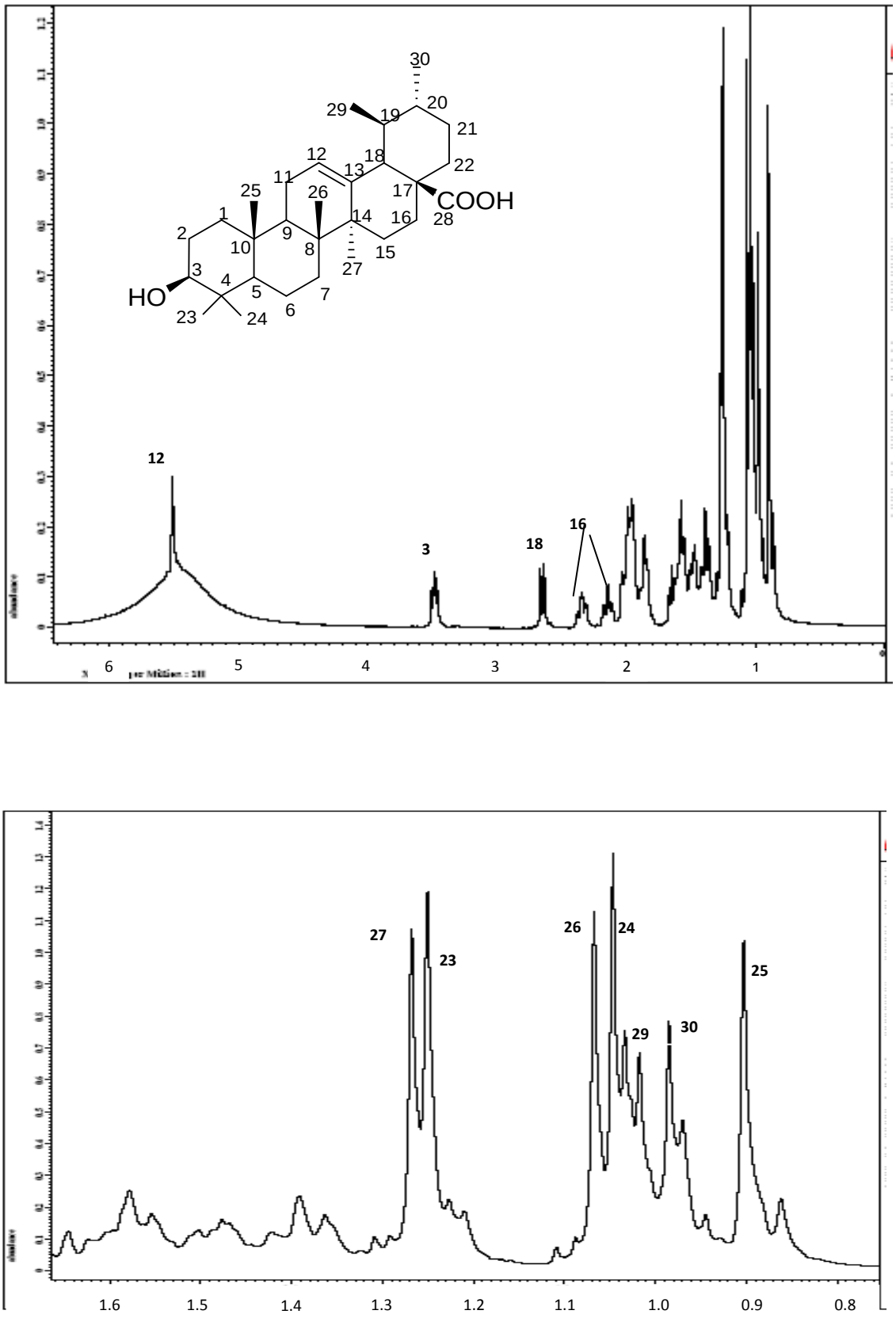

Figure 3.2.1.1: ^{1}H NMR spectrum of ursolic acid **60**

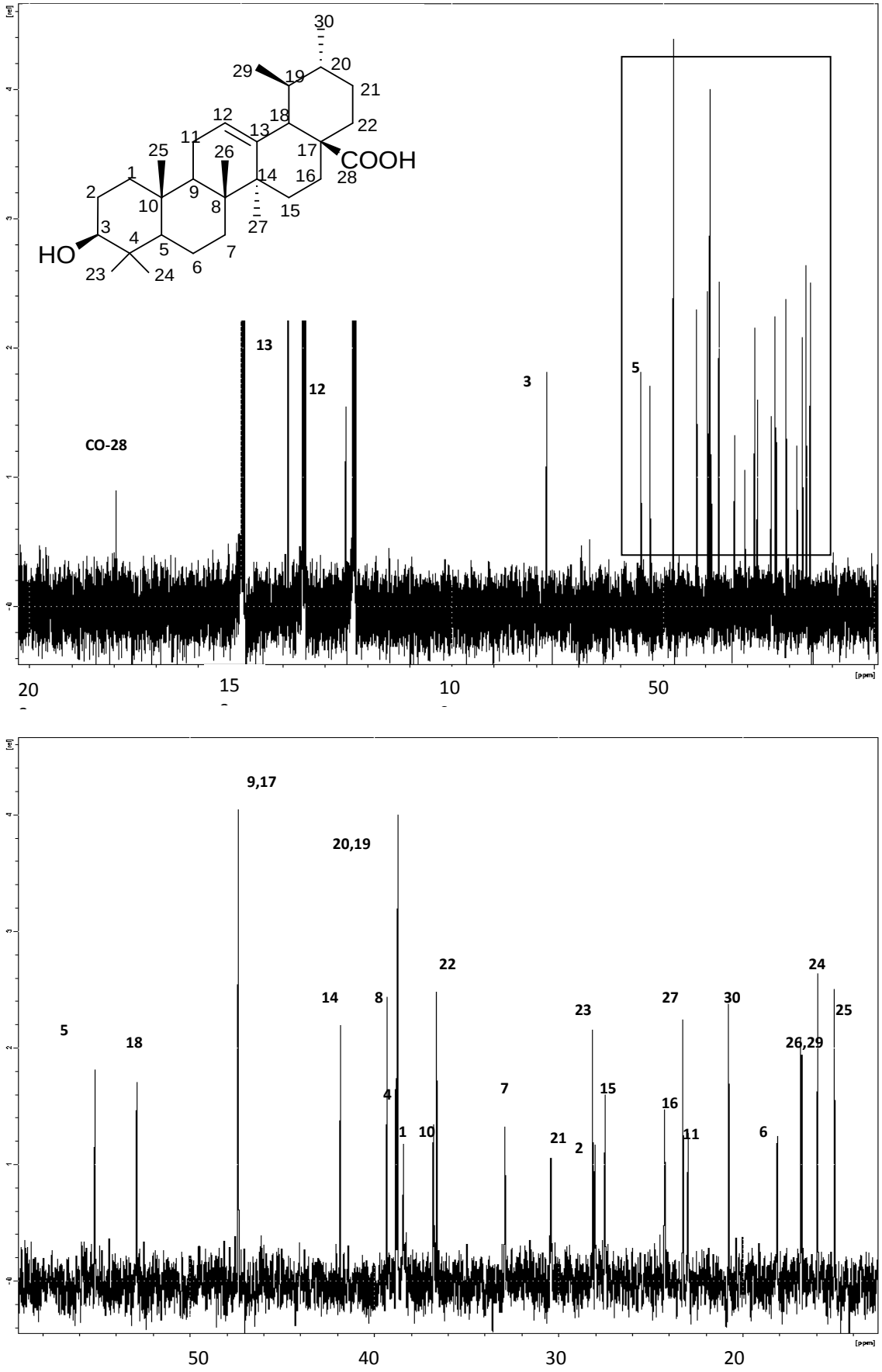

Figure 3.2.1.2: ^{13}C NMR of ursolic acid **60**

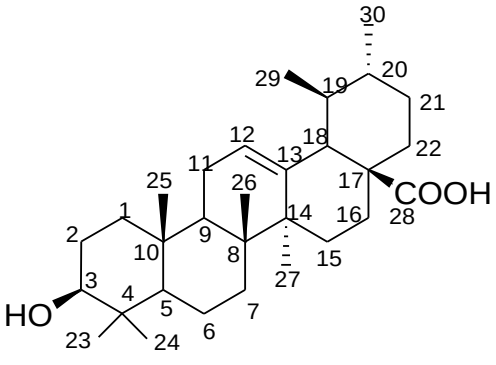

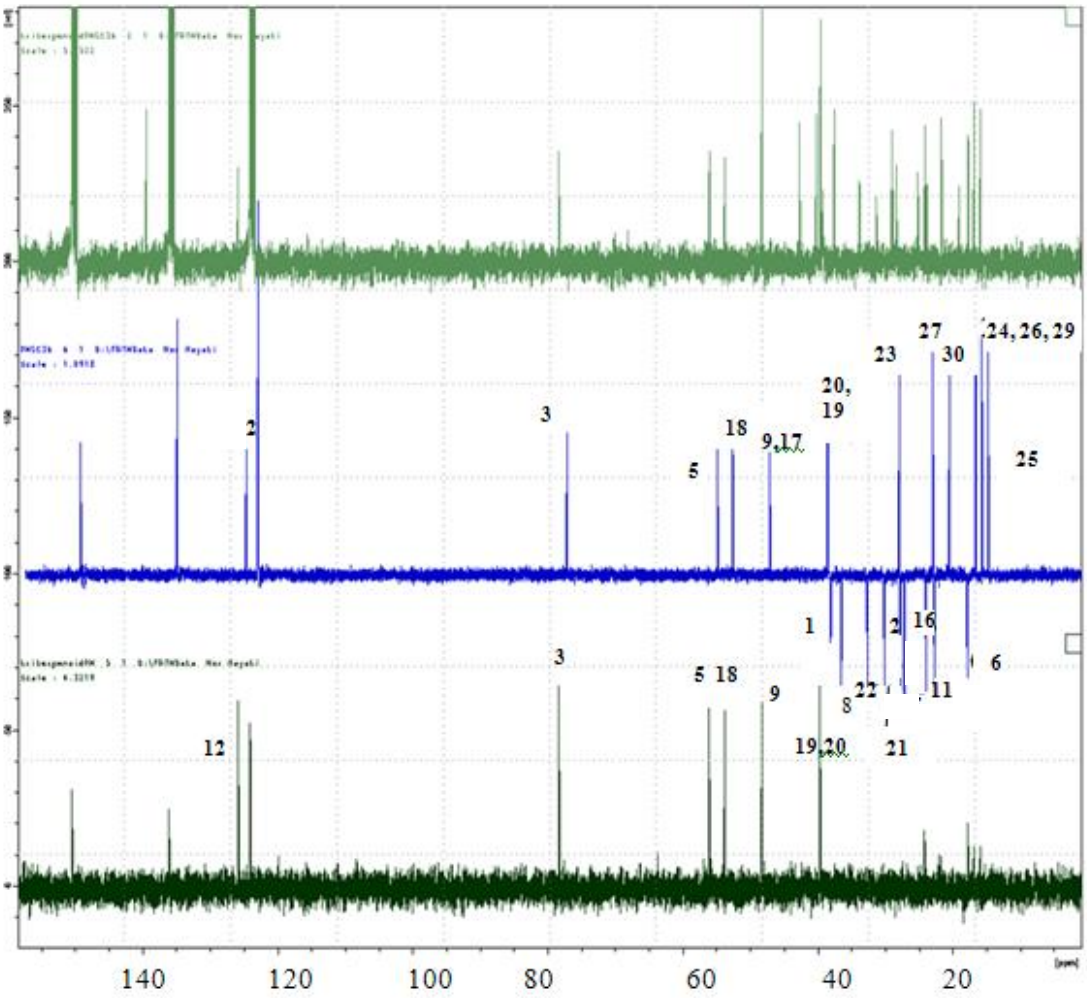

Figure 3.2.1.3: DEPT spectrum of ursolic acid **60**

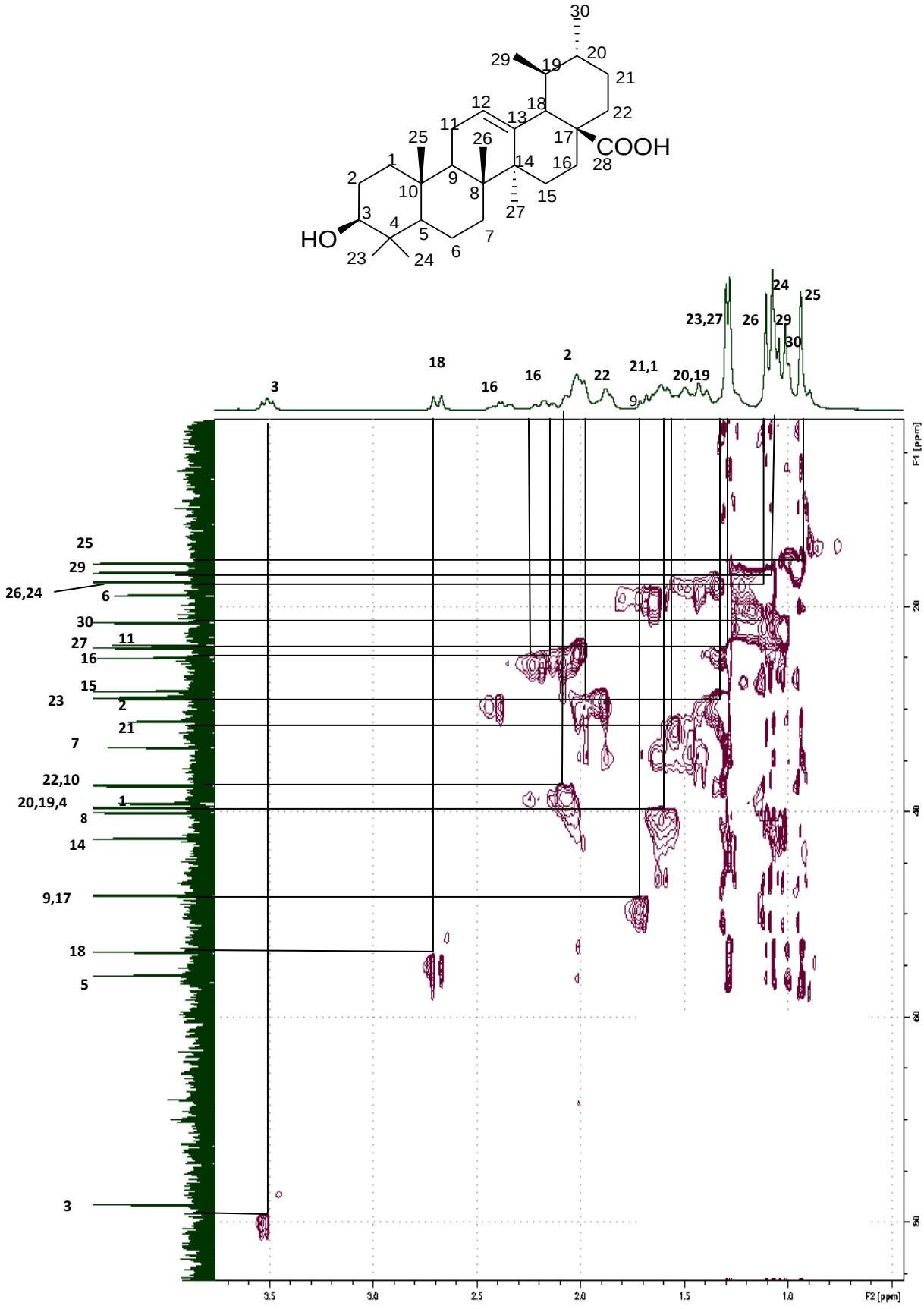

Figure 3.2.1.4: HMQC spectrum of ursolic acid **60**

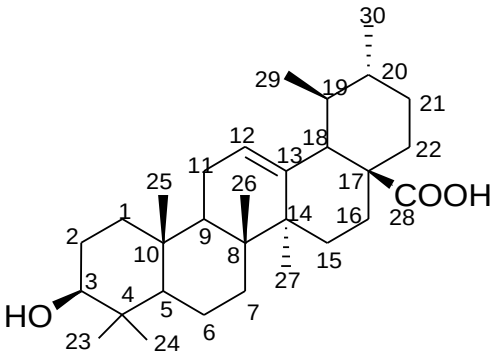

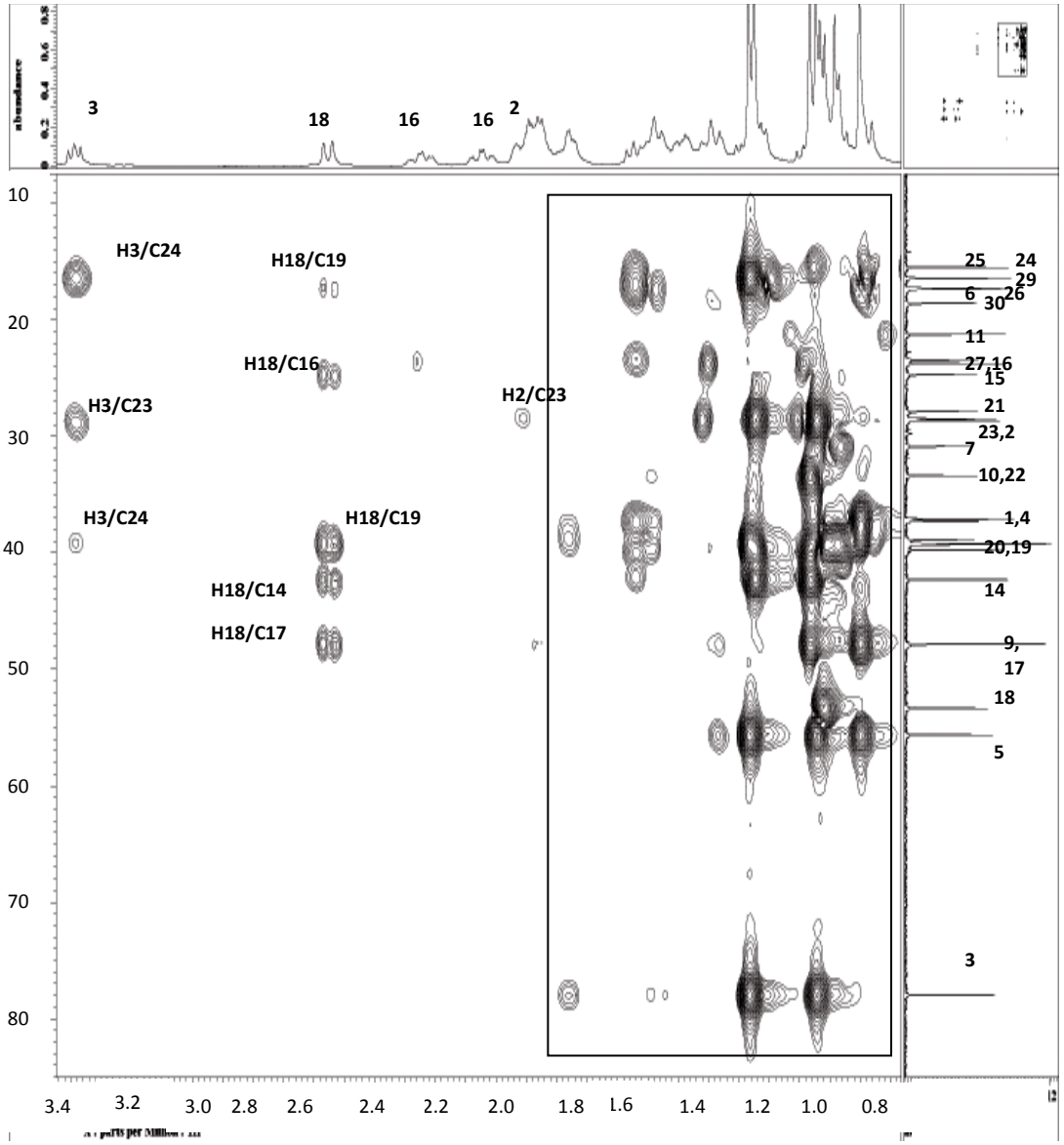

Figure 3.2.1.5a: HMBC spectrum of ursolic acid **60**

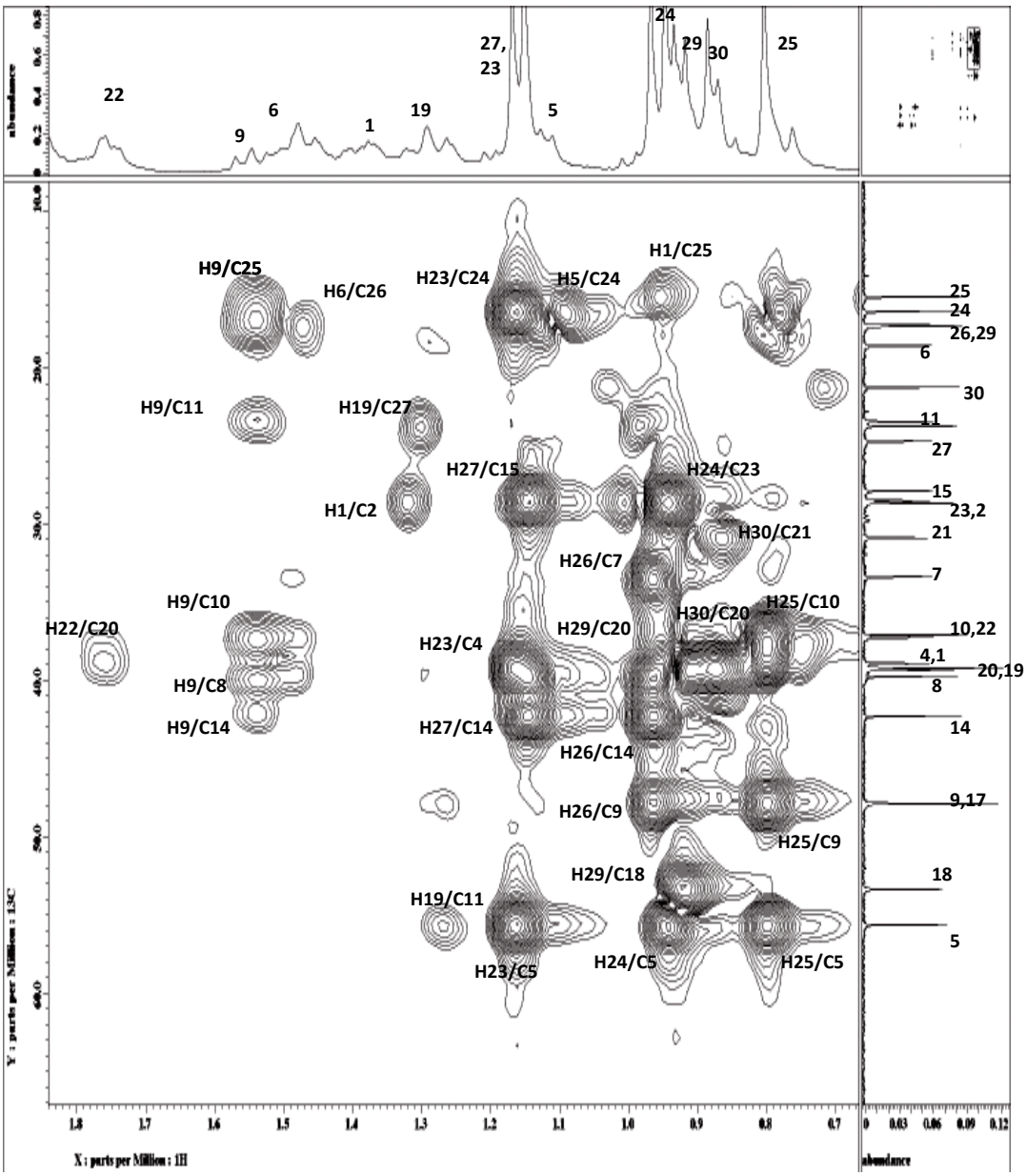

Figure 3.2.1.5b: HMBC spectrum expansion of ursolic acid **60**

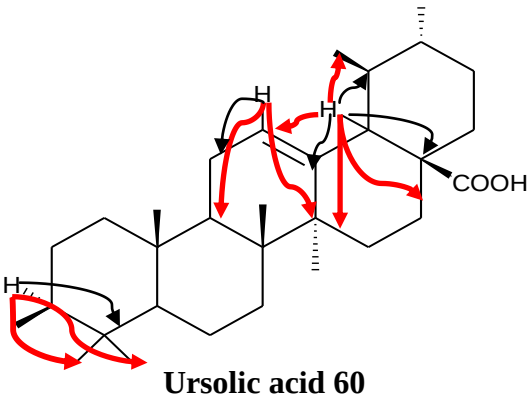

Ursolic acid 60

J^2 Correlations

J^3 Correlations

Figure 3.2.1.6: Selected HMBC correlations in ursolic acid **60**

3.2.2 Compound B: *3α,19α,24-trihydroxyurs-12-en-28-oic acid (barbinervic acid)*

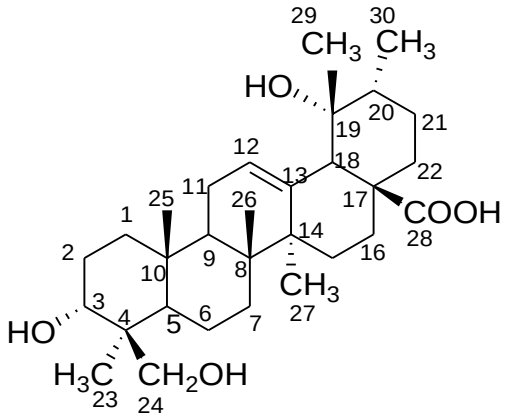

61

Barbinervic acid (3α, 19α, 24-trihydroxyurs-12-en-28-oic acid) **61** (compound B) was isolated as colorless amorphous solid. It produced a pseudo-molecular ion peak $[M+Na]^+$ at m/z 511.34012 by ESI-MS which is consistent with the molecular formula $C_{30}H_{48}O_5$. The IR spectrum gives strong peak at 1688cm^{-1} for C=O, a broad and strong peak between 3691 and 3208 cm^{-1}, and 2937 cm^{-1} for COOH absorptions (Silverstein et al., 1991).

Its ^{1}H NMR (figure 3.2.2.1) is almost similar to compound A. It possess one set of doublets (δ1.16, *J*=9.6 Hz, H-30) which indicate the presence of secondary methyl, five singlets of tertiary methyl at (δ1.65, H-23; 1.0, H- 25; 1.14, H-26; 1.68, H-27; 1.46, H-29) a tri substituted double bond (δ5.64, *brs*, H-12) and two oxymethine protons (δ4.5, *bs*, 1H) for H-3 and (5.08,*bs*, 1H) for OH-19. It showed differences in the total number of methyl groups compared to **60**. The presence of two doublets (δ4.13, *J*=10.8 Hz and δ3.84, *J*=10.8 Hz, H-24) suggested the exocylic methane with geminal coupling (CH_2-). The H-α is deshielded by the electronegative oxygen atom (-OH) and thus shifted downfield in the spectrum. The occurrence of a singlet signal at 3.02 for H-18 as well as a characteristic doublet of triplet signal (δ3.14 *dt*, J_1=12.7 and

J_2= 4.0 Hz) assignable to H-16α, which is shifted downfield by the anisotropic effect due to a 19α-hydroxyl group, similar to those reported on 3α, 19α,24-trihydroxyurs-12-en-28-oic acid (Jie-Ping et al., 2006).

The analysis on ^{13}C NMR (Figure 3.4.2.2) and DEPT spectrum (Figure 3.2.2.3) differentiate thirty resonances into eight quarternary carbons, six methines, ten methylenes and six methyls. The presence of olefinic group was demonstrated by the peaks at δ128 and δ139.7 (C-12, C-13), while three hydroxylated carbon signals at δ69.8, 72.5 and 65.4 (C-3, C-19, C-24). The carboxylic carbon signal was revealed at δ180.6.

The HMQC spectrum (figure 3.2.2.4a and 3.2.2.4b) showed the correlation between proton and carbon bonded together. The structural assignment was further confirmed by the HMBC spectrum illustrated in figure 3.2.2.5a and b. The correlation between H-30 (δ 1.16) and C-19 (δ 5.08) supported the hydroxylated C-19. Another set of correlation between proton H-24 (δ 4.13) and C-4 (δ 43.69) giving an evidence that exocylic methane was position at C-24. Selected HMBC correlation was presented in figure 3.2.2.5.

As a result, with comparison of the spectroscopic data obtained from compound B and the literature, the former was confirmed to be 3α,19α,24-trihydroxyurs-12-en-28-oic acid of 19α-hydroxyursane-type triterpenoids **61**.

Table 3.2.2: ^{1}H NMR [300 MHz, δ_H (*J*, Hz)] and ^{13}C NMR [75 MHz, δ_C] of **61** in C_5D_5N

Position	**^{13}C***	**^{13}C**	**^{1}H(*J*,H)**
1	33.3	33.8	1.35*m*
2	25.7	26.7	1.8 *m*
3	68.9	69.7	4.50 *bs*
4	42.9	43.7	-
5	49.4	48.1	1.80 *m*
6	18.7	18.9	1.75 *m*
7	33.6	33.6	1.2 *m*
8	40.0	41.8	-
9	47.1	47.5	1.4 *m*
10	36.9	37.2	-
11	23.7	24.0	2.2 *m*
12	127.4	128.0	5.64 *s*
13	139.0	139.7	-
14	41.6	40.3	-
15	28.5	29.05	2.14 *m*
16	25.7	26.2	3.14 (*dt*, 12.6, 4.0 Hz)
17	47.4	47.5	-
18	53.7	54.4	3.02 *s*
19	72.1	72.5	5.08*bs*
20	41.9	42.2	2.3 *m*
21	26.4	26.2	2.1 *m*
22	37.7	38.3	2.5 *m*
23	23.1	23.4	1.65*s*
24	64.6	65.5	4.13 (*d*, 10.8 Hz) 3.84 (*d*, 10.8 Hz)
25	15.8	15.8	1.0 *s*
26	16.9	16.9	1.14 *s*
27	24.5	24.4	1.68 *s*
28	179.4	180.6	-
29	26.9	26.9	1.46 s
30	16.8	16.6	1.16 (*d*, 9.6 Hz)

*^{13}CNMR [500MHz, DMSO-d_6]
Jie-Ping et al., 2006

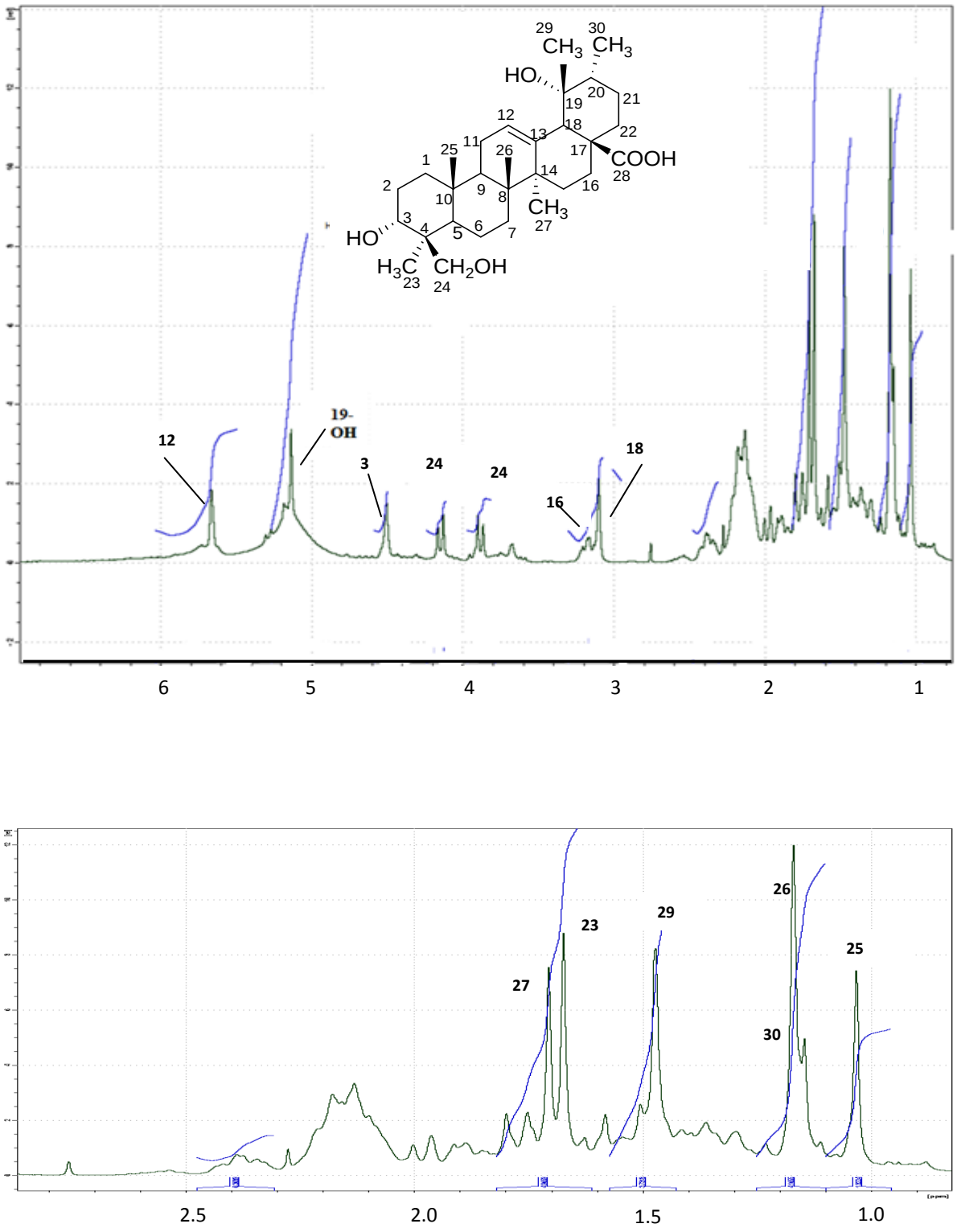

Figure 3.2.2.1: ^{1}H NMR spectrum of barbinervic acid **61**

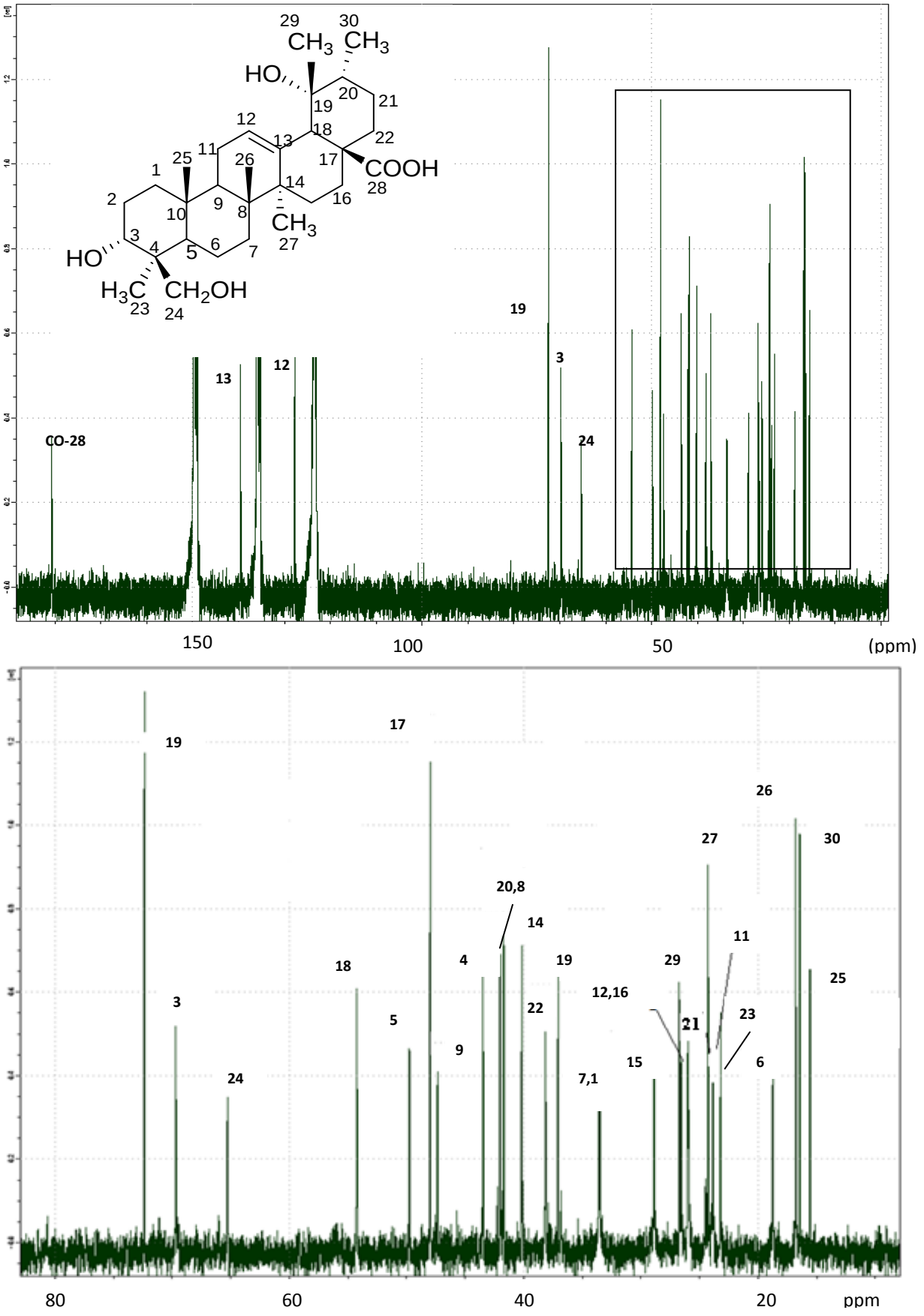

Figure 3.2.2.2: ^{13}C NMR spectrum of barbinervic acid **61**

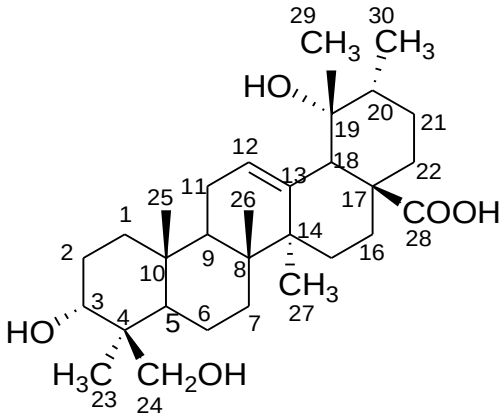

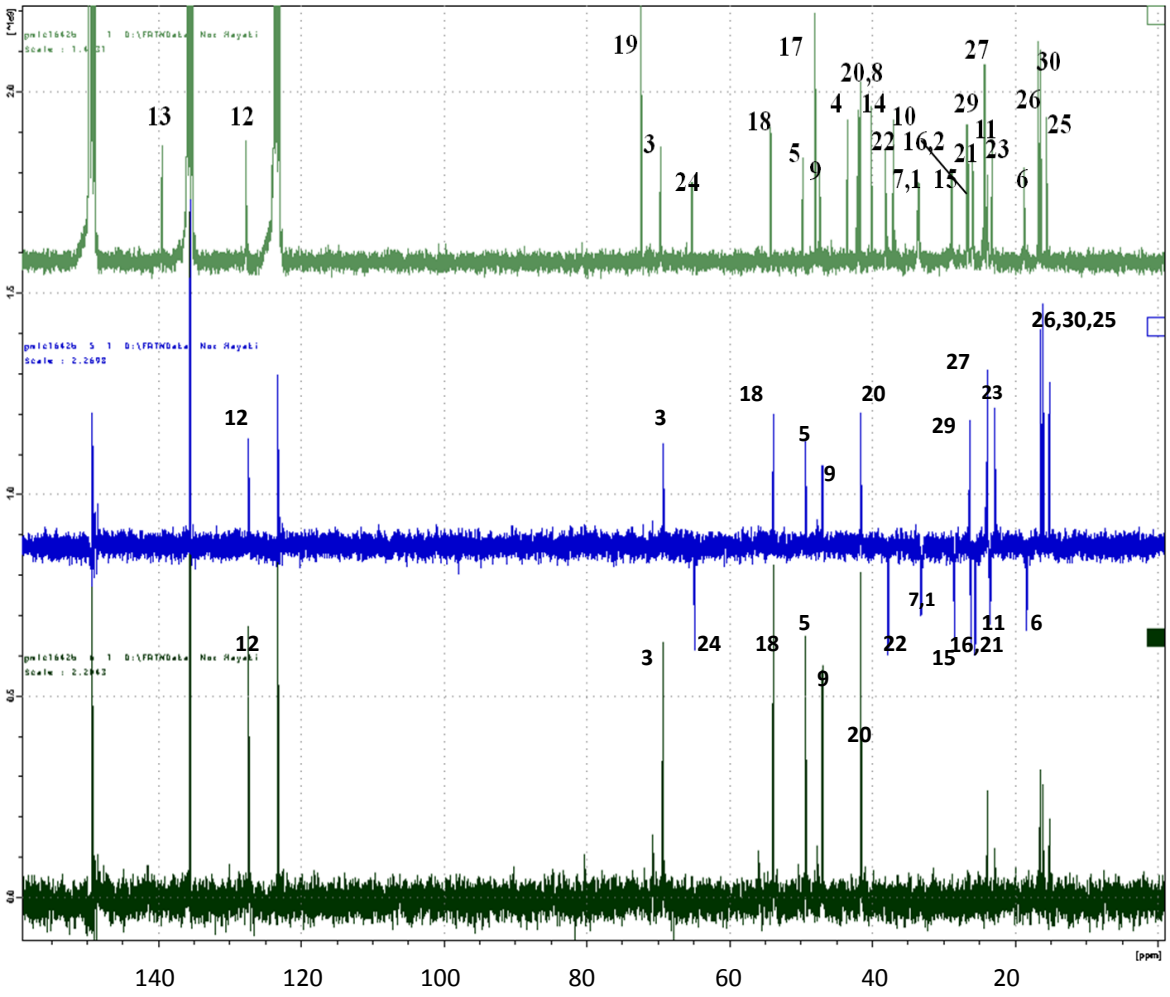

Figure 3.2.2.3: DEPT spectrum of barbinervic acid **61**

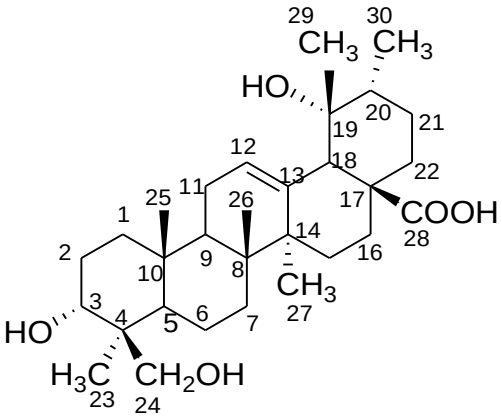

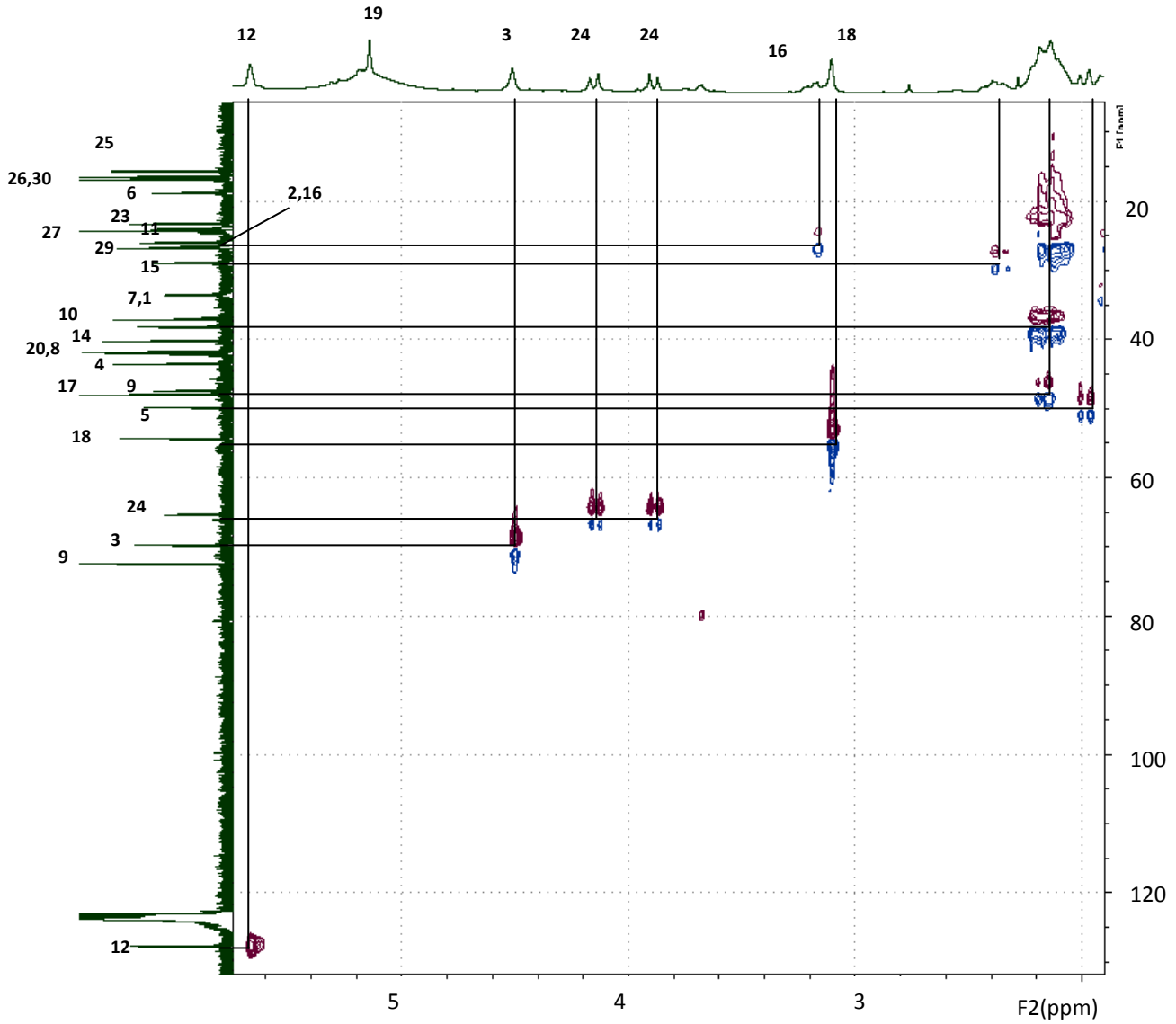

Figure 3.2.2.4a: HMQC spectrum of barbinervic acid **61**

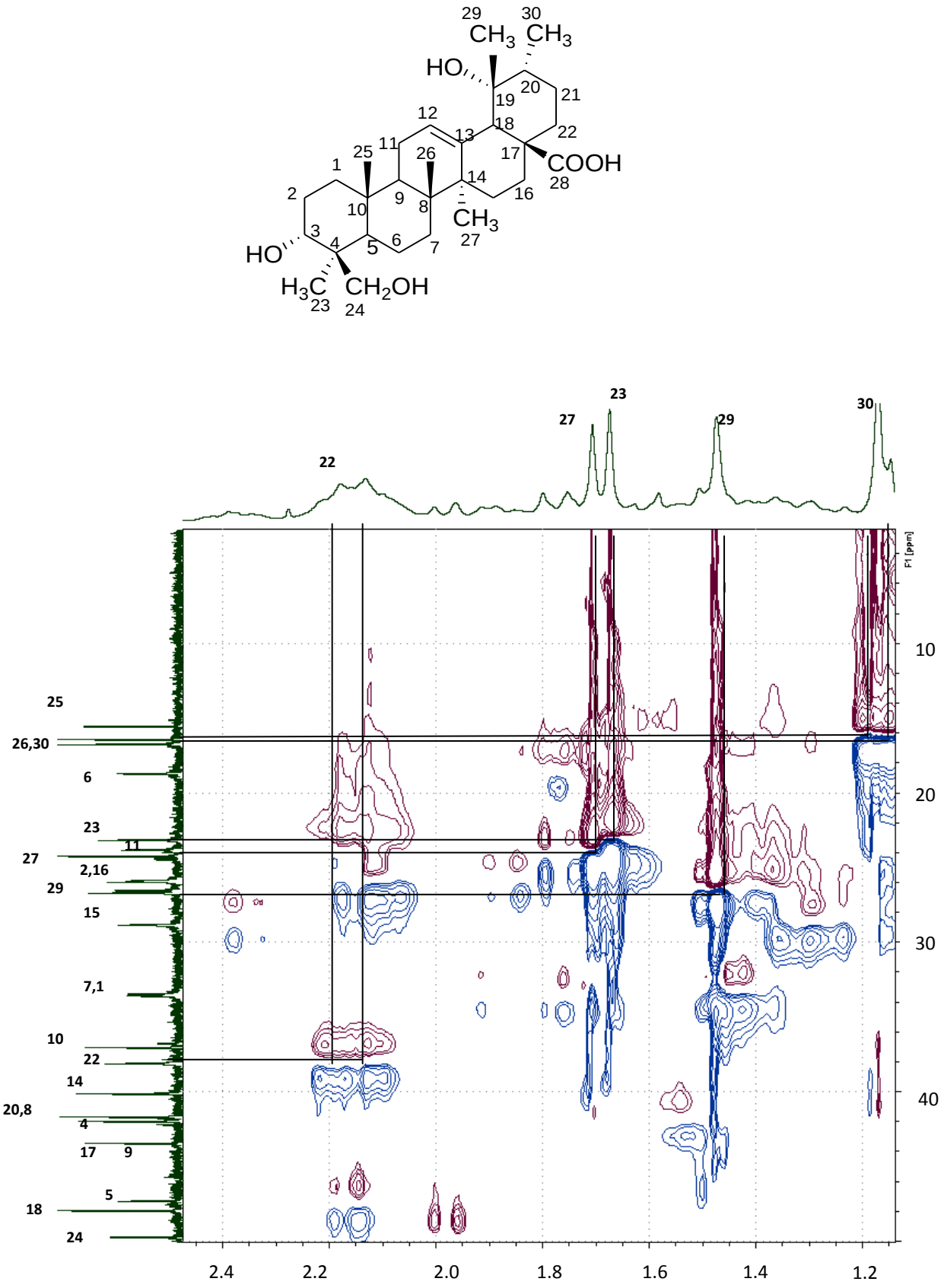

Figure 3.2.2.4b: HMQC spectrum expansion of barbinervic acid **61**

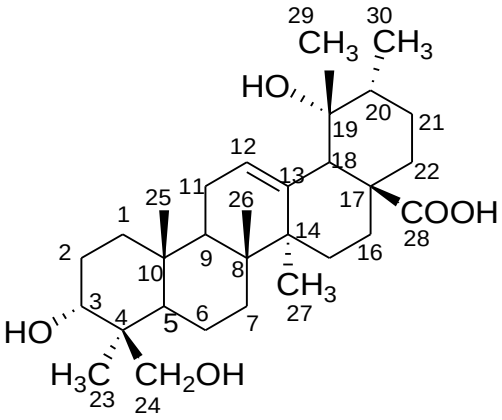

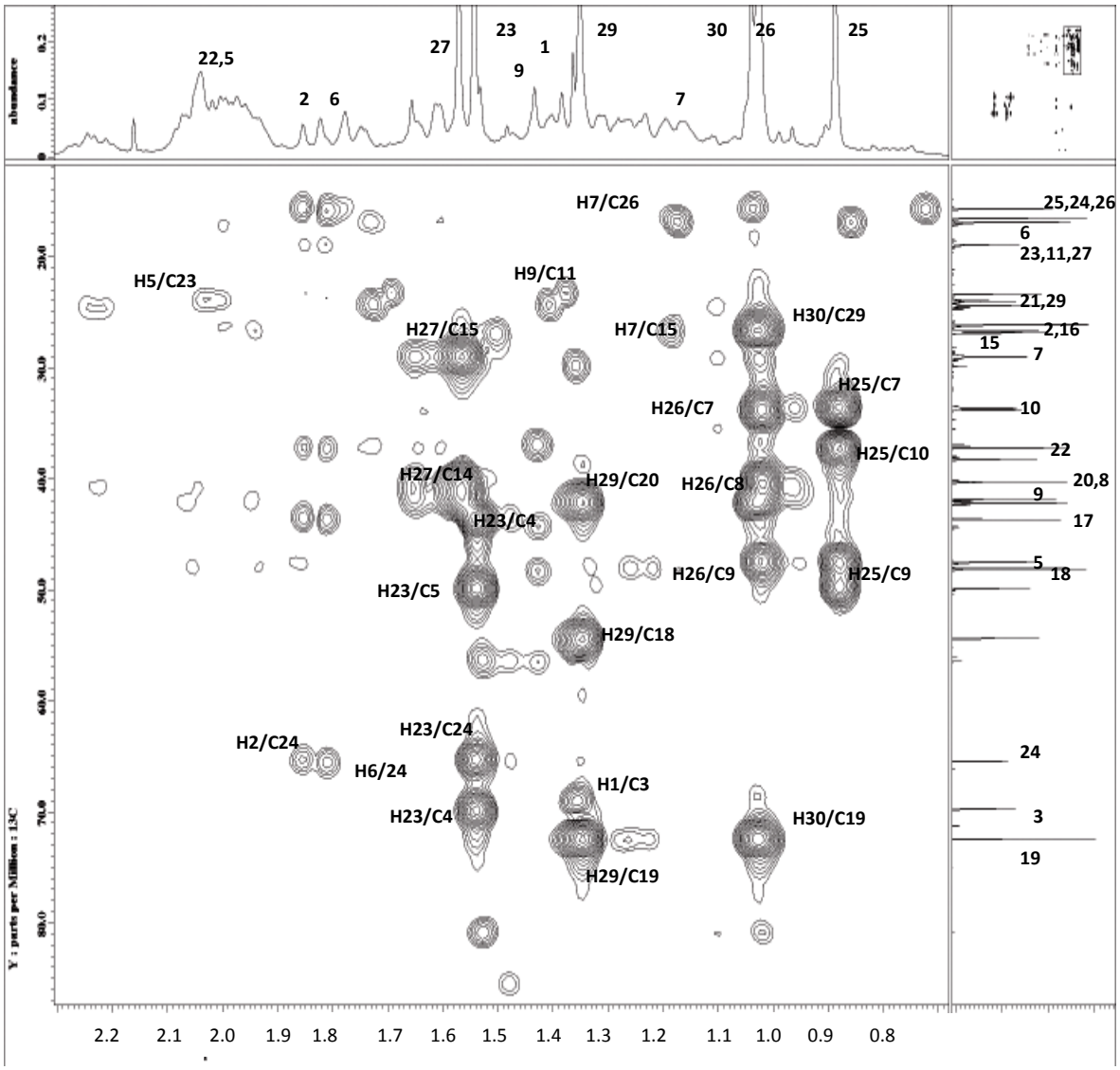

Figure 3.2.2.5a: HMBC spectrum of barbinervic acid **61**

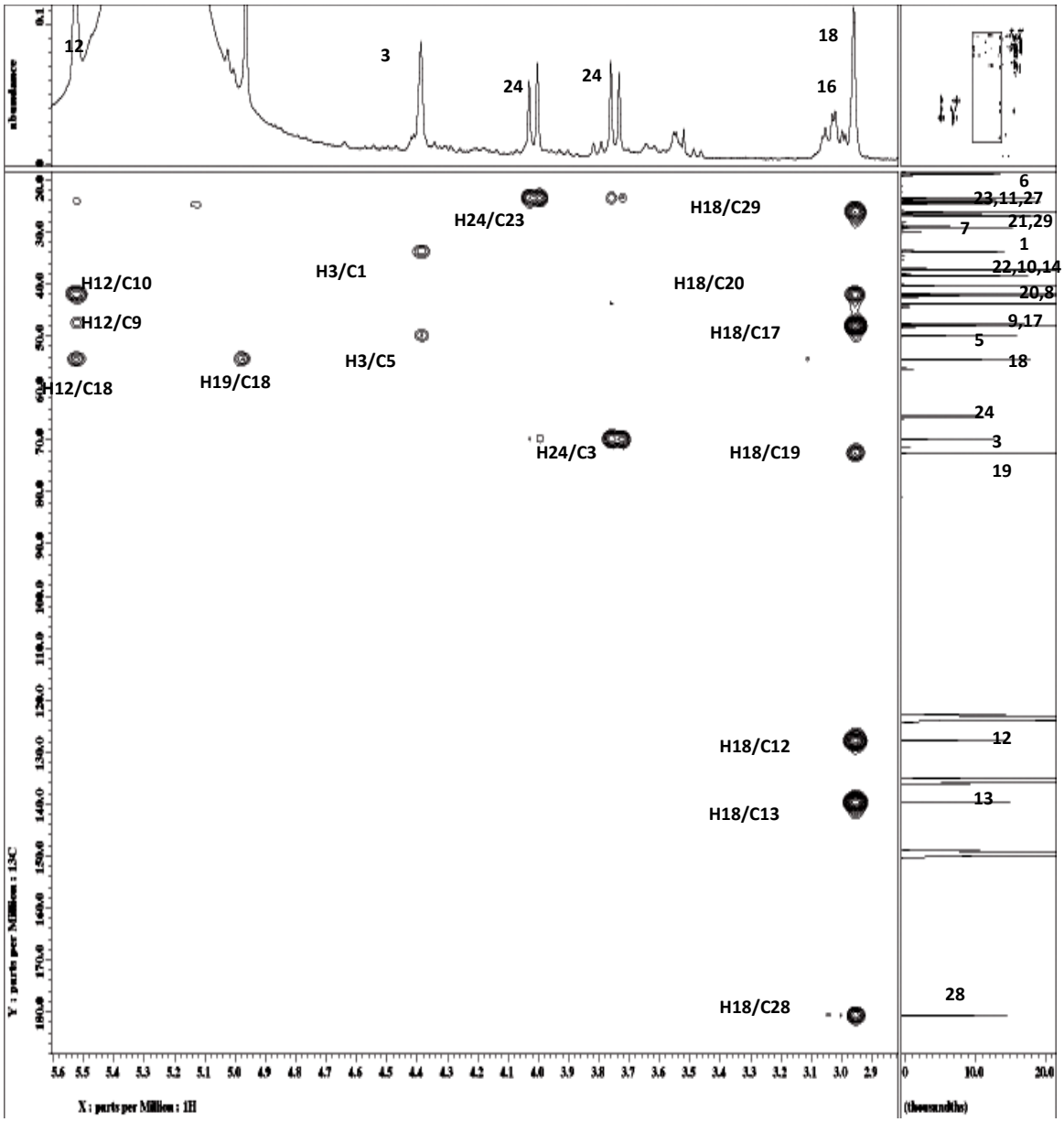

Figure 3.2.2.5b: HMBC spectrum expansion of barbinervic acid **61**

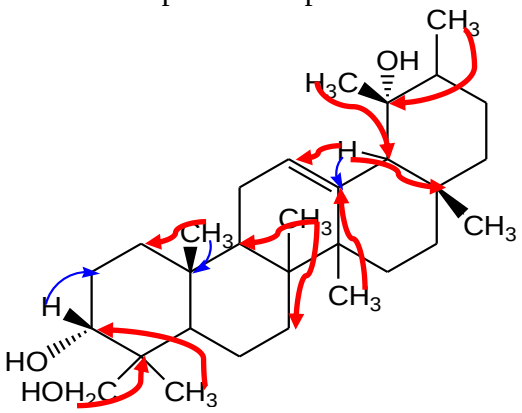

barbinervic acid 61

J_2 Correlations

J_3 Correlations

Figure 3.2.2.6: Selected HMBC correlation in barbinervic acid **61**

3.2.3 Compound C: *3β, 23-dihydroxyurs-12-en-28-oic acid*

(23-hydroxyursolic acid)

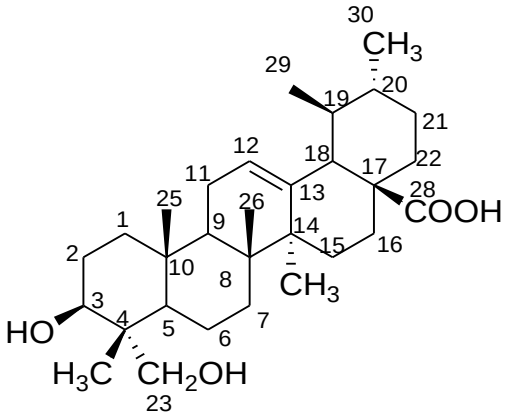

62

23-hydroxyursolic acid (3β,23-dihydroxyurs-12-en-28-oic acid) **62** (compound C) was isolated as white powder. It produced a pseudo-molecular ion peak $[M+Na]^+$ at m/z 495.34546 by ESI-MS which is consistent with molecular formula $C_{30}H_{48}O_4$. Its IR spectrum gives sharp peak at 1689 cm^{-1} for C=O, a broad and sharp peak between 3736 and 3066 cm^{-1}, and 2933 cm^{-1} for OH absorption (Silverstein et al., 1991).

The ^{1}H NMR (figure 3.2.3.1) revealed the presence of two secondary methyl groups with two sets of doublet (δ0.99, *J*=5.0 and 0.94, *J*=5.0 Hz, 3H) and four tertiary methyl groups (δ1.05, H-24; δ 0.97, H-25; δ1.03, H-26; δ1.18, H-27). The tri substituted olefinic double bond (δ5.48) for H-12 was overlapped with the water signal. The presence of an oxymethine proton resonating at δ4.12 (*dd*, *J*=5.9, 10.0 Hz, H-3), could be observable in the ^{1}H NMR of compound **62**. The large coupling constant of H-3 in compound C is similar to that reported by Dong-Hyun et al. (2005) indicated that the H-3 of compound C was α orientated and thus the OH was β orientated.

The occurrence of a doublet at δ2.50, *J*=11.6 Hz, for H-18 as well as a characteristic doublet of triplets signal at δ2.22 (J_1=2.7, J_2=7.8 and J_3=15.0 Hz, 1H) for H-16 suggested that compound C is an urs-12-ene derivative (Chien-Ya et al., 2001). The presence of two doublets (δ4.09, *J*=10.5 Hz and δ3.65, *J*=10.4 Hz, H-23) which represent an AB system, suggested the exocylic methane with geminal coupling (CH_2-) attached to an asymmetric centre. The H23-α was deshielded by the electronegative oxygen atom (OH) and therefore shifted downfield in the spectrum.

The analysis on ^{13}C NMR spectrum (figure 3.2.3.2) together with the DEPT spectrum (figure 3.2.3.3) enable us to distinguish and classify the thirty signals into seven methines, ten methylenes, six methyls and seven quarternary carbons. The ^{13}CNMR spectrum also showed the presence of an olefinic carbon at δ125.2 and δ138.8 (C-12, C-13), two hydroxylated carbons at δ73.8 and δ67.0 (C-3, C-23) and a carboxylic carbon at δ179.7 (C-28).

This was further corroborated by the HMBC spectrum (figure 3.2.3.5a and b) whereby the H-3 (δ4.12) correlated with C-23 (δ62.3), C-24 (δ12.9) which confirmed the assignments of methylene hydroxy in the ring A. Figure 3.2.3.6 summarized the selected HMBC correlations.

Finally, after comparison between the spectroscopic data of compound C and the literature data of the known compound, this compound was confirmed to be 3β, 23-dihydroxyurs-12-en-28-oic acid **62** (Dong-Hyun et al., 2005).

Table 3.2.3: ^{1}H NMR [400MHz, δ_H (*J*, Hz)] and ^{13}C NMR [75 MHz, δ_C] of **62** in C_5D_5N

Position	**^{13}C***	**^{13}C**	**^{1}H(*J*,H)***	**^{1}H (*J*,H)**
1	38.4	38.7		1.05*m*
2	27.2	27.3		1.47 *m*
3	72.8	73.0	4.22(*dd*, 9.6, 6.0 Hz)	4.12 (*dd*, 5.9, 10.0 Hz)
4	42.4	42.7		-
5	48.0	48.2		1.50 *m*
6	18.1	18.3		1.80 *m*
7	30.6	30.8		1.45 *m*
8	39.5	39.2		-
9	47.5	47.8		1.70 *m*
10	36.6	36.8		-
11	23.2	23.4		1.85 *m*
12	125.0	125.4	5.48 *brs*	5.48
13	138.7	139.0		-
14	42.0	42.3		-
15	28.2	28.4		1.24 *m*
16	24.5	24.6		2.22 (*dt*, 2.7, 7.8, 15.0 Hz)
17	47.5	47.8		-
18	53.1	53.3	2.20 (*d*, 11.0 Hz)	2.50 (*d*, 11.6 Hz)
19	39.0	39.7		1.60 *m*
20	38.9	39.2		1.15 *m*
21	37.0	37.2		1.40 *m*
22	32.8	33.0		1.65 *m*
23	67.3	67.3	4.18(*d*, 10.4 Hz) 3.72(*d*, 10.4 Hz)	4.09(*d*,10.5 Hz) 3.65 (*d*,10.5 Hz)
24	12.7	12.9	1.04 *s*	1.05 *s*
25	15.7	15.9	0.96 *s*	0.97*s*
26	17.1	17.3	1.06 *s*	1.03*s*
27	23.4	23.7	1.17 *s*	1.18*s*
28	178.7	179.9		-
29	17.1	17.3	0.98 (*d*, 6.4Hz)	0.99 (*d*, 5.0Hz)
30	20.9	21.2	0.92(*d*, 6.4Hz)	0.94(*d*, 5.0Hz)

*^{1}HNMR [400MHz, C_5D_5N]
*^{13}CNMR [100MHz, C_5D_5N]
(Dong-Hyun et al., 2005)

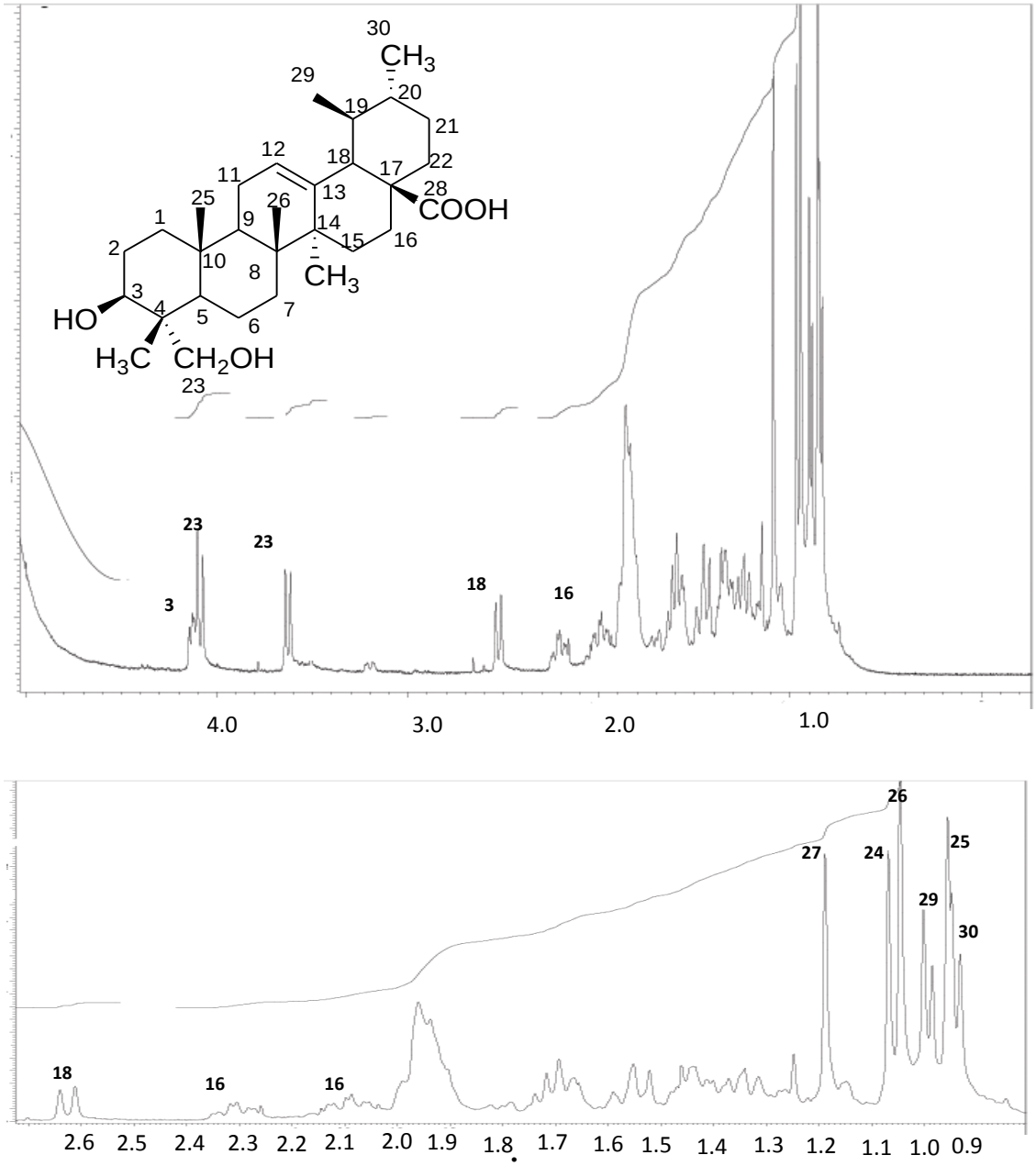

Figure 3.2.3.1: ^{1}H NMR spectrum of 3β-23-dihydroxyurs-12-en-28-oic acid **62**

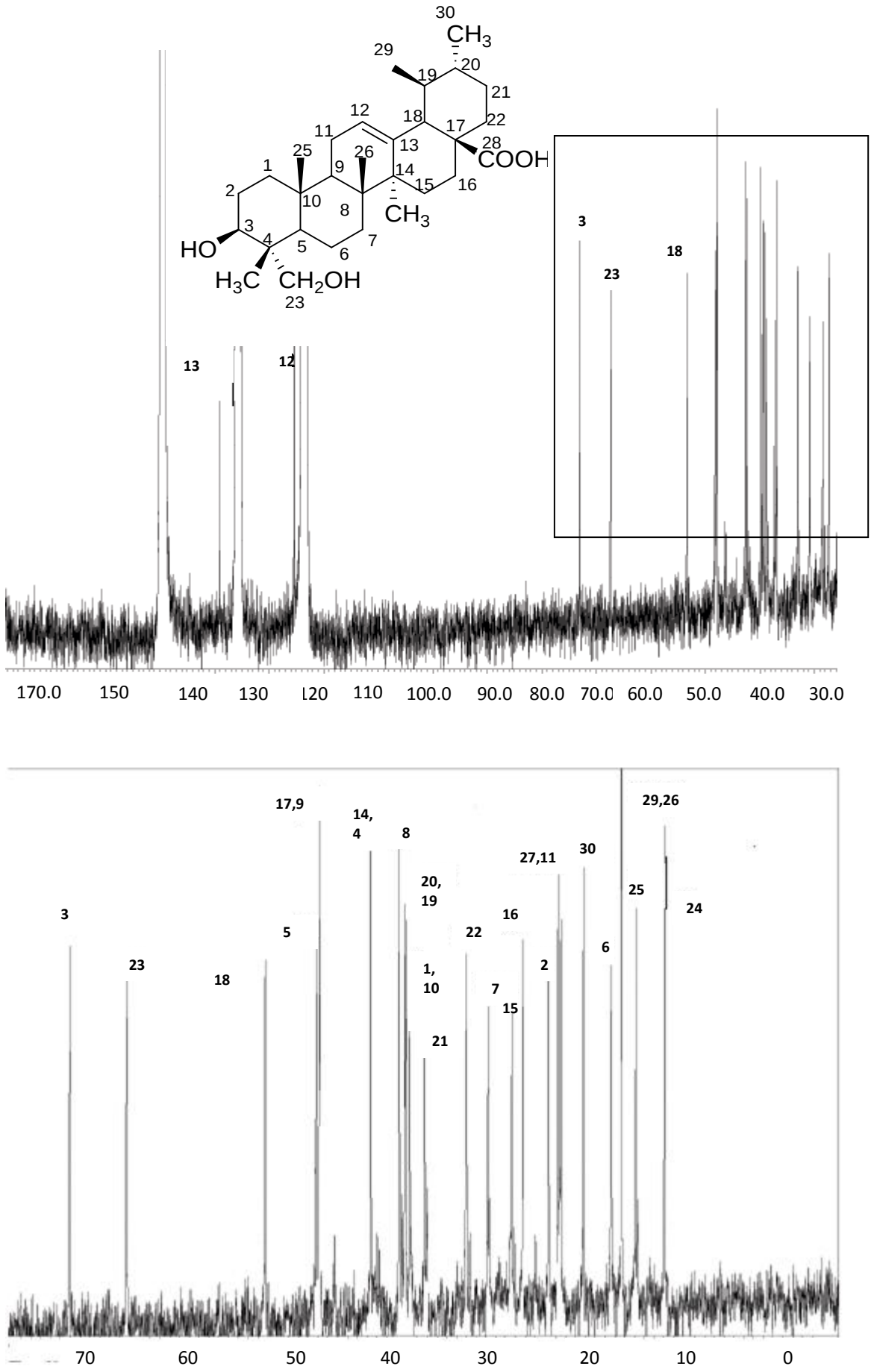

Figure 3.2.3.2: ^{13}C NMR spectrum of 3β-23-dihydroxyurs-12-en-28-oic acid **62.**

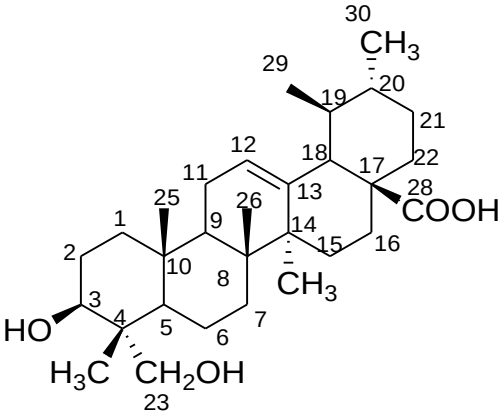

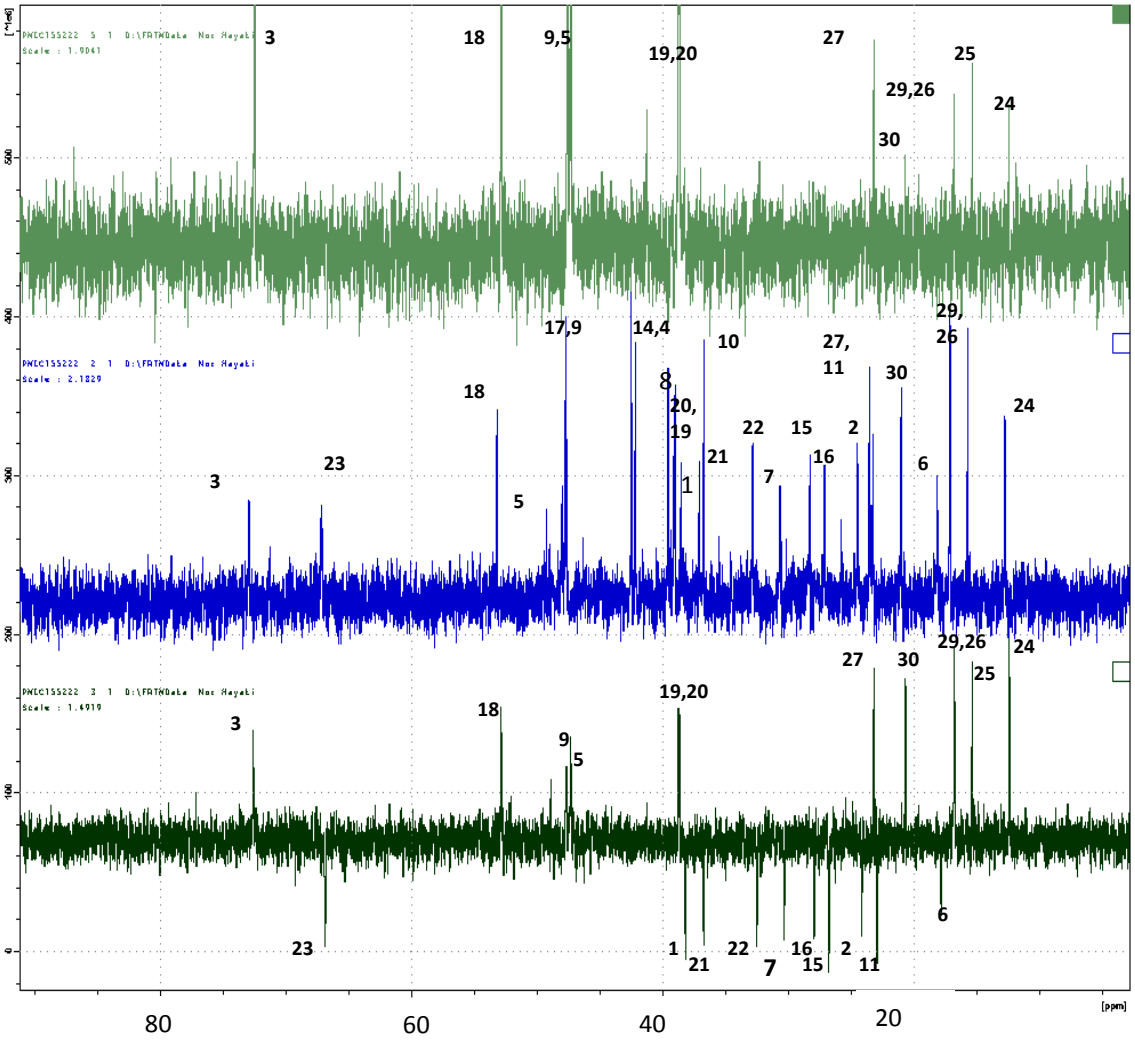

Figure 3.2.3.3: DEPT spectrum of 3β-23-dihydroxyurs-12-en-28-oic acid **62.**

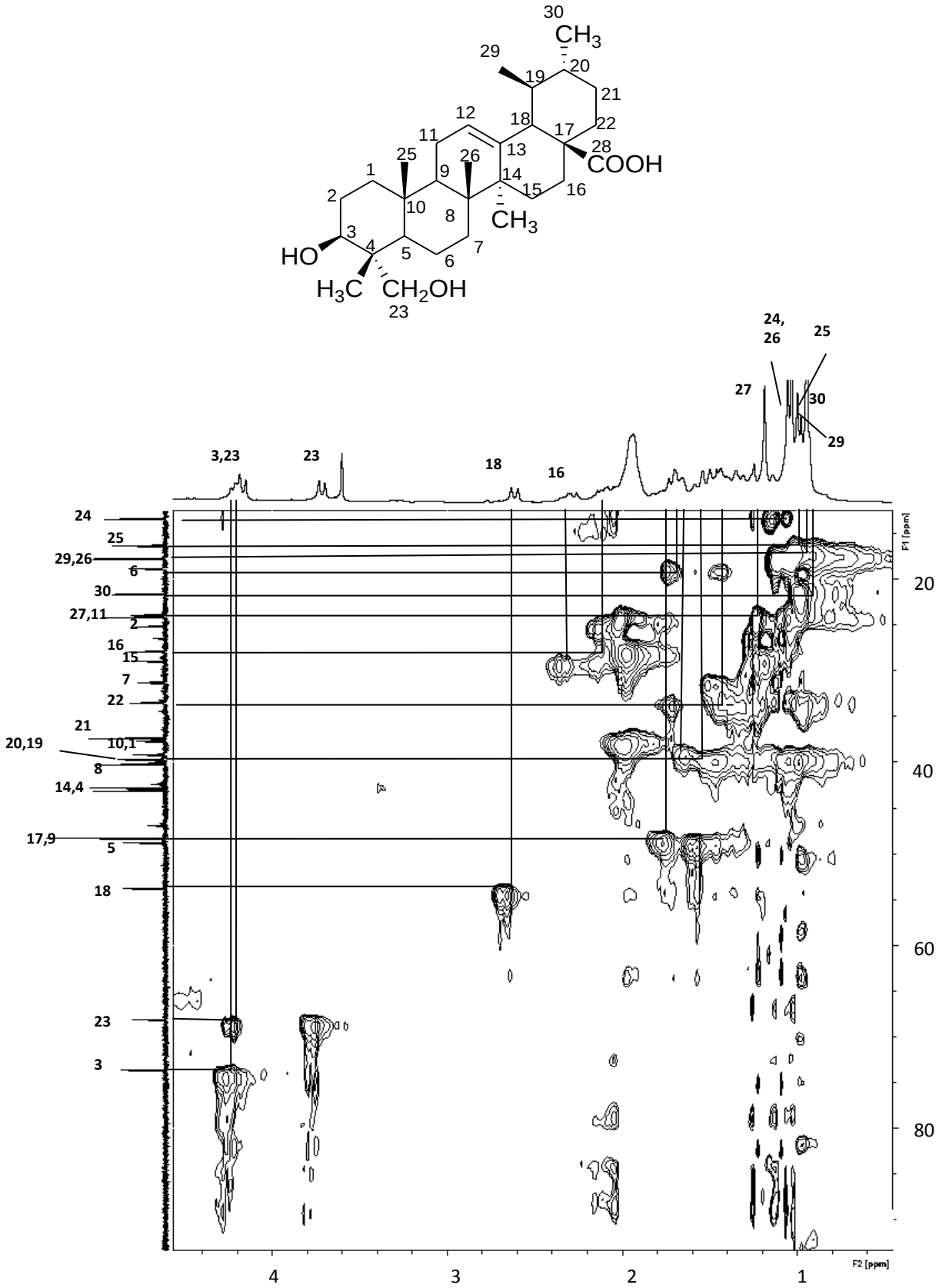

Figure 3.2.3.4: HMQC spectrum of 3β-23-dihydroxyurs-12-en-28-oic acid **62**

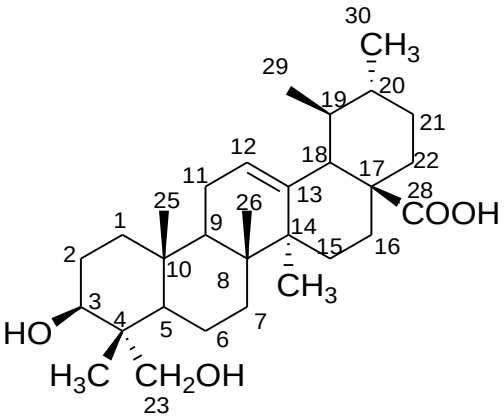

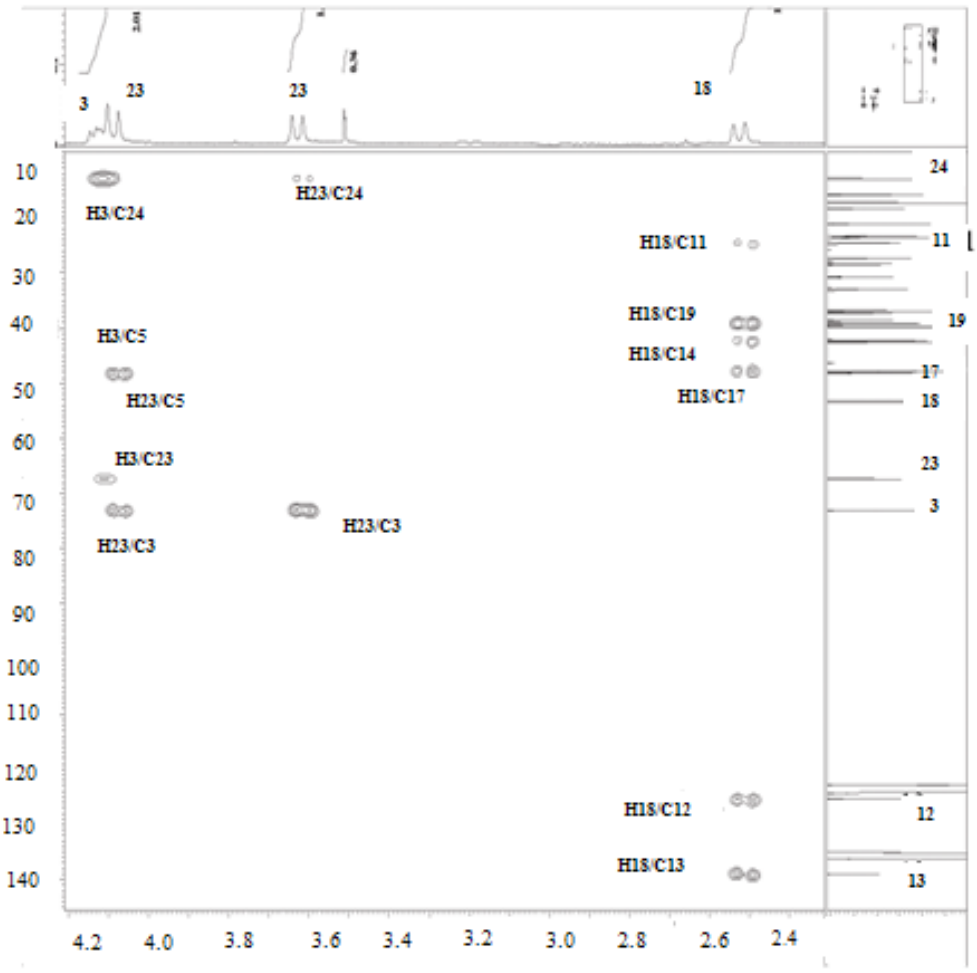

Figure 3.2.3.5a: HMBC spectrum of 3β,-23-dihydroxyurs-12-en-28-oic acid **62**

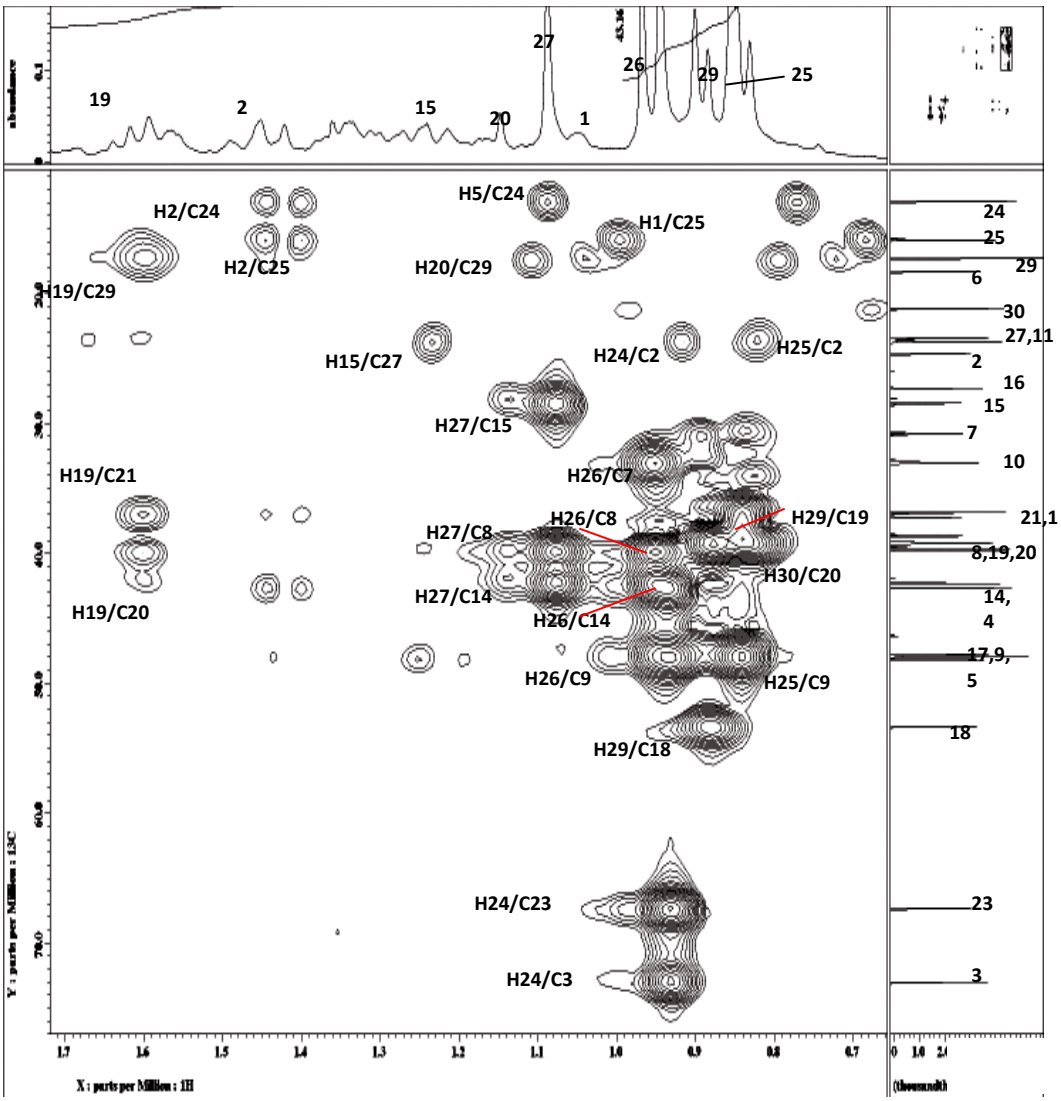

Figure 3.2.3.5b: HMBC spectrum of 3β-23-dihydroxyurs-12-en-28-oic acid **62**

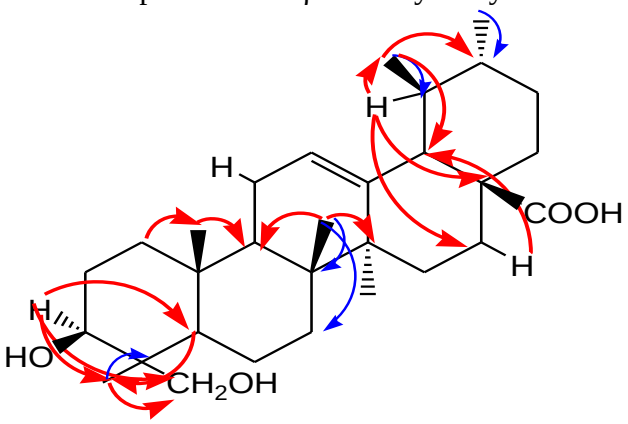

3β-23-dihydroxyurs-12-en-28-oic acid 62

J_2 Correlations
J_3 Correlations

Figure 3.2.3.6: Selected HMBC correlation in 3β-23-dihydroxyurs-12-en-28-oic acid **62**

3.2.4 Compound D:

28-O-β-glucopyranosyl-3α,19α,24-trihydroxyurs-12-en-28-oic acid

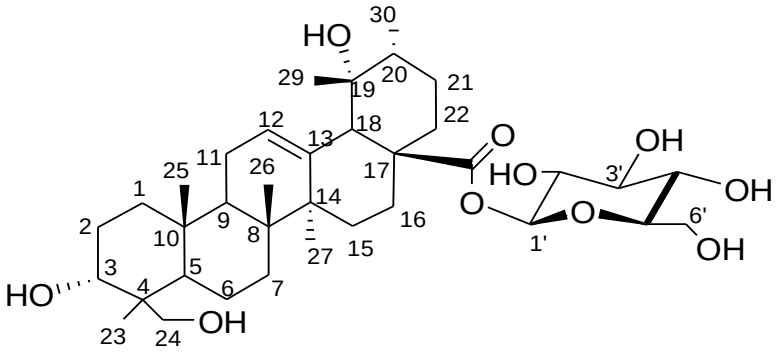

63

28-*O*-β-glucopyranosyl-3α,19α,24-trihydroxyurs-12-en-28-oic acid **63** (compound D) was isolated as brown solid. It produced pseudo-molecular ion peak $[M+Na]^+$ at m/z 673.39362 with ESI-MS which is consistent with molecular formula $C_{36}H_{58}O_{10}$. Its IR spectrum showed a sharp peak at 1724 cm^{-1} for C=O group and broad signal between 3716 and 3018 cm^{-1} for the OH group (Silverstein et al., 1991).

The ^1H NMR spectrum (figure 3.2.4.1) showed one doublet (1.09, J_1=9.6 Hz, 3H) which corresponded to secondary methyl H-30 and five singlet peaks for tertiary methyls (δ 1.64, H-27; δ 1.40, H-29; δ 1.54, H-23; δ 1.06, H-25; δ 1.26, H-26). It also showed a singlet signal at δ2.95 for H-18 as well as a characteristic doublet of triplet signal (δ2.50 , J_1 =5.8, J_2=8.8 and J_3=13.1 Hz, 1H) assignable to H-16α, which is caused downfield by the anisotropic effect due to a 19α-hydroxyl group strong 1,3 diaxial interaction (Jie-Ping et al., 2006). The singlet signal at δ5.60 with an AB_2 patterns H-12 characteristic of tri substituted olefinic proton H-12. A doublet (J=7.9 Hz) of an AB system belongs to anomeric proton H-1' of glucose unit observed at δ 6.33. The H-3 broad singlet was appeared at δ4.39 overlapped with glucose protons signals (H-2'- H-6').

The ^{13}C NMR spectrum (figure 3.2.4.2) together with DEPT (figure 3.2.4.4) distinguished the carbon of compound D into six methanes, ten methylenes, six methyls and eight quarternary carbons for the aglycon skeleton. Another five methanes and one methylene peak was characteristic of the glucose moiety. The signal of carbonyl carbon presence at δ177.5 while the free hydroxylated carbons signal observed at δ69.8 (C-3) and δ73.1 (C-19). Another methylene hydroxy carbon was observed at δ65.5 which was assigned as the C-24. The signal of the glucose and other remaining carbon was listed in table 3.2.3.

The arrangement of the sugar unit which was connected to C-28 was determined by HMBC correlation (figure 3.2.4.5a and b) between H-1' (δ 6.33, *d*) and C-28 (δ177.5). Another set of correlations was between H-24 (δ 65.5) and C-23 (δ23.4). Correlation between H-29 (δ1.40) and C-18 (δ54.9), C19 (δ 73.1) and C-20 (δ42.6) confirmed the position of quarternary hydroxyl to be at C-19. The selected correlation was shown in figure 3.2.4.6.

The HMQC assignment was shown in figure 3.2.4.4a and b. The analysis of the accumulated data and comparison with literature values confirms that compound D was 28-*O*-β-glucopyranosyl-3α,19α,24-trihydroxyurs-12-en-28-oic acid **63** that was reported previously as kakisaponin A (Chen et al., 2007) but was first time reported isolated from this plant.

Table 3.2.4: ^{1}H NMR [400 MHz, δ_H (*J*, Hz)] and ^{13}C NMR [100 MHz, δ_C] of **63** in C_5D_5N.

Position	**^{13}C**	**^{13}C***	**^{1}H (*J*,H)**	**^{1}H (*J*,H)***
1	33.8	34.0	1.40*m*	1.47*m*
2	26.8	26.1	1.85*m*	1.82*m*
3	69.8	70.0	4.39*m*	4.37*m*
4	44.4	43.9	-	-
5	50.6	50.2	1.95 (*bd*, 12.4 Hz)	1.90 (*bd*, 12.1 Hz)
6	19.1	19.3	1.72*m*	1.65*m*
7	33.8	34.1	2.05*m*	2.05*m*
8	41.2	40.8	-	-
9	48.3	47.9	2.02*m*	2.01*m*
10	37.9	37.5	-	-
11	24.3	24.4	2.05*m*	2.02*m*
12	128.9	128.5	5.60*bs*	5.55 *brs*
13	139.7	139.3	-	-
14	42.6	42.2	-	-
15	29.0	29.2	2.50 (*dt*, 8.8, 5.8, 13.0 Hz),	1.82*m*
16	26.5	26.5	3.10 (*dt*, 8.8, 5.8, 13.0 Hz)	2.46*m*
17	49.1	48.7	-	-
18	54.9	54.5	2.95*s*	2.91*s*
19	73.1	72.7	-	-
20	42.6	42.2	1.40*m*	1.33*m*
21	26.5	26.7	1.26*m*	1.26*m*
22	37.5	37.5	1.92*m*	2.04*m*
23	23.4	23.6	1.54*m*	1.58*s*
24	65.5	65.8	3.88 (*d*, 10.9 Hz) 4.14(*d*, 11.0 Hz)	3.82 (*d*, 10.8 Hz) 4.08 (*d*, 10.8 Hz)
25	15.9	16.1	1.06*s*	1.02*s*
26	17.2	17.4	1.26*s*	1.22s
27	24.3	24.5	1.64	1.60 *s*
28	177.5	177.0	-	-
29	26.8	27.0	1.40	1.36*s*
30	16.5	16.7	1.09 (*d*, 9.6 Hz)	1.04 (*d*, 6.1 Hz)
1'	95.7	95.9	6.33 (*d*, 8.1 Hz)	6.28 (*d*, 8.1 Hz)
2'	73.8	74.1	4.14 (*t*, 8.2 Hz*)*	4.19 *m*
3'	78.8	79.0	4.25 (*t*, 8.7 Hz)	4.21*m*
4'	71.0	71.3	4.33 (*t*, 9.2 Hz)	4.29*m*
5'	79.1	79.3	4.11*m*	4.02 *m*
6'	62.1	62.4	4.45 (*d*, 8.5 Hz) 4.50 (*d*, 8.5 Hz)	4.43 (*d*, 9.2 Hz) 4.34 (*d*, 9.2 Hz)

* ^{13}CNMR [100MHz, C_5D_5N]
*^{1}HNMR [400MHz, C_5D_5N]
Chen et al., 2007

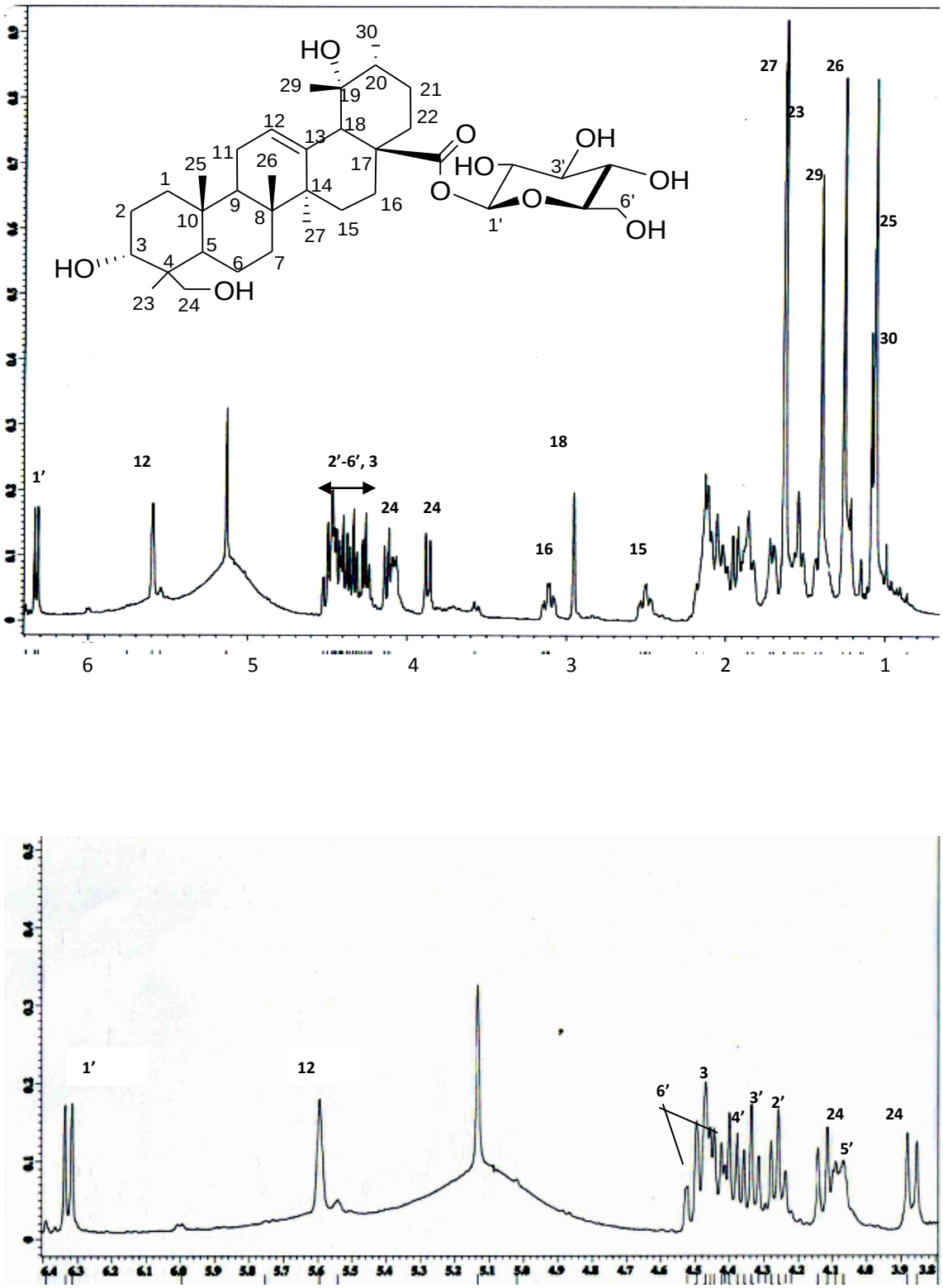

Figure 3.2.4.1: ^{1}H NMR spectrum of 28-*O*-β-glucopyranosyl-3α,19α,24-trihydroxyurs -12-en-28-oic acid **63**

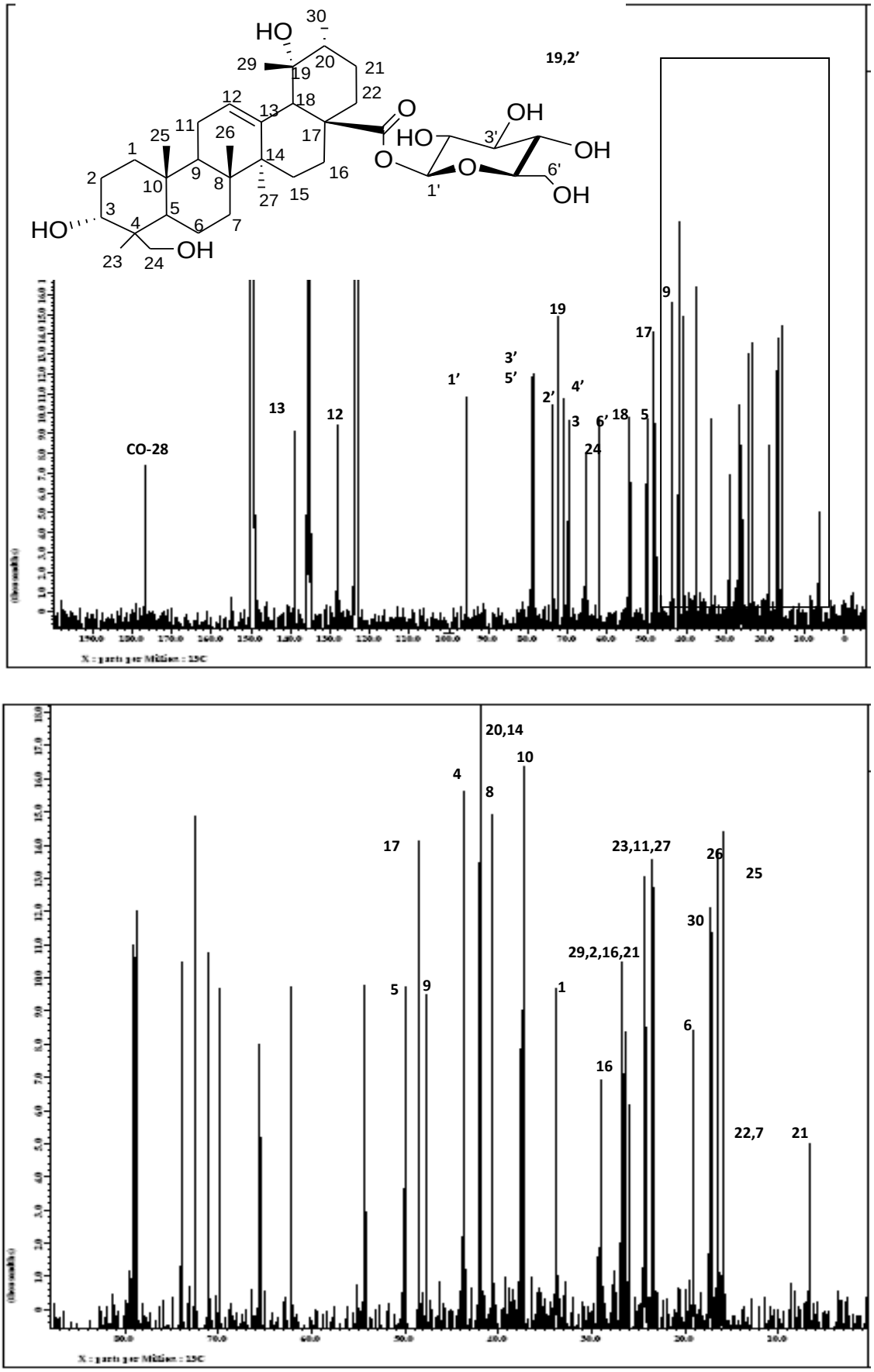

Figure 3.2.4.2: ^{13}C NMR spectrum of 28-*O*-β-glucopyranosyl-3α,19α,24-trihydroxyurs-12-en-28-oic acid **63**

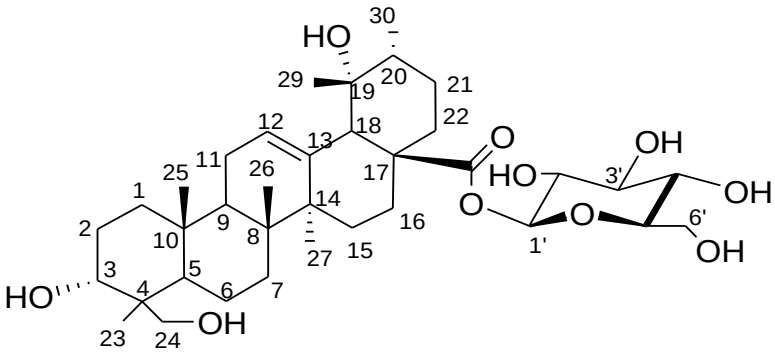

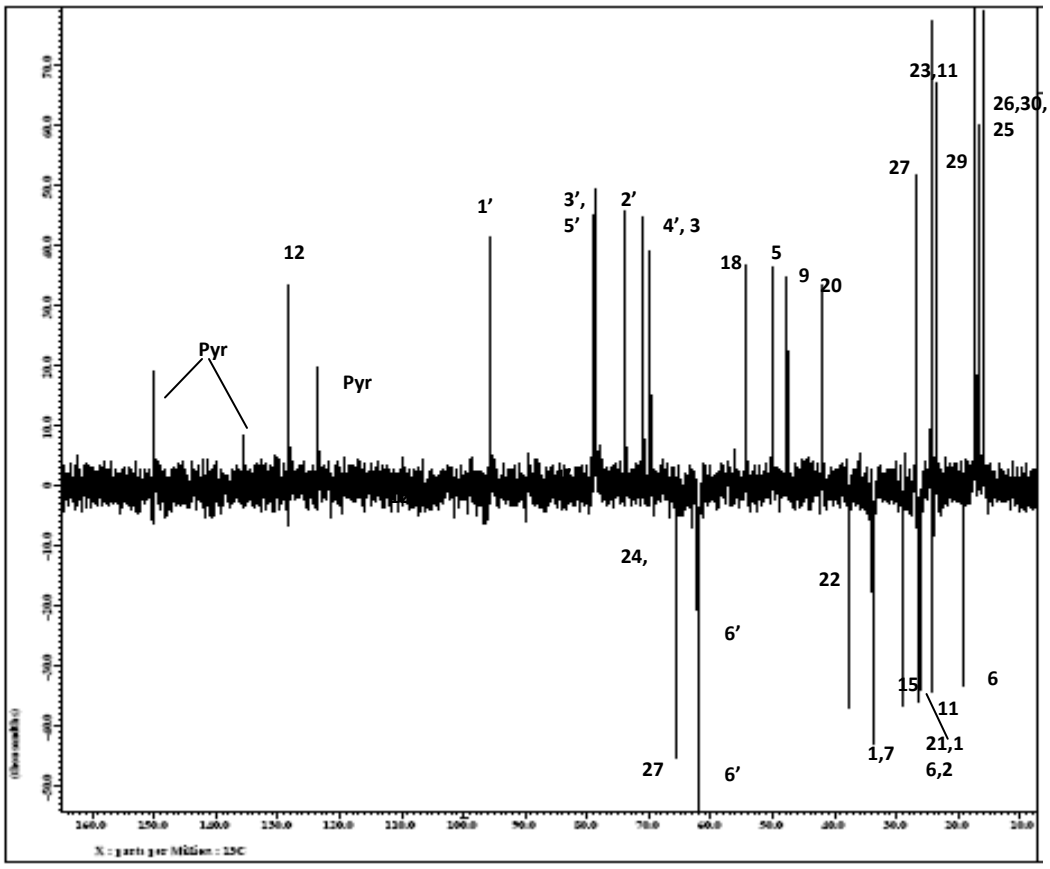

Figure 3.2.4.3: DEPT spectrum of 28-*O*-β-glucopyranosyl-3α,19α,24-trihydroxyurs-12-en-28-oic acid **63**

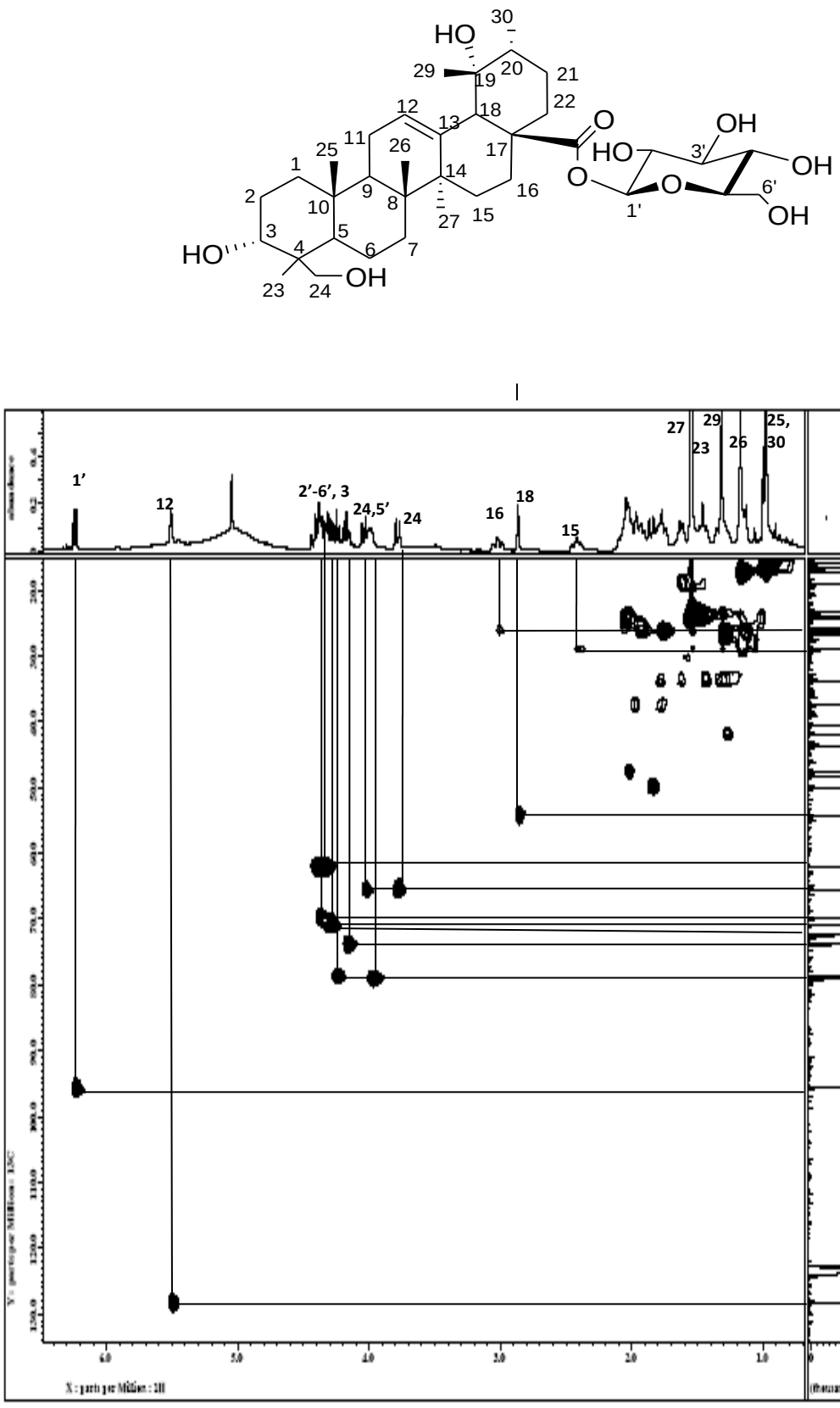

Figure 3.2.4.4a: HMQC spectrum of 28-*O*-β-glucopyranosyl-3α,19α,24-trihydroxyurs-12-en-28-oic acid **63**

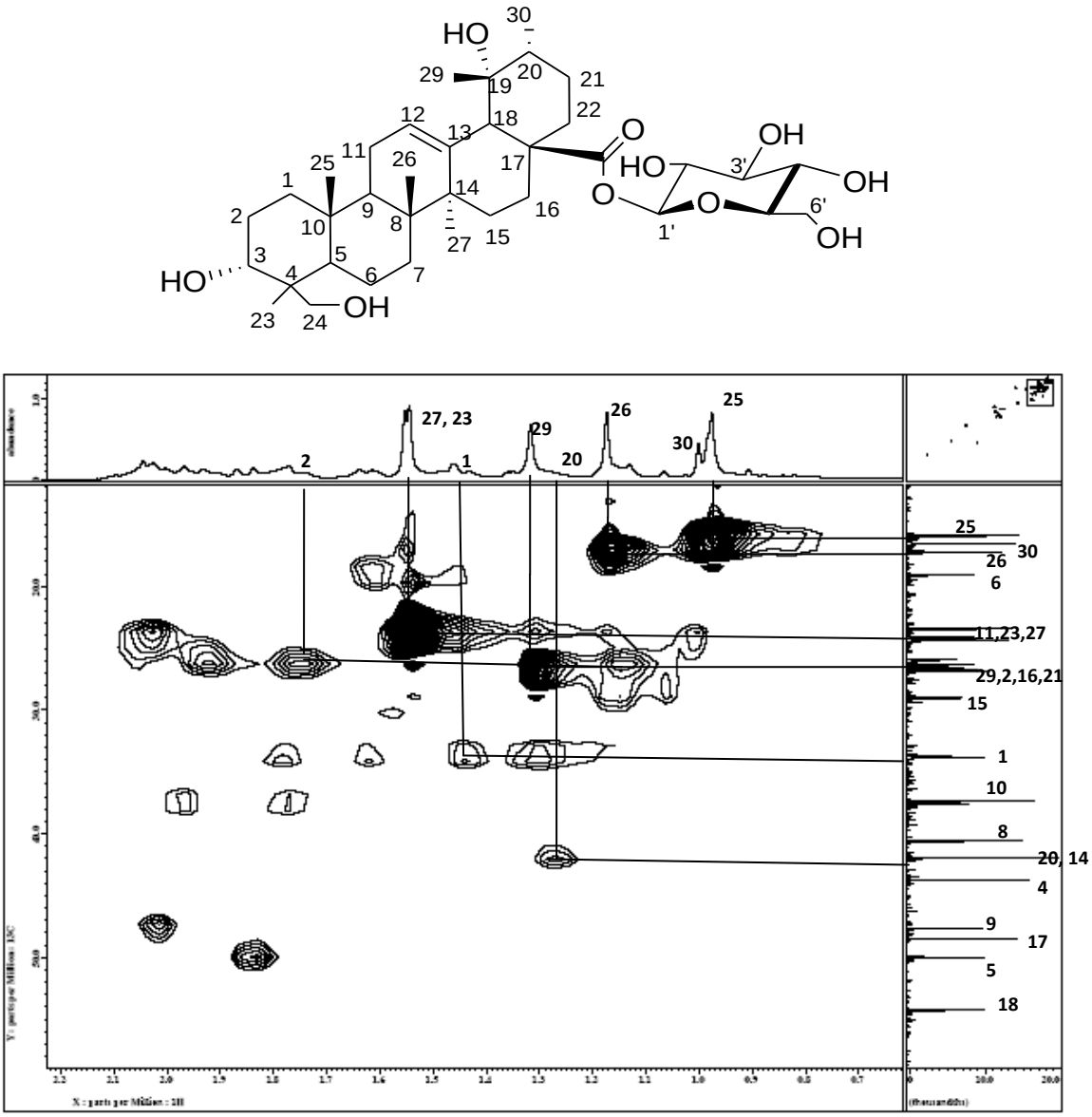

Figure 3.2.4.4b: HMQC spectrum of 28-*O*-β-glucopyranosyl-3α,19α,24-trihydroxyurs-12-en-28-oic acid **63**

5

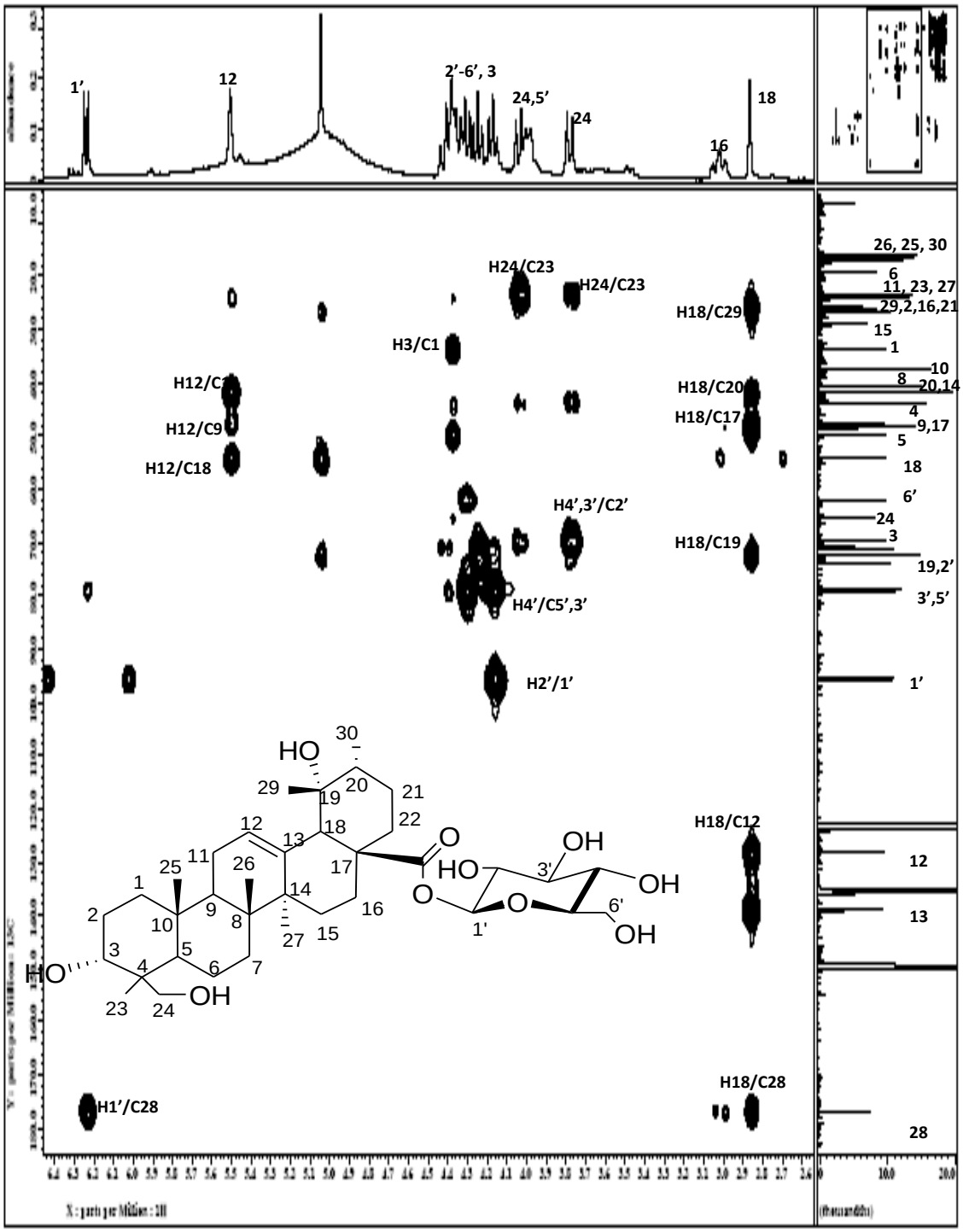

Figure 3.2.4.5a: HMBC spectrum of 28-*O*-β-glucopyranosyl-3α,19α,24-trihydroxyurs-12-en-28-oic acid **63**

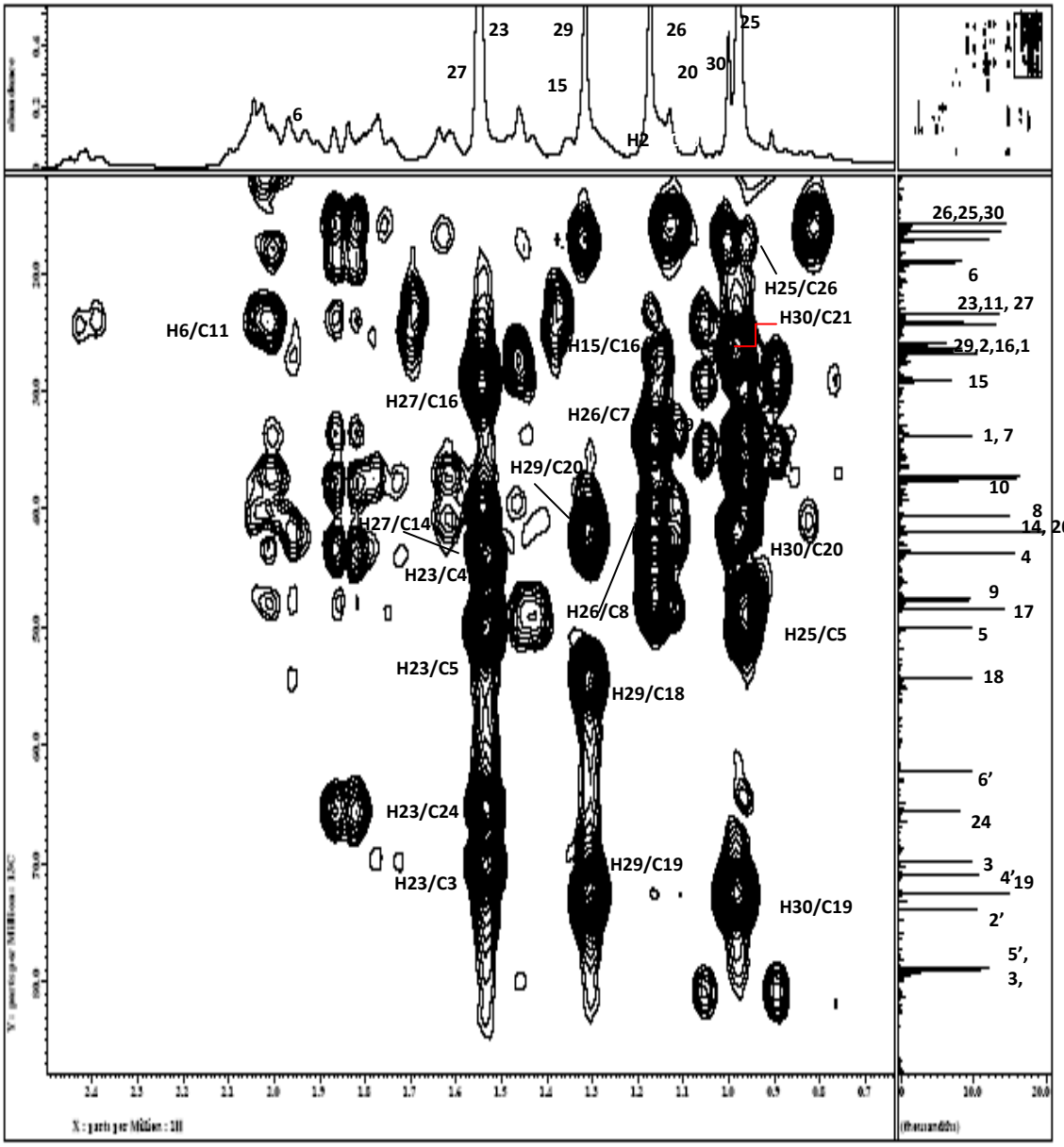

Figure 3.2.4.5b: HMBC spectrum expansion of 28-*O*-β-glucopyranosyl-3α,19α,24-trihydroxyurs-12-en-28-oic acid **63**

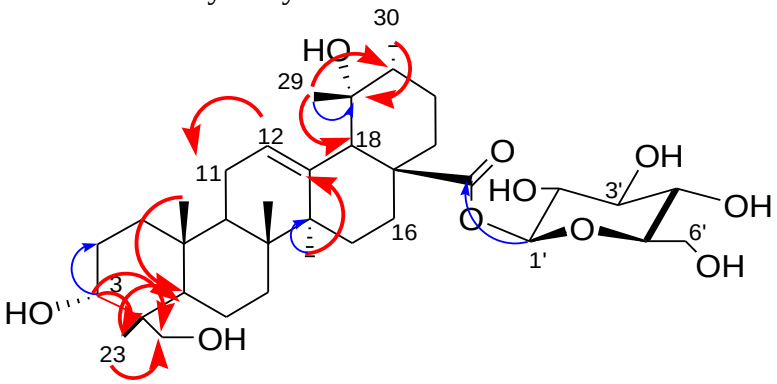

28-*O*-β-glucopyranosyl-3α,19α,24-trihydroxyurs-12-*en*-28-oic acid 63

J^2 Correlations

J^3 Correlations

Figure 3.2.4.6: Selected HMBC correlation in 28-*O*-β-glucopyranosyl-3α,19α,24-trihydroxyurs-12-en-28-oic acid **63**

3.2.5 Compound E: *3β-acetylolean-12-en-28-oic acid*

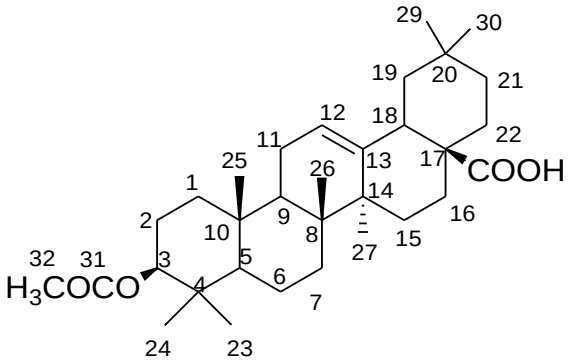

64

3β-acetylolean-12-en-28-oic acid **64** (compound E) was isolated as colorless crystal. It produced pseudo-molecular ion peak $[M-H]^-$ at m/z 497.36142 with ESI-MS which is consistent with molecular formula $C_{32}H_{50}O_4$. Its IR spectrum showed two sharp peaks at 1722 cm^{-1} and 1694 cm^{-1} for C=O and 2947 cm^{-1} for OH group (Silverstein et al., 1991).

The ^{1}H NMR spectrum (figure 3.2.5.1) indicate the presence of seven quarternary methyls at (δ1.02,H-30; δ0.99, H-29; δ1.30, H-27; δ0.86, H-26; δ0.94, H-25; δ0.96, H-24; δ0.91, H-23) and one additional methyl at 2.07 (s, 3H) of the acetyloxy group. An AX_2 spin system could be observed at 3.35 (*dd*, J_1=4.6 and J_2=13.3 Hz, 1H) was indicative of H-18 which is next to H19. As compare to ursolic acid **60**, the secondary methyl signals were not observed in the ^{1}H NMR proton, thus suggested that the structure was oleanane type instead of ursane.

The ^{13}C NMR and DEPT spectrum (figure 3.2.5.2 and 3.2.5.3) showed five methines, ten methylenes, eight methyls and nine quarternary carbons on compound E. It exhibited down field signal at δ180.1 and δ170.2 attributable to the carbonyl carbon of

C-28 and C-31 respectively. The methyl carbon of C-29 gave rise to a downfield peak at δ33.0 due to the deshielding effect of carbonyl carbon C-31. The methane carbon C-19 experienced the deshielding effect from the carbonyl carbon to give a down field signal at δ46.4. The other signals are similar to those of ursolic acid **60**.

The HMQC spectrum was showed in figure 3.2.5.4 (a) and (b). This compound was further confirmed by the correlations detected in the HMBC spectrum (figure 3.2.5.5 (a) and (b)) between H-11 (δ1.79) and C-12 (δ 123.6), C-13 (δ 139); H-21(δ 1.8) and C-30 (δ 23.5) and C20 (δ 30.7). Complete assignments were shown in the HMBC spectrum (figure 3.2.5.5a and b) and the selected correlation was presented in figure 3.2.5.6.

Finally, after extensive comparison of the spectroscopic data obtained from compound E with the literature values (Kazuhito et al., 1997), the former was confirmed to be 3β-acetylolean-12-en-28-oic acid **64**.

Table 3.2.5.: ^{1}H NMR [300 MHz, δ_H (*J*, Hz)] and ^{13}C NMR [75 MHz, δ_C] of **64** in C_5D_5N

Position	**^{13}C***	**^{13}C**	**^{1}H(*J*,H)***	**^{1}H(*J*,H)**
1	38.0	38.0		1.50,1.15*m*
2	23.5	23.5		1.45 *m*
3	80.9	80.5	4.5 (*dd*, 7,1Hz)	4.73 (*dd*, 5.0,11.1Hz)
4	37.6	37.6		-
5	55.2	55.3		1.00 *m*
6	18.1	18.2		1.50 *m*
7	32.4	33.0		1.65 *m*
8	39.2	39.4		-
9	47.5	47.6		1.20 *m*
10	36.9	36.9		-
11	22.8	23.4	1.97 (*dt*, 3.5,14.0 Hz)	1.85 *m*
12	122.5	123.6	5.27 (*t*, 3.5Hz)	5.5 *bs*
13	143.6	139.0		-
14	41.5	41.7		-
15	27.6	28.0		1.40 *m*
16	23.3	23.6		2.10,1.90 *m*
17	46.5	46.2		-
18	40.8	41.0	2.82 (*dd*, 4.5,13.5Hz)	3.35 (*dd*, 4.6,13.3Hz)
19	45.8	46.4		1.91 *m*
20	30.6	30.7		0.90 *m*
21	33.7	33.9		1.50 *m*
22	32.4	32.8		1.90 *m*
23	28	27.9	0.86*s*	0.94 *s*
24	16.6	16.7	0.87*s*	0.86 *s*
25	15.3	15.1	0.87*s*	0.91 *s*
26	17.1	17.1	0.74*s*	0.97 *s*
27	25.8	25.9	1.13*s*	1.30 *s*
28	184.3	180.1		-
29	33	33.0	0.94*s*	1.02 *s*
30	23.5	23.5	0.97*s*	1.04 *s*
32	21.3	20.9	2.05*s*	2.07*s*
31	171.1	170.5		-

*^{1}HNMR [90 and 270MHz] in $CDCl_3$
*^{13}CNMR [25 and 67.5MHz] in $CDCl_3$
(Kazuhito et al., 1997)

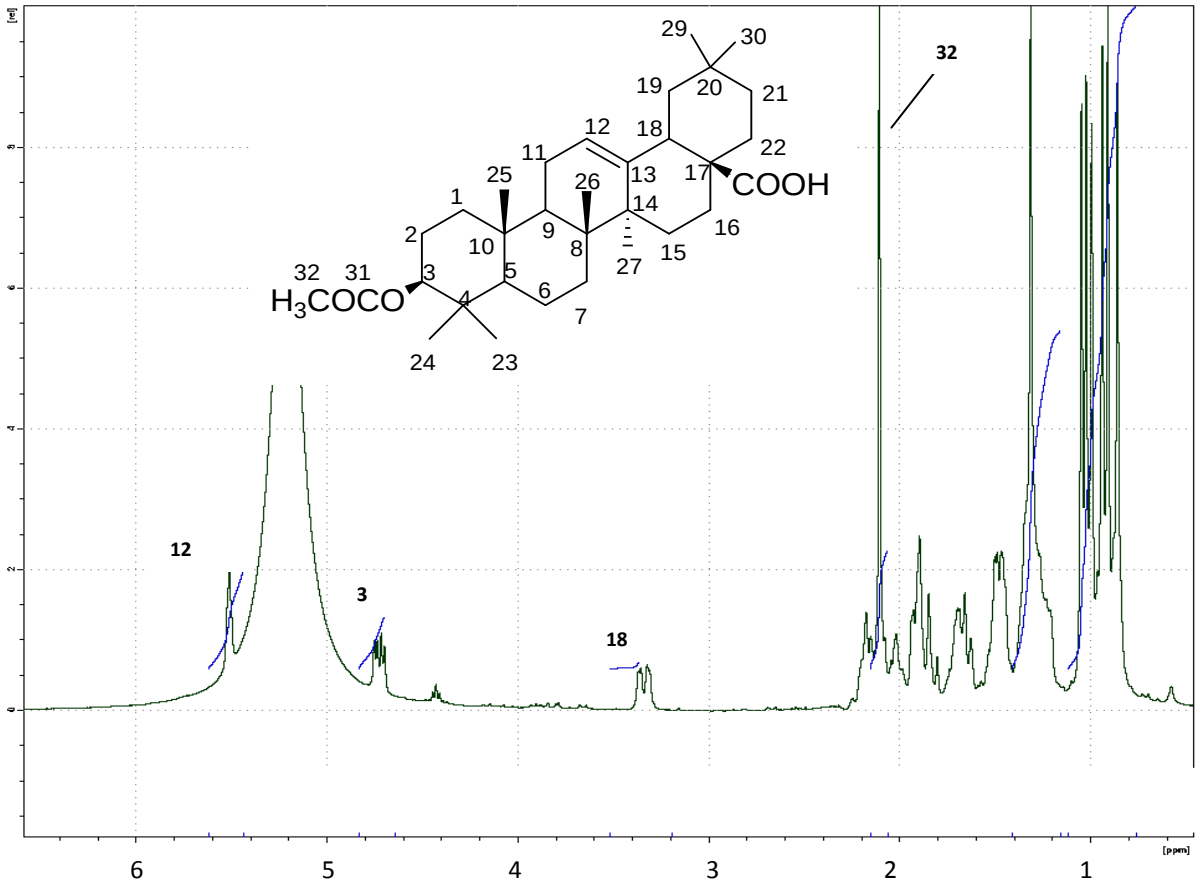

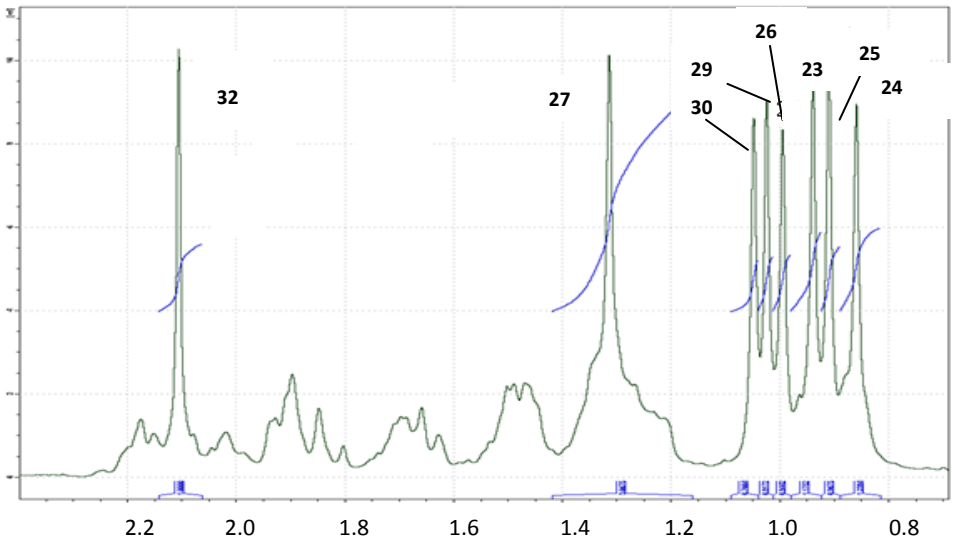

Figure 3.2.5.1: ^{1}H NMR spectrum of 3β-acetylolean-12-en-28-oic acid **64**

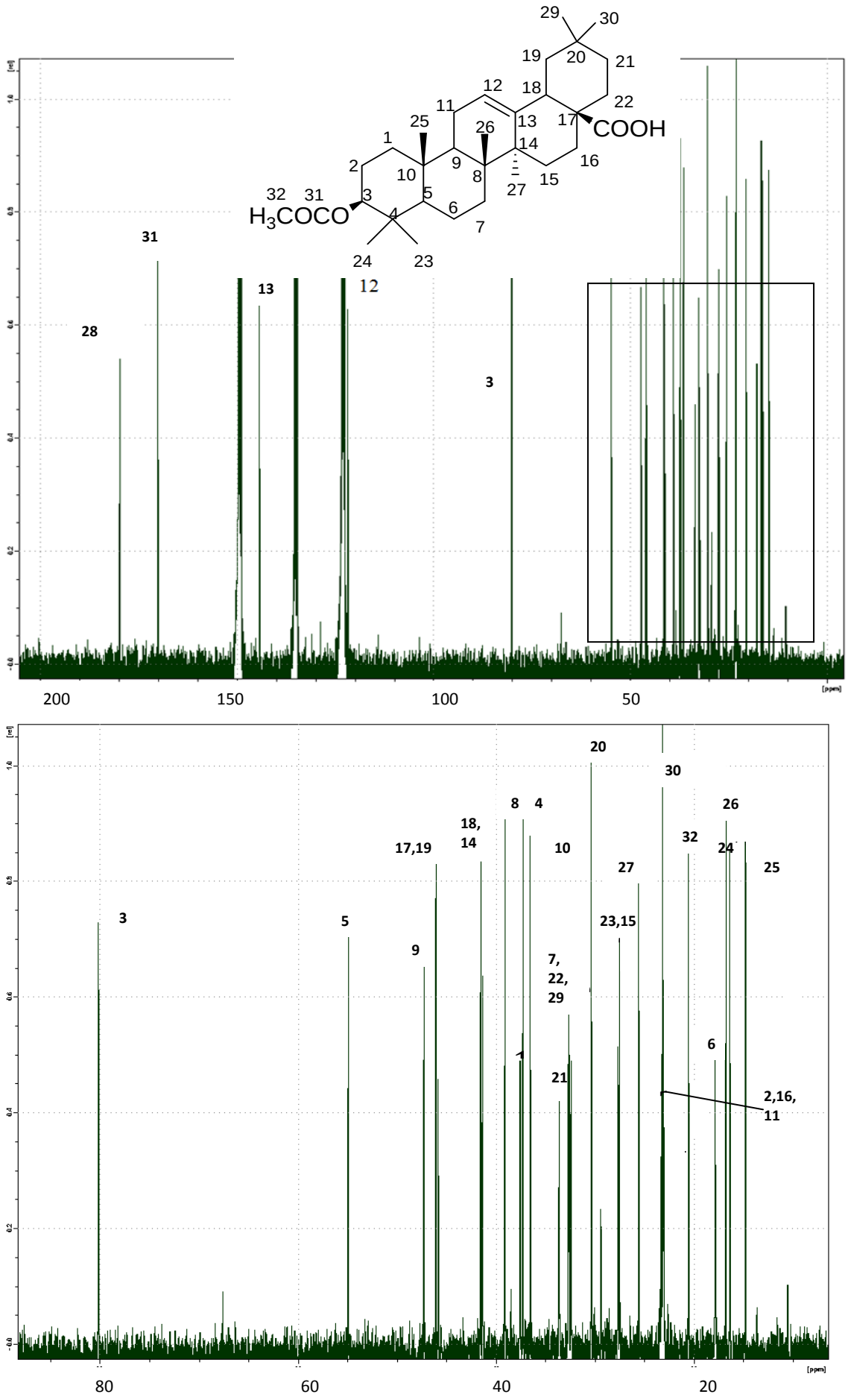

Figure 3.2.5.2: ^{13}C NMR spectrum of 3β-acetylolean-12-en-28-oic acid **64**

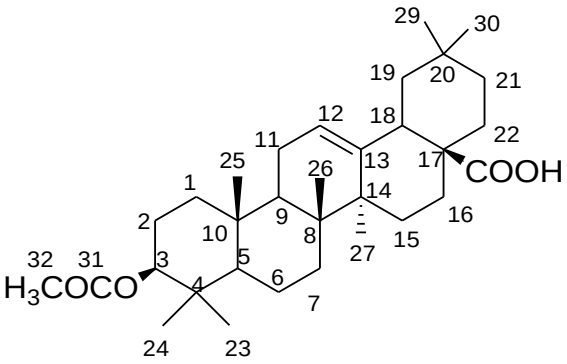

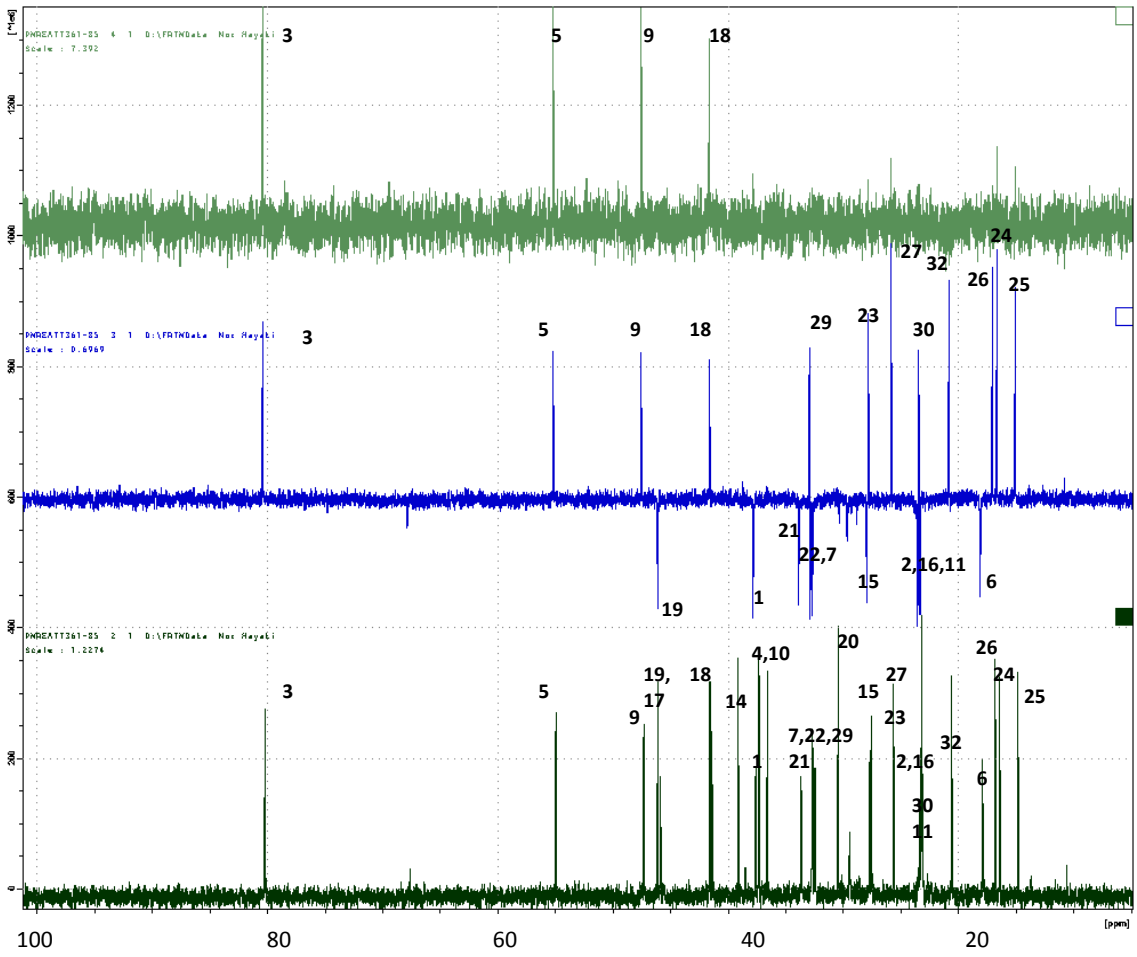

Figure 3.2.5.3: DEPT spectrum of 3β-acetylolean-12-en-28-oic acid **64**

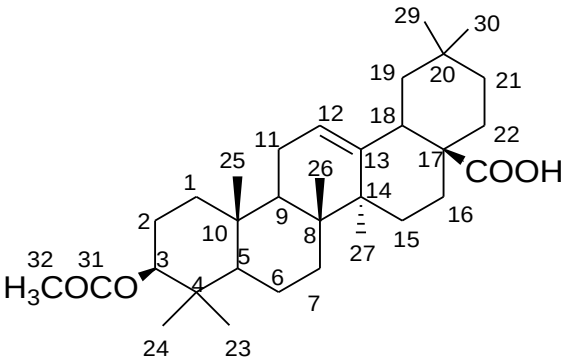

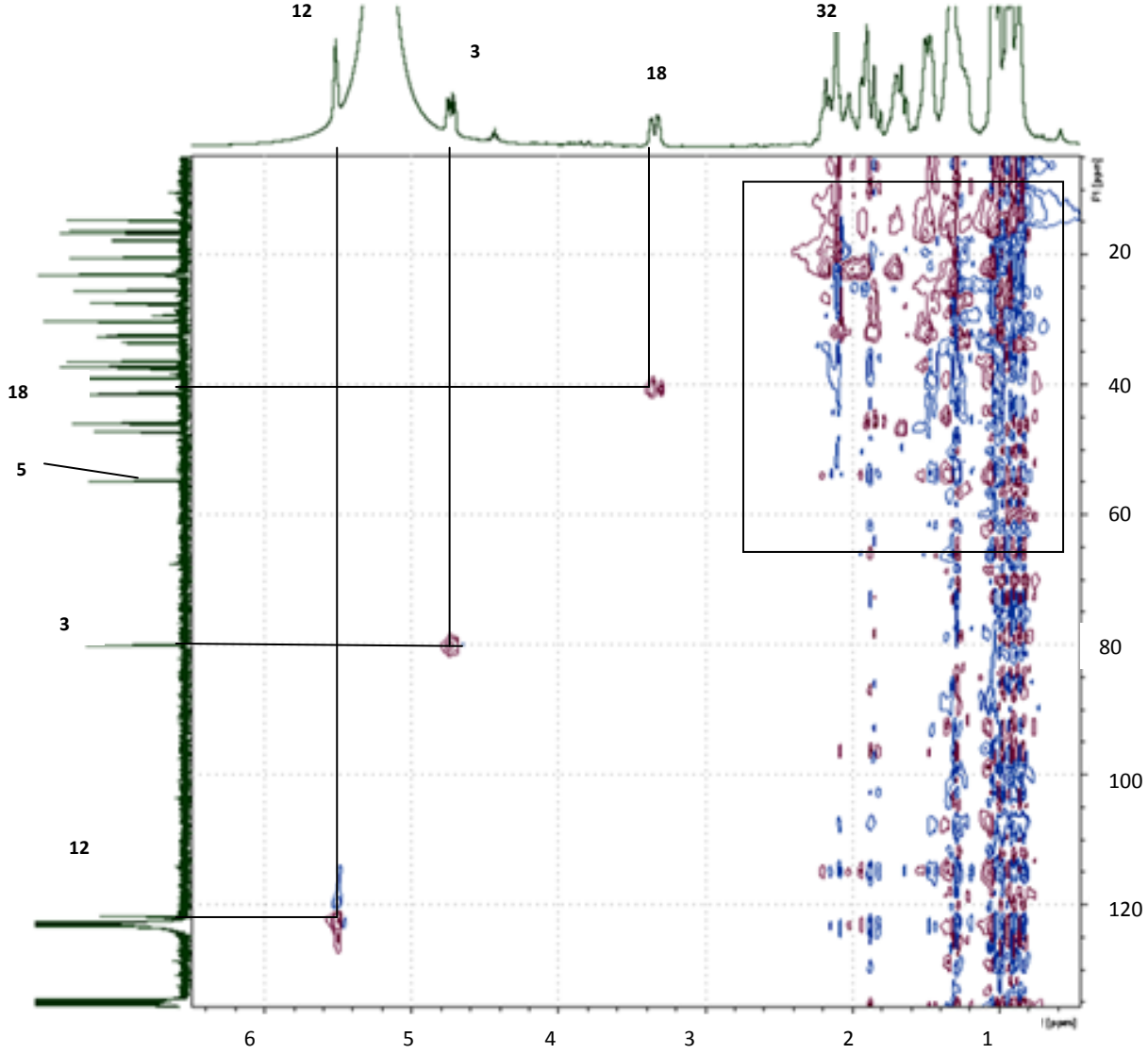

Figure 3.2.5.4 (a): HMQC spectrum of 3β-acetylolean-12-en-28-oic acid **64**

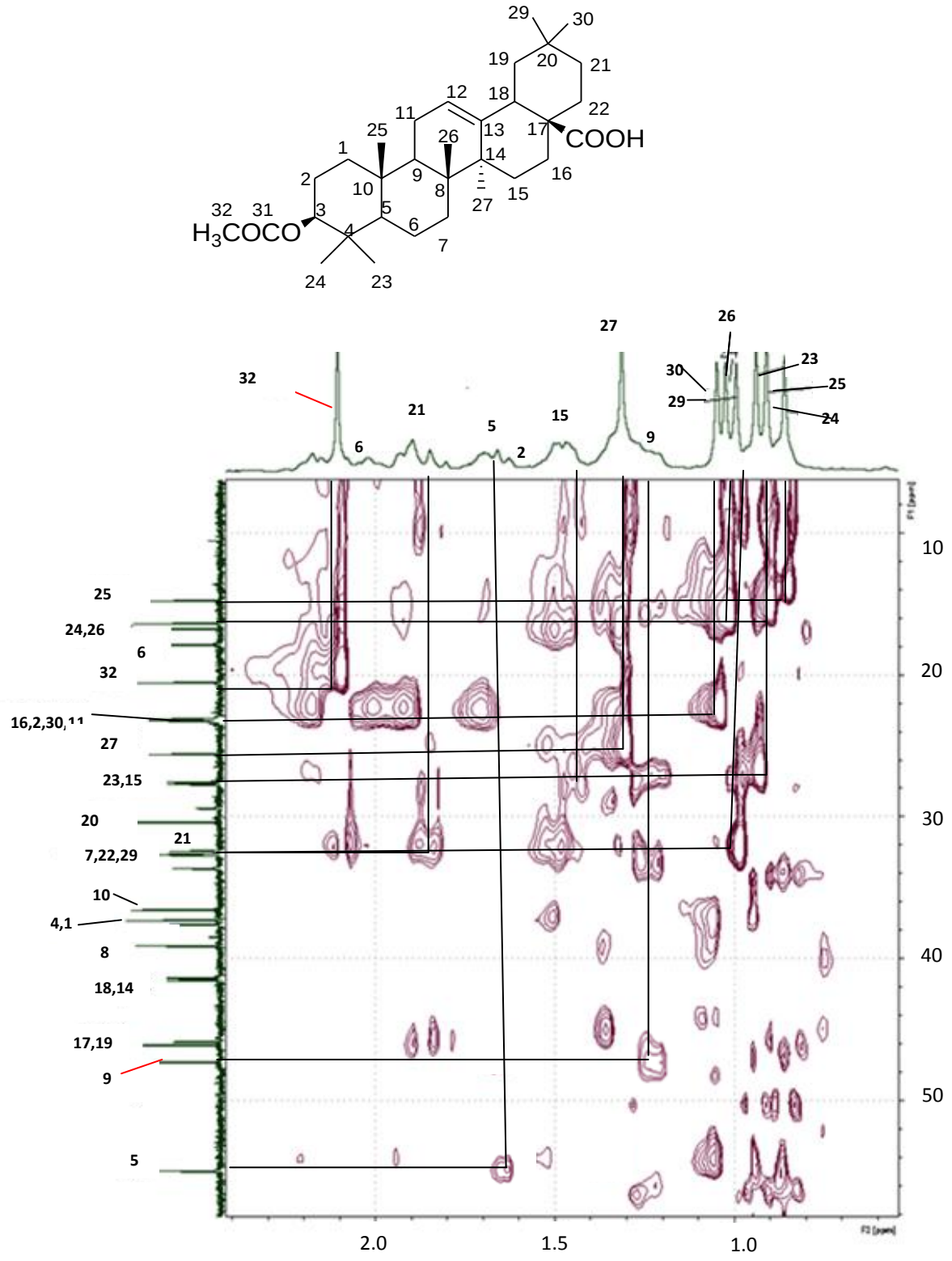

Figure 3.2.5.4 (b): HMQC spectrum of 3β-acetylolean-12-en-28-oic acid **64**

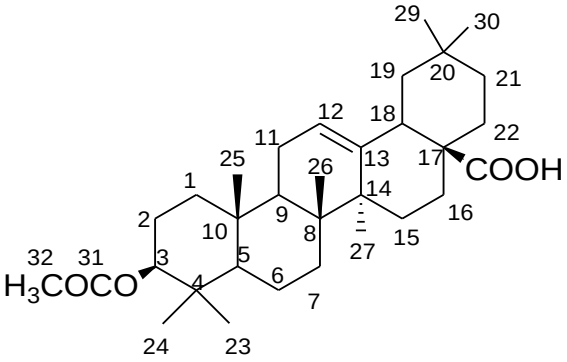

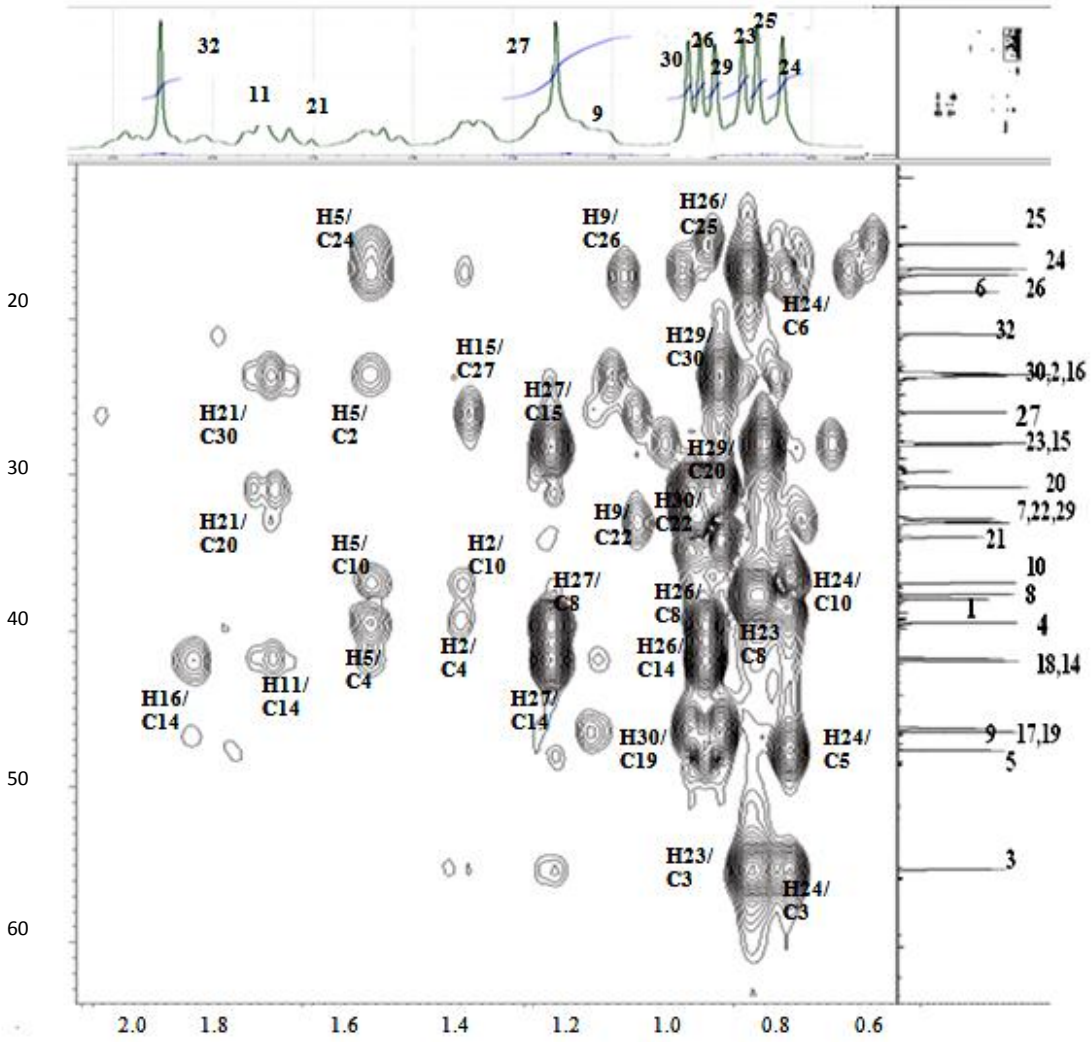

Figure 3.2.5.5(a): HMBC spectrum of 3β-acetyloxean-12-en-28-oic acid **64**

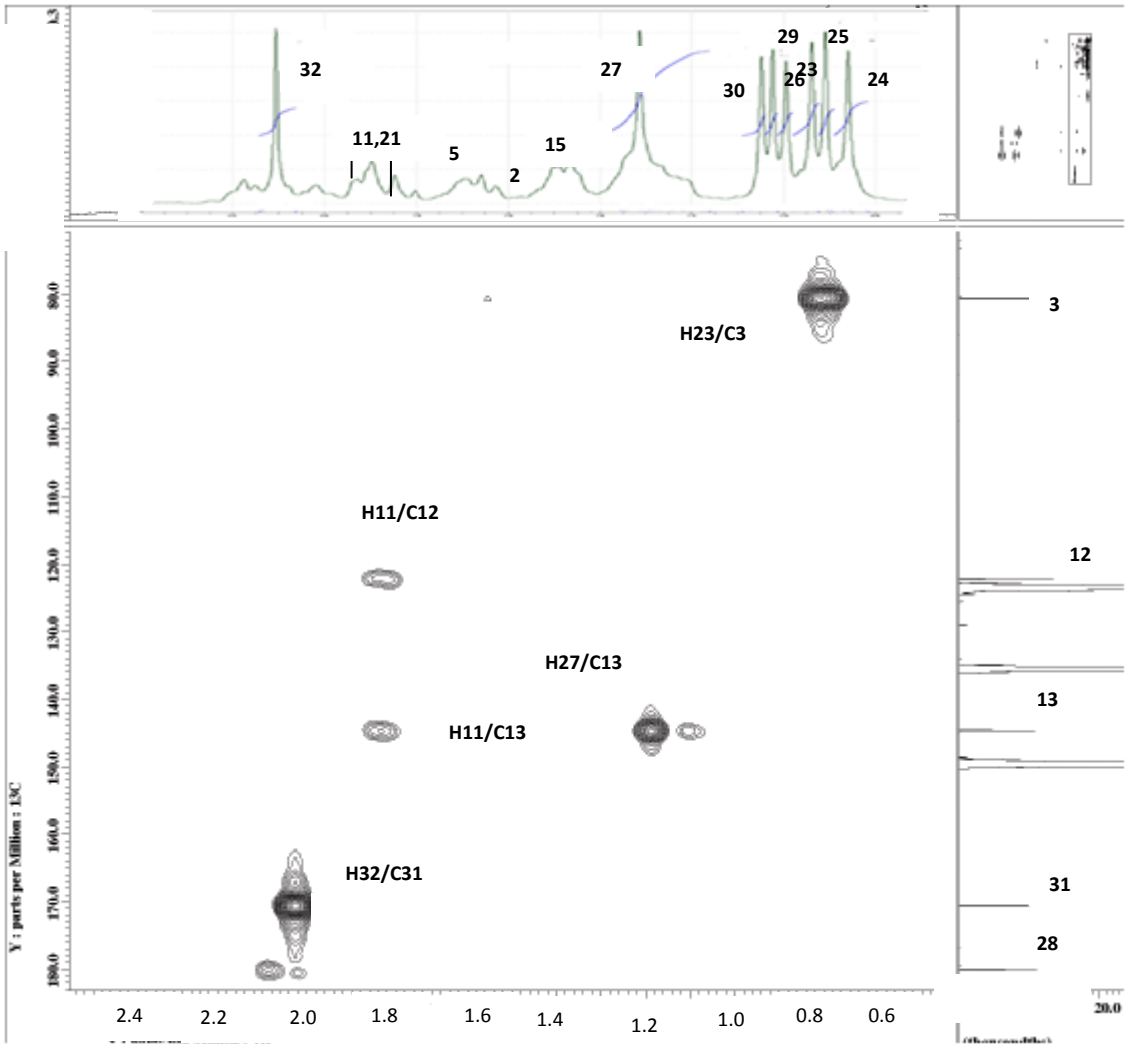

Figure 3.2.5.5(b): HMBC spectrum expansion of 3β-acetylolean-12-en-28-oic acid **64**

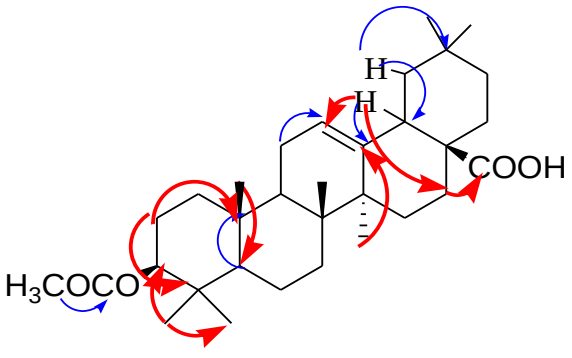

3β-acetylolean-12-en-28-oic acid 64

J_2 Correlations

J_3 Correlations

Figure 3.2.5.6: Selected HMBC correlation in 3β-acetylolean-12-en-28-oic acid **64**

3.2.6 Compound F: *3β-hydroxyurs-11-en-13,28-olide*

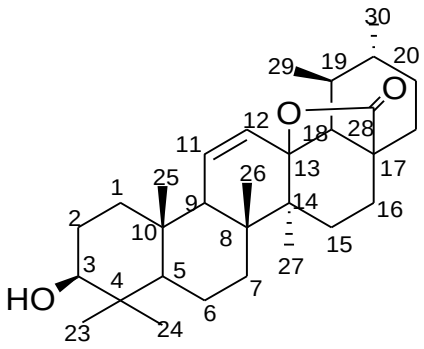

65

3β-hydroxyurs-11-en-ursane-13,28-olide **65 (c**ompound F) was isolated as white amorphous powder. It produced pseudo-molecular ion peak $[M+Na]^+$ at m/z 477.33621 with ESI-MS which is consistent with molecular formula $C_{30}H_{46}O_3$. It showed strong signal at 2884cm^{-1} in the IR spectrum for OH group and a sharp signal at 1687 cm^{-1} for the stretching C=O (Silverstein et al., 1991).

Its ^{1}H NMR (figure 3.2.6.1) exhibited two sets of doublets (table 3.2.6.1) resonated at δ 0.88 (*d, J* =6.1 Hz, H-29, 3H), δ 1.08 (*d, J* =6.1 Hz, H-30, 3H) and five singlet of tertiary methyl protons (δ1.29,H-23; δ1.26, H-27; δ1.23,H-24; δ1.08,H-26; δ0.94, H-25). It also showed two sets of broad doublets of tri substituted olefinic protons at δ6.10 (*brd, J*=10.3 Hz, H-11, 1H) and δ5.70 (*brd, J*=10.3 Hz, H-12, 1H). The presence of an oxymethine proton resonating at δ3.50 (*brt, J*=8.4 Hz), was revealed in the ^{1}H NMR of compound F. Compared to compound A, the signal for H-18 was shifted to the upper field due to the steric effect of the lactone ring. However, the doublet of triplets signal (δ 2.15, J_1=5.6, $J_{2=}$13.7 and $J_{3=}$19.5 Hz, 1H) and δ2.05 (m, 1H) could be assigned to be of the H-16 protons.

The ^{13}C NMR (fig. 3.2.6.2) showed thirty resonances. It showed the lactone carbon signal at δ180.7 and one C-O bonded qarternary carbon signal resonated at δ90.7, two olefinic carbons resonated at δ130.6 and δ135.0 which assignable to be of C-11 and C-12, respectively. The ^{13}C NMR spectrum showed five sp^3 quarternary carbon signals resonated at δ46.4, δ43.4, δ43.2, δ40.7 and δ37.8 of C-17, C-14, C-8, C-4 and C-10 respectively. A hydroxylated carbon was revealed at δ77.6 (C-3) together with other five sp^3 methine carbon resonated at δ1.7, δ56.3, δ54.6, δ41.5 and δ39.4 attributable to be C-5, C-18, C-9, C-19 and C-20 respectively.

Finally, after thorough comparison on the empirical data of compound F together with the known compounds (Masaaki et al., 1983), this compound was identified as 3β-hydroxyurs-11-en-ursane-13,28-olide **65** with additional double bond between C-11 and C-12 (Mulholland et al., 2011)

Table 3.2.6: ^{1}H NMR [300 MHz, δ_H (*J*, Hz)] and ^{13}C NMR [75 MHz, δ_C] of **65** in C_5D_5N

Position	**^{13}C***	**^{13}C**	**^{1}H(*J*,H)**
1	39.1	39.8	
2	27.4	29.1	
3	79.0	79.2	3.5 (*t*, 8.4 Hz)
4	38.9	40.7	-
5	55.3	56.3	
6	17.8	19.3	
7	34.2	32.7	
8	42.3	43.4	-
9	51.4	54.6	
10	37.1	37.8	-
11	**18.9**	**125.5**	**6.1 (*d*, 10.3 Hz)**
12	**34.7**	**130.6**	**5.7 (*d*,10.3 Hz)**
13	93.2	90.7	-
14	43.3	43.2	-
15	27	27.1	
16	22.9	24.4	2.15 (*dt*, 5.5, 13.7, 19.5 Hz), 2.05*m*
17	45.7	46.4	-
18	61.2	61.7	
19	38.7	40.7	
20	39.9	39.4	
21	30.8	31.2	
22	31.6	31.2	
23	28	29.6	1.29*s*
24	15.3	17.1	1.23 *s*
25	16.4	19.2	0.94 *s*
26	18.5	20.4	1.09 *s*
27	17.4	19.4	1.26 *s*
28	180.6	180.8	-
29	17.6	19.4	0.88 (*d*, 6.1 Hz)
30	19.5	20.6	1.08 (*d*, 6.1 Hz)

*^{13}CNMR [22.5MHz]
*^{1}HNMR [89.55MHz] $CDCL_3$
(Masaaki et al., 1983)

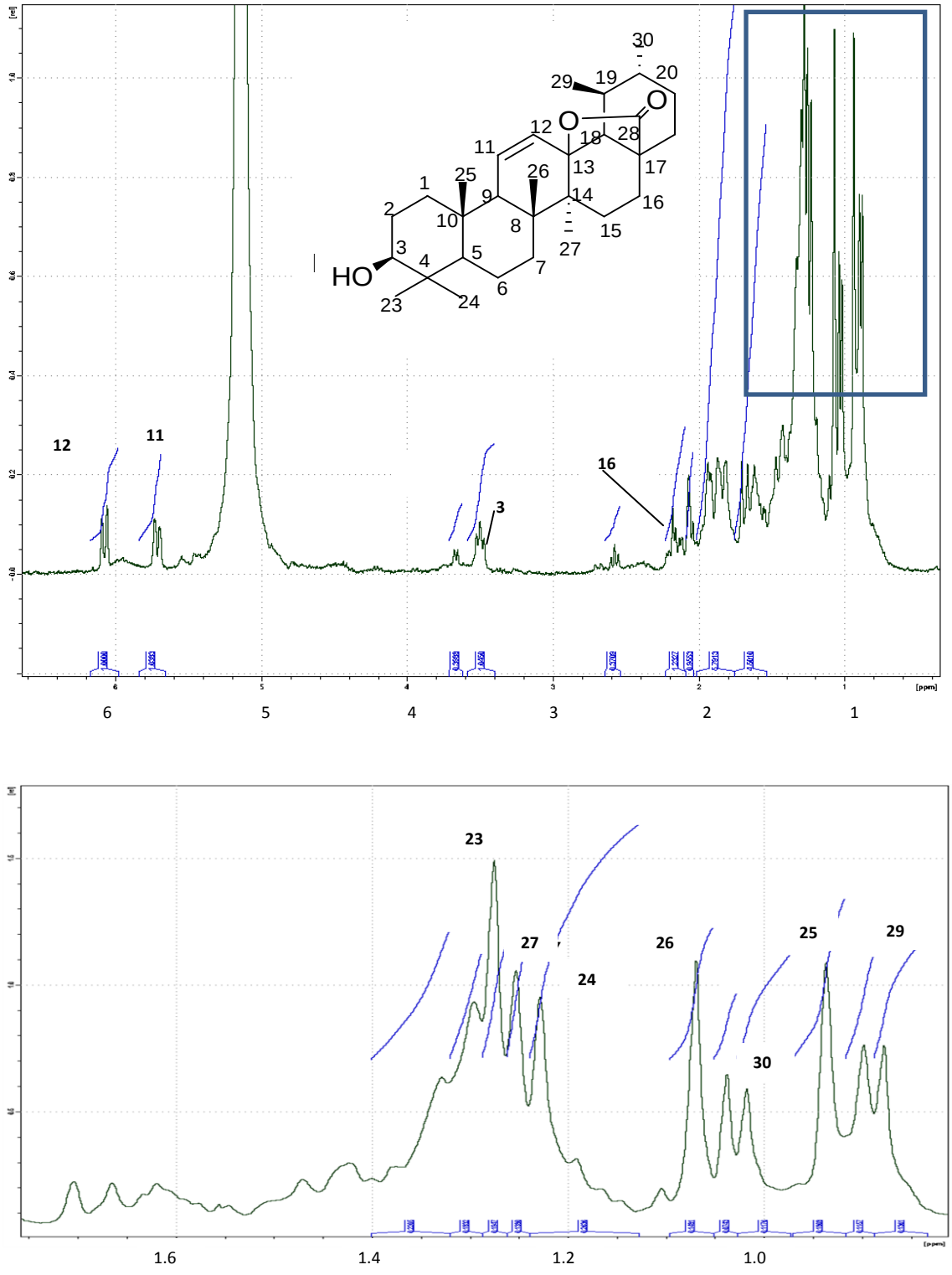

Figure 3.2.6.1: ^{1}H NMR spectrum of 3β-hydroxyurs-11-en-13,28-olide **65**

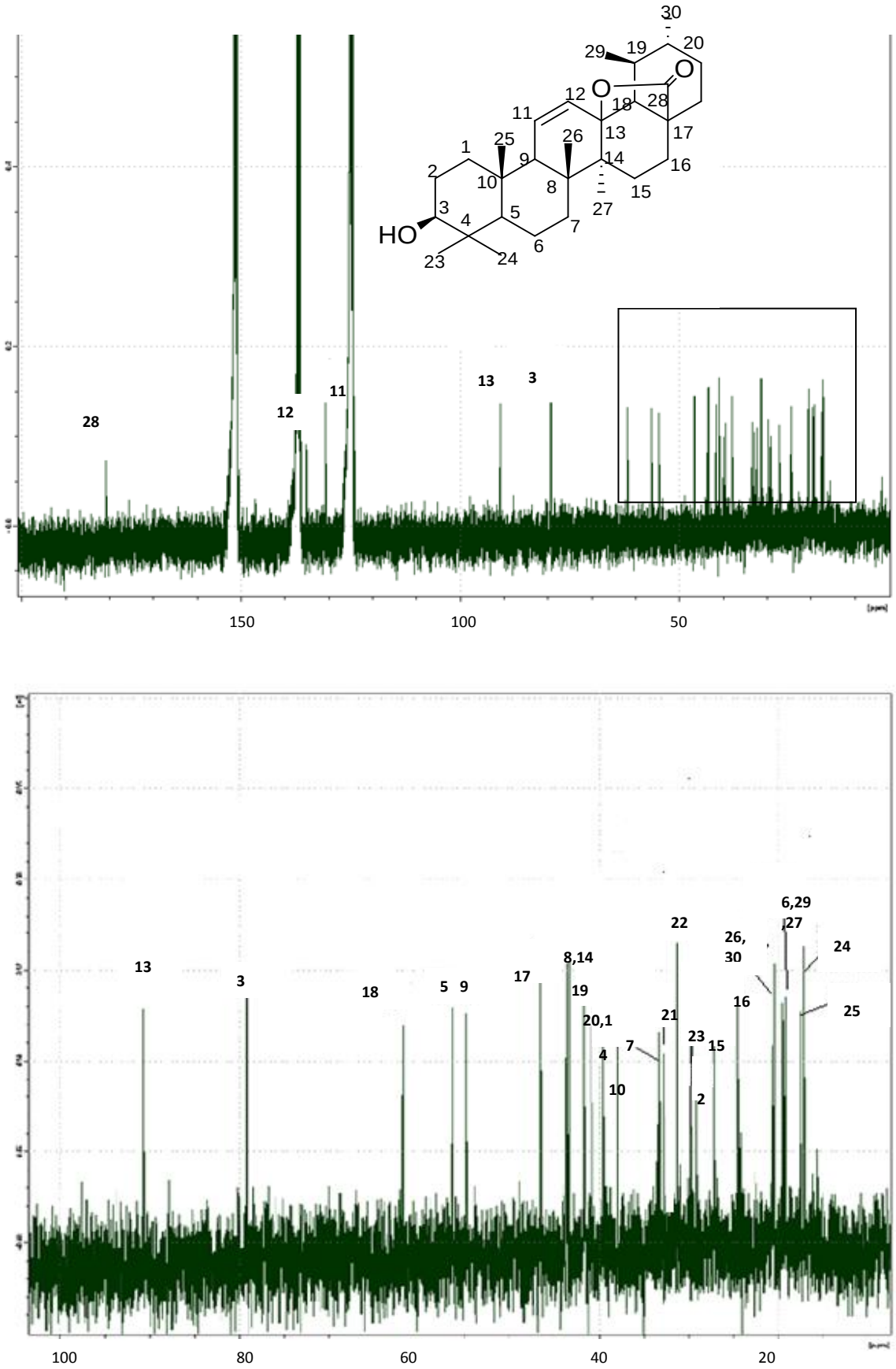

Figure 3.2.6.2: ^{13}C NMR spectrum of 3β-hydroxyurs-11-en-13, 28-olide **65**

3.2.7 Compound G: *Prismalayanoside*

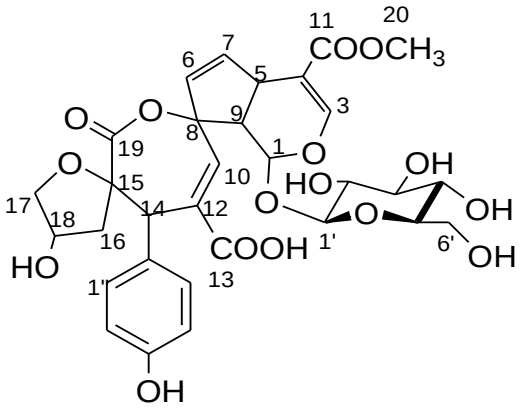

66

Prismalayanoside **66** (compound G) was isolated as yellowish amorphous solid. It produced pseudo-molecular ion peak $[M+Na]^+$ at m/z 685.17523 (calcd. 685.16944) with ESI-MS which is consistent with the molecular formula of $C_{31}H_{33}O_{16}$ (figure 3.2.7.0). The UV spectrum showed maximum absorption at 234, 292 and 314 nm typical for the iridoid of plumerin type (Biswanath et al., 2007). The IR absorptions band at 3375 cm^{-1} (strong and broad signal) and 1686 cm^{-1} (strong signal) show the presence of α,β-unsaturated carboxylic acid (Silverstein et al., 1991), whereas, the absorptions at 1754 and 1639 cm^{-1} suggested the presence of an iridoic enol ether system conjugated with an ester carbonyl group (Wu et al., 2009).

The ^1H NMR spectrum in MeOD (figure 3.2.7.1 a) was characterized by a doublet for H-1 at δ5.25 (*d*, *J*=5.1 Hz) which was split by proton H-9 at δ3.00 (*dd*, J_1=5.2 and $J_{2=}$ 7.2 Hz), an olefinic proton at δ7.60*s* (*d*, J_1=1.4 Hz, H-3) and carbomethoxy group 3.80 (*s*, H-20) (table 3.2.7). These signals were consistent with the characteristic structural features of an enol ether system conjugated with a carbomethoxy group of iridoid skeletons (Wu et al., 2009). An AB spin system between *cis*-olefinic protons, H-7 and

H-6 showed by the two doublet signals resonated at δ5.62 (*dd, J_1*=5.5 and *J_2*=2.0 Hz) and δ6.50 (*dd, J_1*=5.5 and *J_2*=2.3 Hz) respectively. The small coupling constant of these disubstituted protons, H-6 and H-7, indicated that the double bonds were located in a five membered ring (Wu et al., 2009). The anomeric proton of glucose, H-1' was resonated at δ4.80 (*d, J*=7.8 Hz). The big coupling constant value of H-1' substantiated the *β*-configuration of the glucopyranose unit (Kim et al., 2006). The signals for the other glucose protons (H-2', H-3', H-4', H-5' and H-6') were resonated between 3.2-4.0 ppm and overlapped with the proton signals of H-5, H-17, H-18. The ^{1}H NMR spectrum in C_5D_5N showed a better resolution for the H-2', H-3', H-4', H-5', H-6', H-5, H-17 and H-18 (figure 3.2.7.1b). The coupling constant values of the sugar unit further supported the glucose type of sugar in this compound (table 3.2.7).

Besides the above mentioned signals of cylopentanopyran ring system with a sugar moiety, other peaks were of an isolated olefinic protons at δ7.70*s* (H-10) and a downfield singlet at δ4.12 which is attributable to the isolated H-14 (figure 3.2.7.1a, MeOD). A pair of doublet signal at the aromatic region of δ7.35 (*d, J*=8.5 Hz) and δ 6.80 (*d, J*=8.5 Hz) were the signal of two sets of chemically equivalent protons of the *para*-substituted aromatic ring; H-2'', H-6'' and H-3'', H-5'', respectively. The spin system AA'BB' was indicated by the presence of a pair of *dd* signal at δ2.60 (*dd, J*=6.7, 12.9 Hz) and δ2.10 (*dd, J*=8.5, 13.6 Hz) which is attributable to H-16. Three sets of protons were found overlapped with the glucose protons signals: H-5 (4.05, *m*), H-17 (3.83, *m*) and H-18 (4.0, *m*).

In the ^{1} H NMR (C_5D_5N) however, the signals of H-5, H-17 and H-18 could be observed at 3.98 (*bd*, 7.8 Hz), [4.09 (*dd*, 13.7, 4.1), 3.87 (*m*)] and 4.65*m*, respectively.

The signal for H-5 was split into the broad doublet by H-6 and H-9. The multiplicity of H-18 because of its correlation with H_2-17 and H_2-16.

Combined analysis of the ^{13}C NMR (figure 3.2.7.2, MeOD) and the DEPT (figure 3.2.7.3, MeOD) spectra showed thirty one carbon signals which consisted of one methyl, three methylene, eighteen methine and nine quartenary carbons. In comparison with prismatomerin **63** and gaertneroside **21** (Krohn et al., 2007), prismalayanoside **66** showed three additional peaks which are shifted down field at δ79.4 (C-15), δ62.3C-17) and δ77.9 (C-18), probably due to the deshielding effect of the electronegative oxygen atom (table 3.2.7).

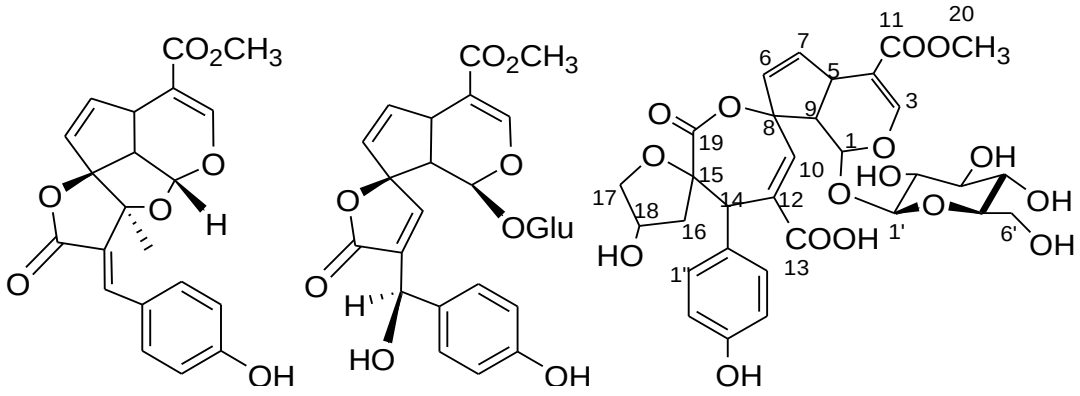

67 **23** **66**

The other additional signals were methine carbon at δ46.7 of C-14, methylene carbon at δ34.9 (C-16) and two carbonyl carbons at δ178.7 and δ173.3 of C-13 and C-19, respectively. The downfield chemical shift of C-8 (δ 98.5) indicated that this quaternary carbon is oxygenated.

The analysis on COSY (figure 3.2.7.4 a) and HMQC (figure 3.2.7.5) spectra showed the correlations between H-6 (δ 6.50), H-7 (δ 5.62), H-5 (δ 4.05), H-9 (δ 3.00) and H-1(δ 5.25), thus supported the *cis*-fused cylopentanopyran ring sytem found in iridoid skeletons which particularly the plumieride type iridoids (Kuigoua et al., 2010). In figure 3.2.7.4 b (C_5D_5N), the COSY correlation between H-18 (δ 4.66) and H-16a (δ

3.87), H-16b (δ 3.13) and H-17 (δ 4.10), H-17b (3.87) suggested the presence of the five membered ring D.

The structure was further confirmed with the HMBC spectrum (figure 3.2.7.6a and b, MeOD). The expected $^{1}J_{CH}$ and $^{2}J_{CH}$ correlation for the aglycon cylopentanopyran ring (ring A and B) were observed. It showed correlation between H-3 (δ 7.6) and C- 1 (δ 94.6), C-4 (δ 111.0), C-5 (δ 40.6), C-11 (δ 168.8); H-5 (δ 4.05) and C-9 (δ 51.0), C-4 (δ 111.0), C-7 (δ 130.1), C-6 (δ 141.8), C-3 (δ 152.6); H-6 (δ 6.5) and C-5 (δ 40.6), C-9 (δ 51.0), C-8 (δ 98.5) C-7 (δ 130.1); H-7 (δ 5.62) and C-5 (δ 40.6), C-9 (δ 51.0), C-8 (δ 98.5), C-6 (δ 141.8); H-9 (δ 3.0) and C-8 (δ 98.5). The cross peak between H-1' (δ 4.80) and C-1 (δ 94.6) confirmed the site of attachment of the glucose moiety at C-1.

The unusual seven-membered unsaturated spiro lactone ring (ring C) attached to C-8 was constructed by the long range correlations in the HMBC spectrum between H-10 (δ 7.7) and C-14 (δ 47.8), C-8 (δ 98.5), C-13 (δ 174.5), C-12 (δ 131.8); H-14 and C-18, C-1", C-12, 2", 6", C-10 (δ 151.5), C-13 (δ174.5); H-16 (δ 2.10) and C-17 (δ 62.8), C-18 (δ 78.1) , C-15 (δ 77.8) (figure 3.2.7.7). The HMBC spectrum (figure 3.2.7.6 c, C_5D_5N), showed better view on the correlation between H-18 and C-14, H-17 and H-17 and C-16, C-15 thus further supported the five-membered ring D unit.

The ROESY / NOESY experiment (figure 3.2.7.9, CD_3OD) showed interactions between H-9 and H-5, H-6 and H-5, H-7, thus indicated that all these protons are cofacial (Krohn et al., 2007). The H-10 was of α-position relative to C-8 as the chemical shift of C-9 was δ 51.0 (Kanchanapoom et al., 2002). Thus, the cross peaks between H-1/H-10 and H-5/H-9 confirmed that the linkage between C-8 and C-10 was α-oriented,

H-1 was α and in equatorial conformation whereas H-5 and H-6 were β-oriented. The correlations were summarized in figure 3.2.7.8.

From the 3D minimization of the molecular structure of prismalayanoside resulted in a skewed/pleated octalactone ring. Therefore, the methylene proton of H-16b was oriented within the proximity to H-10. The ROESY confirmed the configuration from the interaction between H-16b and H-10 thus implied that C-16 is *β*-oriented (figure 3.2.7.8).

Thorough examination of all spectral data obtained led to the conclusion that prismalayanoside **66** was assigned as the novel compound having unprecedented spiro-hepta-lactone ring.

Table 3.2.7: ^{1}H NMR [300 MHz, δ_H (*J*, Hz)] and ^{13}C NMR [75 MHz, δ_C] of **66** in CD_3OD[a] and C_5D_5N[b].

	^{1}H (*J*,H)[a]	^{1}H (*J*,H)[b]	^{13}C[a]	^{13}C[b]
1	5.25 (*d*, 5.1 Hz)	6.01 (*d*, 3.2 Hz)	94.6	94.3
3	7.60(*d*, 1.4)	7.75 (*d*, 0.9 Hz)	152.6	152.2
4	-	-	111.0	110.9
5	4.05*m*	3.96 (*brd*, 7.8 Hz)	40.6	39.5
6	6.50 (*dd*, 2.3, 5.5 Hz)	6.50 (*dd*, 5.5, 2.8 Hz)	141.8	140.5
7	5.62(*dd*, 5.5, 2.3 Hz)	5.51 (*dd*, 5.5, 1.8 Hz)	130.1	130.2
8	-	-	98.5	97.6
9	3.0(*dd*, *J*=5.2, 7.2 Hz)	3.38 (*dd*, 8.2, 3.6 Hz)	51.0	50.6
10	7.70*s*	8.30*s*	151.5	151.2
11	-	-	168.8	167.2
12	-	-	131.8	133.8
13	-	-	174.5	173.3
14	4.12*s*	4.83*s*	47.8	48.5
15	-	-	79.4	79.5
16	2.60 (*dd*, 7.7, 13.8 Hz), 2.10 (*dd*, 7.7, 13.8 Hz)	2.87(*dd*, 13.7, 7.5 Hz), 3.13 (*dd*, 13.7, 7.5 Hz)	35.9	38.5
17	3.85*m*	4.10(*dd*, 13.7, 4.1 Hz), 3.87*m*	62.3	62.6
18	4.0*m*	4.66*m*	77.9	78.7
19	-	-	179.9	178.0
20	3.80*s*	3.59*s*	52.2	51.7
1'	4.80 (*d*, 7.8 Hz)	5.36 (*d*, 7.8 Hz)	100.3	101.4
2'	3.37-3.50*m*	4.12 (*brd*, 8.2 Hz)	74.6	75.0
3'	3.37-3.50*m*	4.24 (*t*, 9.1 Hz)	79.2	79.0
4'	3.37-3.50*m*	4.42 (*bd*, 8.7 Hz)	71.3	71.4
5'	3.37-3.50*m*	3.89*m*	79.0	79.4
6'	3.7(*dd*, 4.3, 12.8Hz), 3.55 (*dd*, 4.3, 12.8 Hz)	4.45 (*dd*, 11.9, 1.8 Hz),4.4(*dd*, 11.9, 5.5Hz)	63.9	63.8
1"	-	-	127.5	127.7
2"	7.35 (*d*, 8.5 Hz)	7.67 (*d*, 8.7 Hz)	130.9	132.3
3"	6.80 (*d*, 8.5 Hz)	7.14 (*d*, 8.7 Hz)	116.6	116.6
4"	-	-	157.5	159.1
5"	6.80 (*d*, 8.5 Hz)	7.14 (*d*, 8.7 Hz)	115.5	116.6
6"	7.35 (*d*, 8.5 Hz)	7.67 (*d*, 8.7 Hz)	130.9	132.3

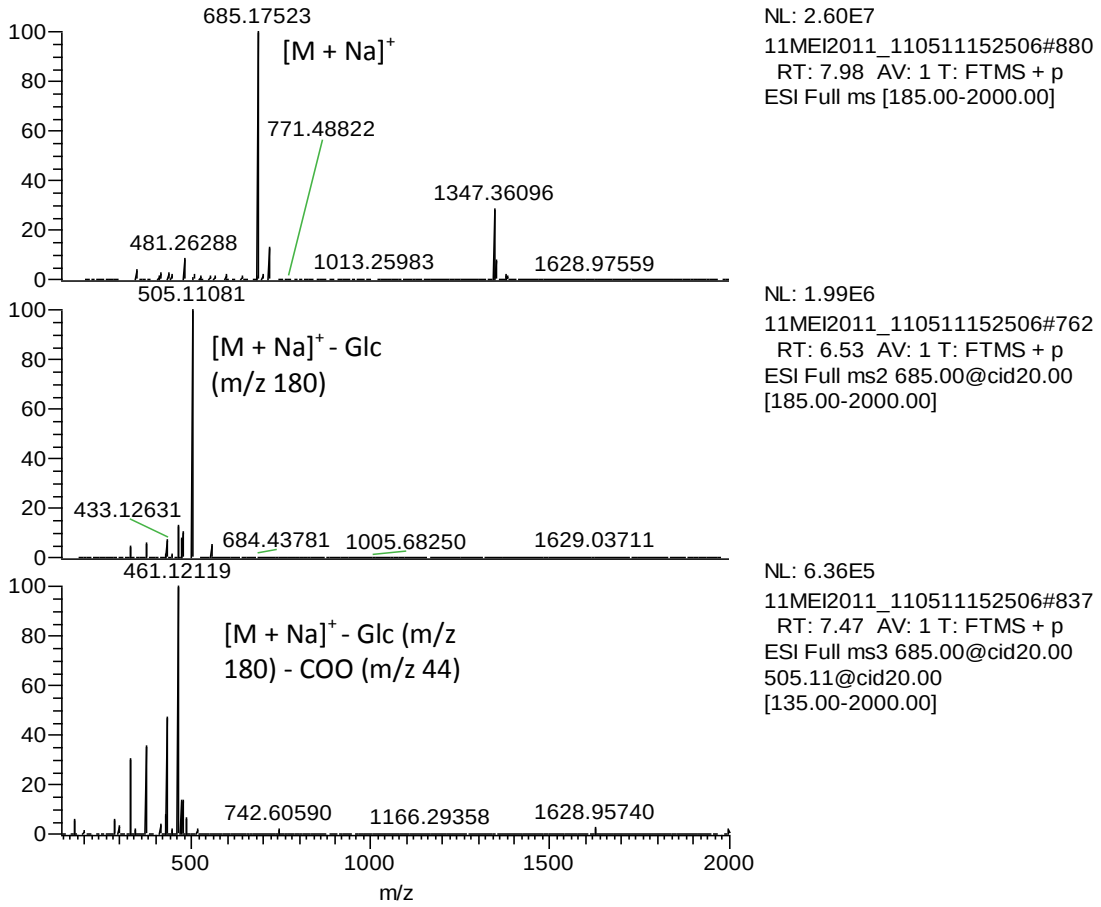

Figure 3.2.7.0: Mass spectrum of prismalayanoside **66**

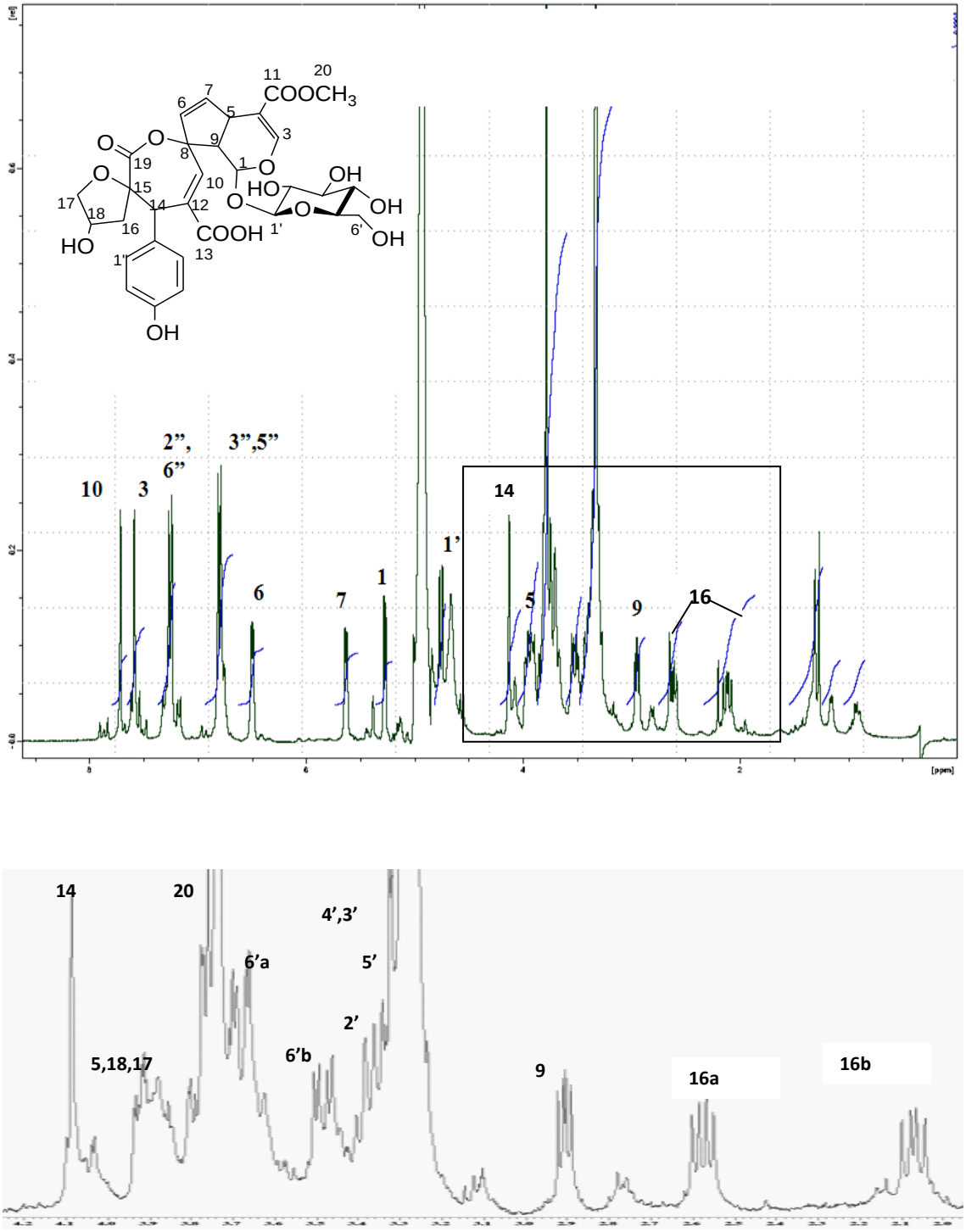

Figure 3.2.7.1a: ^{1}H NMR spectrum of prismalayanoside **66** in MeOD

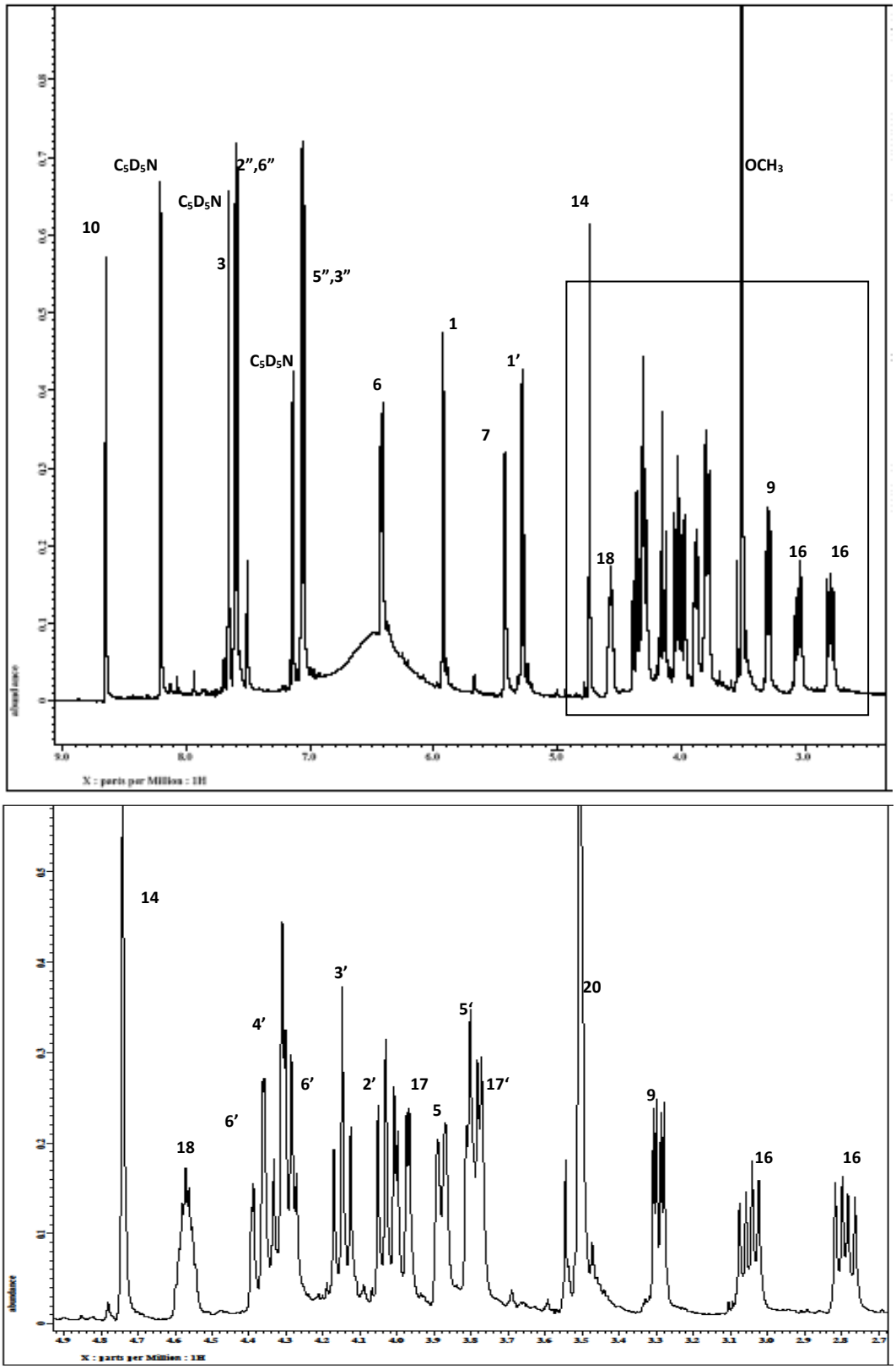

Figure 3.2.7.1b: ^{1}H NMR spectrum of prismalayanoside **66** in C_5D_5N

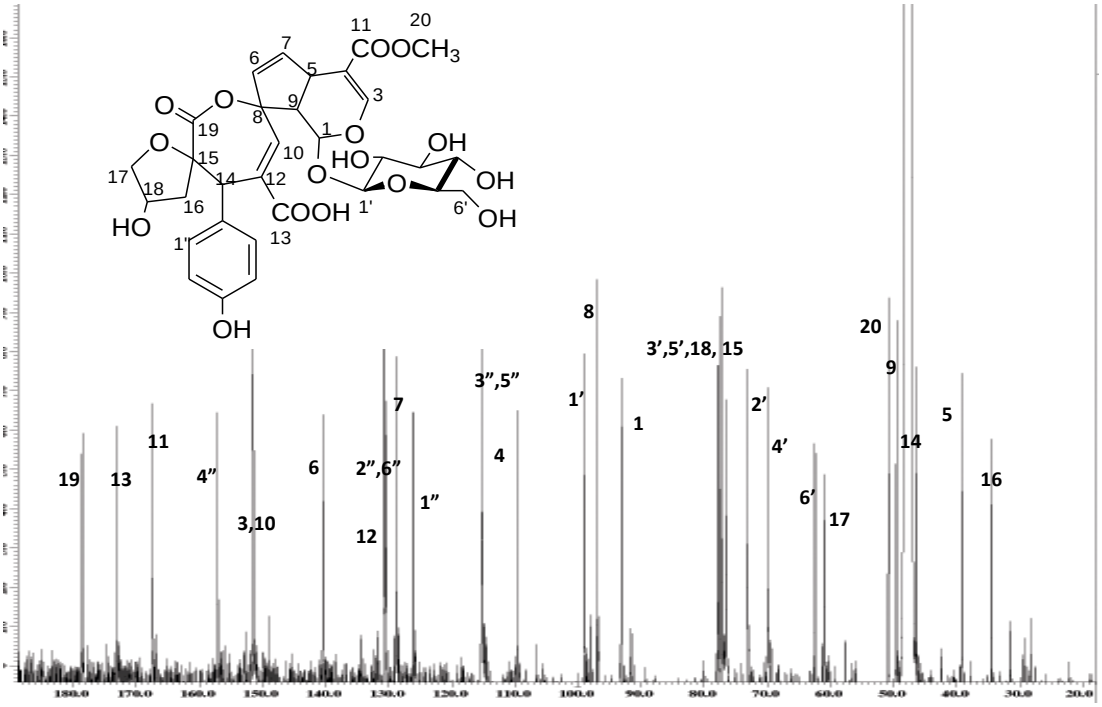

Figure 3.2.7.2a: ^{13}C NMR spectrum of prismalayanoside in MeOD **66**

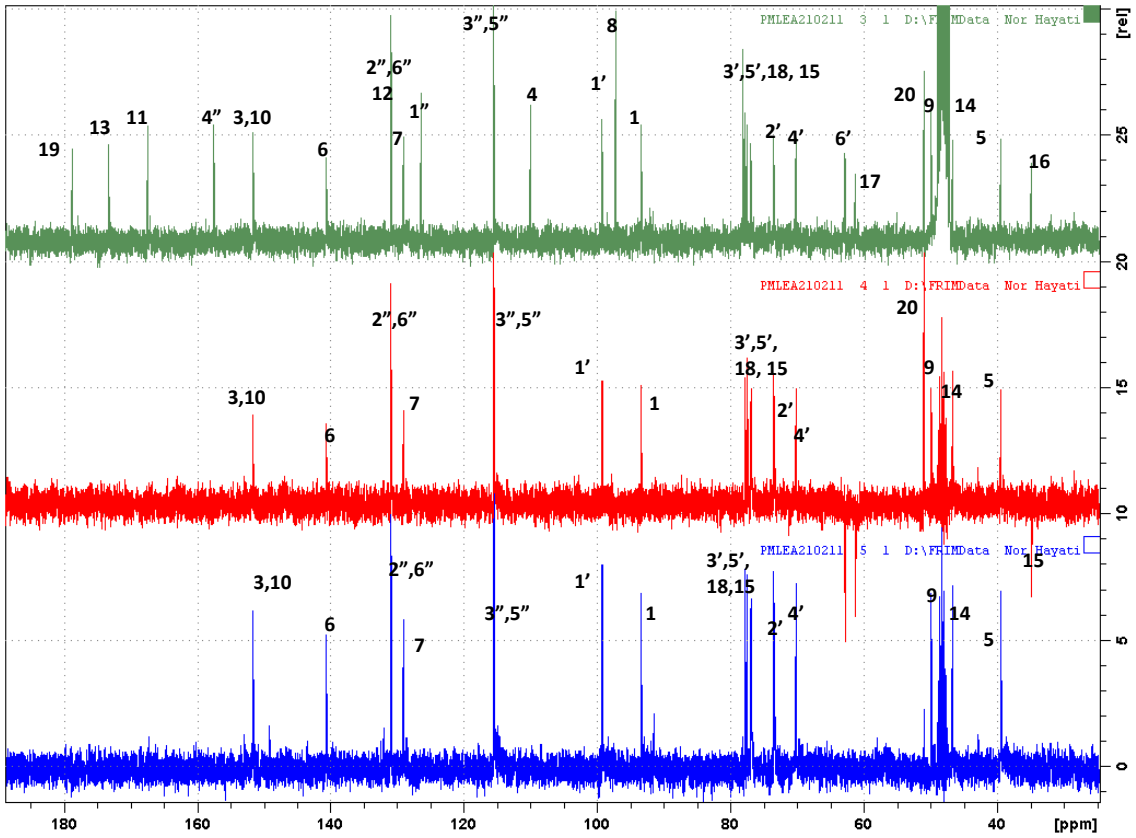

Figure 3.2.7.3: DEPT spectrum of prismalayanoside in MeOD **66**

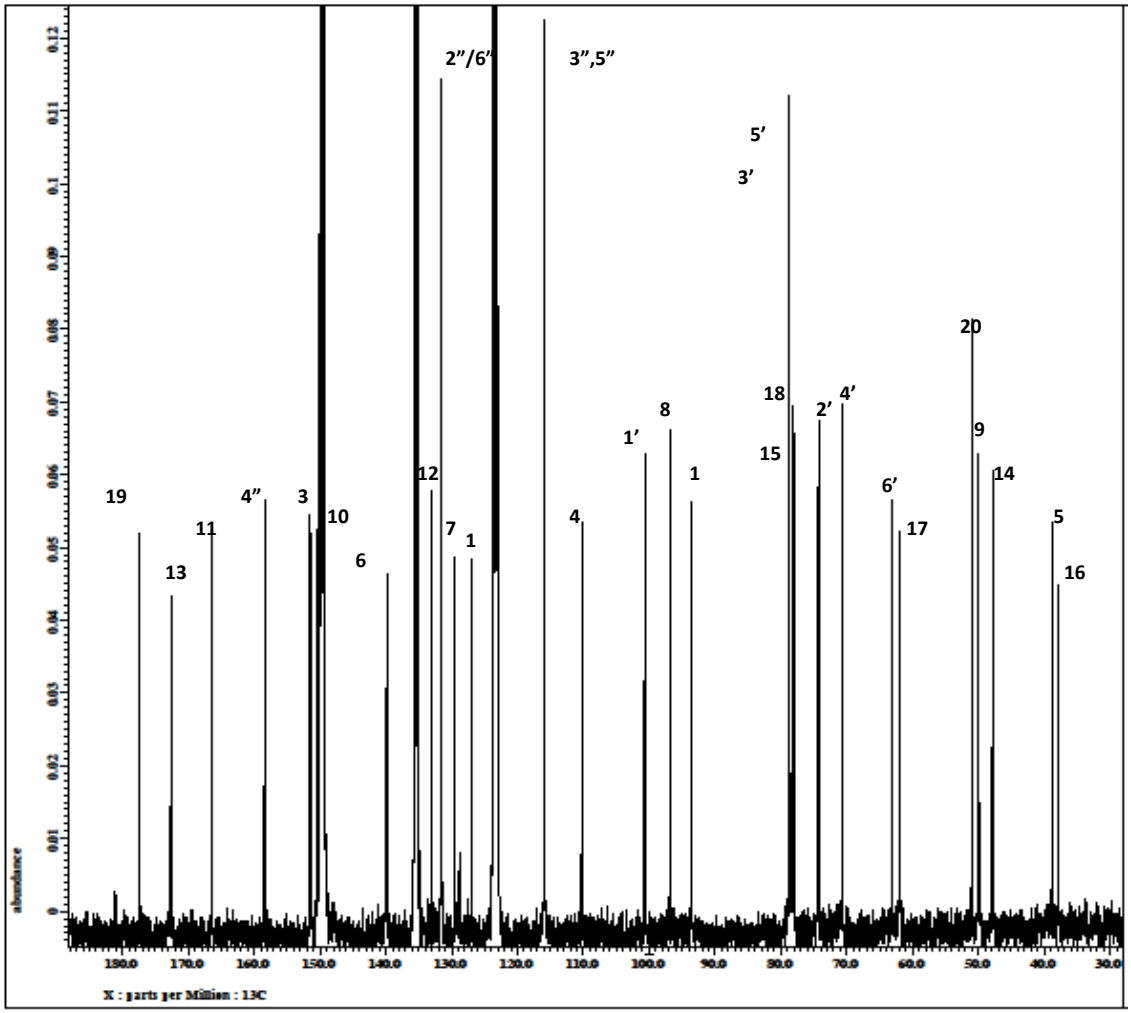

Figure 3.2.7.2 b: ^{13}C NMR spectrum of prismalayanoside **66** in C_5D_5N

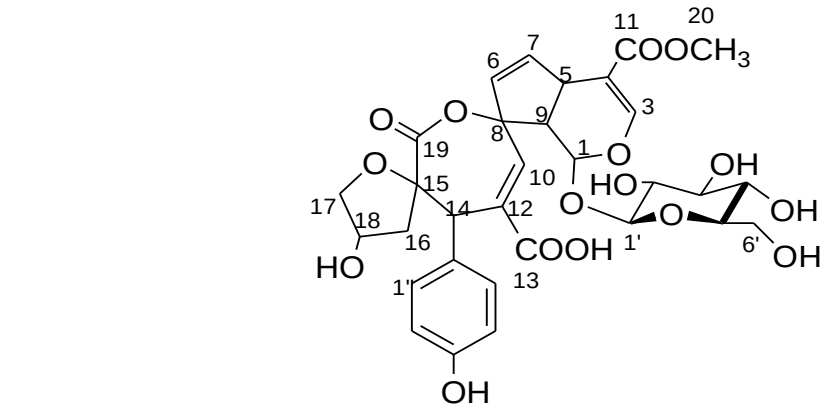

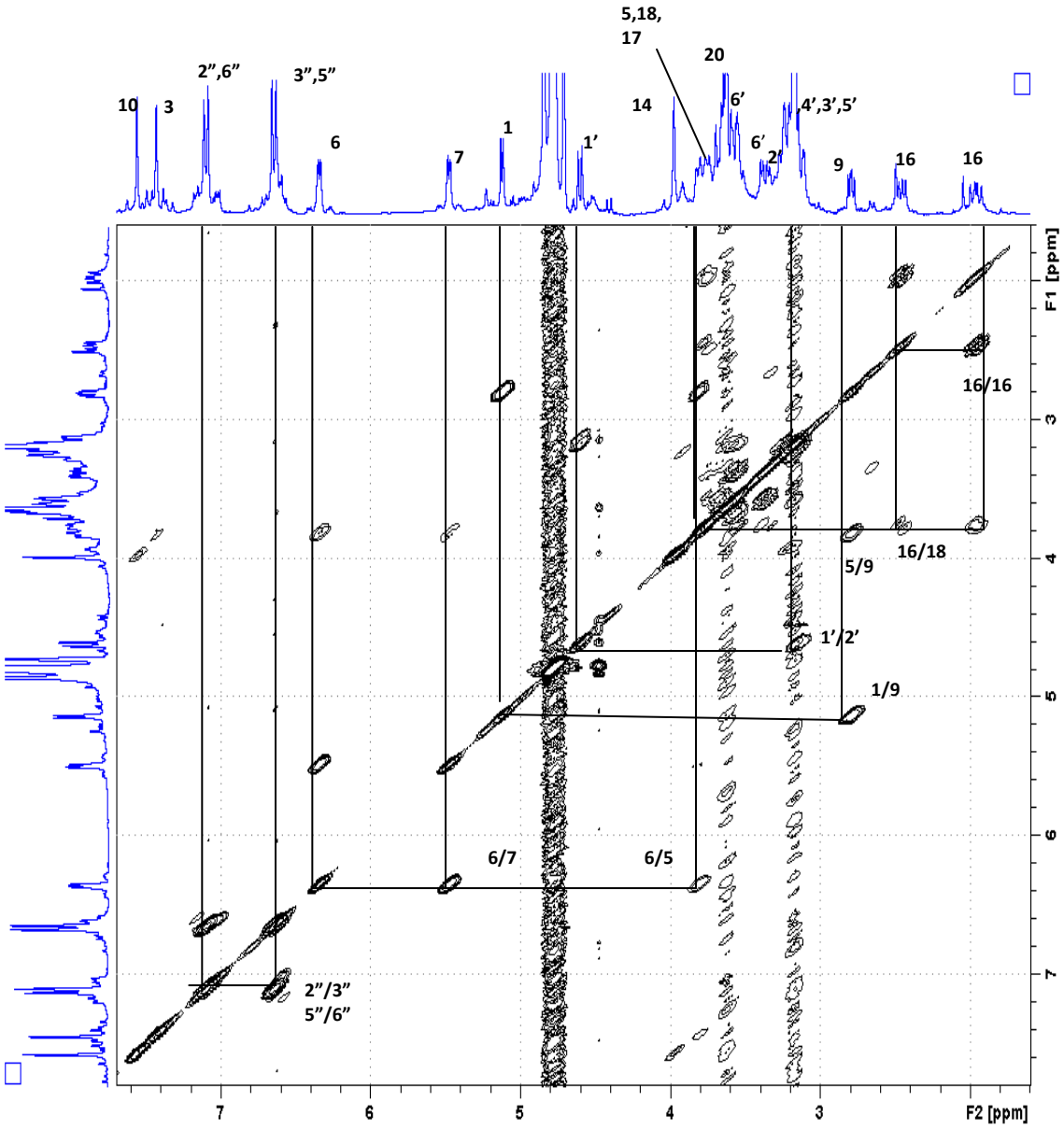

Figure 3.2.7.4a: COSY spectrum of prismalayanoside **66** in MeOD

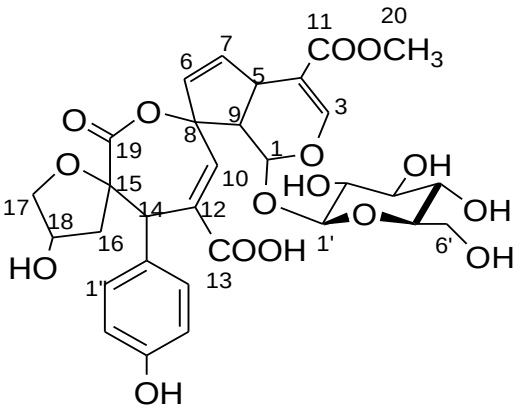

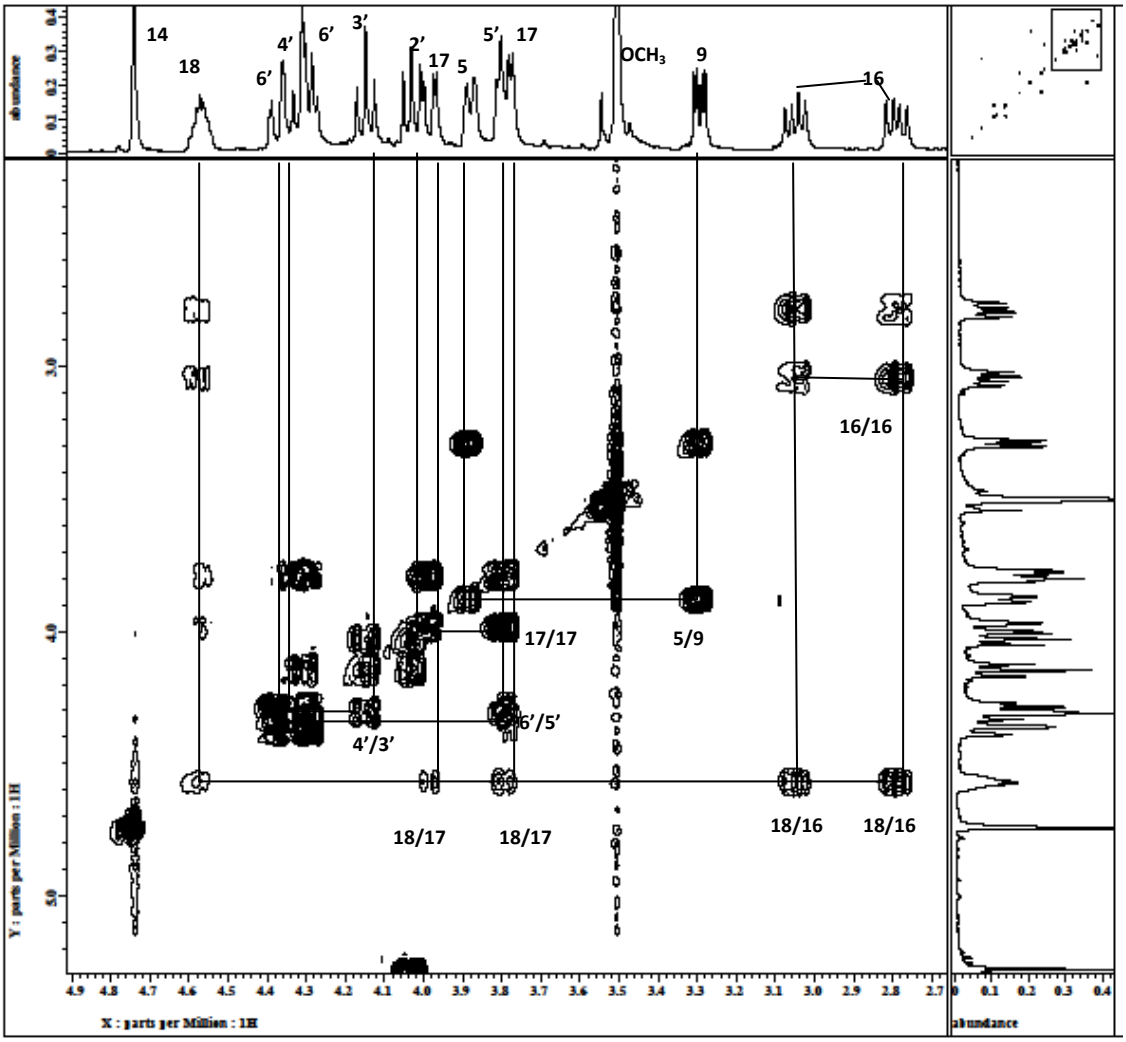

Figure 3.2.7.4b: COSY spectrum of prismalayanoside **66** in C_5D_5N

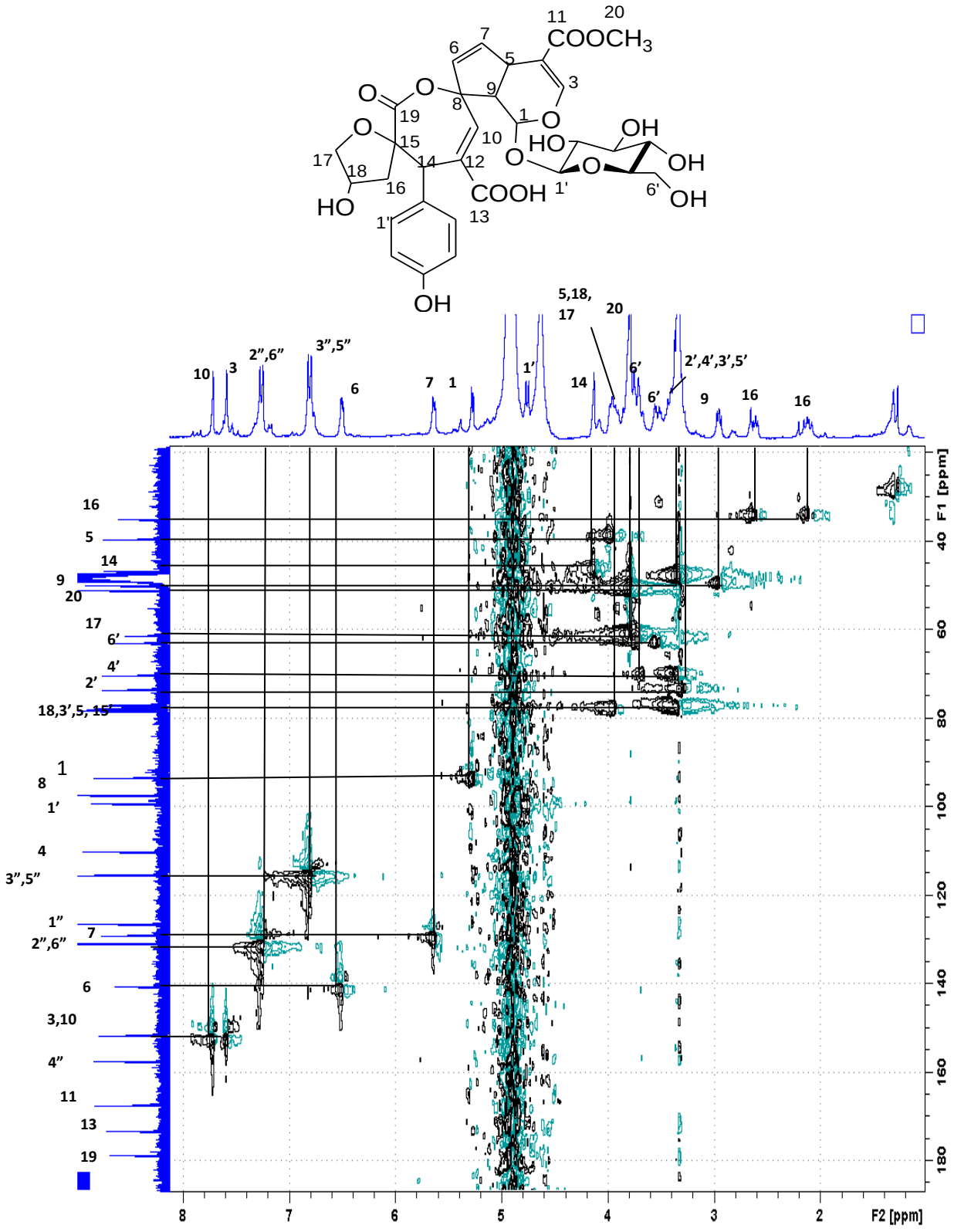

Figure 3.2.7.5a: HMQC spectrum of prismalayanoside **66** in MeOD

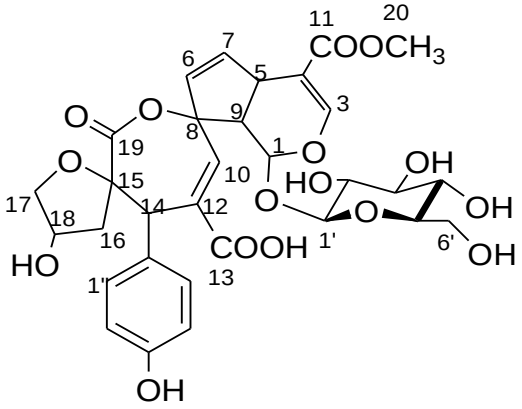

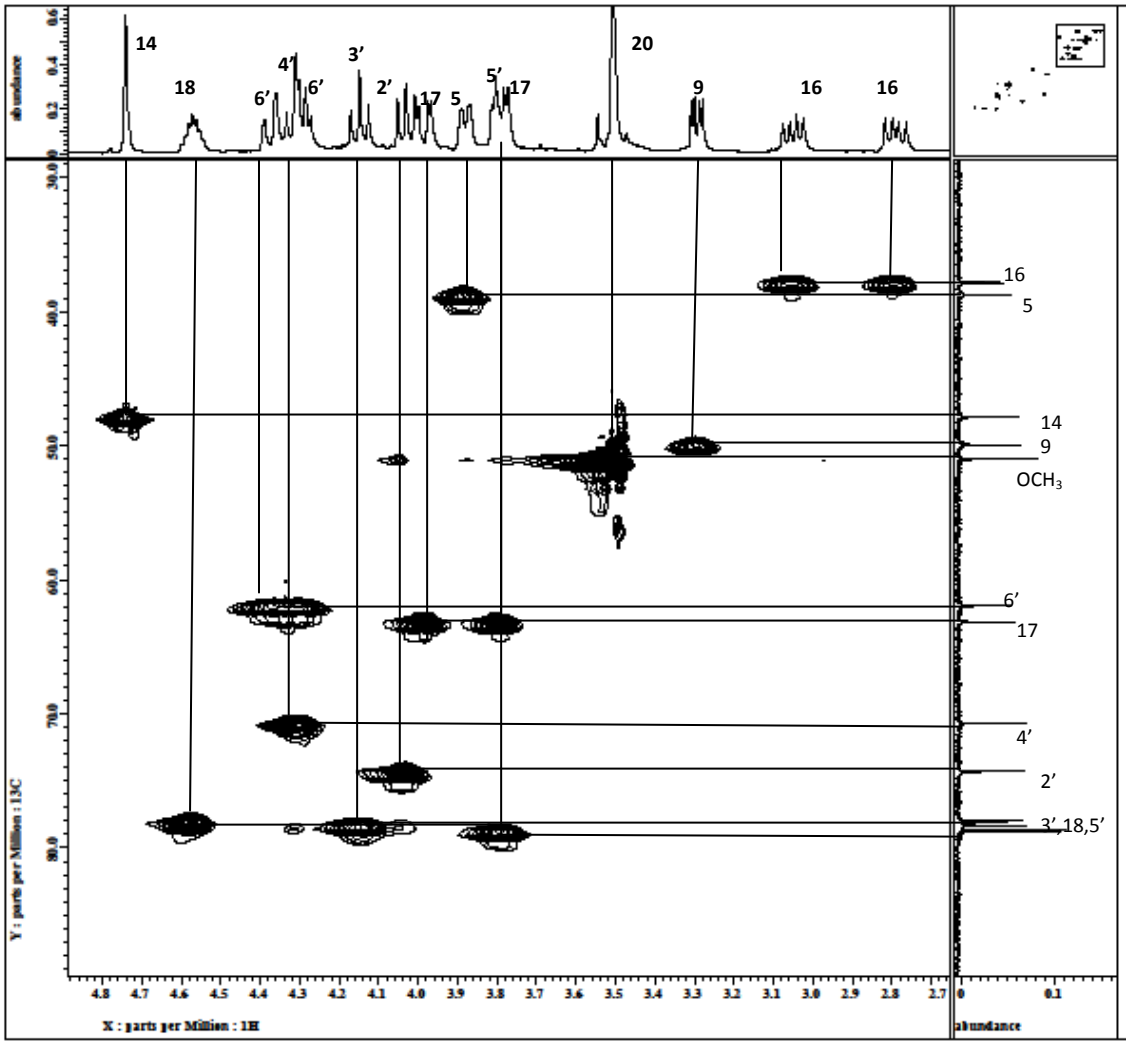

Figure 3.2.7.5b: HMQC spectrum of prismalayanoside **66** in C_5D_5N

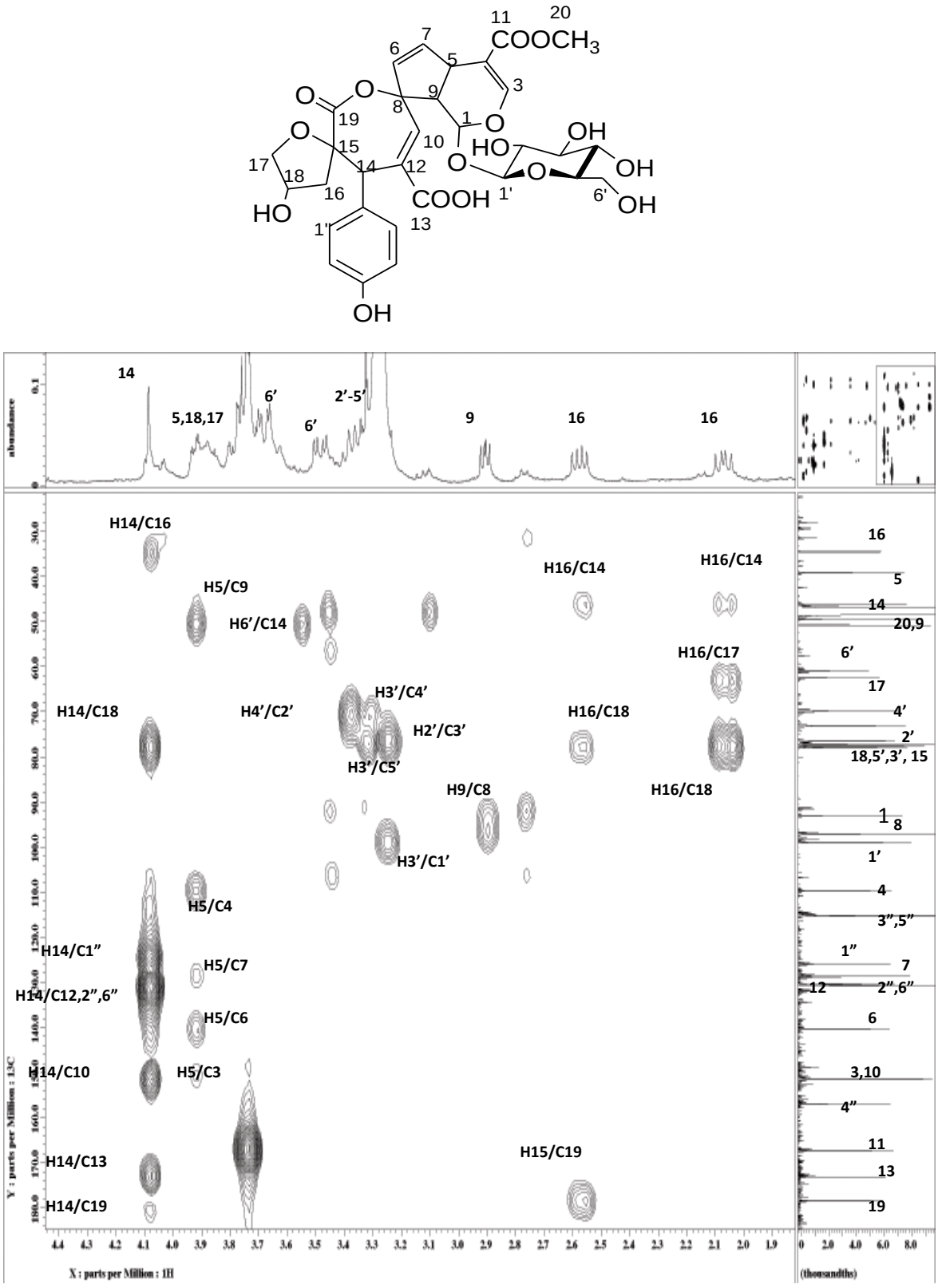

Figure 3.2.7.6a: HMBC spectrum of prismalayanoside **66** in MeOD

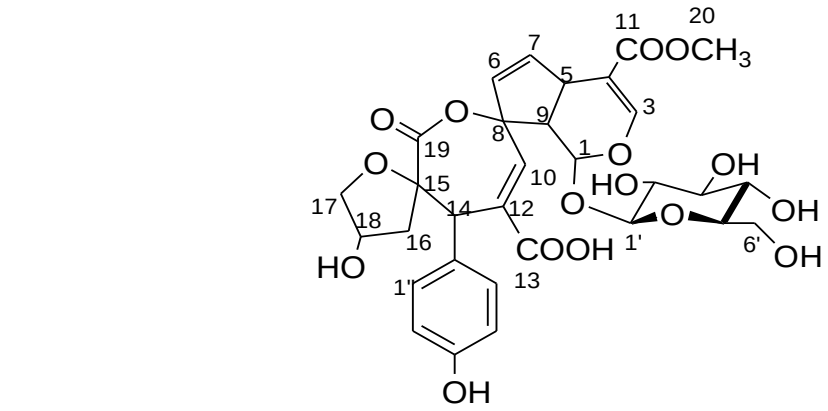

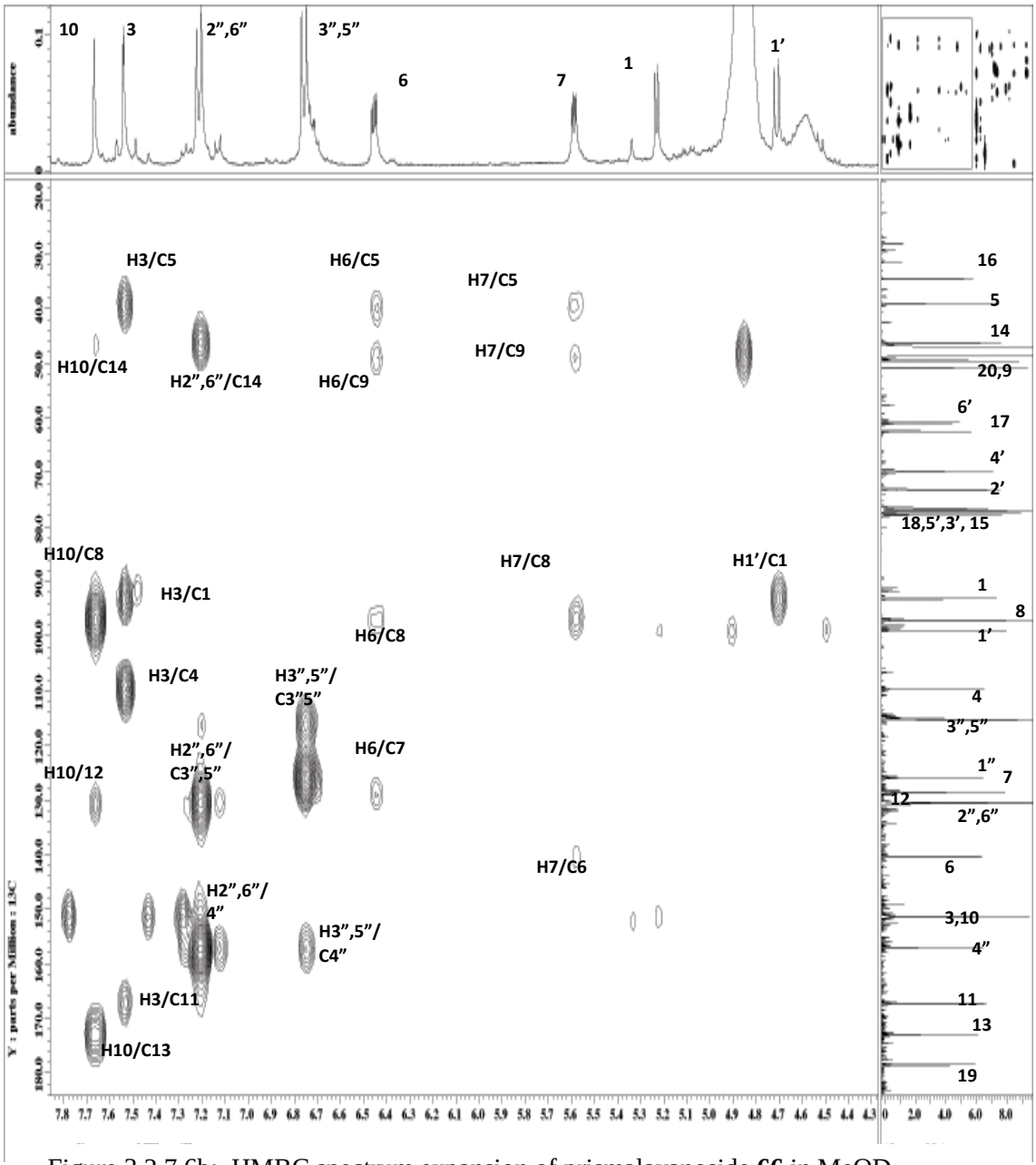

Figure 3.2.7.6b: HMBC spectrum expansion of prismalayanoside **66** in MeOD

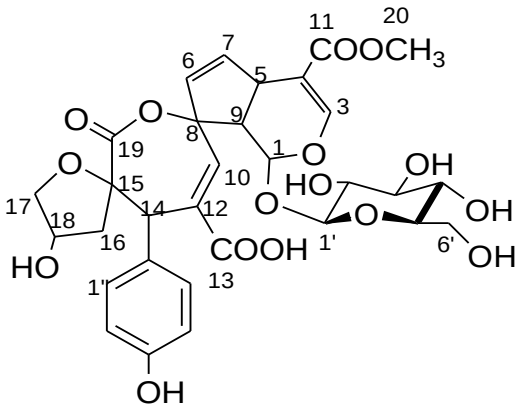

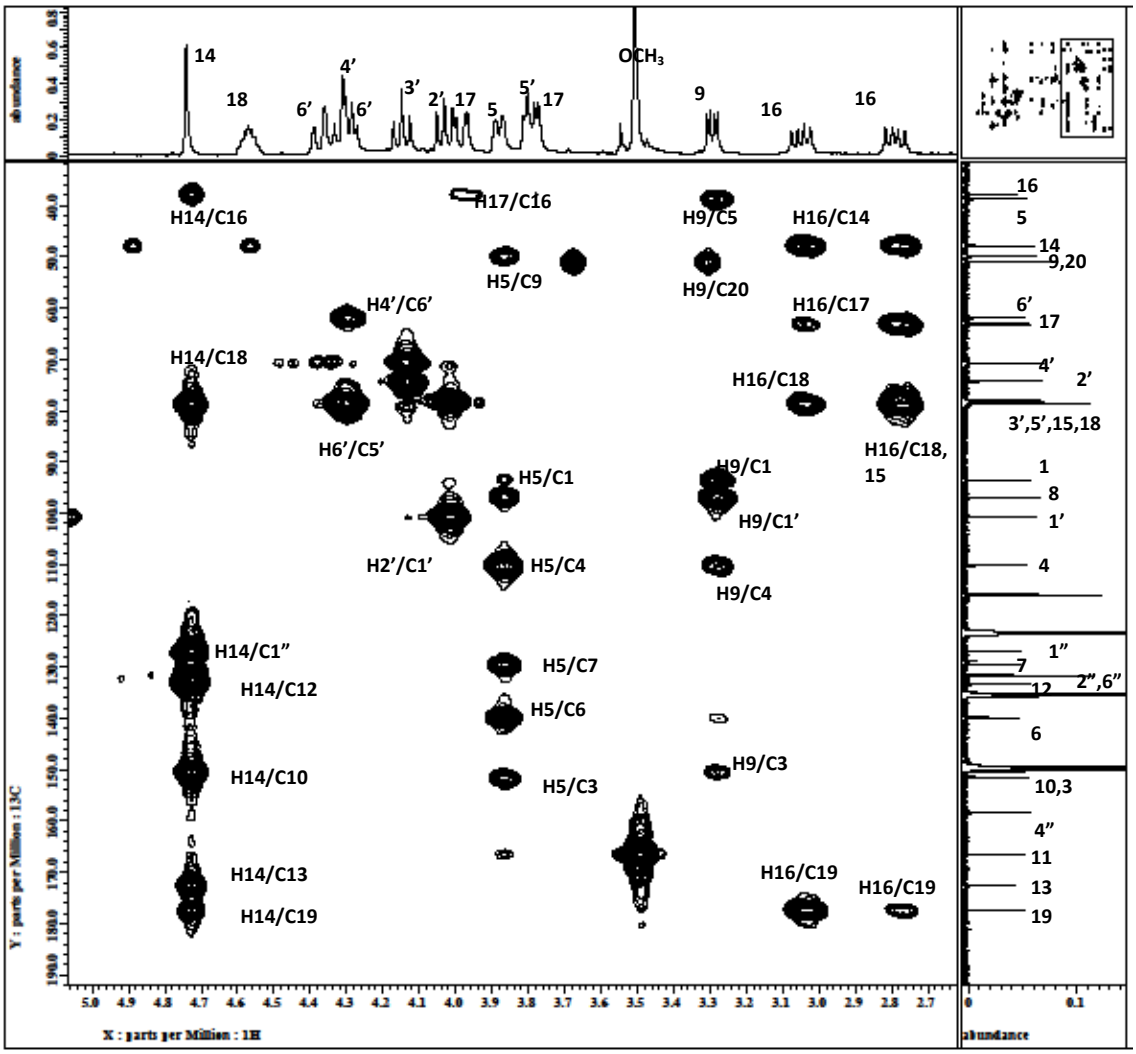

Figure 3.2.7.6c: HMBC spectrum expansion of prismalayanoside **66** in C_5D_5N

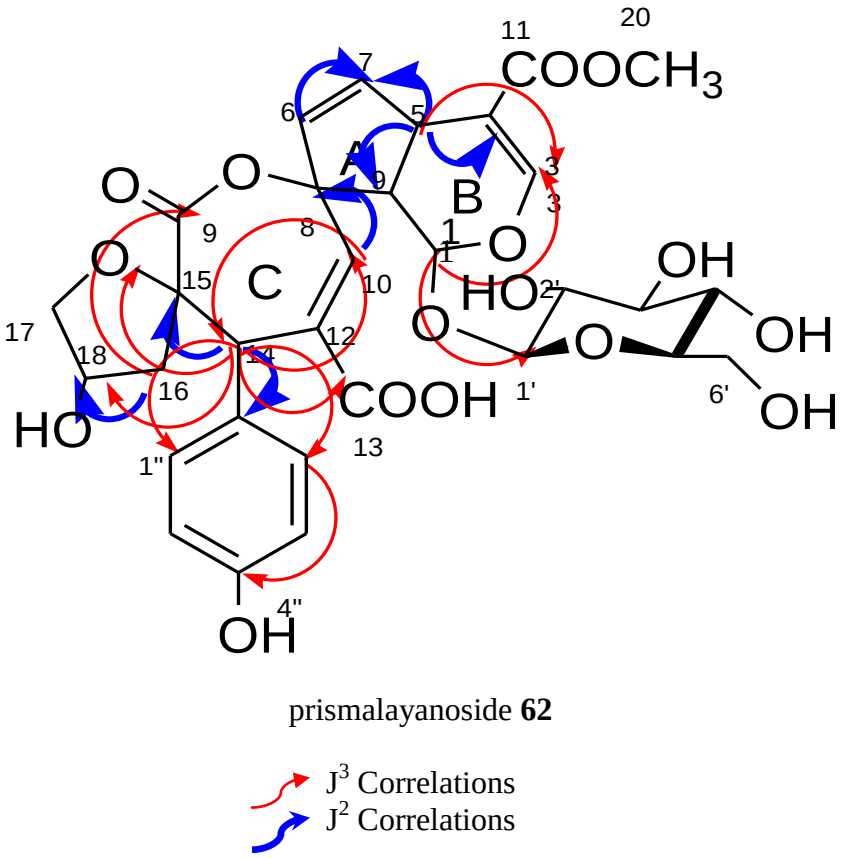

prismalayanoside **62**

Figure 3.2.7.7: Selected HMBC correlation of prismalayanoside **66**

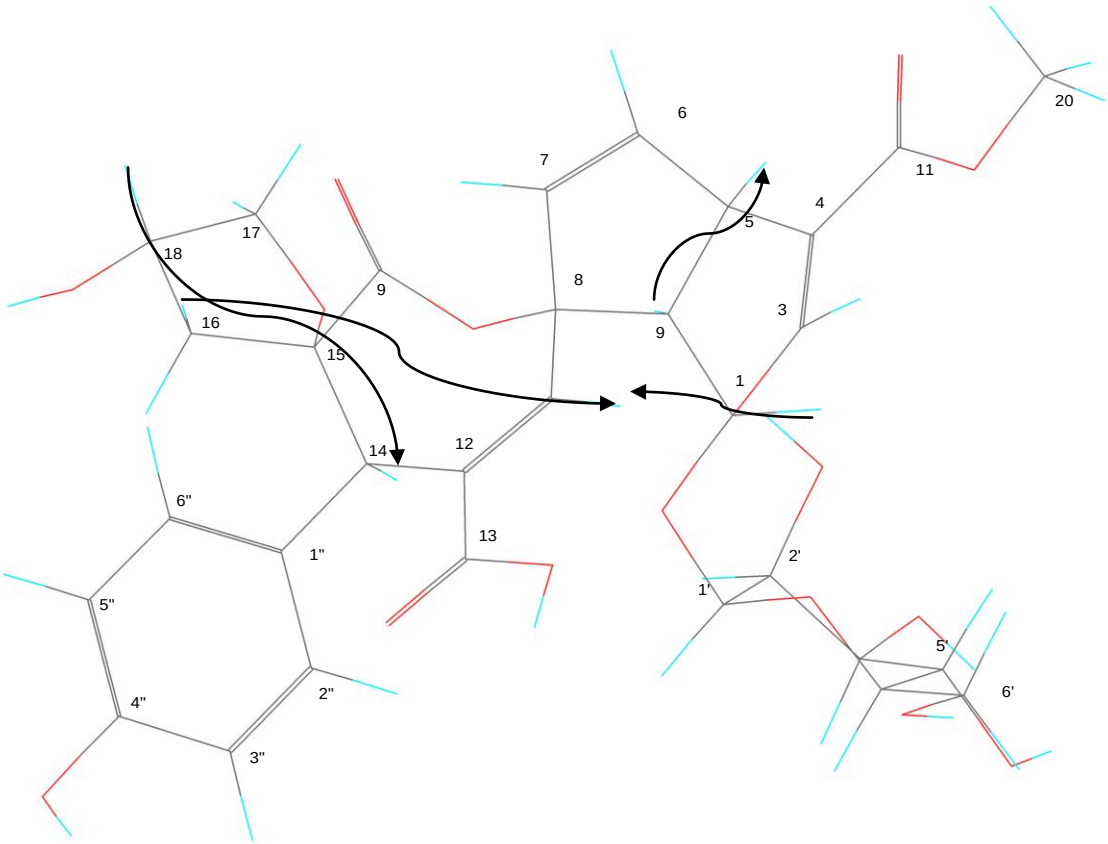

Figure 3.2.7.8: Selected NOESY correlation of prismalayanoside **66**

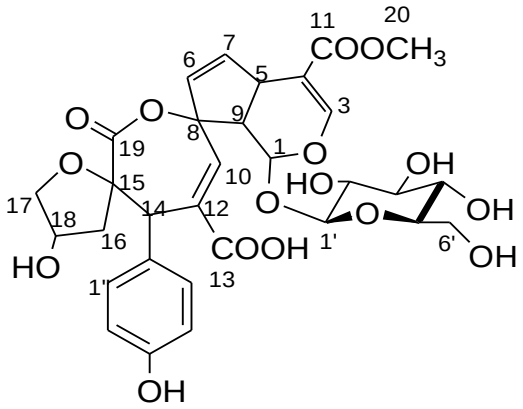

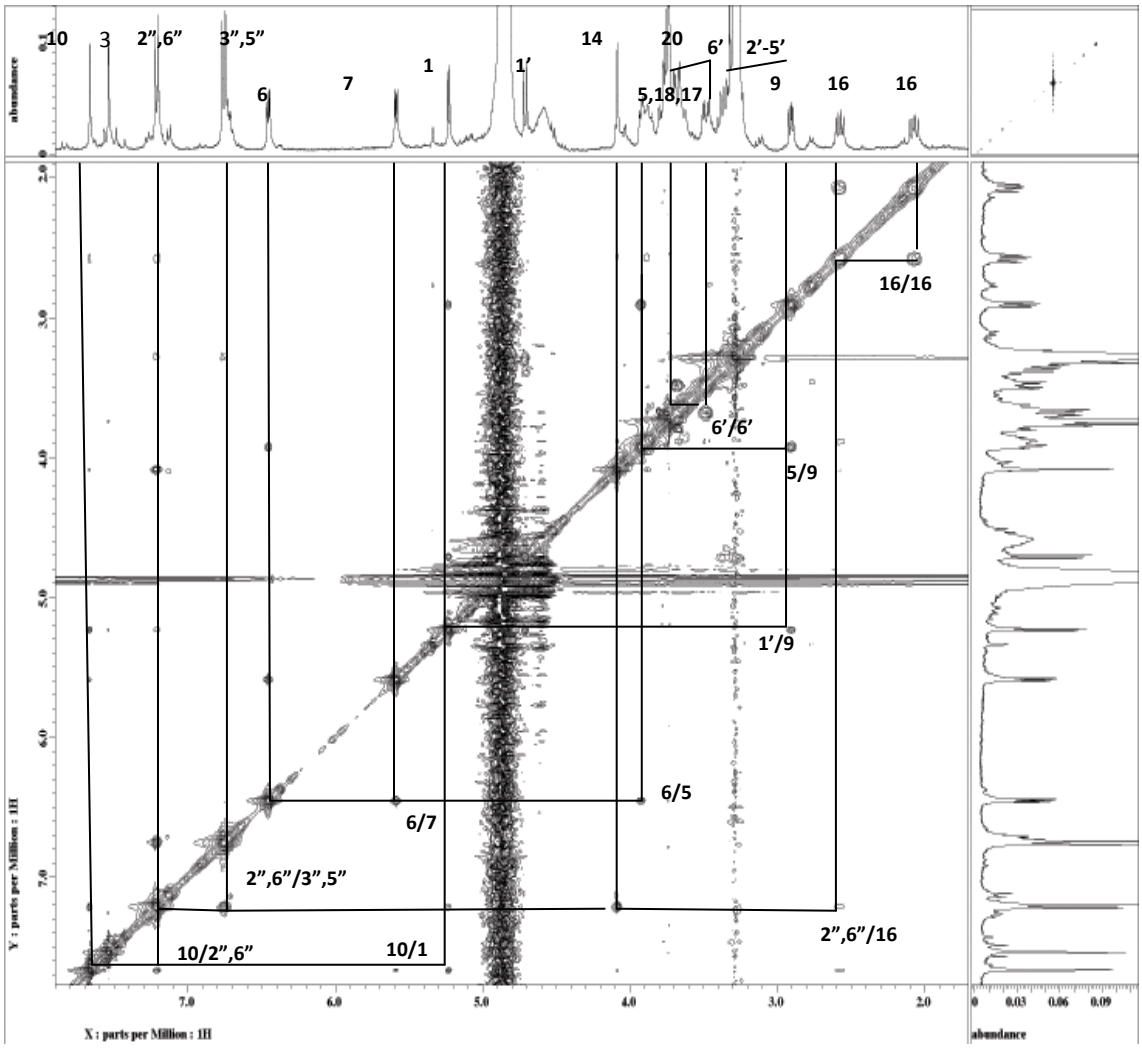

Figure 3.2.7.9: NOESY spectrum of prismalayanoside **66** in MeOD

3.2.8 Compound H: *Asperulosidic acid*

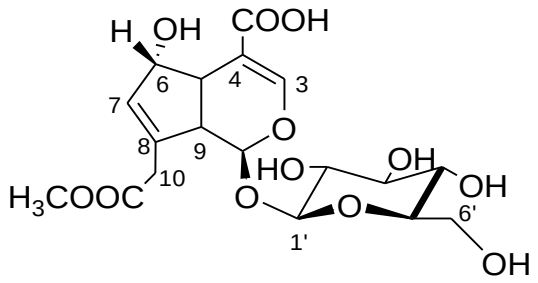

68

Asperulosidic acid **68 (**compound H) was isolated from the roots and leaves as brown amorphous powder. It produced the pseudo-molecular ion peak $[M-H]^+$ at m/z 431.11816 with ESI-MS which is consistent with molecular formula $C_{18}H_{24}O_{12}$. The IR spectrum indicated the presence of OH groups (3365 cm^{-1}) and the conjugated enol-ether system characteristic of an iridoid (1688 cm^{-1} and 1636 cm^{-1}) (Ling, 2003; Silverstein et al.,1991).

The ^1H NMR spectrum (figure 3.2.8.1) was characterized by a doublet for the H-1 at δ5.09 (*J*=9.0 Hz), a singlet for the H-3 (δ7.70), a doublet for the H-10 (δ4.85, *J*=15.8 Hz) (table 1.4.8.1). Another proton, H-5 and 9 resonated at δ3.01 (*t, J*=6.3 Hz) and δ2.65 (*t, J*=8.3 Hz), respectively. The anomeric proton of glucose (δ 4.77, *J*=7.8 Hz, H-1') and a singlet for H-7 (δ6.05). A strong peaks resonating at δ2.10 corresponding to three protons were attributable to the methyl protons attached to the carbonyl carbon.

The ^{13}C NMR (figure 3.2.8.2) and DEPT spectra (figure 3.2.8.3) indicate the presence of seventeen carbons; three quarternary carbons, eleven methines, two methylenes and one methyl group. A signal at δ170.6 corresponding to the carbonyl carbon attached to the methyl carbon the signal for which resonated at δ20.7 (table 3.2.8). Another carbonyl carbon resonated at δ172.6 could be assigned to C-11. The peaks at δ155.4 and

δ131.8 might be attributable to the methine sp^2 carbons at position C-3 and C-7, respectively.

The quartenary carbon of C-4 and C-8 resonated at δ108.1 and δ145.8 respectively. The peaks at δ101.2 and δ75.3 corresponded to the methine carbon type which were deshielded due to the oxygen neighbouring atom. Another signal at δ46.1 and δ42.3 and δ63.7 could be assigned to methine carbon C-9, C-5 and methylene carbon C-10 respectively. The former was deshielded due to the attachment to the oxygen atom. The HMQC spectrum (figure 3.2.8.4) of compound H shows the complete assignments of ^{1}H and ^{13}C signals.

As a result, by comparison of the spectroscopic data obtained from compound H with the literature values (Inouye et. al., 1969, Ling S.K., 2003), the former was confirmed to be asperulosidic acid **68**.

Table 3.2.8: ^{1}H NMR [300 MHz, δ_H (*J*, Hz)] and ^{13}C NMR [75 MHz, δ_C] of **68** in CD_3OD.

Position	**^{13}C***	**^{13}C**	**^{1}H(*J*,H)**	**^{1}H(*J*,H)***
1	101.1	101.1	5.09 (*d*, 9.0 Hz)	5.05
3	154.9	155.4	7.70*s*	7.62*d*
4	109.0	108.1	-	-
5	42.6	42.3	3.00*t*	3.02*t*
6	75.4	75.2	4.90*s*	4.90*s*
7	131.8	131.8	6.05*s*	6.01*d*
8	145.9	145.8	-	-
9	46.3	46.1	2.65*t*	2.62*t*
10	63.7	63.7	4.85, 4.94, *m*.	4.85*d* 4.94*d*
11	172.5	172.5	-	-
12				
$\underline{CO}OCH_3$	172.5	172.5	-	-
$CO\underline{OCH_3}$	20.8	20.8	2.10	2.09
1'	100.5	100.4	4.75	4.72*d*
2'	74.9	74.8	3.25-3.50*m*	3.24*m*
3'	78.5	78.3	3.25-3.50*m*	3.38*m*
4'	71.5	71.4	3.25-3.50*m*	3.26*m*
5’	78.5	78.1	3.25-3.50*m*	3.26*m*
6’	62.9	63.0	3.65, 3.90*m*	3.85(*dd*, 1.8, 12.0 Hz), 3.62 (*dd*, 6.0,12.0

* ^{1}H NMR [300 MHz, CD_3OD]
*^{13}CNMR [75MHz, CD_3OD]
Ling, 2003

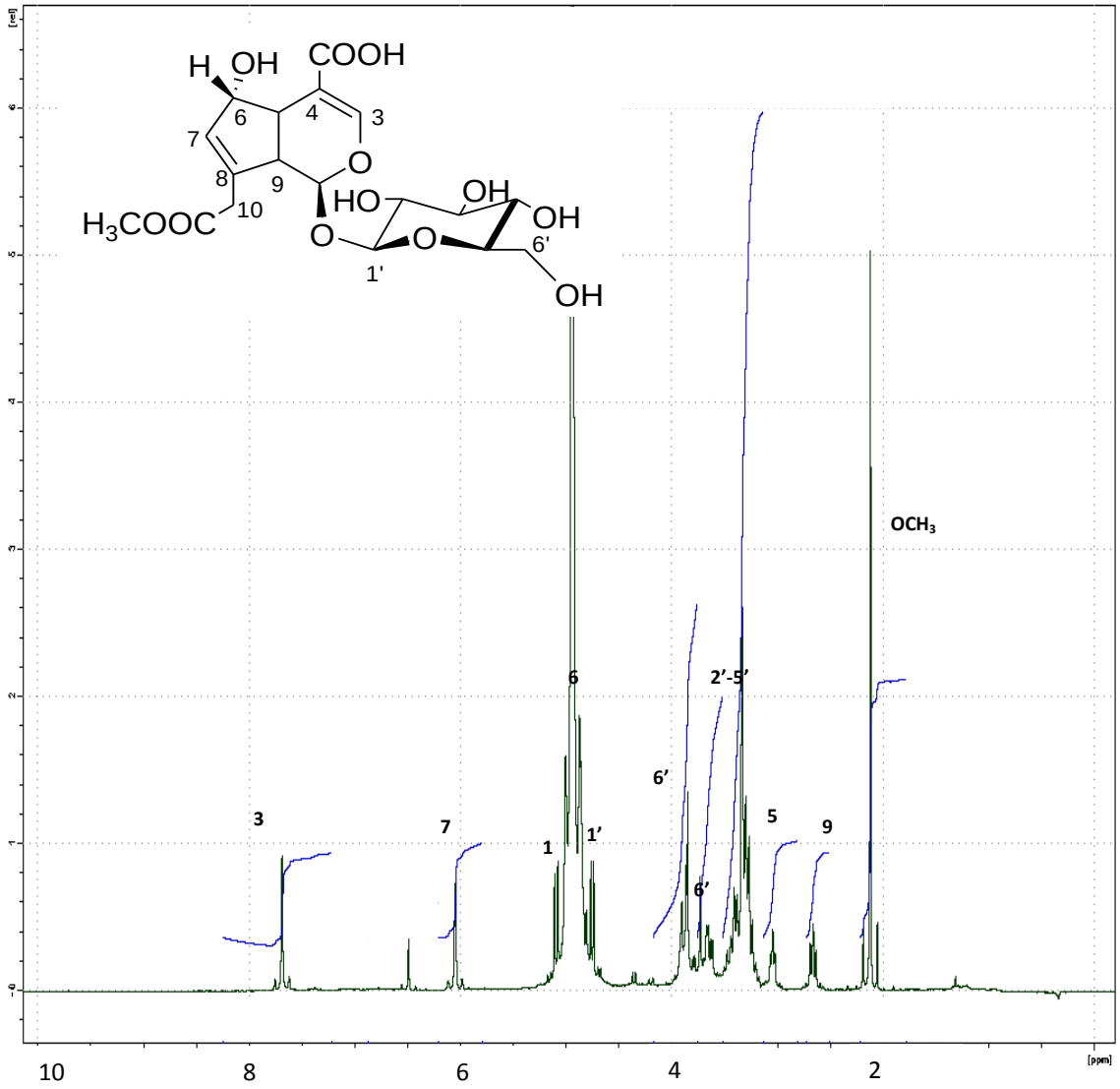

Figure 3.2.8.1: ^{1}H NMR spectrum of asperulosidic acid **68**

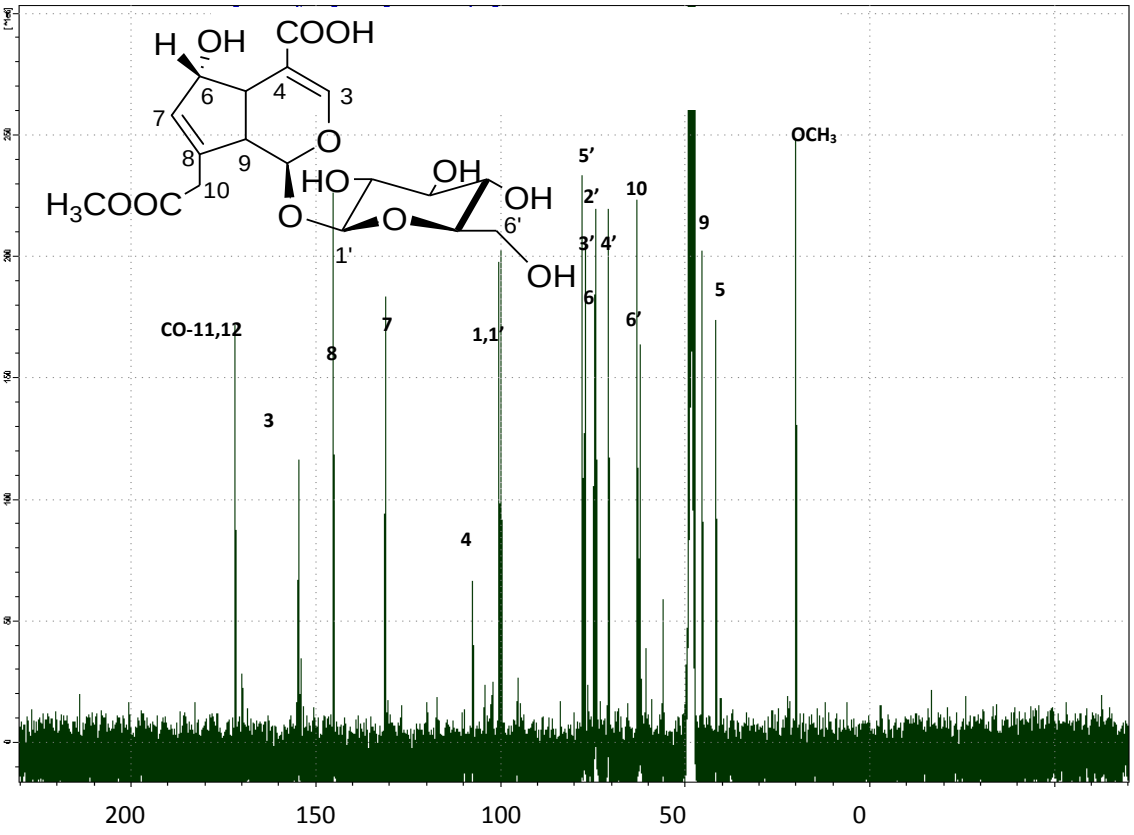

Figure 3.2.8.2: ^{13}C NMR spectrum of asperulosidic acid **68**

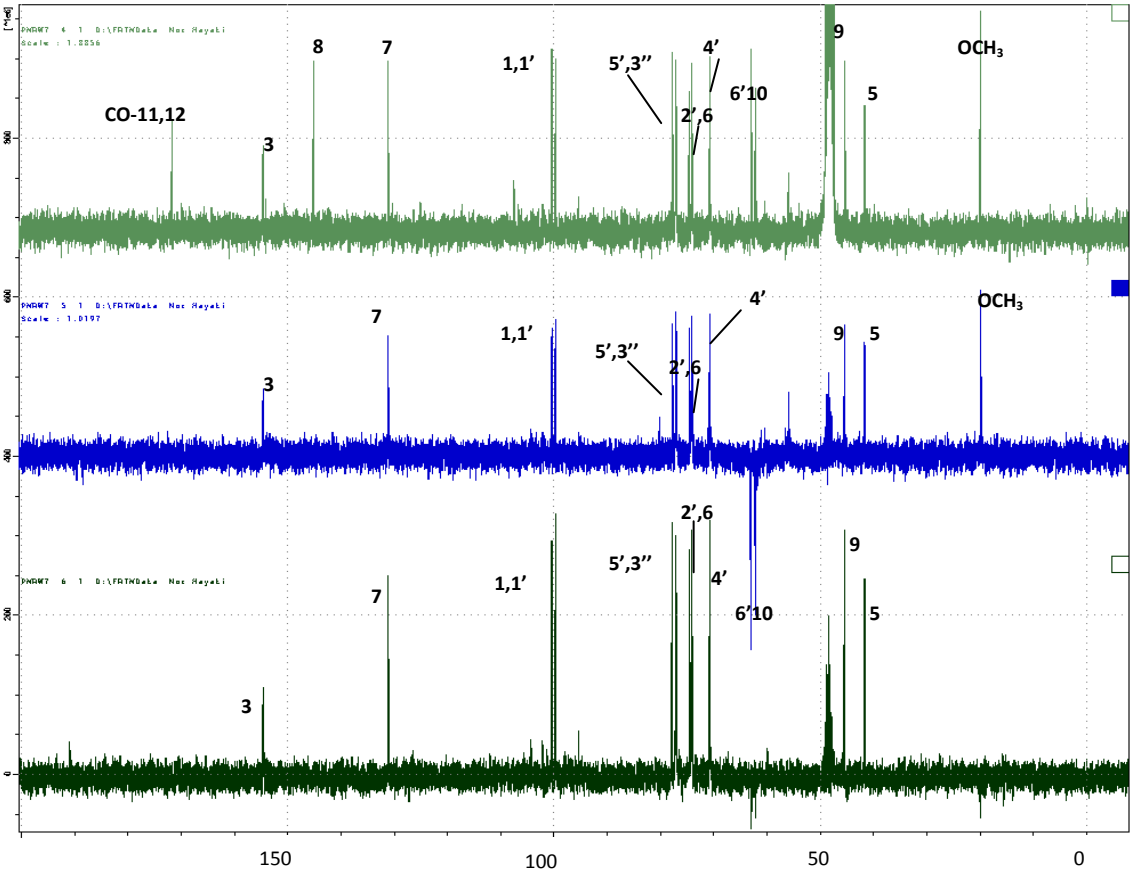

Figure 3.2.8.3: DEPT spectrum of asperulosidic acid **68**

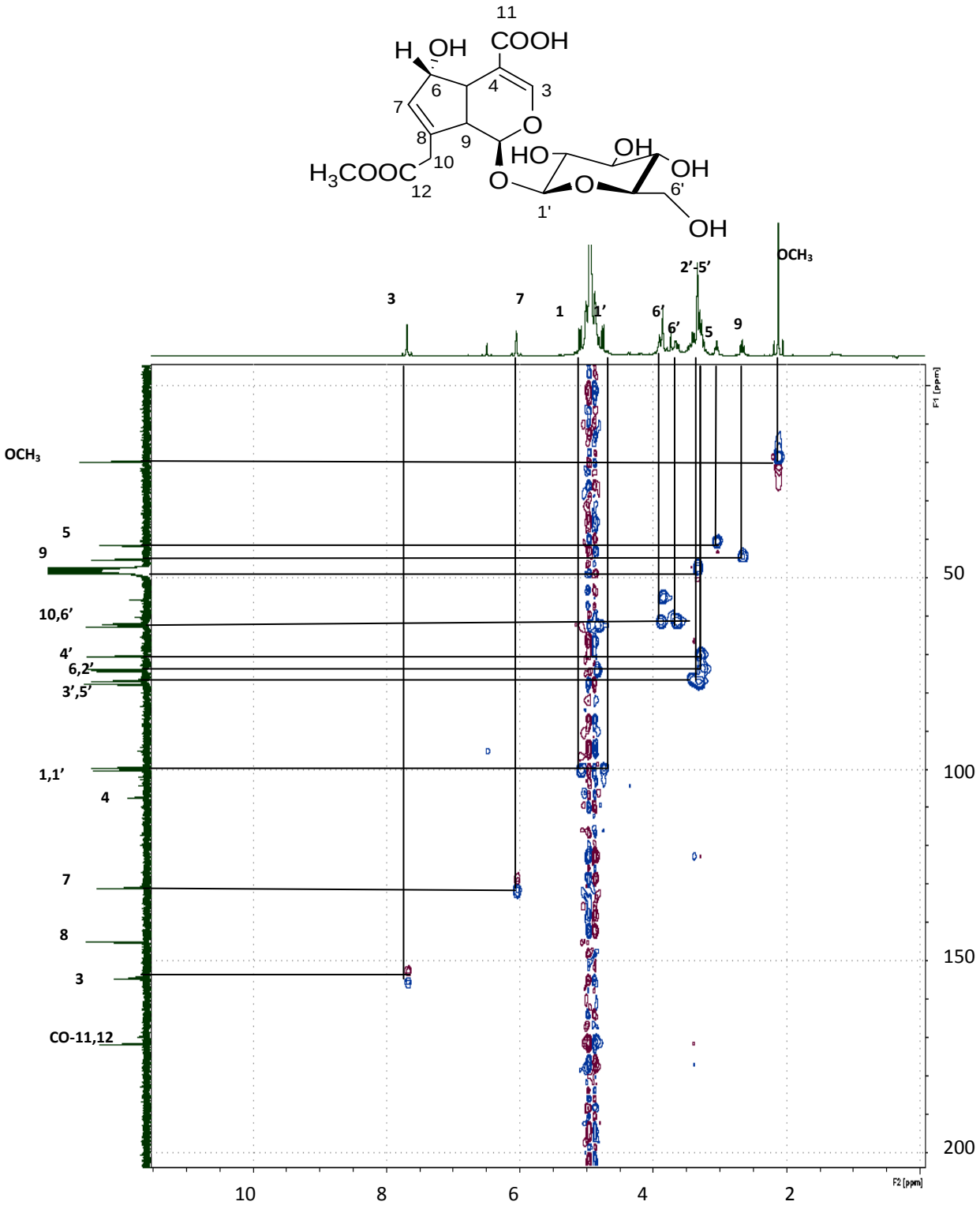

Figure 3.2.8.4: HMQC spectrum of asperulosidic acid **68**

3.2.9 Compound I: *Asperuloside*

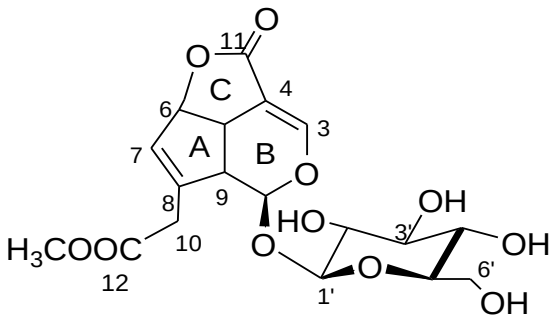

69

Asperuloside **69** (compound I) was isolated as white amorphous powder. It produced pseudo-molecular ion peak $[M+K]^+$ at m/z 453.11 with ESI-MS which is consistent with molecular formula $C_{18}H_{22}O_{11}$. Its IR spectrum showed the presence of OH groups (3360cm^{-1}) and a conjugated enol-ether system of an iridoid (1689 cm^{-1} and 1635cm^{-1}) (Ling, 2003) .

The ^{I}H NMR (figure 3.2.9.1) showed a broad singlet signal at δ7.35 for H-3 which is characteristic for the iridoids (table 3.2.9). Another signal resonated at δ5.98 (*bs*, 1H), δ5.74 (*bs*, 1H), δ5.59 (*d, J* =6.2 Hz) which assigned to H-1, H-7 and H-6 respectively. The signal for H-1 was shifted to lower field due to the steric effect of ring C. The steric effect also shifted the signal of H-5, H-9 and H-10 at δ3.70 (*m*, 1H), δ3.50 (*m*, 1H) and δ4.95 (*d, J*=14.7 Hz) and δ4.72 (*d, J*=14.7 Hz) respectively. The signal of H-10 was overlapped with the CD_3OD signal.

The anomeric proton, H-1', resonating at δ4.74 (*d, J*=7.8 Hz) clearly indicated that the dissacharide moiety should be in a pyranoside form. Other signals for the glucose protons (H-2', H-3', H-4', H-5') resonated between δ4.0 – δ3.2.

Finally, by comparison of the obtained spectroscopic data with the literature review (Briggs, 1963, Inouye, 1970, Ling, 2003), compound I was identified as asperuloside **69**.

Table 3.2.9: ^{1}H NMR [300 MHz, δ_H (*J*, Hz)] and ^{13}C NMR [75 MHz, δ_C] of **69** in CD_3OD.

	^{13}C*	**^{13}C**	**^{1}H(*J*,H)***	**^{1}H(*J*,H)**
1	93.3	92.3	5.95(*brs*, *J*=1.5 Hz)	5.98*bs*
3	150.3	153.7	7.29 (*d*, *J*=2.1 Hz)	7.35*bs*
4	106.1	105.1	-	-
5	37.4	36.4	3.64*m*	3.70*m*
6	86.3	85.3	5.56 (*d*, *J*=6.3 Hz)	5.59 (*d*, *J*=6.2 Hz),
7	128.9	127.9	5.73 *bs*	5.74 *bs*
8	144.2	143.2	-	-
9	45.2	44.2	3.34*m*	3.5*m*
10	61.9	60.3	4.9 (d, *J*=15.3 Hz), 4.8 (*d*, *J*=15.3 Hz)	4.95 (*d*, *J*=14.7 Hz), 4.72 (*d*, *J*=14.7 Hz)
11	172.2	171.4	-	-
12	172.2	171.6	-	-
OCH_3	20.6	19.7	2.08*s*	2.10*s*
1'	100	98.9	4.67 (*d*, *J*=8.1 Hz)	4.74(*d* , *J*=7.8 Hz)
2'	74.6	73.6	3.19 (*dd*, *J*= 8.1, 9.0 Hz)	3.19*m*
3'	77.8	76.8	3.38 (*t*, *J*=9.0 Hz)	3.40*m*
4'	71.5	70.5	3.27 (t, *J*=9.0 Hz)	3.3*m*
5’	78.3	77.3	3.3*m*	3.4*m*
6’	62.5	61.7	3.92 (*dd*, *J*= 2.1, 12.0 Hz), 3.67 (*dd*, 6.0,12.0Hz)	3.97*m*, 3.69*m*

* ^{1}H NMR [300 MHz, CD_3OD]
*^{13}C NMR [75MHz, CD_3OD]
(Ling, 2003)

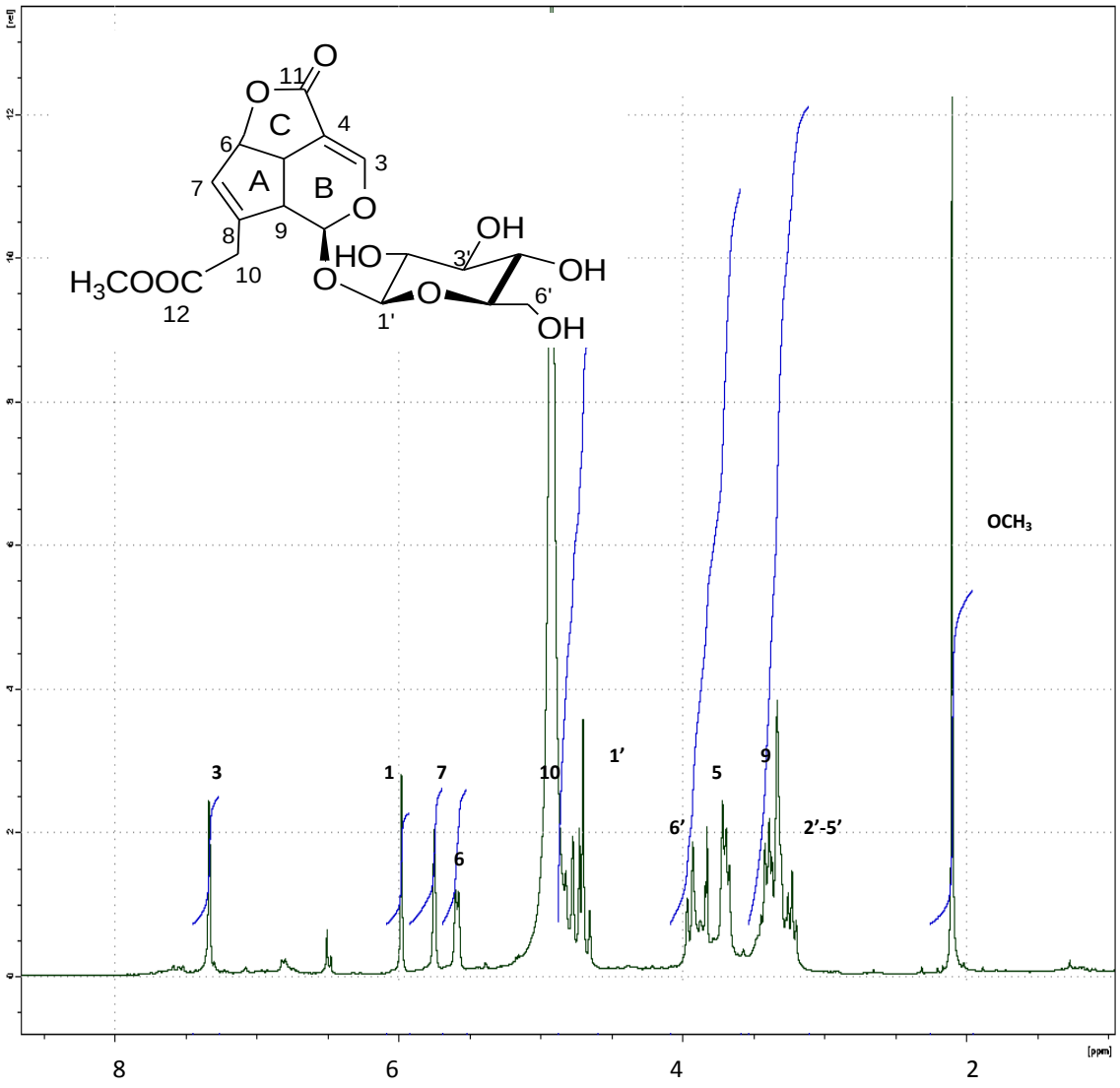

Figure 3.2.9.1: ^{1}H NMR spectrum of asperuloside **69**

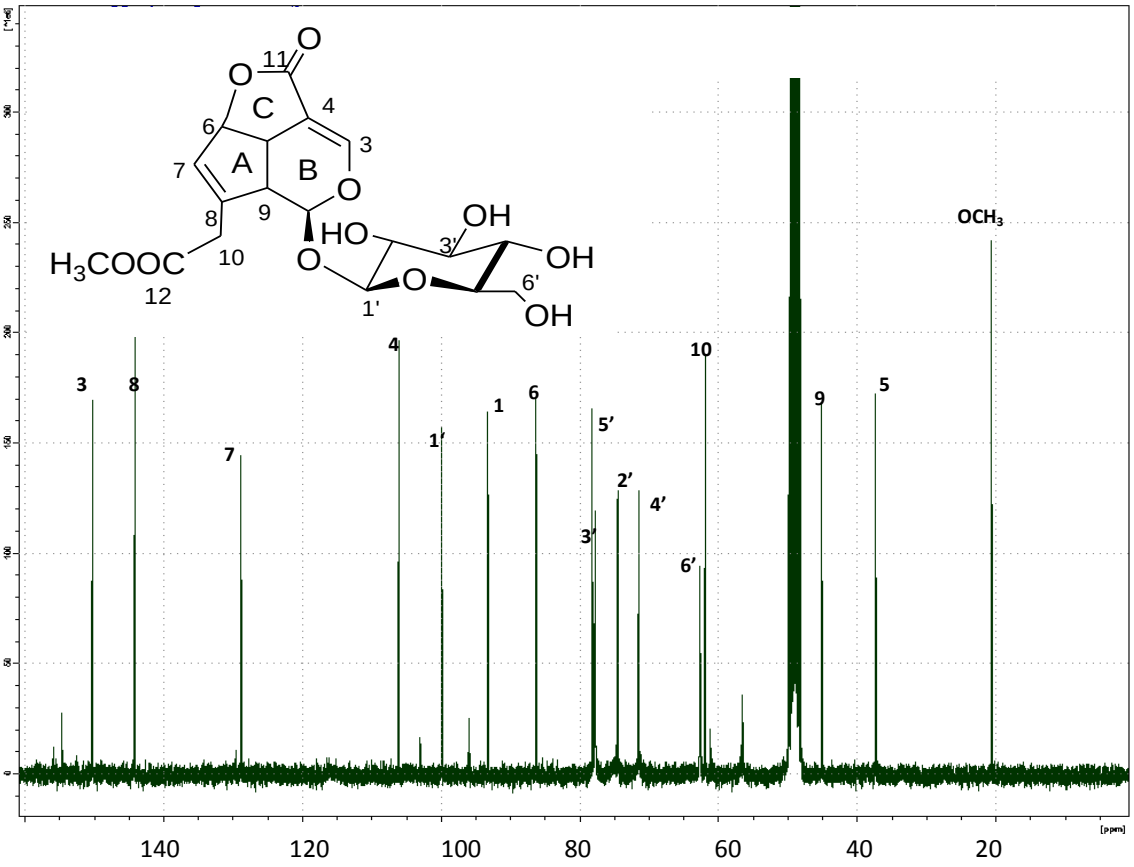

Figure 3.2.9.2: ^{13}C NMR spectrum of asperuloside **69**

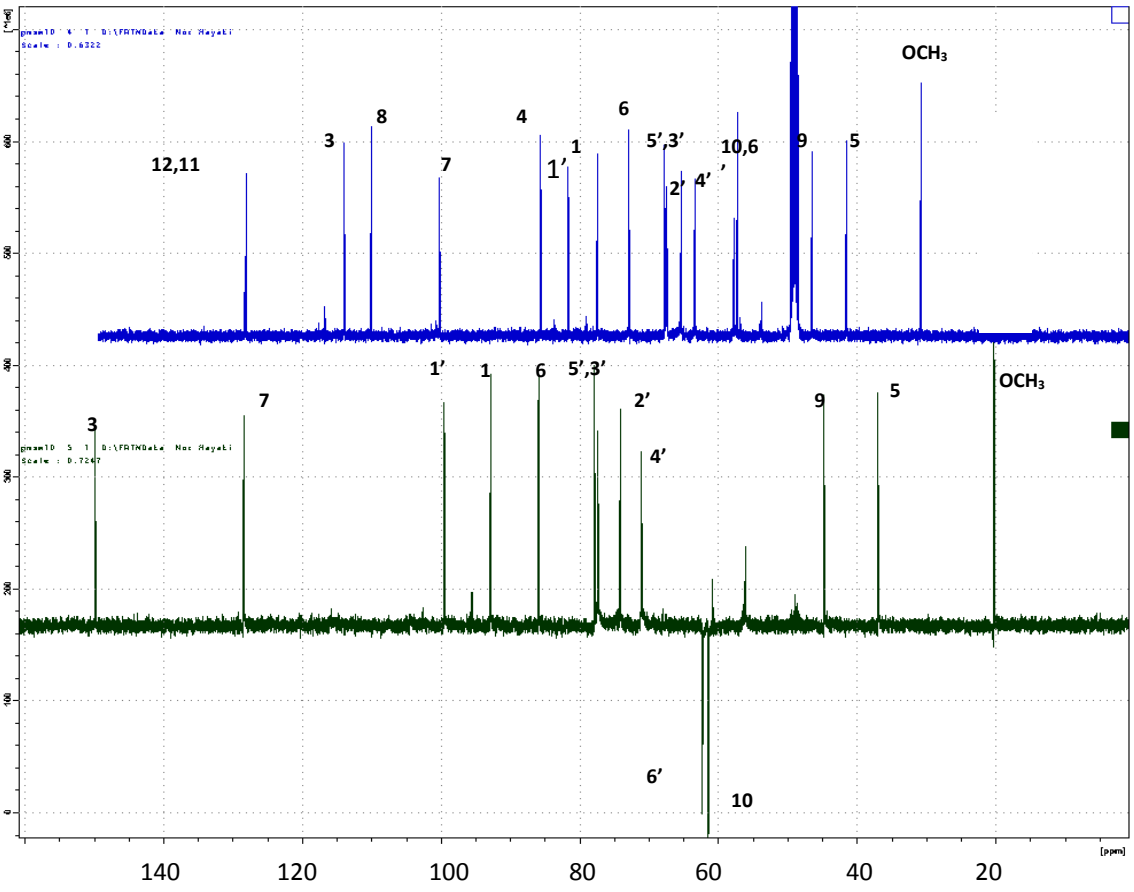

Figure 3.2.9.3: DEPT spectrum of asperuloside **69**

3.2.10 Compound J: *Scandoside*

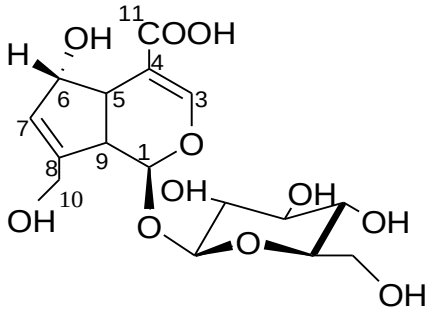

70

Scandoside **70** (compound J) was isolated as brown amorphous powder. It produced pseudo-molecular ion peak $[M-H]^-$ at m/z 389.10745 with ESI-MS which is consistent with molecular formula $C_{16}H_{22}O_{11}$. Its IR spectrum showed a broad signal at 3369 cm^{-1} for OH and a sharp signal at 1635 cm^{-1} for the presence of C=O group (Silverstein et al.,1991).

The ^1H NMR (figure 3.2.10.1) showed a broad singlet (table 3.2.10) for the H-3 characteristic of iridoids at δ7.66. Another signals observed at δ5.09 (*d*, *J*=9.0 Hz, H-1), δ2.55 (*t*, *J*=8.0 Hz, H-9). An oxymethylene proton of H-10 appear at δ4.50 and δ4.25 as two doublet (*J*=15.8 and *J*=15.6 Hz). The anomeric proton resonating at δ4.76 (H-1', *d*, *J*=7.8 Hz) clearly indicated that the sacharide moiety should be in a pyranoside form (Ling, 2003). The sequential *trans* diaxial relationship of H-1' to H-5' (*J*=9.0-9.5 Hz), with the corresponding carbon signals established that the sugar unit was that of a β-glucopyranosyl moiety. Other signals for the glucose resonated at δ3.89 and δ3.67 (H-6', 2xd, *J*=11.8 Hz).

The ^{13}C NMR (figure 3.2.10.2, table 3.2.10) indicated the glucose signals at δ99.2, δ77.4, δ76.8, δ73.9, δ70.6 and δ61.8 represent C-6', C-1', C-3' ,C-2', C-4' and C-5' respectively which experience the deshielding effect due to the neighbouring oxygen atom. The two sp^2 carbons *i.e* C-3 and C-7 gave signals at δ150.3, δ128.8 respectively. The C-3 experienced a deshielding effect from the C=O of the carboxylate moiety due to its β position from the group. The C-6, C-1 and C-10 gave rise to down field signal at δ74.4, δ100.4 and δ60.7 respectively due to the deshielding effect of the next oxygen atom. The signals at δ41.7, δ44.8, δ150.4 and δ107.6 could be attributable to C-5, C-9, C-8 and C-4 respectively.

Figure 3.2.10.3 showed the DEPT spectrum of compound J. This spectrum distinguished the C, CH, CH_2 and CH_3 signals present in this compound. Figure 3.2.10.5 showed the COSY spectrum of compound J and this provides further support for the proton assignments from the ^1H NMR spectrum. The ^1H-^1H COSY correlation was shown in figure 3.2.10.4. HMQC spectrum in figure 3.2.10.5 showed the C-H correlation of compound J.

Analysis of all spectral data obtained and comparison with literature (Inouye et al., 1968, Ling, 2003) led to the conclusion that compound J was assigned as scandoside **70**.

Table 3.2.10: ^{1}H NMR [300 MHz, δ_H (*J*, Hz)] and ^{13}C NMR [75 MHz, δ_C] of **70** in CD_3OD

	^{13}C*	**^{13}C**	**^{1}H(*J*,H)**	**^{1}H(*J*,H)***
1	101.1	100.4	5.09 (*d*, 9.0 Hz)	4.97 (*d*, 9.0 Hz)
3	153.2	150.3	7.66*s*	7.48 (*d*, 1.5Hz)
4	111.6	107.6	-	-
5	43.4	41.7	3.05*bt*	3.04 (*ddt*, 1.5, 6.3, 8.4 Hz)
6	75.8	74.4	4.90*m*	4.88*m*
7	129.7	128.8	6.03*s*	5.98 (*d*, 2.1 Hz)
8	151.5	150.4	-	-
9	46.2	44.8	2.55 (*t*, 8.0 Hz)	2.52 (*dd*, 8.1, 8.4 Hz)
10	61.8	60.7	4.50 (*d*, 15.8 Hz)	4.45 (*d*, 15.9 Hz)
			4.25 (*d*, 15.6 Hz)	4.20 (*d*, 15.9 Hz)
11	173.9		-	-
1'	75.0	70.6	4.76 (*d*, 7.7 Hz)	4.72 (*d*, 8.1 Hz)
2'	77.8	76.8	3.40(d, 9.0 Hz)	3.23 (*dd*, 8.1, 9.3 Hz)
3'	71.6	73.9	3.2-3.2 *m*	3.4 (*t*, 9.3 Hz)
4'	78.5	77.4	3.2-3.2 *m*	3.26*m*
5'	62.8	61.8	3.2-3.2 *m*	3.26*m*
			3.89 (*d*, 11.7 Hz),	3.84 (*dd*, 2.0, 12.0 Hz)
6'	100.3	99.2	3.67 (*d*, 11.8 Hz)	3.65 (*dd*, 5.4, 12.0 Hz)

* ^{1}H NMR [300 MHz, CD_3OD]

*^{13}CNMR [75MHz, CD_3OD]

(Ling, 2003)

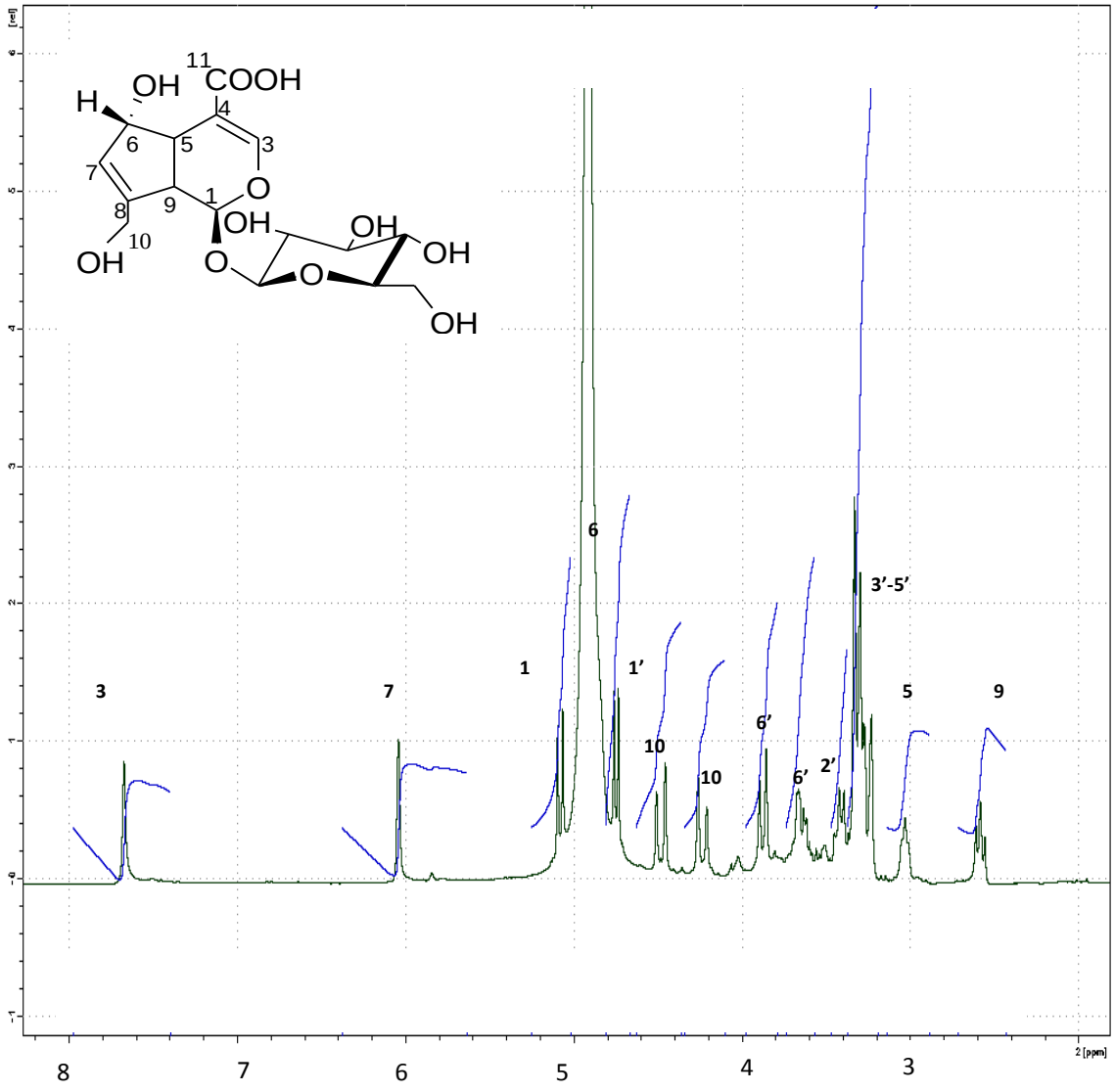

Figure 3.2.10.1: ^{1}H NMR spectrum of scandoside **70**

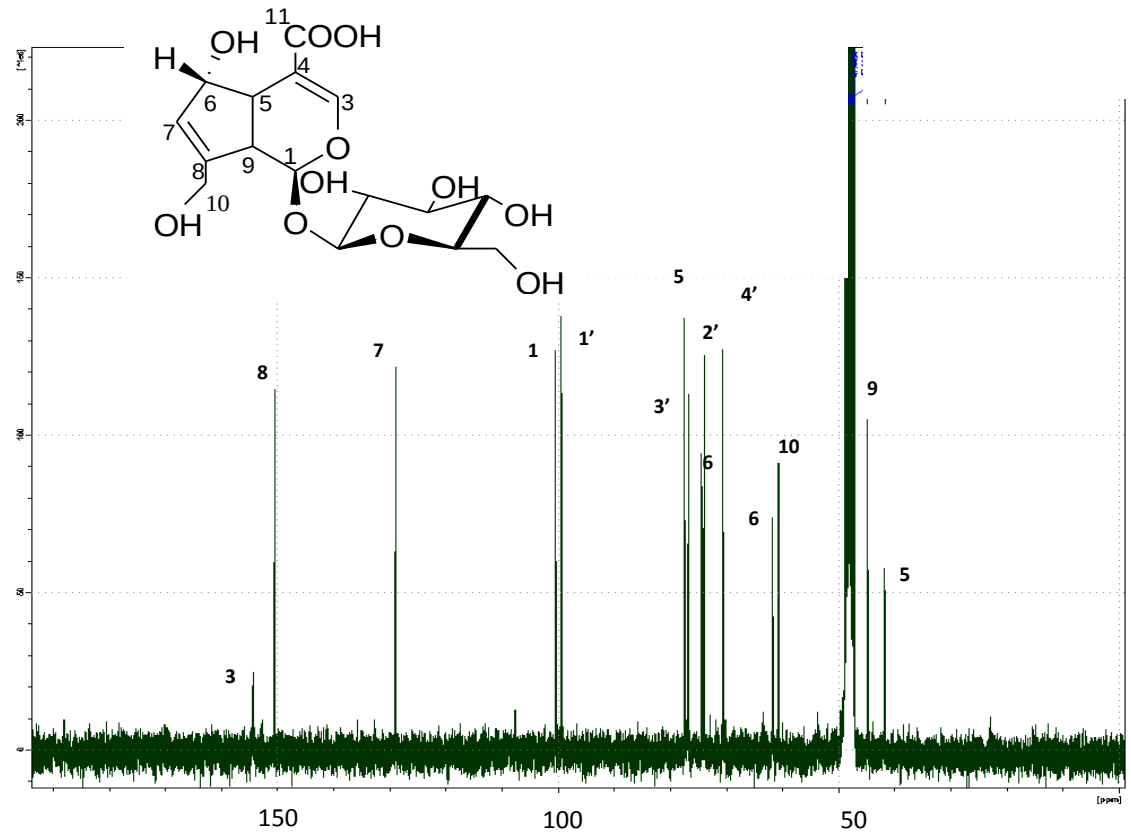

Figure 3.2.10.2: ^{13}C NMR spectrum of scandoside **70**

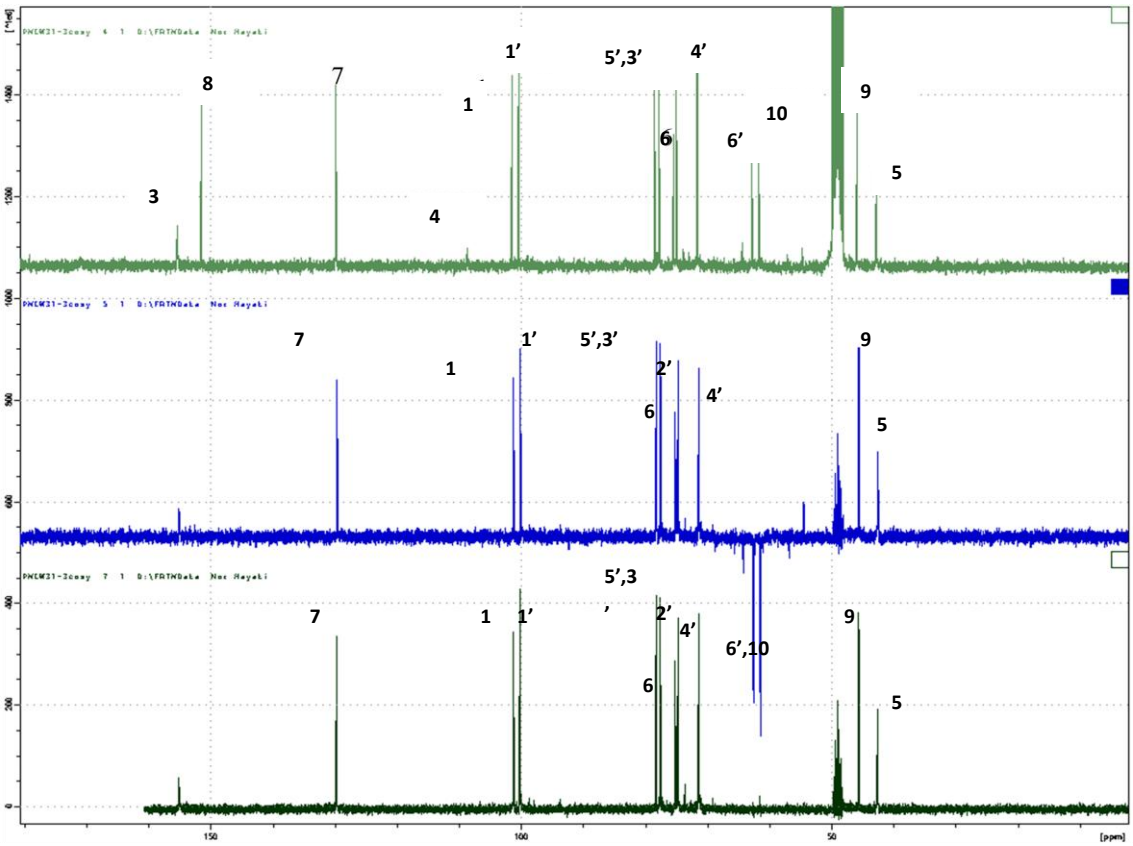

Figure 3.2.10.3: DEPT spectrum of scandoside **70**

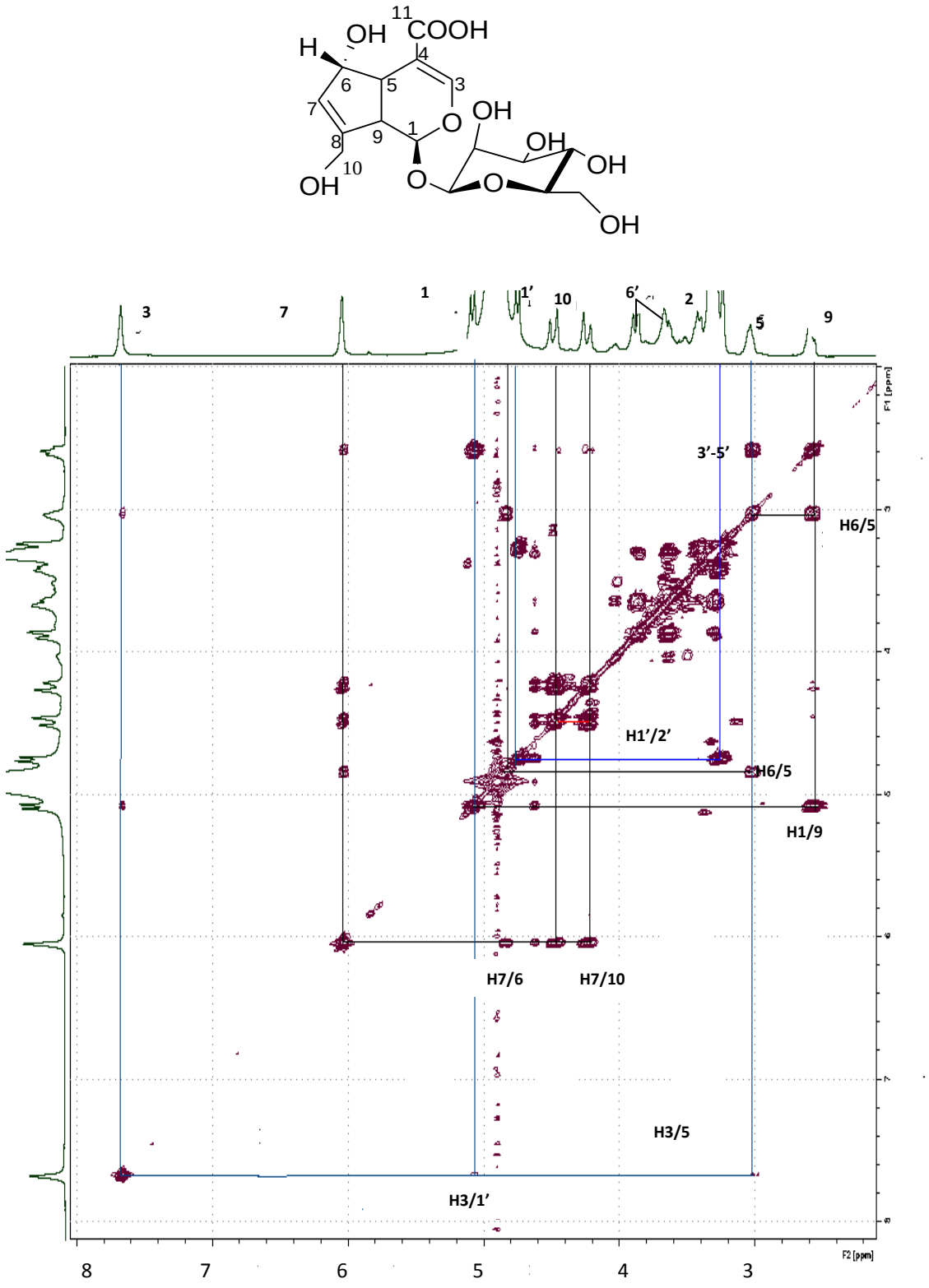

Figure 3.2.10.4: COSY spectrum of scandoside **70**

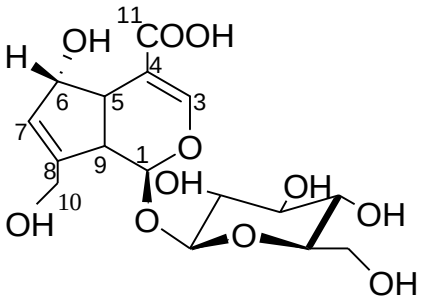

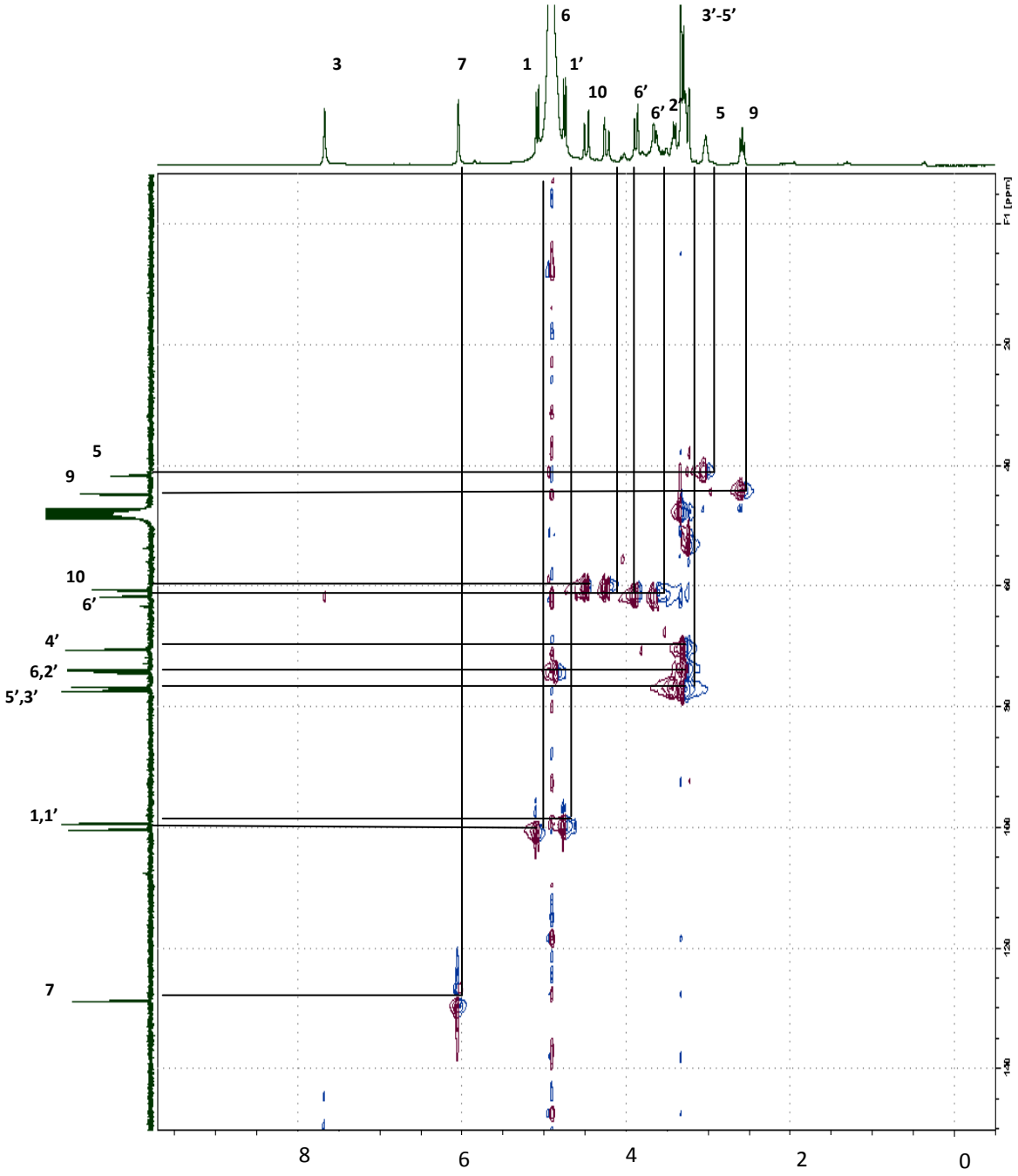

Figure 3.2.10.5: HMQC spectrum of scandoside **70**

3.2.11 Compound K: *Lucidin-3-methyl ether*

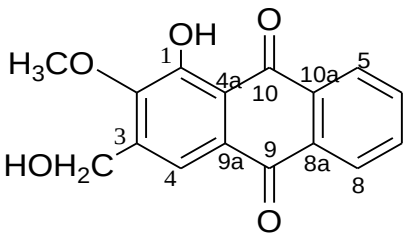

71

Lucidin-3-methylether (4-hydroxy-2-hydroxymethyl-3-*O*-methoxy-9,10-anthraquinone) **71** (**c**ompound K) was isolated as yellow amorphous powder. It produced pseudo-molecular ion peak $[M - H]^-$ at m/z 283.05963 with ESI-MS which is consistent with molecular formula $C_{16}H_{12}O_5$. The UV spectrum recorded in methanol showed maximum absorption at 283, 247, 203 nm. The IR spectrum exhibits absorption due to OH groups (3306 cm^1) and a strong signal of C=O (1647 cm^{-1}) (Silverstein et al., 1991).

The ^{1}H NMR (figure 3.2.11.1) showed one methoxy peak at δ 3.64 (s, 3H), one oxymethylenes at δ 4.86 (s, 3H), aromatic proton signals at δ8.9 (*dd*, J_1=2.1, J_2=8.1 Hz, H-5), 8.18-8.27*m* (H-6, 7) and 8.40 (*dd*, J_1=2.1, J_2=8.1 Hz, H-8). The data demonstrate a similarity to those of damnacanthol **69** but with additional one singlet peak resonated at δ13.17. It was the chelated proton from the hydroxyl group attached to C-1. Thus, it makes this compound different from damnacanthol **71**.

Its ^{13}C NMR (figure 3.2.11.2) showed 16 signals for all the carbons present in this anthraquinone. The complete assignments were summarized in table 3.2.11 also similar to those of damnacanthol **71.** The ^{13}CNMR spectrum of this compound indicated the presence of eight quarternary carbons, six methines, one methylene and one methyl

group. The methine carbon which resonated at lower field of 109.7 was seen to have J_2 correlation to OH-1 in the HMBC spectrum (figure 3.2.11.3), thus supported its position at C-2. Another important J_2 correlation was between the oxymethylene (CH_2OH) and methoxy (CH_3OH) proton and carbon. The complete HMBC correlation was summarized in figure 3.2.11.4.

Hence, this compound was demonstrated to be 4-hydroxy-2-hydroxymethyl-3-*O*-methoxy-9,10-anthraquinone **71** (Kitajima et. al., 1998).

Table 3.2.11: ^{1}H NMR [300 MHz, δ_H (*J*, Hz)] and ^{13}C NMR [75 MHz, δ_C] of **71** in DMSO-d_6

	^{13}C	**^{1}H (*J*/H)**	**^{1}H (*J*/H)***
1	108.4	13.17*s*	13.14*s*
2	109.7		
3	164.9		
4	164.5	7.50*s*	7.45*s*
4a	134.5		
5	127.5	8.90 (*dd*, *J*=2.1, 8.1 Hz)	8.28-8.32*m*
6	135.3	8.18-8.27*m*	7.78-7.84*m*
7	135.2	8.18-8.27, *m*	7.78-7.84*m*
8	127.1	8.40 (*dd*, *J*=2.1, 8.1 Hz)	8.28-8.32*m*
8a	133.5		
9	182.3		
9a	117.4		
CH_2O	58.4	4.86*s*	4.89*s*
OCH_3	61.9	3.64*s*	4.06*s*
10a	133.6		
10	186.8		

* ^{1}H NMR [125.65MHz, DMSO-d_6], ^{13}C NMR [500 MHZ, DMSO-d_6] Kitajima et al., 1998

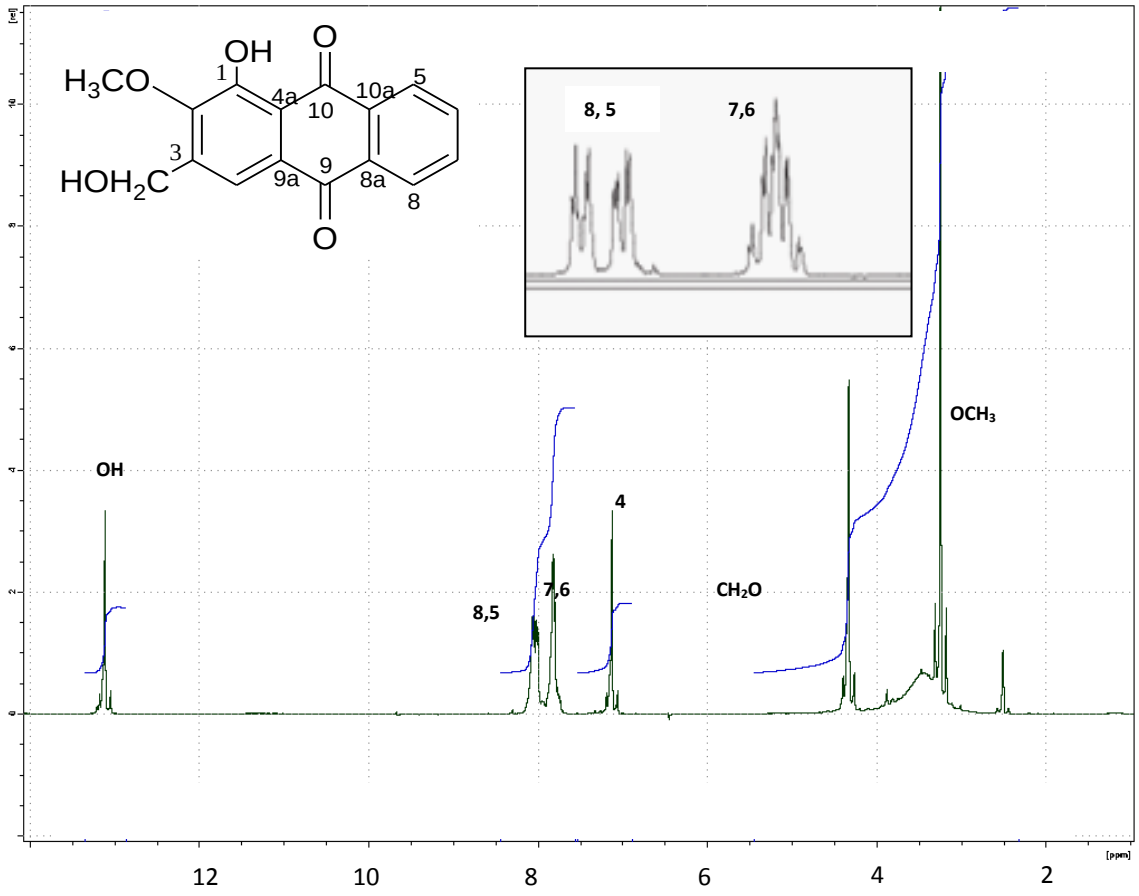

Figure 3.2.11.1: ^{1}H NMR spectrum of lucidin -3-methyl ether **71**

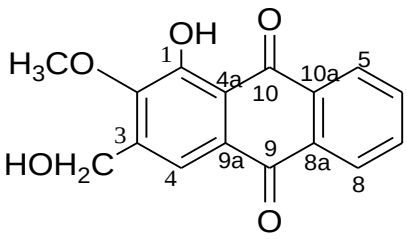

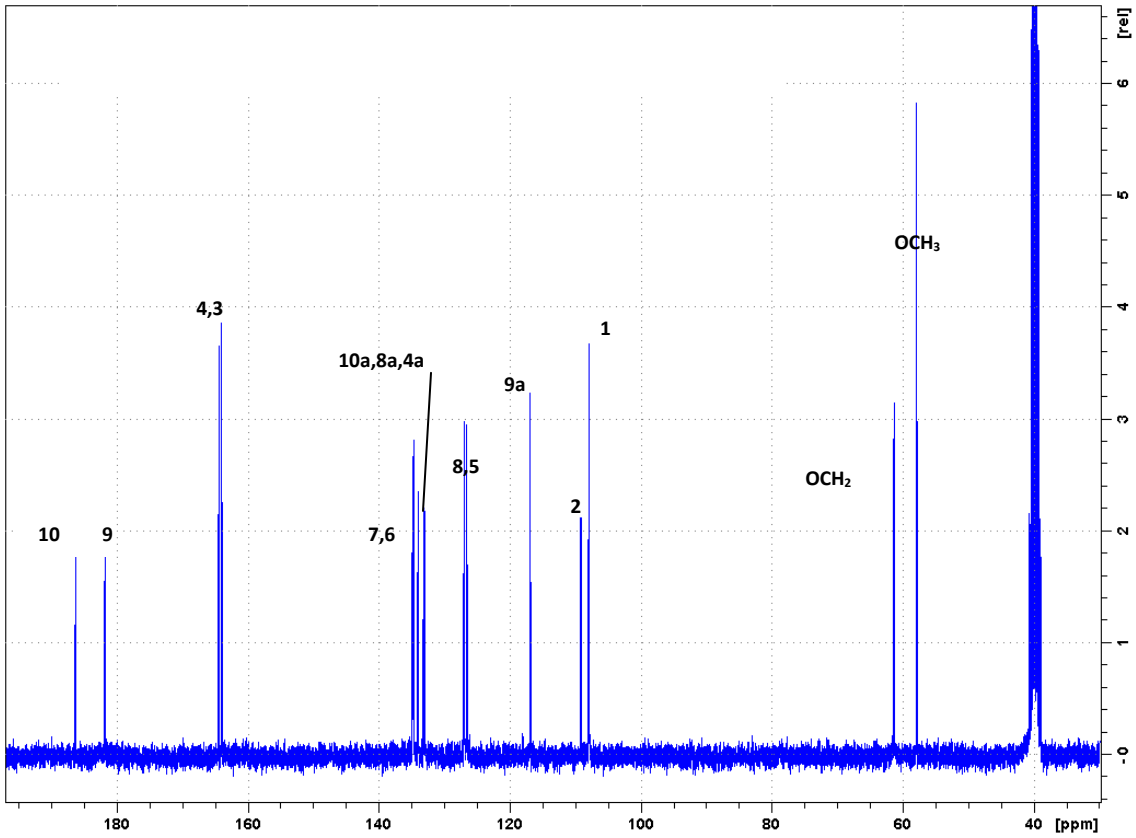

Figure 3.2.11.2: ^{13}C NMR spectrum of lucidin-3-methyl ether **71**

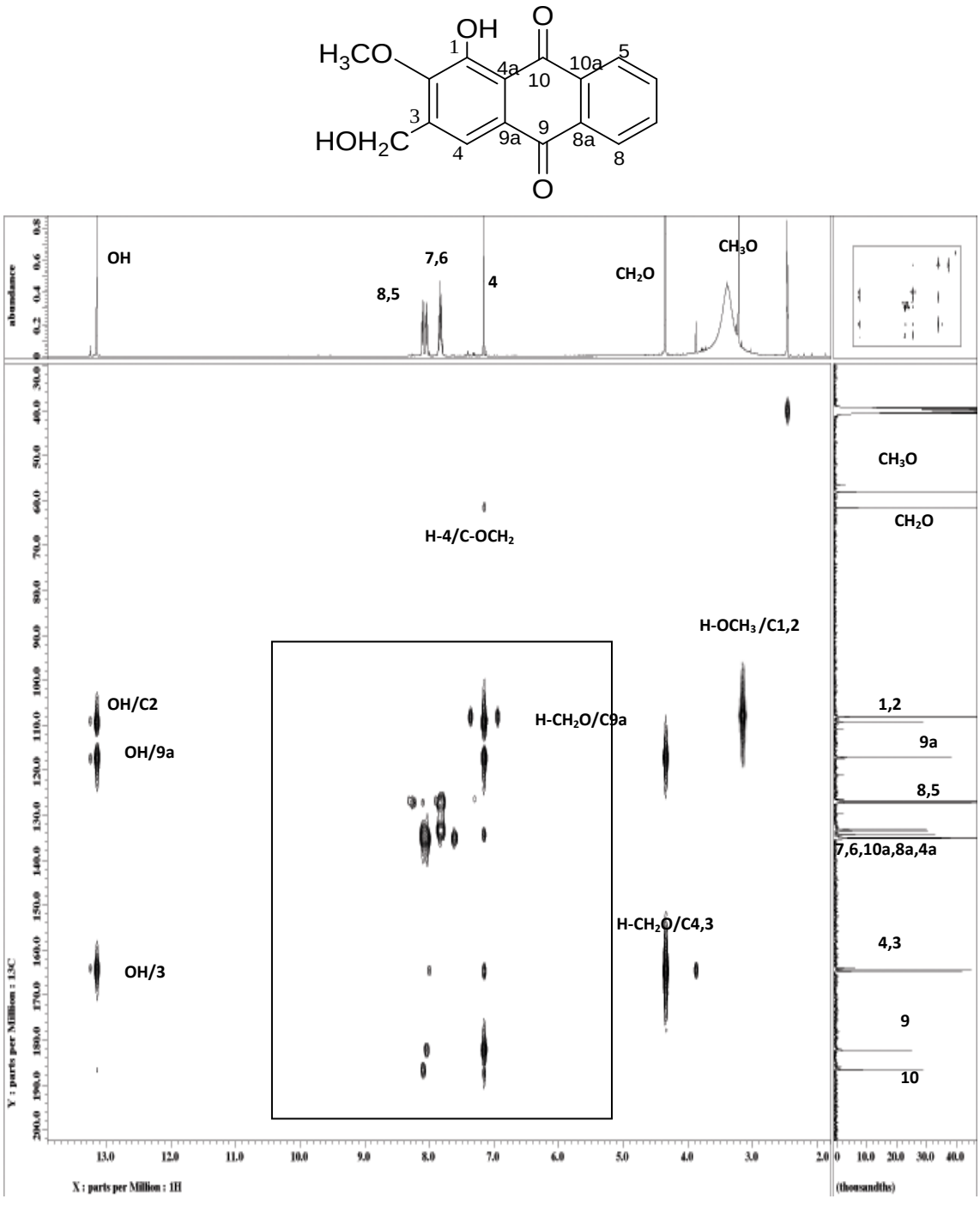

Figure 3.2.11.3a: HMBC spectrum of lucidin-3-methyl ether **71**

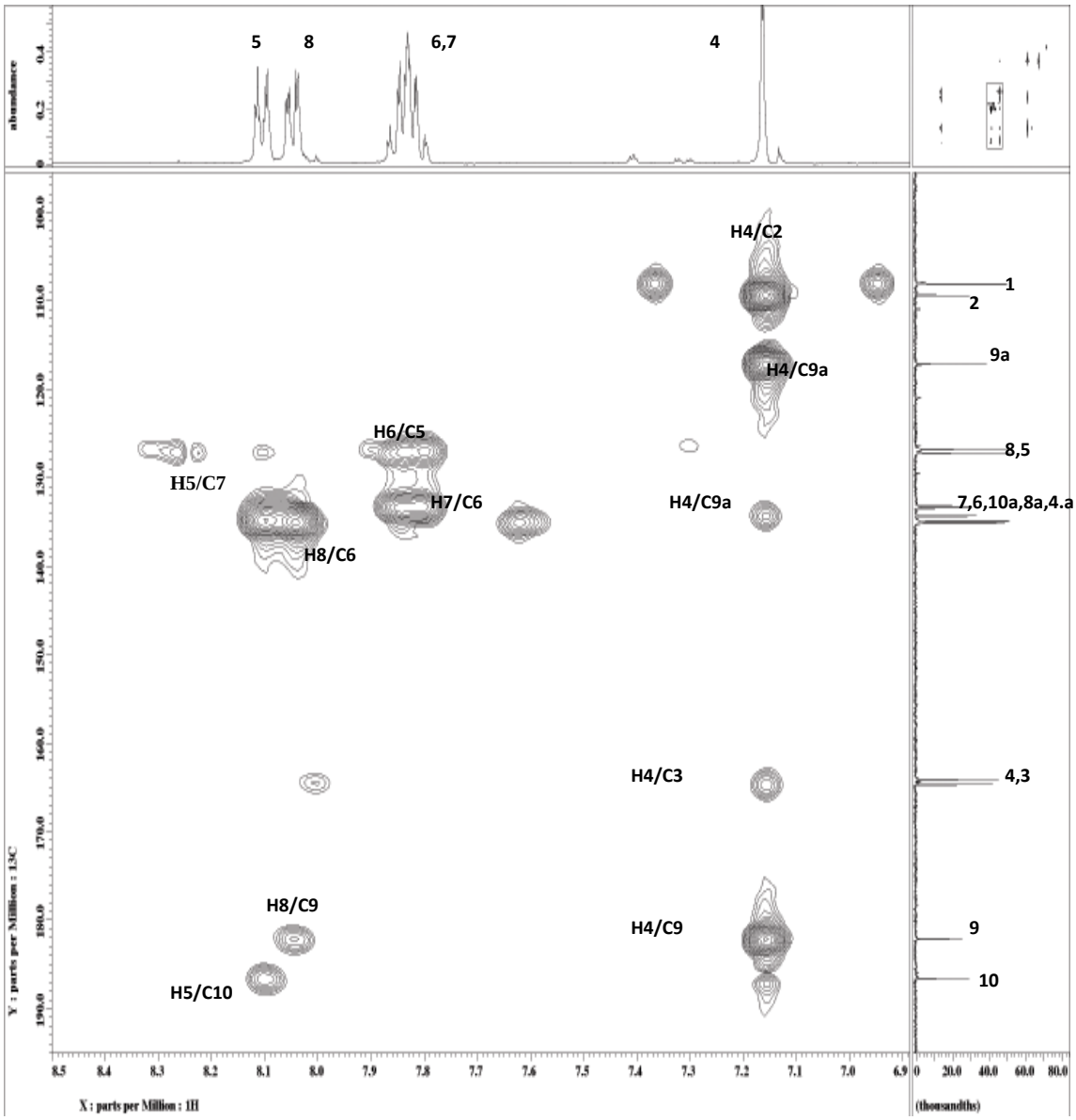

Figure 3.2.11.3b: HMBC spectrum expansion of lucidin-3-methyl ether **71**

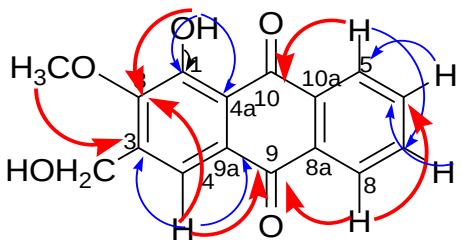

lucidin-3-methyl-ether 71

J^2 correlations

J^3 correlations

Figure 3.2.11.4: Selected HMBC correlation in lucidin-3-methyl ether **71**

3.2.12 Compound L: *Rubiadin-1-methyl ether*

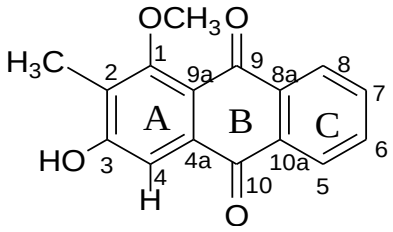

11

Rubiadin-1-methylether **11 (c**ompound L) was isolated as yellow amorphous powder from two fractions, it produced pseudo-molecular ion peak $[M-H]^-$ at m/z 267.06534 with ESI-MS which is consistent with molecular formula $C_{16}H_{12}O_4$. The UV spectrum recorded in MeOH showed maxima absorptions at 280, 238 and 204 nm. In the IR spectrum, important absorptions were observed at 3306 cm^{-1} for OH groups and 1650 cm^{-1} for C-H aromatics group (Silverstein et al., 1991). The strong signal which is attributable to C=O group could be observed at 1672 cm^{-1}.

Its ^1H NMR (figure 3.2.12.1) showed an A_2B_2 type of aromatic proton signals at δ8.18 (*dd*, J_1=7.4 and J_2=1.8 Hz, H-8), δ8.12 (*dd*, J_1=7.4 and J_2=1.8 Hz, H-5), δ7.90 (*dt*, J_1=7.4 and J_2=1.8 Hz, H-6) and δ7.80 (*dt*, J_1=7.4 and J_2=1.8 Hz, H-7) for the ring (table 3.2.12). A singlet δ7.48 for an isolated aromatic proton could be attributable to proton H-4. Another signal resonated at δ3.83 (*s*, 3H) and δ2.13 (*s*, 3H). The former was a signal for the methoxy protons as it resonated at lower field due to the deshielded effect of the oxygen atom, while the latter was the signal for the aromatic methyl protons.

The ^{13}C NMR (figure 3.2.12.2) together with the DEPT spectrum (figure 3.2.12.3) distinguished sixteen carbons into nine quarternary carbons, five methines and two

methylenes groups. Two quarternary carbonyl carbons at δ182.8 and δ180.3 were assigned to be C-10 and C-9 respectively. The C-10 was deshielded interspace by the neighboring oxygen atom of the methoxy group at C-1. Peaks at position δ126.1-δ134.7 were indicative of the sp^2 carbons of the benzene ring. The quarternary carbon resonated at δ161.8 (C-3), δ160.8 (C-1), δ134.7 (C-4a), δ133.9 (C-8a), δ132.2 (C-10a), δ126.3 (C-2) and δ118.1 (C-9a). The C-3 and C-1 experience a deshielding effect from the neighbouring oxygen atom. The methoxy and methyl carbon resonated at δ60.8 and δ9.2 respectively.

Consequently, comparison of the empirical data with the literature values (Lee, 1968; Kohei et. al, 2010) of a known compound led to the conclusion that compound L was rubiadin-1-methylether **11**.

Table 3.2.12: ^{1}H NMR [300 MHz, δ_H (*J*, Hz)] and ^{13}C NMR [75 MHz, δ_C] of **11** in DMSO-d_6

	^{13}C	**^{13}C***	**^{1}H(*J*,H)**	**^{1}H (*J*,H)***
1	160.8	161.1	-	-
2	126.3	126.6	-	-
3	161.8	162.3	-	-
4	109.2	109.5	7.48*s*	7.51*s*
4a	134.7	135.0	-	-
5	126.2	126.5	8.12 (*d*, *J*=7.4, 1.8 Hz)	8.1 (*dd*, *J*=7.4, 1.4 Hz)
6	134.7	134.2	7.90 (*dt*, *J*=7.4, 1.8 Hz)	7.83(*td*, *J*=7.4, 1.4 Hz)
7	133.5	133.8	7.80 (*dt*, *J*=7.4, 1.8 Hz)	7.89 (*td*, *J*=7.5, 1.4 Hz)
8	126.8	127.1	8.18 (*d*, *J*=7.4, 1.8 Hz)	8.15(*dd*, *J*=7.5, 1.4 Hz)
8a	133.9	135.0	-	-
9	180.3	180.6	-	-
9a	118.1	118.34	-	-
10	182.8	183.1	-	-
10a	132.2	132.5	-	-
CH_3	9.2	9.5	2.13*s*	2.16*s*
OCH_3	60.8	61.1	3.83*s*	3.79*s*

* ^{1}H NMR [400MHz, DMSO-d_6],
* ^{13}C NMR [100MHz, DMSO-d_6]
Kohei et al, 2010

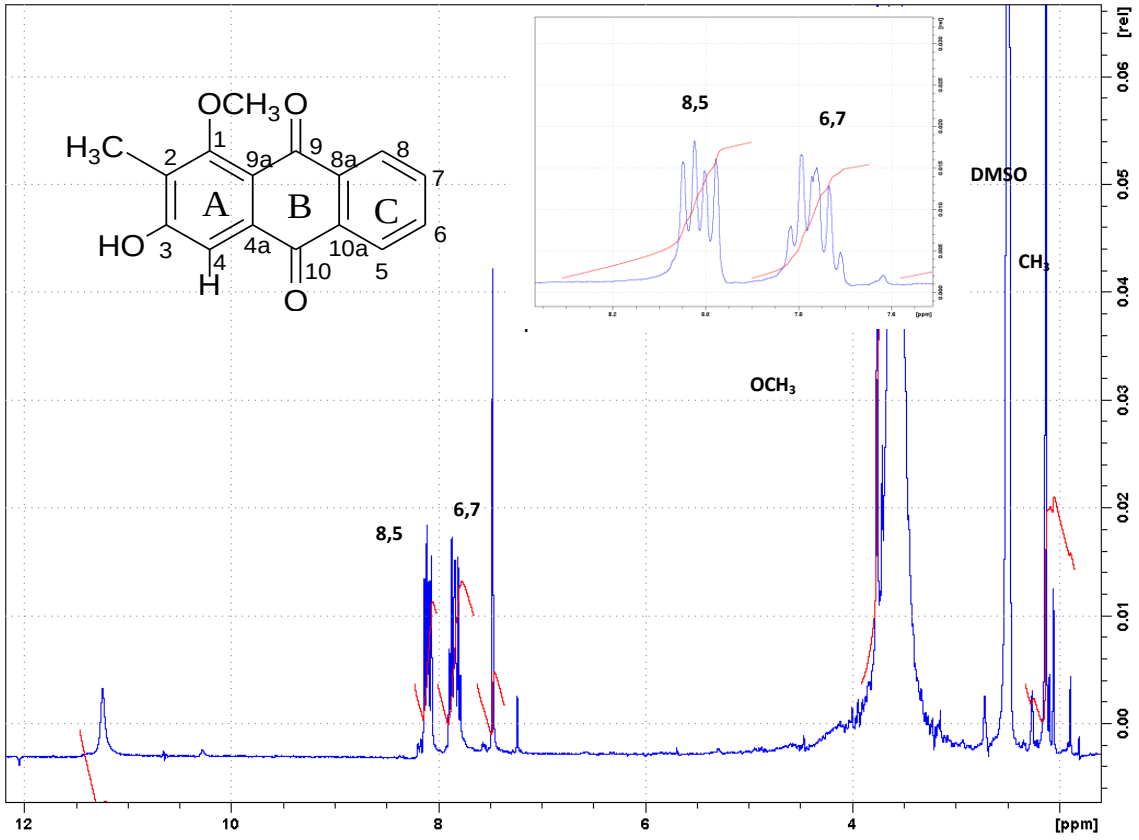

Figure 3.2.12.1: ^{1}H NMR spectrum of Rubiadin-1-methylether **11**

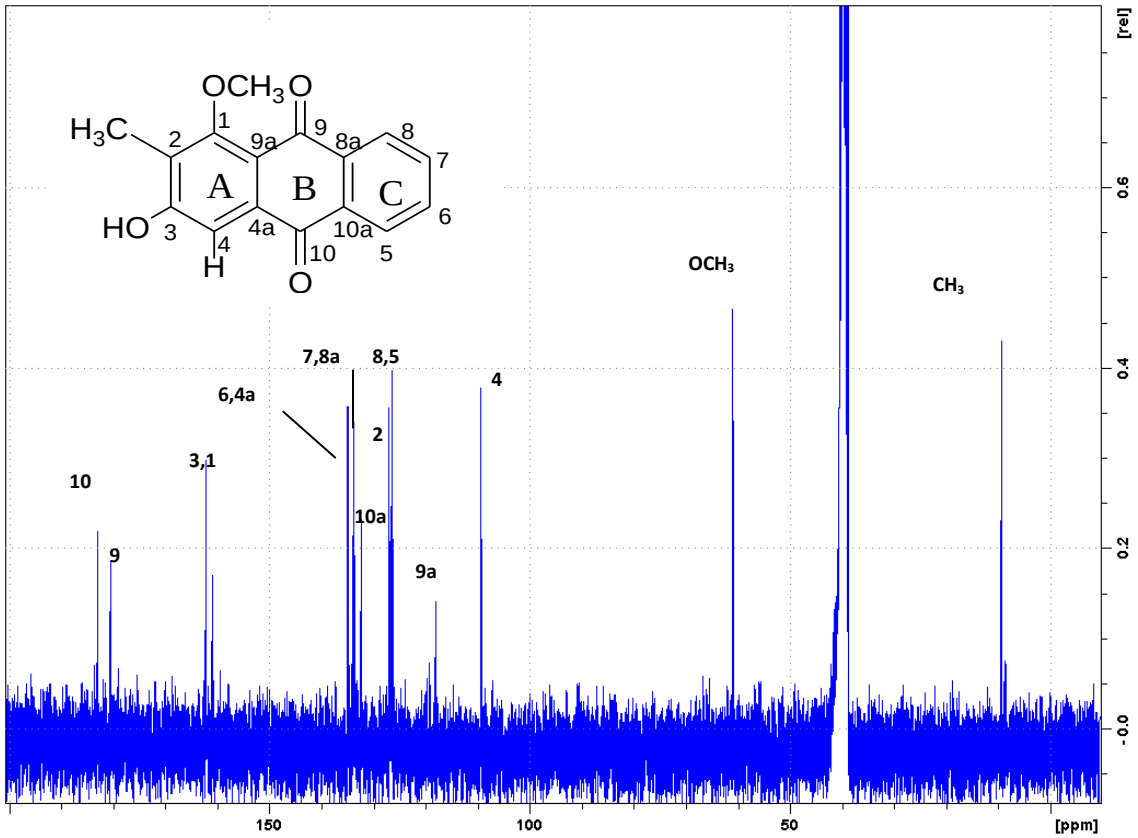

Figure 3.2.12.2: ^{13}C NMR spectrum of Rubiadin-1-methylether **11**

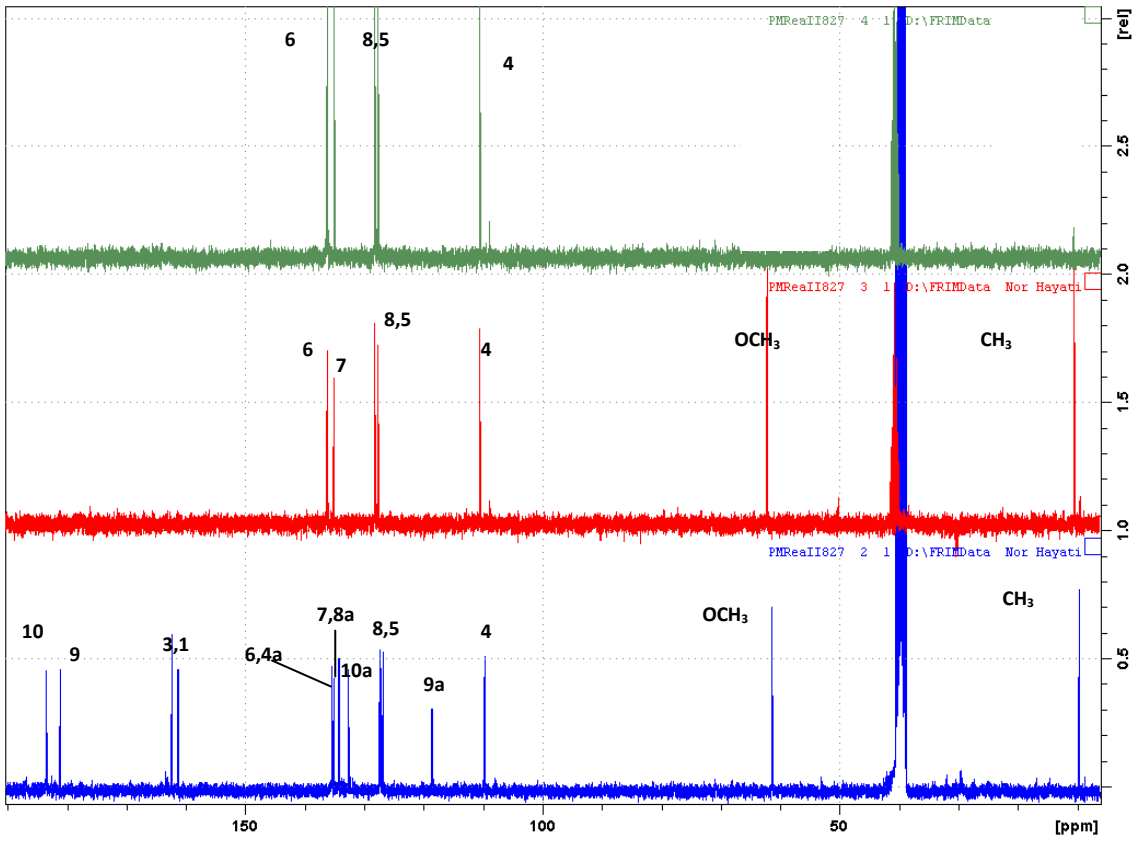

Figure 3.2.12.3: DEPT spectrum of Rubiadin-1-methylether **11**

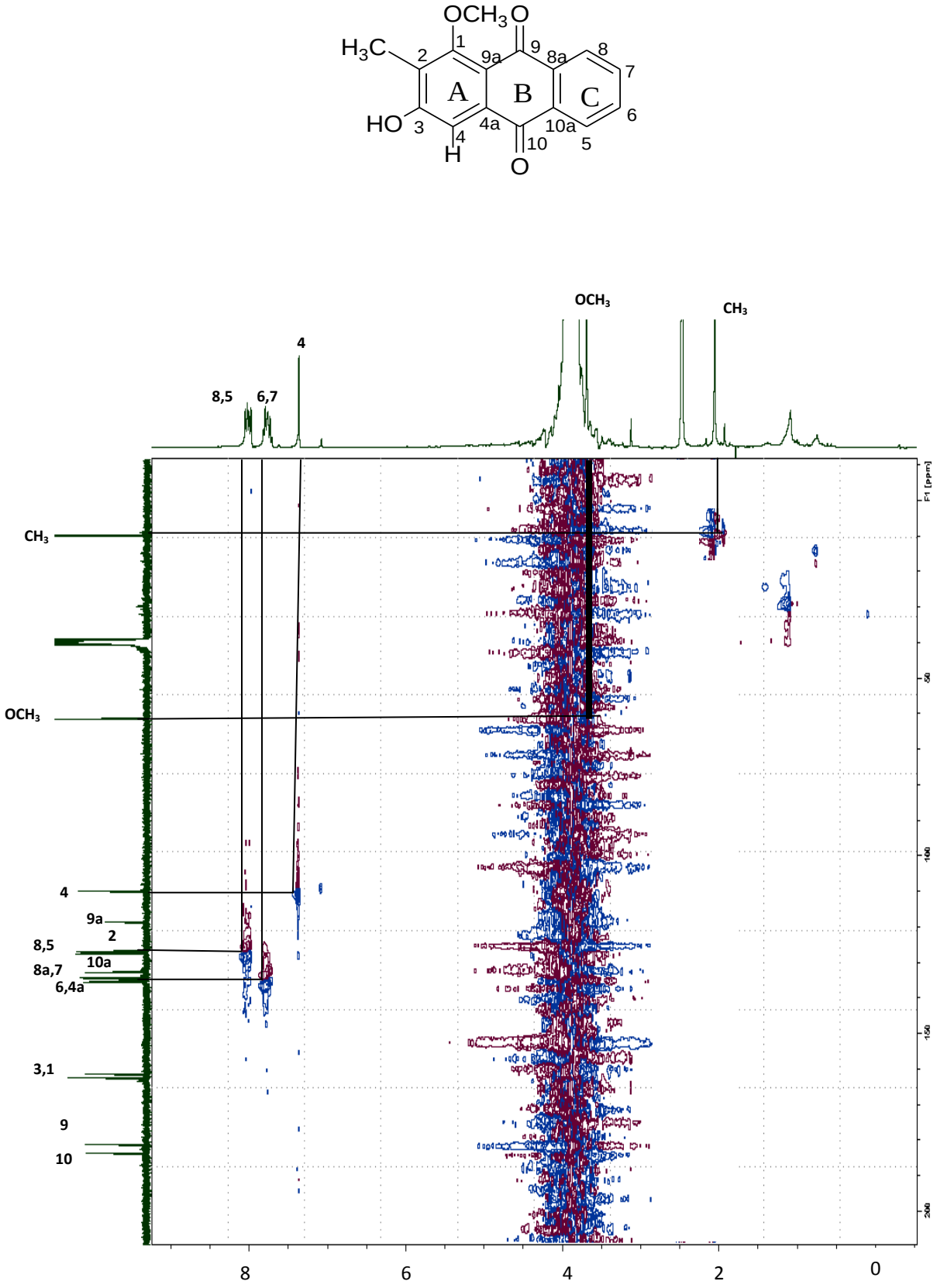

Figure 3.2.12.4: HMQC spectrum of Rubiadin-1-methylether **11**

3.2.13 Compound M: *Damnacanthol*

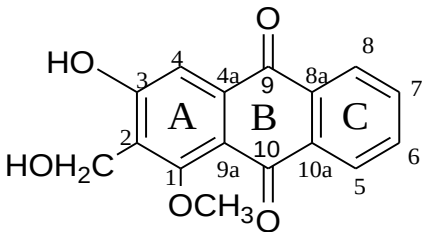

72

Damnacanthol **72 (c**ompound M) was isolated as yellow amorphous powder. It produced pseudo-molecular ion peak $[M-H]^-$ at m/z 283.05991 with ESI-MS which is consistent with molecular formula $C_{16}H_{12}O_5$. The UV spectrum recorded in MeOH exhibited maximum absorptions at 278, 239, 203 nm. The IR spectrum showed broad bands for OH groups (3300 cm^{-1}), C-H aromatic signal (1647 cm^{-1}) and a sharp signal at 1672 cm^{-1} of C=O function (Silverstein et al., 1991).

The ^1H NMR spectrum (figure 3.2.13.1) showed an A_2B_2 aromatic spin system at δ8.10 (*dd*, J_1=7.5 and J_2=1.2 Hz, 1H, H-8), δ8.06 (*dd*, J_1 =1.2 and J_2=7.5 Hz, 1H, H-5), δ7.86 (*dt*, J_1=7.5 and J_2=1.1 Hz, 1H, H-6) and δ7.77 (*dt*, J_1 =7.5 and J_2=1.2 Hz,1H, H-7) which could be assigned to be protons in the ring A (table 3.2.13). It also showed an isolated aromatic proton at δ7.48 (1H). Other signals include an overlapped singlet of two hydrogens at δ4.54 and a singlet for three hydrogens at δ3.80 which indicated the presence of oxymethylene and methyl groups, respectively. Both signals protons were shifted down field due to the deshielding effect by the neighbouring oxygen.

The ^{13}C NMR spectrum (figure 3.2.13.2) together with the DEPT spectrum (figure 3.2.13.3) confirmed the presence of sixteen carbons of which nine are quarternary

carbons, five methines, one methylene and one methyl group. Two quarternary chelated carbon at δ183.4 and δ180.8 were attributable to the carbonyl carbon of C-10 and C-9, respectively. Two oxygenated quarternary carbons resonated at δ163.0 and δ162.5 attributed to C-3 and C-1 respectively. Another quarternary carbon resonated at δ136.2, δ135.4, δ133.9 and δ118.6 which was attributable to C-4a, C-8a, C-10a and C-9a respectively. The upfield shift of C-3 and downfield shift of C-9a can be attributed to the substituted OH-3 and its shielding effect on the para carbon, C-9a. The C-4 carbon was shifted to upper field (δ110.6) compared to the other aromatic carbon C5-C8 due to the shielding effect of methoxy on C-1 on the para carbon, C-4. The methoxy group itself resonated at δ63.2 while the methylene carbon resonated at δ52.9.

Finally, after thorough comparison of the empirical data with the literature values of the knowm compound (Kohei et. al, 2010) we concluded that compound M was damnacanthol **72**.

Table 3.2.13: ^{1}H NMR [300 MHz, δ_H (*J*, Hz)] and ^{13}C NMR [75 MHz, δ_C] of **72** in DMSO-d_6

Position	**^{13}C***	**^{13}C**	**^{*1}H(*J*,H)**	**^{1}H(*J*,H)**
				-
1	161.7	162.5	-	-
2	128.8	129.6	-	-
3	162.2	163.0	7.52*s*	7.48*s*
4	109.8	110.6	-	-
4a	135.4	136.2	-	-
5	126.1	126.9	8.11 (*dd*, *J*=7.5, 1.5 Hz)	8.06 (*dd*, *J*=7.5, 1.2 Hz)
6	133.4	134.2	7.83 (*td*, *J*=7.5, 1.4 Hz)	7.86 (*dt*, *J*=7.5, 1.1 Hz)
7	134.6	135.4	7.89 (*td*, *J*=7.5, 1.5 Hz)	7.77 (*dt*, *J*=7.5, 1.2 Hz)
8	126.6	126.9	8.16 (*dd*, *J*=7.5, 1.4 Hz)	8.10 (*dd*, *J*=7.5, 1.2 Hz)
8a	134.6	135.3	-	
9	178.0	180.8	-	-
9a	117.9	118.6		
10	182.6	183.4	-	-
10a	132.0	133.9	-	-
CH_2O	52.2	52.9	4.57*s*	4.54*s*
OCH_3	62.4	63.2	3.87*s*	3.80*s*

*^{1}H NMR [400MHz] in DMSO-d_6
*^{13}C NMR [100 MHz] in DMSO-d_6
(Kohei et al., 2010)

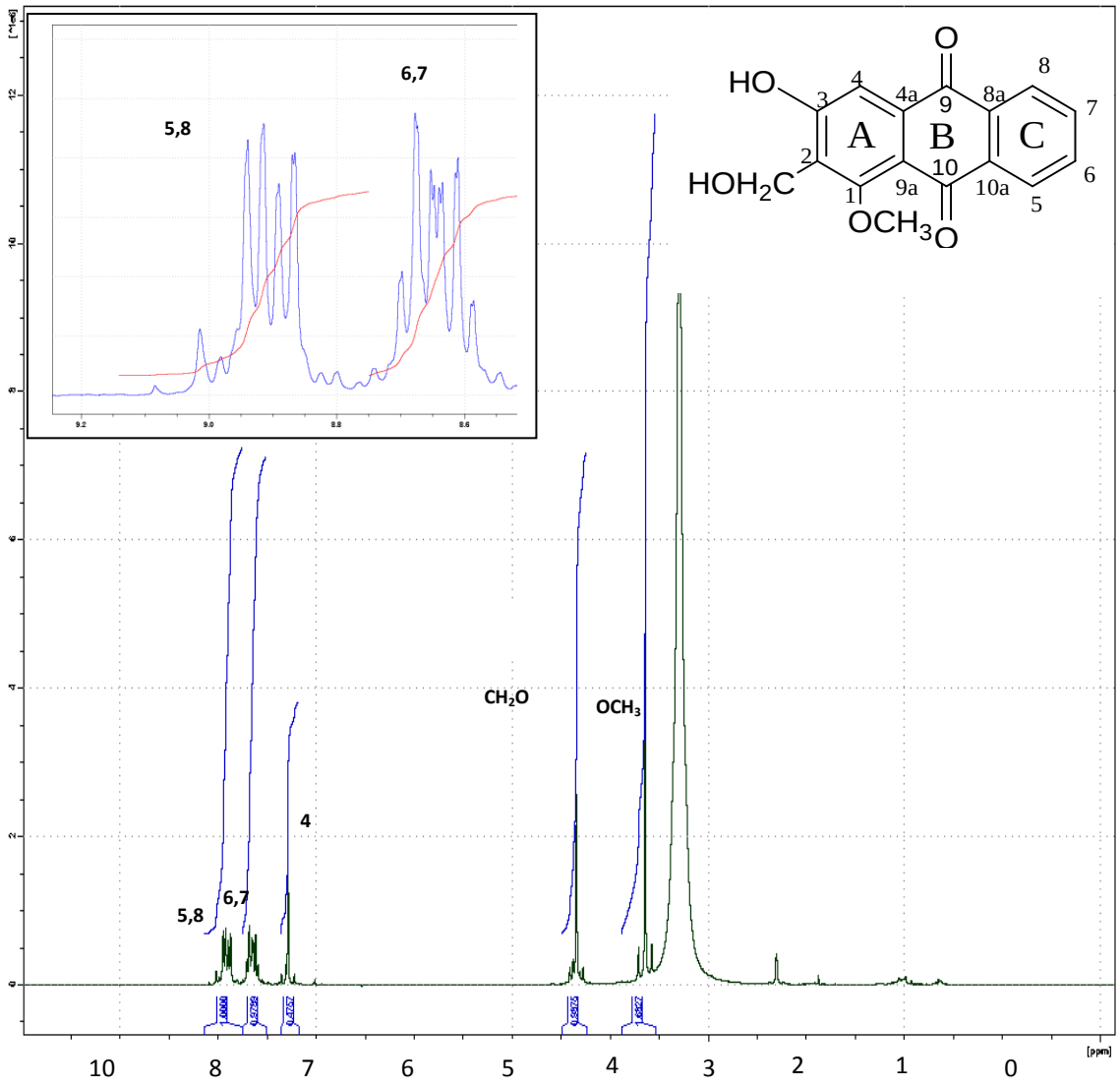

Figure 3.2.13.1: ^{1}H NMR spectrum of damnacanthol **72**

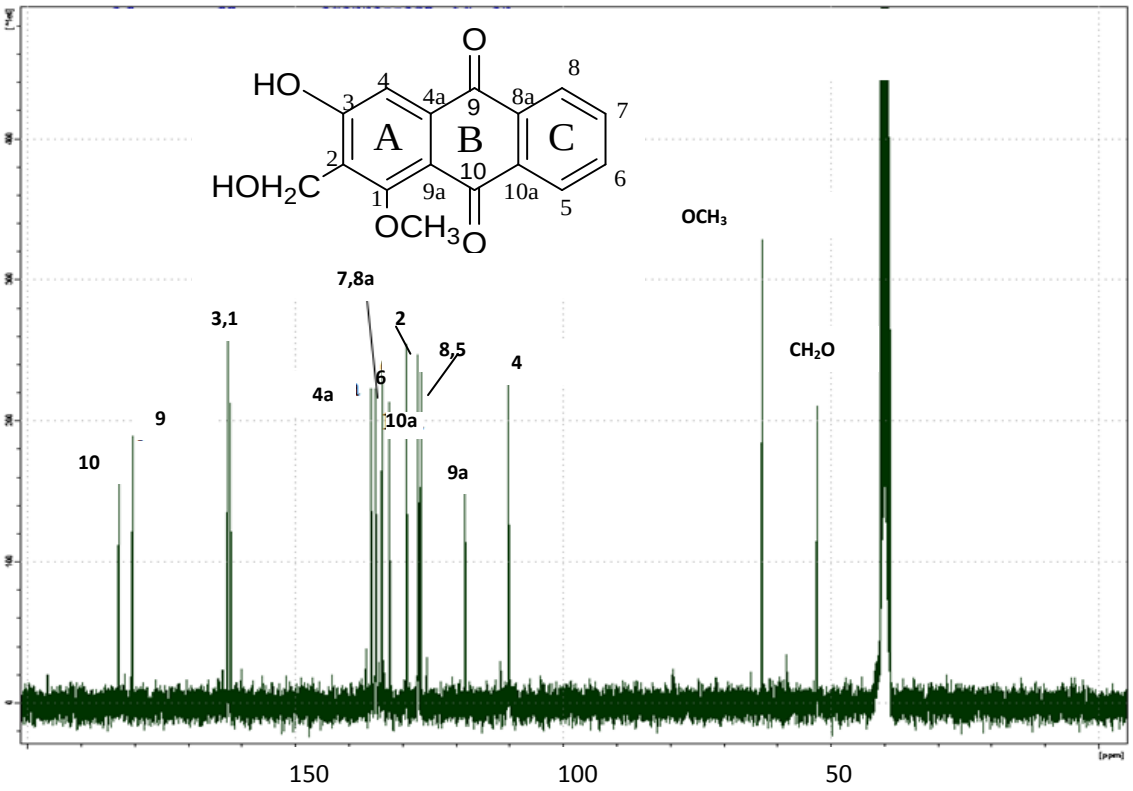

Figure 3.2.13.2: ^{13}C NMR spectrum of damnacanthol **72**

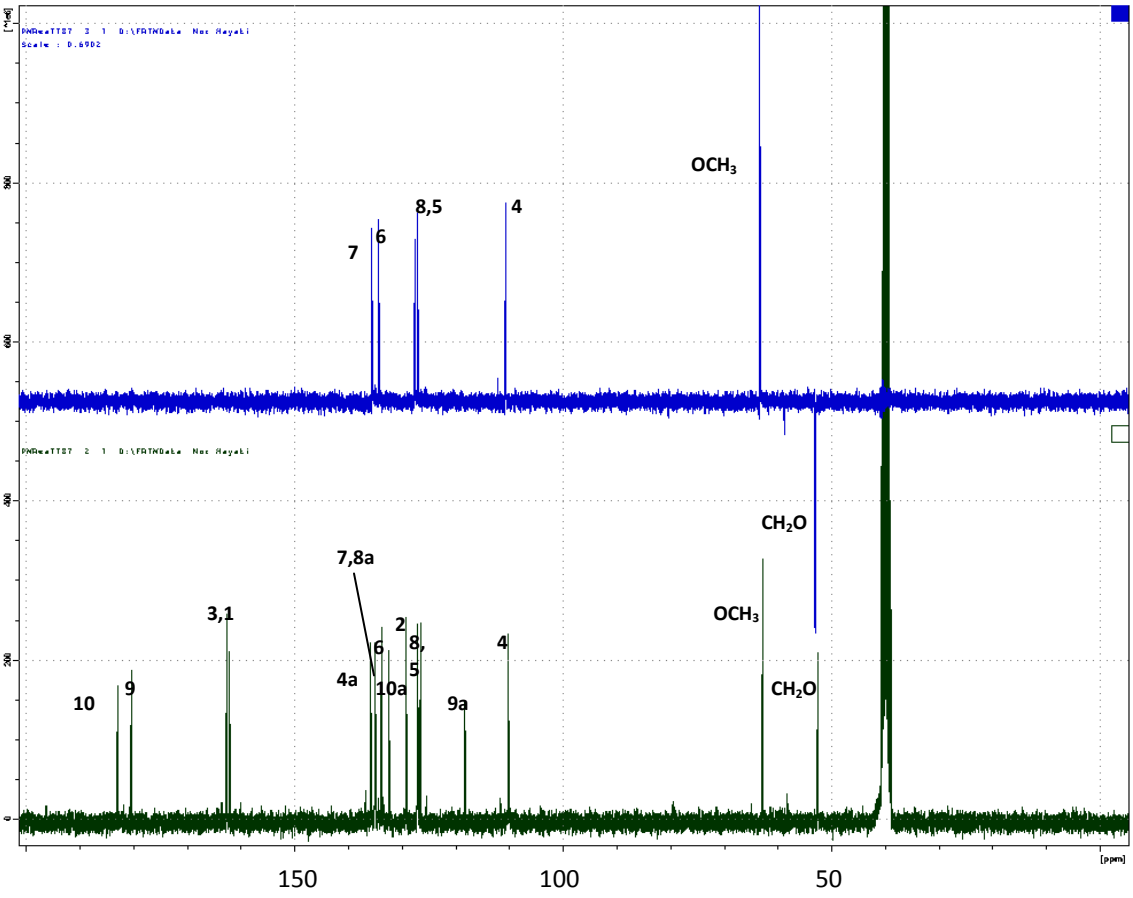

Figure 3.2.13.3: DEPT spectrum of damnacanthol **72**

3.2.14 Compond N: *Rubiadin*

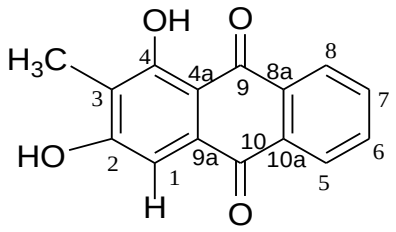

10

Rubiadin **10** (compound N) was isolated as yellowish orange crystals. It produced pseudo-molecular ion peak $[M - H]^-$ at m/z 253.04933 with ESI-MS which is consistent with molecular formula $C_{15}H_{10}O_4$. It showed maximum UV absorption at 409, 279, 245 and 206 nm. The IR spectrum showed a broad band for OH groups (3391 cm^{-1}) and a signal for C-H aromatic at 1621 cm^{-1} (Silverstein et al.,1991) . It also showed a strong signal at 1660 cm^{-1} due to C=O function.

The ^1H NMR spectrum (figure 3.2.14.1) showed aromatic proton signal on A_2B_2 spin system for ring C at δ8.21 (*dd*, J_1=7.0 and J_2=1.7 Hz, 1H, H-8), δ8.13 (*dd*, J_1=7.0 and J_2= 1.7 Hz, H-5, 1H), δ7.90 (*dt*, J_1 =7.0 and J_2= 1.7 Hz, H-6, 7, 2H) (table 3.2.14). It also showed a methyl proton signal at δ2.07 (*s*, 3H).

Both the ^{13}C NMR (figure 3.2.14.2) and DEPT spectrum (figure 3.2.14.3) were employed to analyze the carbon of this compound. Two quarternary carbon of carbonyl groups resonated at δ185.9 and δ182.2 attributable to C-10 and C-9 respectively. A quarternary carbon which resonated at δ162.6 could be assigned to C-4 which was deshielded to lower field by the hydroxyl group. The other carbon signals (C-6, C-7, C-5, C-8, C-9a, C-8a, C-10, C-9, C-4a, C-10a and C-4) are almost similar to the

previously discussed compound (K-M) except for additional peaks resonated at δ8.30. The later was sp^3 carbon of methyl group.

Analysis of all spectral data obtained and comparison with literature values of a known compound (Lee, 1968, Kohei et al., 2010) led to the conclusion that compound N was rubiadin **10**.

Table 3.2.14: ^{1}H NMR [300 MHz, δ_H (*J*, Hz)] and ^{13}C NMR [75 MHz, δ_C] of **10** in DMSO-d_6

	^{13}C	**^{13}C***	**^{1}H(*J*,H)**	***^{1}H(*J*,H)**
1	108.1	108.9	7.15*s*	7.19*s*
2	162.6	162.4	-	-
3	108.5	107.4	-	-
4	162.6	162.9	13.15*s*	13.05 *s*
4a	133.3	131.6	-	-
5	126.8	126.6	8.13 (*dd*, *J*=7.0, 1.7 Hz)	8.08 (*dd*, *J*=7.0, 2.1 Hz)
6	134.7	134.3	7.90 (*dt*, *J*=7.0, 1.7 Hz)	7.84 (*td*, *J*=7.0, 1.7 Hz)
7	134.5	134.4	7.90 (*dt*, *J*=7.0, 1.7 Hz)	7.87 (*td*, *J*=7.2, 2.1 Hz)
8	126.5	126.3	8.21 (*dd*, *J*=7.0, 1.7 Hz)	8.14 (*dd*, *J*=7.2, 1.7Hz)
8a	131.9	132.9	-	-
9	182.2	181.7	-	-
9a	117.3	117.3	-	-
10	185.9	186.1	-	-
10a	133.0	132.8	-	-
CH_3	8.3	8.1	2.07*s*	2.03*s*

*^{1}H NMR [400 MHz] in DMSO-d_6
*^{13}C NMR [100 MHz] in DMSO-d_6
(Kohei et al., 2010)

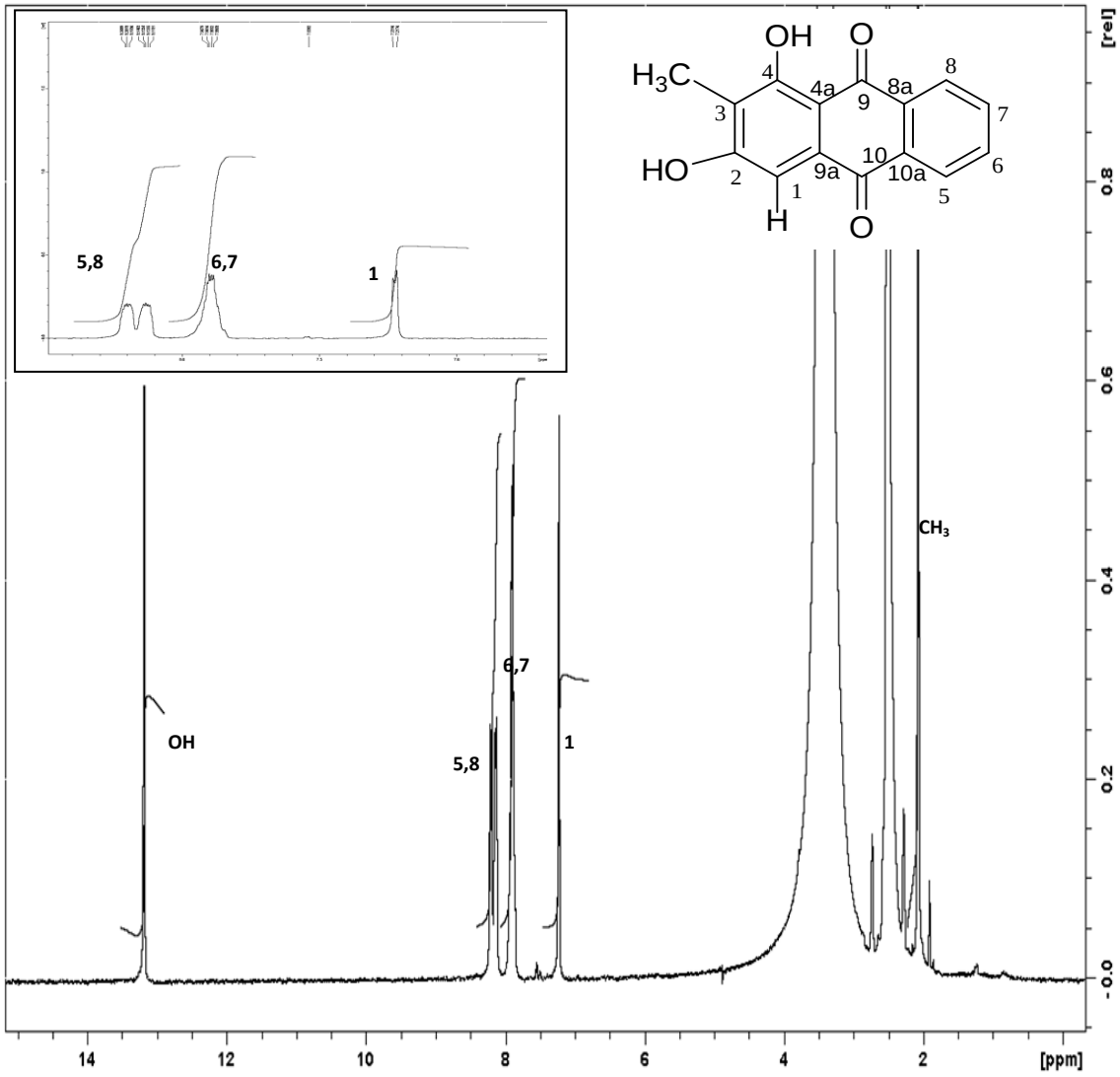

Figure 3.2.14.1: ^{1}H NMR spectrum of rubiadin **10**

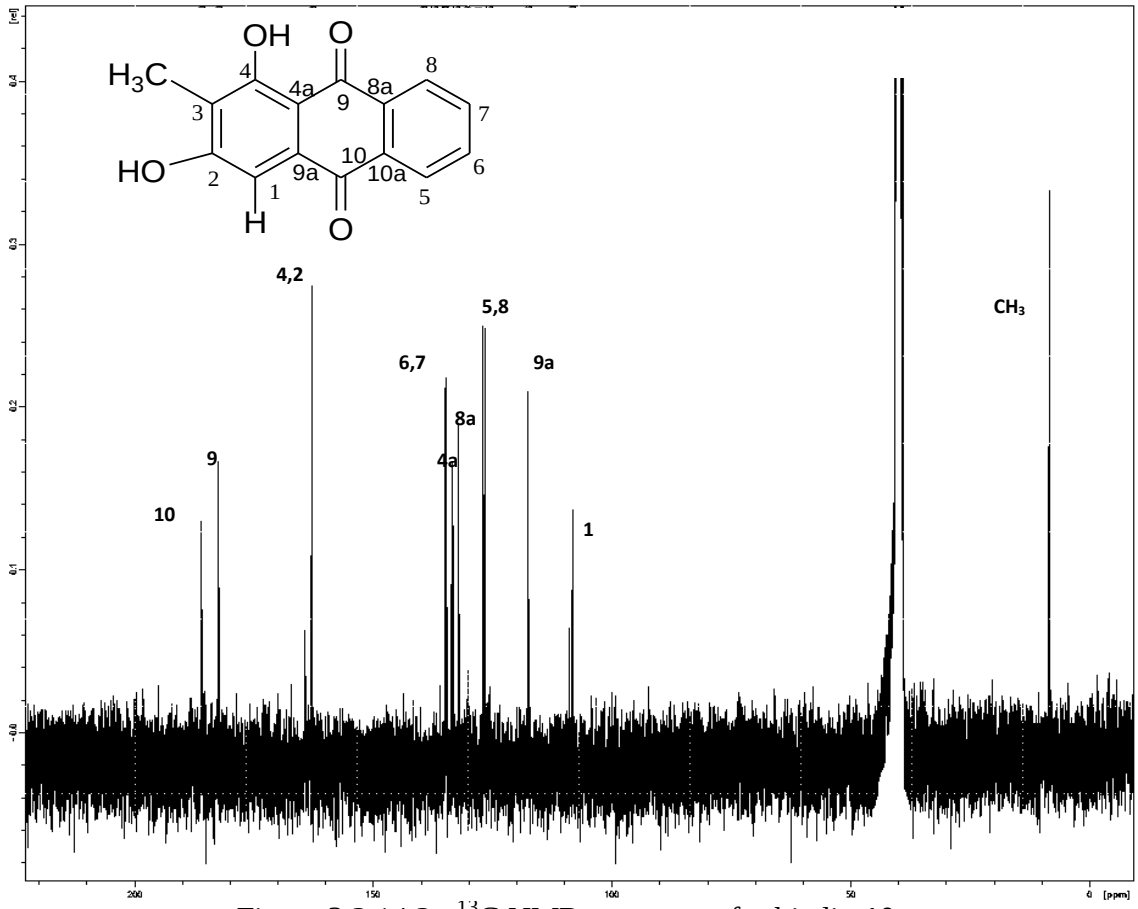

Figure 3.2.14.2: ^{13}C NMR spectrum of rubiadin **10**

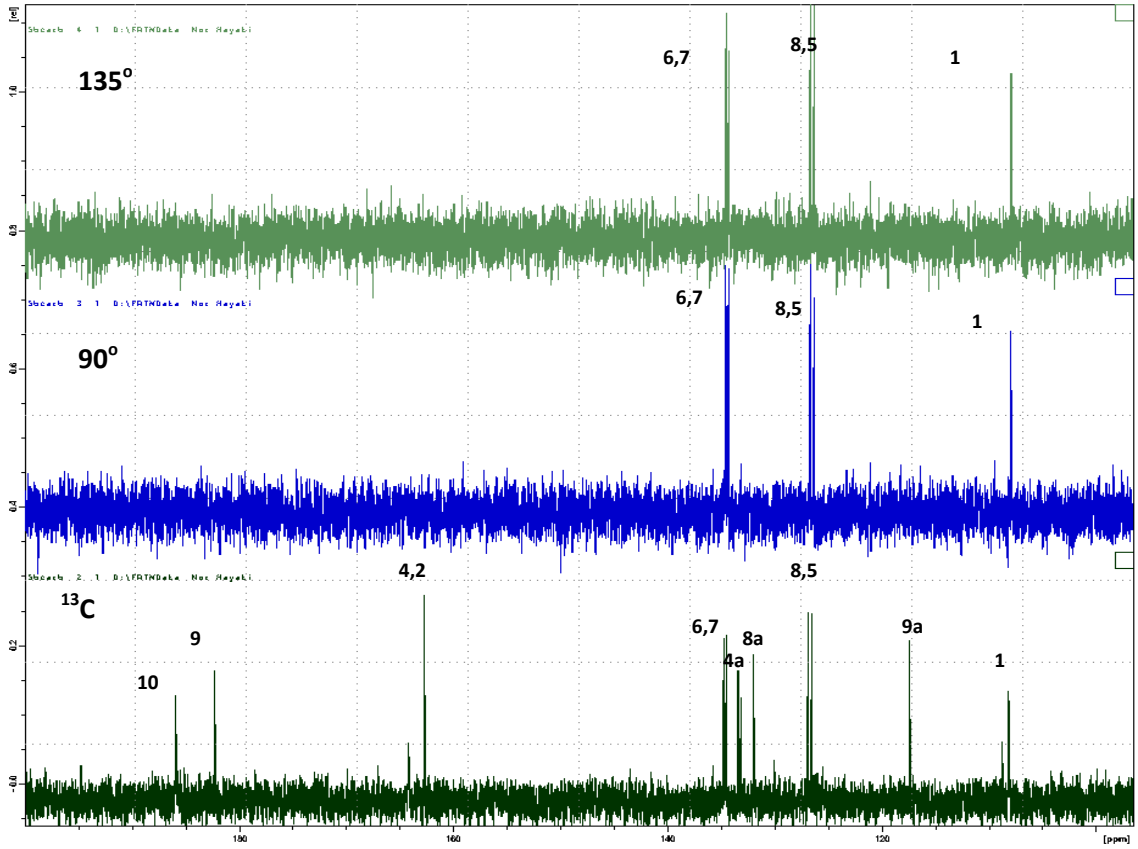

Figure 3.2.14.3: DEPT spectrum of rubiadin **10**

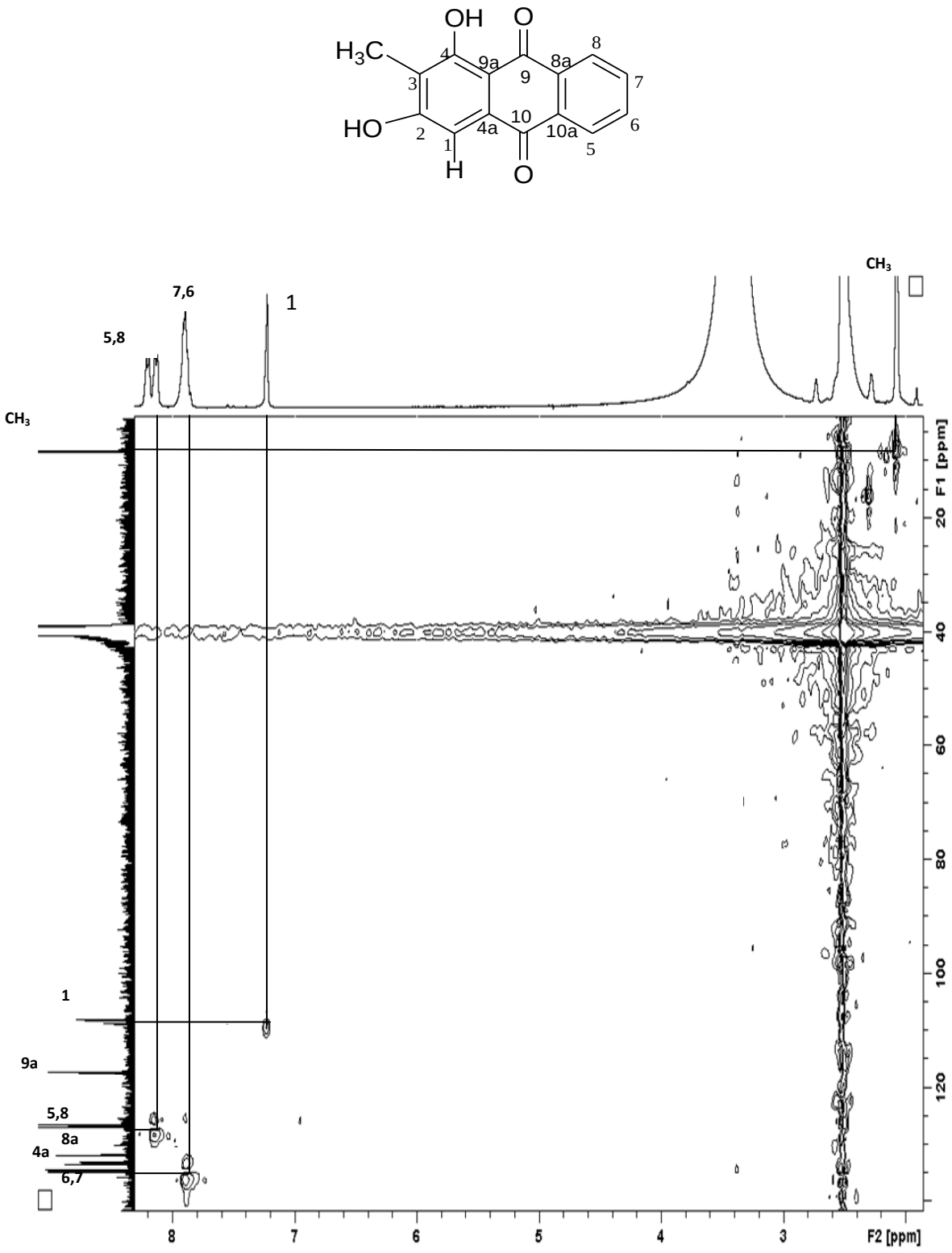

Figure 3.2.14.4: HMQC spectrum of rubiadin **10**

3.2.15 Compound O: *1-ethyl-3-hydroxymethyl-4-hydroxy-9,10-anthraquinone*

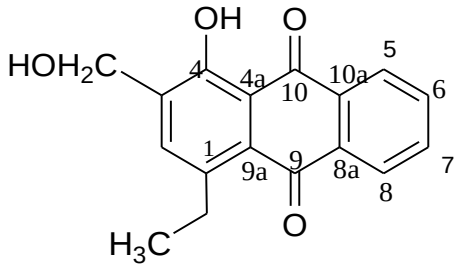

(The position of substituents at C-2,C-3 and C-4 were not confirmed)

73

1-ethyl-3-hydroxymethyl-4-hydroxy-9,10-anthraquinone **73** (compound O) was isolated as yellowish orange powder. It produced pseudo-molecular ion peak $[M - H]^-$ at m/z 283.26373 with ESI-MS which is consistent with molecular formula $C_{16}H_{12}O_5$. The UV spectrum showed maxima absorption at 277, 239 and 204 nm. The IR spectrum indicated the presence of OH and C=O group with the broad signal at 3395 cm^{-1} and sharp signal at 1700 cm^{-1}, respectively (Silverstein et al., 1991).

Its ^1H NMR spectrum (figure 3.2.15.1) showed aromatic proton signals at δ8.28 (*dd*, *J*=7.2, 1.2 Hz, 1H, H-8), δ8.17 (*dd*, J_1=7.2 and J_2=1.2 Hz, 1H, H-5) , δ7.82 (*dt*, *J*=7.5 and J_2=1.2 Hz, 1H, H-7) and δ7.76 (*dt*, J_1=7.5 and J_2=1.2 Hz, 1H, H-6) representing the insulated A_2B_2 spin system for ring C (table 3.2.15). A singlet peak resonated at δ4.66 (2H) shifted downfield due to the deshielding effect of the neighbouring oxygen and anisotropic effect of the aromatic ring. A quartet corresponding to two protons of an ethyl groups was observed rather downfield at δ3.63. This may be due to the anisotropic effect caused by the adjacent carbonyl group. The respective methyl protons resonated as a triplet at δ1.20.

The ^{13}C NMR (figure 3.2.15.2) and DEPT spectrum (figure 3.2.15.3) showed the presence of seventeen carbons; nine quarternary carbons, five methines, two methylenes and one methyl group. Four aromatic sp^2 carbons resonated at δ135.4, δ134.9, δ127.9, δ127.5 which could be assigned to be methine carbons of C-6, C-7, C-8 and C-5 respectively. Another sp^2 carbon resonated at δ118.2 and δ111.1 attributable to the quarternary C-9a and C-4. The sp^3 carbon of the methylene groups resonated at δ67.1, δ81.5 while of the methyl carbon at δ15.4. The former was shifted downfield due to the deshielding effect of the aromatic ring while the second was deshielded by the neighbouring oxygen atom.

Complete assignments of ^1H-^1H and ^1H-^{13}C signals were established by COSY (figure 3.2.15.4) and HMQC (figure 1.4.15.5) correlation spectra, respectively. The COSY spectrum showed the correlation between the methyl and methylene protons.

Finally, by comparison of the empirical data with the literature values of a knowm compound brought to the conclusion that compound O was 1-ethyl-3-hydroxymethyl-4-hydroxy-9,10-anthraquinone **73**.

Table 3.2.15: ^{1}H NMR [300 MHz, δ_H (*J*, Hz)] and ^{13}C NMR [75 MHz, δ_C] of **73** in DMSO

	^{13}C	**^{1}H(*J*,H)**
1	*ND*	-
2	111.1	7.20*s*
3	*ND*	-
4	*180.0*	-
4a	*ND*	-
5	127.5	8.17 (*dd*, *J*=7.2, 1.2 Hz)
6	135.4	7.76 (*dt*, *J*=7.5, 1.2Hz)
7	134.9	7.82 (*dt*, *J*=7.5, 1.2 Hz)
8	127.9	8.28 (*dd*, *J*=7.2, 1.2Hz)
8a	*ND*	-
9	184.1	-
9a	118.5	-
10	187.1	-
10a	ND	-
CH_3	15.4	1.20 (*t*, *J*=6.9 Hz)
CH_2O	81.5	4.66 *s*
CH_2	67.1	3.63 (*q*, *J*=6.9 Hz)

ND=not detected

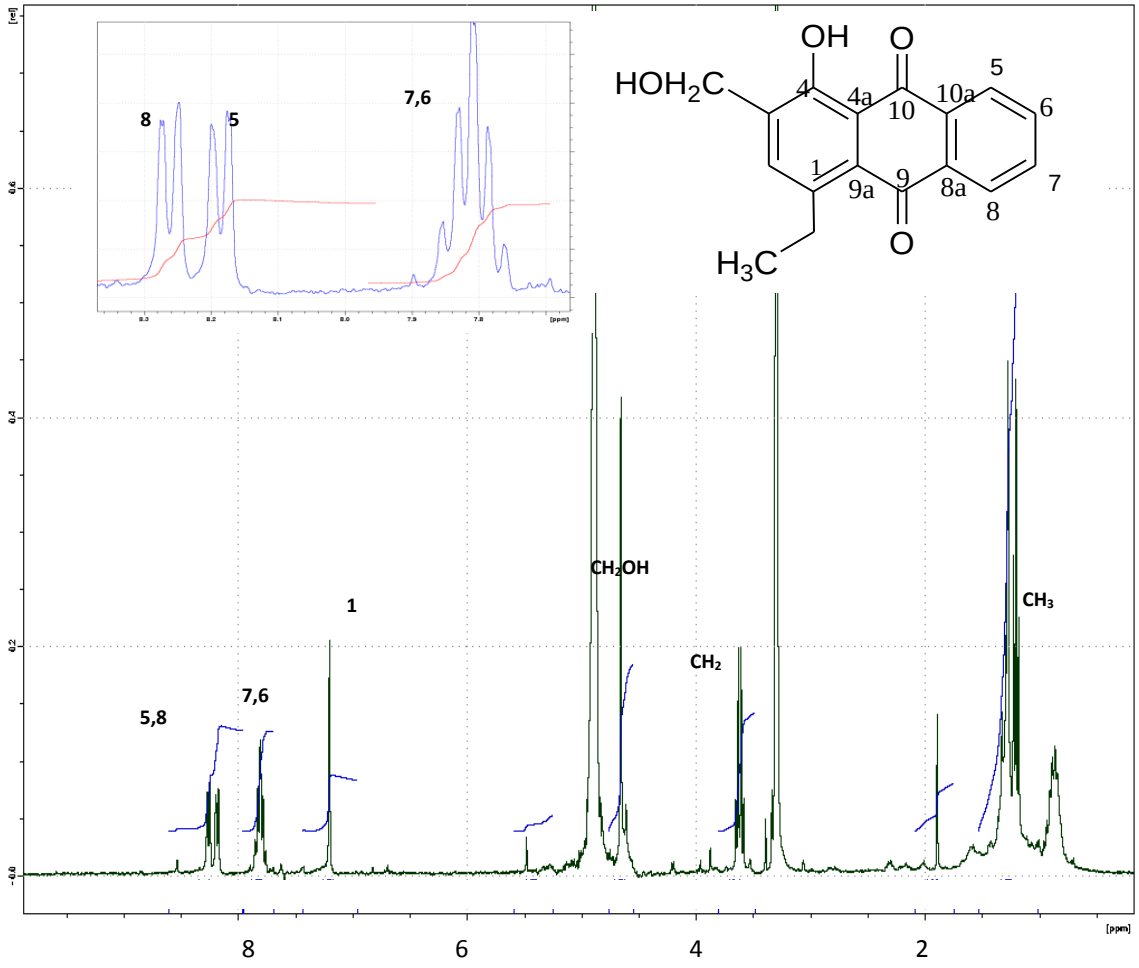

Figure 3.2.15.1: ^{1}H NMR spectrum of 1-ethyl-3-hydroxymethyl-4-hydroxy-9,10-anthraquinone **73**

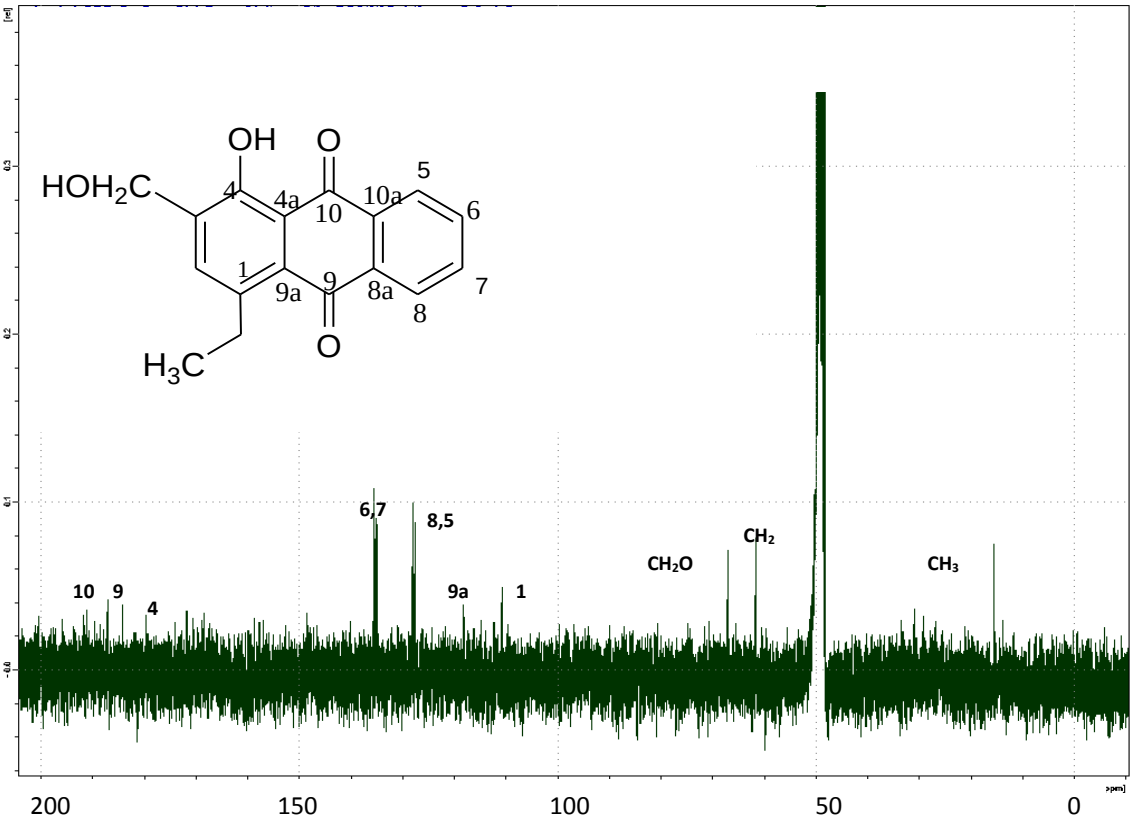

Figure 3.2.15.2: ^{13}C NMR spectrum of 1-ethyl-3-hydroxymethyl-4-hydroxy-9,10-anthraquinone **73**

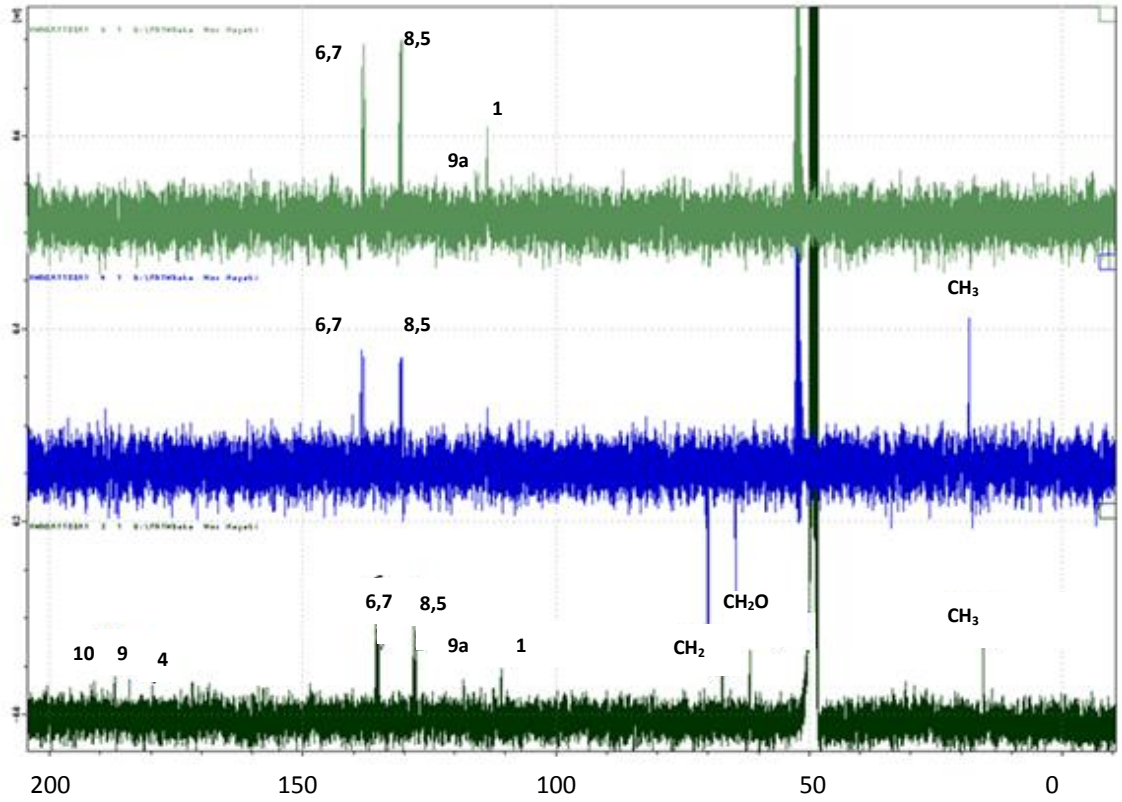

Figure 3.2.15.3: DEPT spectrum of 1-ethyl-3-hydroxymethyl-4-hydroxy-9,10-anthraquinone **73**

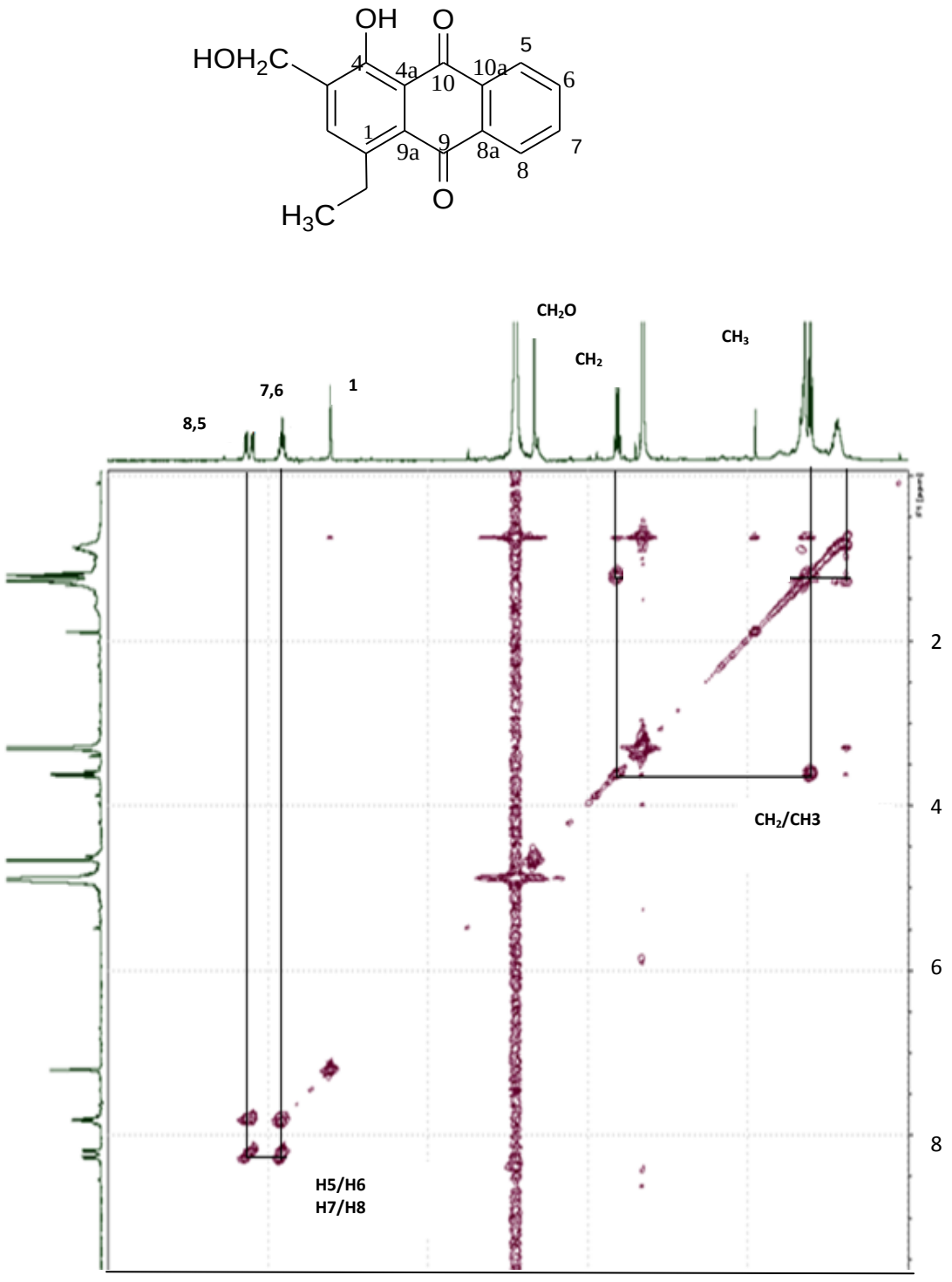

Figure 3.2.15.4: COSY spectrum of 1-ethyl-3-hydroxymethyl-4-hydroxy-9,10-anthraquinone **73**

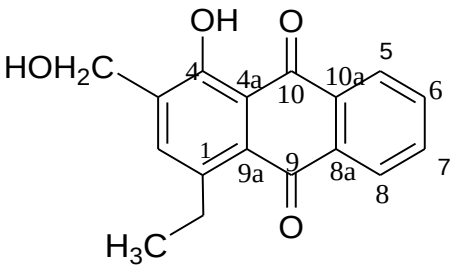

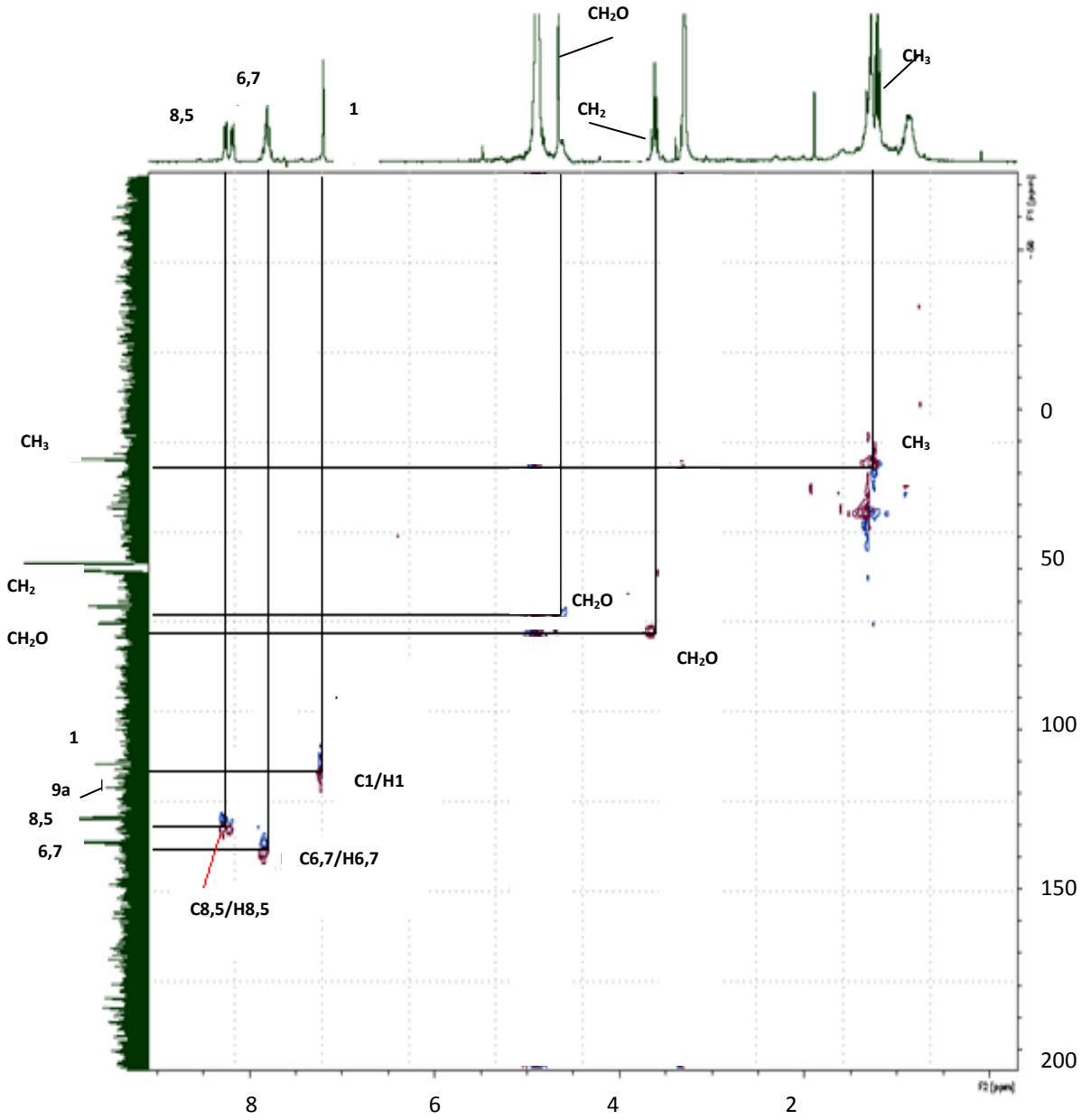

Figure 3.2.15.5: HMQC spectrum of 1-ethyl-3-hydroxymethyl-4-hydroxy-9,10-anthraquinone **73**

3.2.16 Compound P: *2-methoxy-3-oxyhydroxymethyl-9,10-anthraquinone*

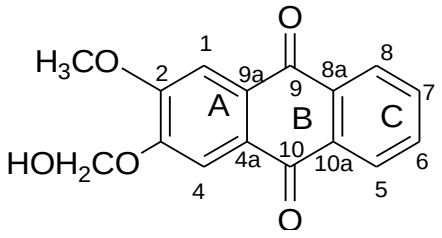

74

Compound 2-methoxy-3-oxyhydroxymethyl-9,10-anthraquinone **74** (compound Q) was isolated as yellowish powder. It produced pseudo-molecular ion peak $[M+Na]^+$ with ESI-MS 307.05450 which is consistent with molecular formula $C_{16}H_{12}O_5$. The UV spectrum showed maximum absorption at 279, 239 and 203 nm. The IR spectrum showed sharp signal for C=O group at 1724 cm^{-1} , C-H aromatic at 1672 cm^{-1} and a strong broad band for the OH function at 3309 m^1 (Silverstein et al., 1991 .

The ^{1}H NMR spectrum (figure 3.2.16.1) showed the aromatic protons resonated at δ9.03 (*bd, J*=6.7Hz, H-8), δ8.98 (*bd, J*=6.7Hz, H-5), δ8.73 (*dt, J_1*=4.1 and *J_2*= 7.3 Hz, H-6) and δ8.65 (*dt, J_1*=7.4 and *J_2*=4.1Hz, H-7), a typical signal for ring C protons (table 3.2.17). Two isolated aromatic protons resonated at δ8.50 (*d, J*=3.2Hz) and δ8.30 (*s*) could be assigned to be H-1 and H-4 respectively. Another signal could be observable at δ5.43 (*s*, 2H) and δ4.66 (*s*, 3H) which belongs to hydroxyl methyl and methoxy protons respectively.

The ^{13}C NMR (figure 3.2.16.2) showed similar signals as those of damnacanthol (compound M) but with additional peak at δ168.6 and δ130.4. The former was sp^2 quarternary carbon C-2 which (figure 3.2.16.4) resonated downfield due to the deshielding effect of oxygen atom. The later was methine sp^2 carbon of C-1. The DEPT

(figure 3.2.16.3) and HMQC (figure 3.2.16.4) spectra help to complete the structure assignment of compound Q.

Finally by comparing the empirical data with the literature values of the known compounds brought to conclusion that compound P was 2-methoxy-3-oxyhydroxymethyl-9,10-anthraquinone **74**.

Table 3.2.16: ^{1}H NMR [300 MHz, δ_H (*J*, Hz)] and ^{13}C NMR [75 MHz, δ_C] of **74** in DMSO-d_6

	^{13}C	**^{1}H(*J*,H)**
1	130.5	8.50 (*d*, *J*=3.2 Hz)
2	163.3	-
3	168.7	-
4	111.5	8.3 *s*
4a	137.0	-
5	136.2	8.98 (*bd*, *J*=6.7 Hz)
6	128.4	8.73 (*dt*, *J*=7.4, 4.1 Hz)
7	127.8	8.65 (*dt*, *J*=7.4, 4.1 Hz)
8	136.3	9.03 (*bd*, *J*=6.7 Hz)
8a	133.3	-
9	181.6	-
9a	120.0	-
10	184.3	-
10a	133.3	-
CH_2O	53.8	5.43*s*
CH_3O	64.1	4.66*s*

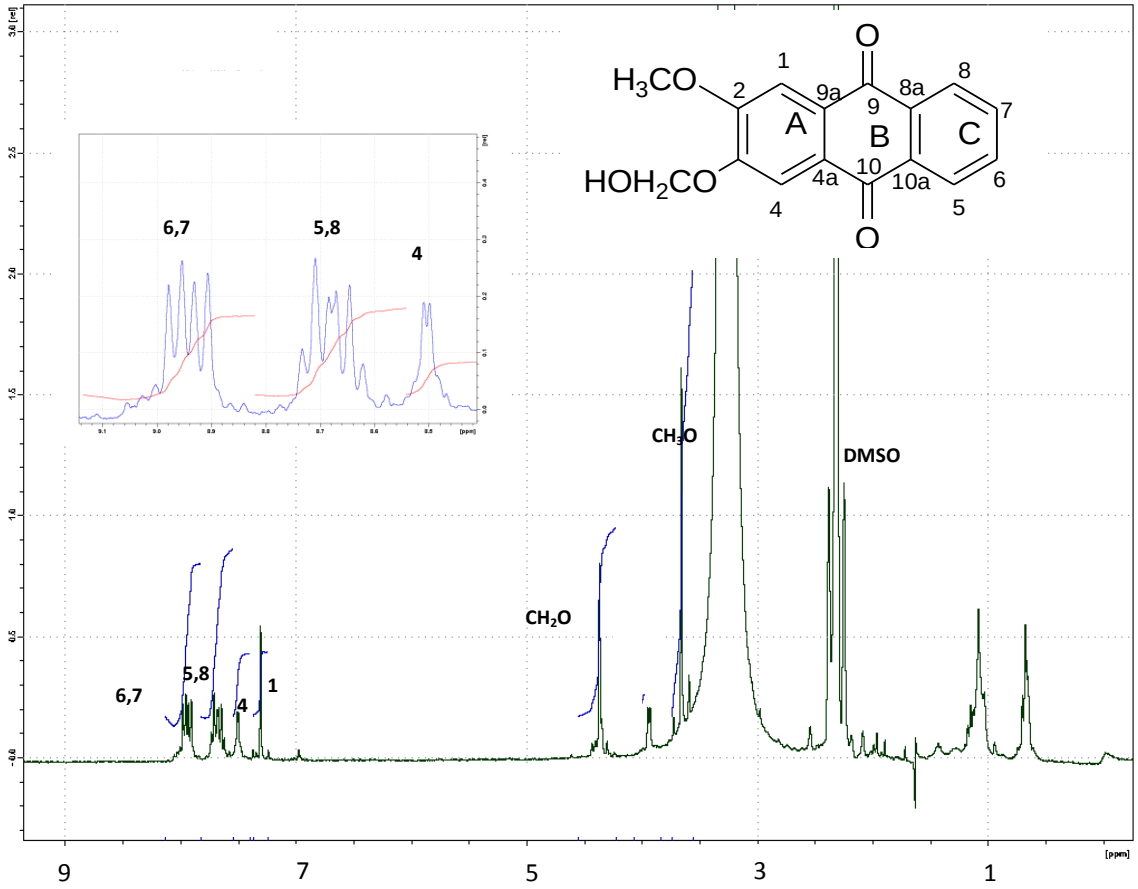

Figure 3.2.16.1: ^{1}H NMR spectrum of 2-methoxy-3-oxyhydroxymethyl-9,10-anthraquinone **74**

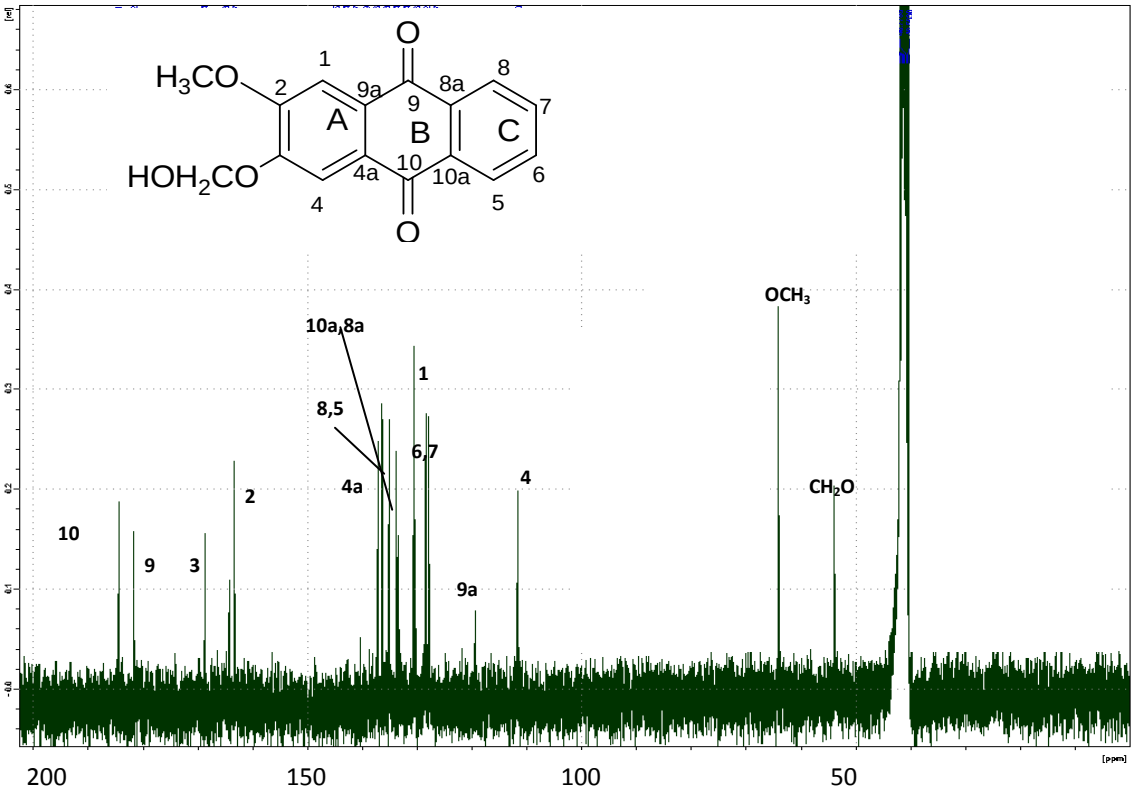

Figure 3.2.16.2: ^{13}C NMR spectrum of 2-methoxy-3-oxyhydroxymethyl-9,10-anthraquinone **74**

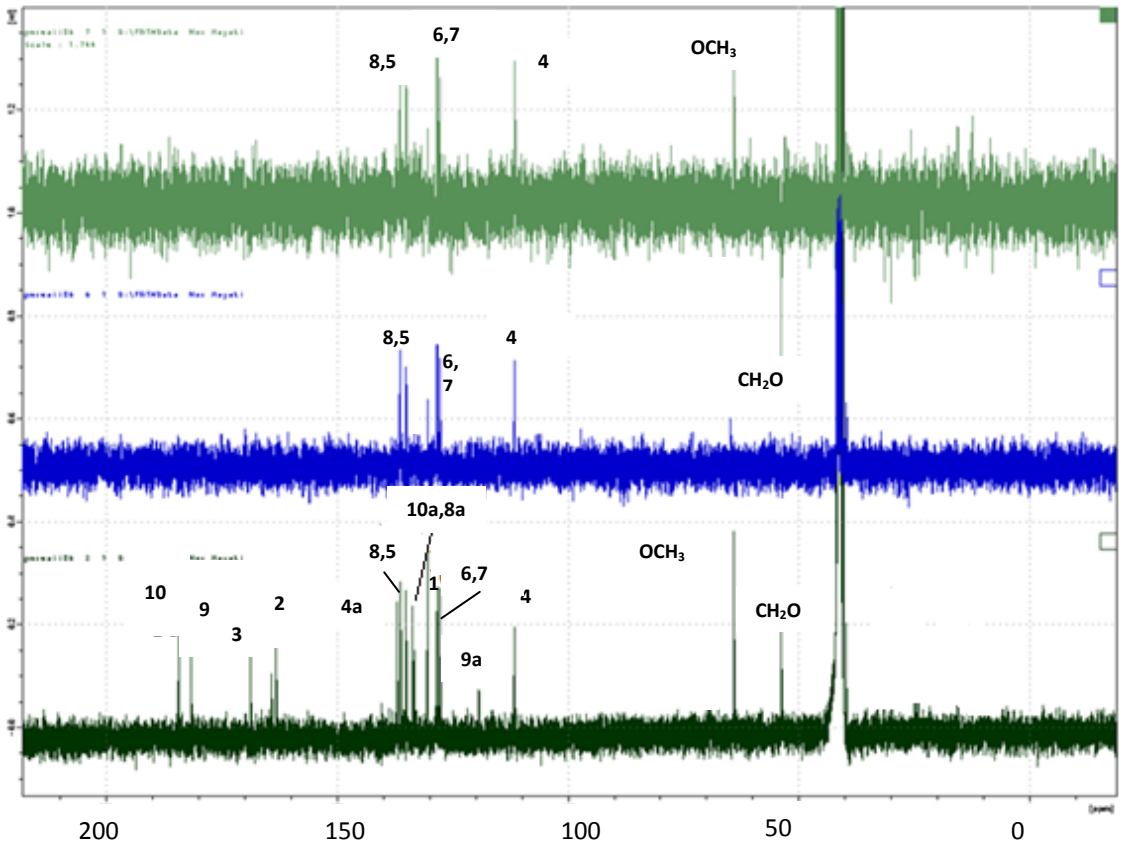

Figure 3.2.16.3: DEPT spectrum of 2-methoxy-3-oxyhydroxymethyl-9,10-anthraquinone **74**

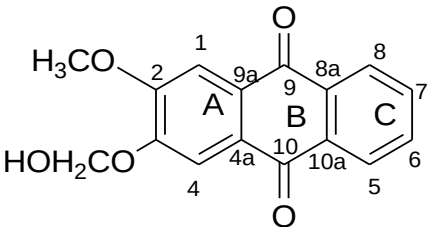

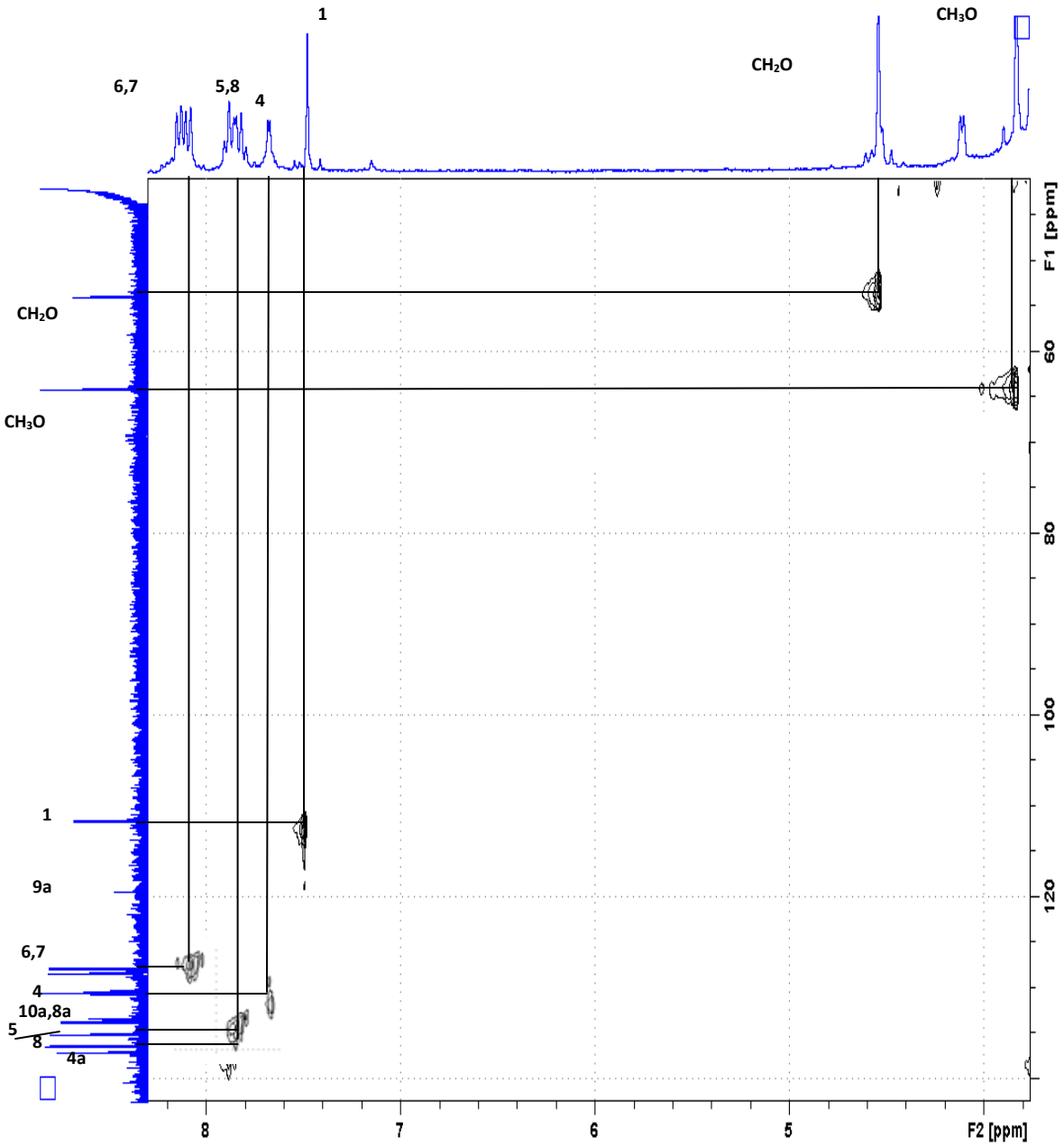

Figure 3.2.16.4: HMQC spectrum of 2-methoxy-3-oxyhydroxymethyl-9,10-anthraquinone **74**

3.2.17 Compound Q: *Lucidin-ω-methyl ether*

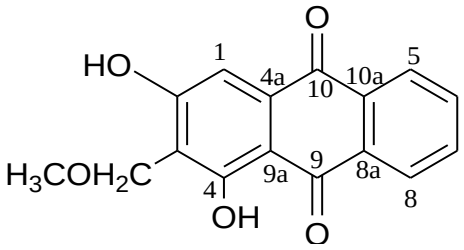

21

Lucidin-***ω***-methylether **21** (compound Q) was isolated as yellowish powder. It produced pseudo-molecular ion peak $[M - H]^-$ at m/z 283.05991 with ESI-MS which is consistent with molecular formula $C_{16}H_{12}O_5$. Its UV spectrum showed maximum absorption at 410, 280, 245, 205 nm. The IR spectrum indicate the presence of OH function with a broad band at 2929 cm^{-1} , C-H (1623cm^{-1}) and C=O function with the strong signal at 1730 cm^{-1}, 1674 cm^{-1} (Silverstein et al.,1991.

The ^{1}H NMR spectrum (figure 3.2.17.1) showed a singlet signal δ13.32 assignable to be the chelated proton at C-1 (table 3.2.17). Another peak was broad singlet, assigned to be of the hydroxyl protons. The aromatic protons signal resonated at δ8.29 (*dd*, J_1=1.8 and J_2=7.2 Hz, H5), δ7.82 (*dt*, J_1=1.8 and J_2=7.2 Hz, H-6), δ7.78 (*dt*, J_1=1.8 and J_2=7.2 Hz, H-7), δ8.32 (*dd*, J_1=1.8 and J_2=7.2 Hz, H-8). A singlet at δ7.35 (1H) was the isolated aromatic proton of H-1. Another singlet signals appear at δ4.95 (*s*, 2H) and δ3.60 (*s*, 3H) attributable to oxygenated methylene and methoxy protons.

The ^{13}C NMR (figure 3.2.17.2) showed two quarternary carboxyl carbons of C-10 and C-9 resonated at δ186.9 and δ182.2, respectively. Another quarternary sp^2 carbon could be observed at δ164.0(C-4) and δ161.8 (C-2). Both of them were dishielded and shifted to the lower field by the electronegative oxygen neighbour of the hydroxyl

group. The methylene and methoxy carbons both resonated at δ68.9 and δ59.5 respectively.

After the comparison of the empirical data together with the literature review (Kohei et al., 2010) of the known compound, it can be concluded that compound Q was lucidin- ***ω*** -methylether **21**.

Table 3.2.17: ^{1}H NMR [300 MHz, δ_H (*J*, Hz)] and ^{13}C NMR [75 MHz, δ_C] of **21** in DMSO-d_6

	^{13}C	**^{13}C***	**^{1}H(*J*,H)**	***^{1}H(*J*,H)**
1	109.7	109.8	7.35*s*	7.22*s*
2	161.8	161.8	9.40*bs*	9.37*s*
3	*ND*	134.1	-	
4	164.0	164.0	13.32*s*	13.22*s*
4a	*ND*	133.5	-	
5	134.1	134.1	8.29 (*dd*, *J*=7.2, 1.8 Hz)	8.08 (*dd*, *J*=7.1, 1.4 Hz)
6	127.3	126.7	7.82 (*dt*, *J*=7.2, 1.8 Hz)	7.85 (*dt*, *J*=7.1, 1.4Hz)
7	126.7	126.7	7.78 (*dt*, *J*=7.2, 1.8 Hz)	7.88 (*dt*, *J*=7.1, 1.4Hz)
8	134.1	134.0	8.32 (*dd*, *J*=7.2, 1.8 Hz)	8.15 (*dd*, *J*=7.1, 1.4Hz)
8a	127.3	127.3	-	-
9	182.2	182.2	-	-
9a	114.3	114.3	-	-
10	186.9	186.9	-	-
10a	*ND*	133.5	-	-
CH_2O	68.9	68.9	5.0*s*	4.40*s*
OCH_3	59.3	59.4	3.64*s*	3.25*s*

*^{1}H NMR [400.1 MHz]
*^{13}C NMR [100.1 MHz, δ_C] in $CDCl_3$
ND= not detected
(Kohei et al., 2010)

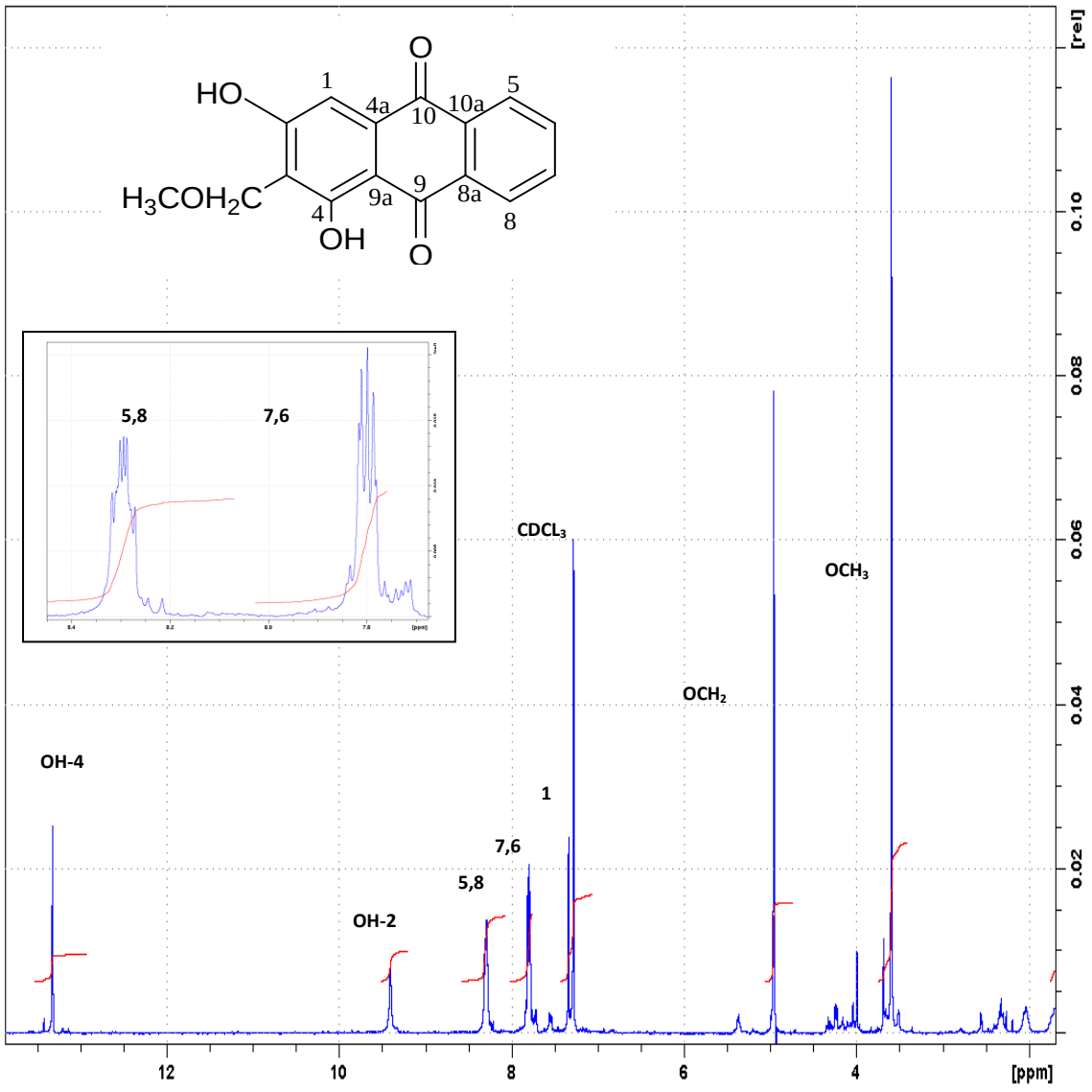

Figure 3.2.17.1: ^{1}HNMR spectrum of lucidin- ω -methyl ether **21**

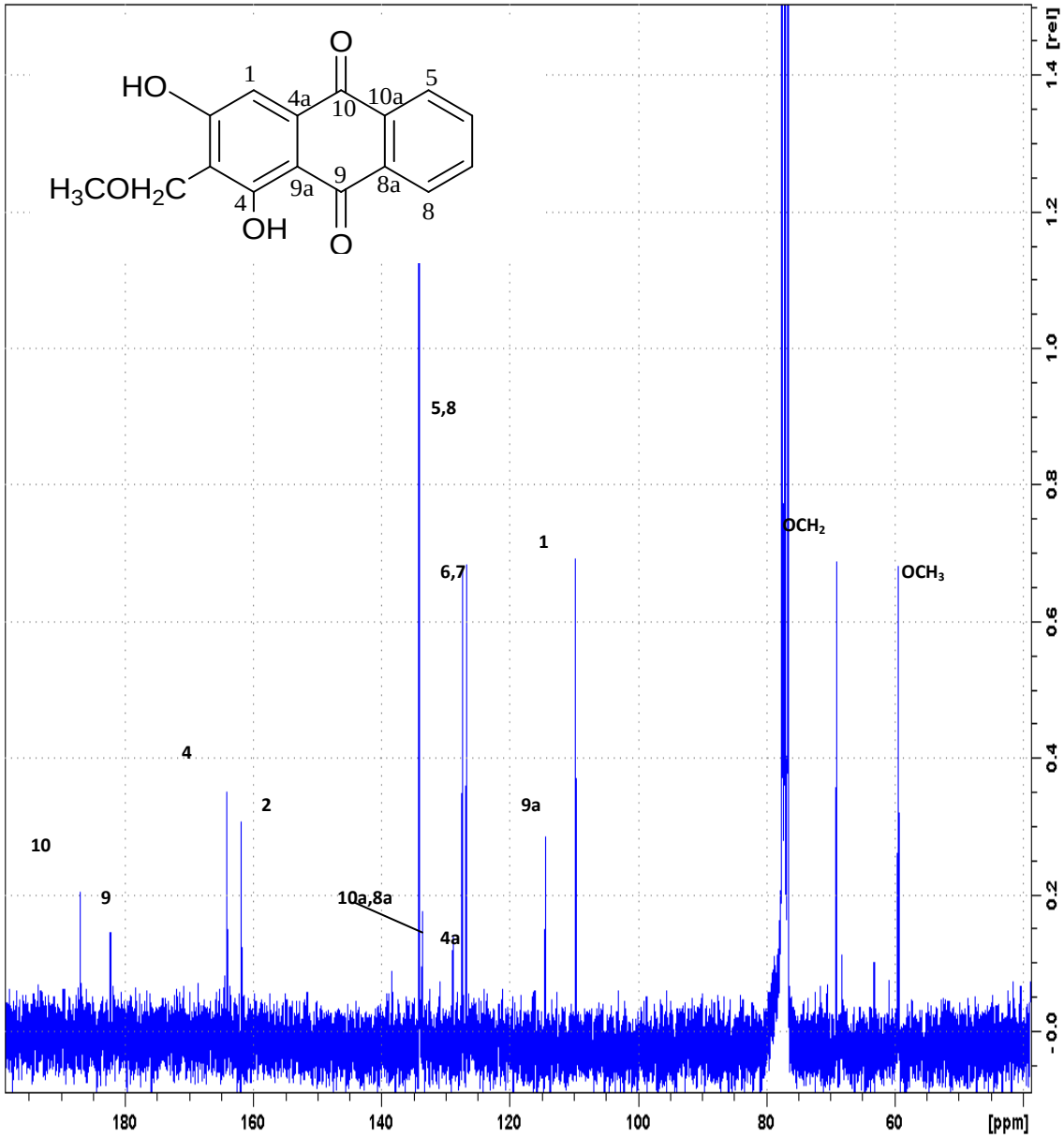

Figure 3.2.17.2: ^{13}C NMR spectrum of lucidin-ω-methyl ether **21**

CHAPTER 4:

SYNTHESIS

4.1 Introduction

The compound ursolic acid **60** was identified as the most active compound on hyaluronidase activity inhibition (chapter 5.4.2). Based on Lipinski rules of five which mentioned that the orally administered drugs should have the molecular weight less than five hundred, not more than five hydrogen bond donor groups, ten or less hydrogen bond acceptor groups and calculated log *P* value less than five (Lipinski et al., 2001), ursolic acid **60** (456.707 g/mol) was found to follow the rules and thus has the 'druglike' properties. Eventhough this compound has log *P* value of 7.317 (Maurya et al., 2012) which violating the Lipinski's rule of five, but since the number of violating is no more than one, thus it is still acceptable.

In order to study structure activity relationships of ursolic acid, the compound needs to be modified in order to obtain derivatives with various functionalities. Thus, the obtained derivatives together with ursolic acid **60** will be investigated with respect to their structure activity relationship quantitatively towards the hyaluronidase activity inhibition. The synthetic modifications were executed as described by Chao-Mei et al. (2005), with slight changes on the solvents and reagents used.

Eight analogues were obtained (**75-81**) and they were tested for their inhibitory activity towards hyaluronidase. Scheme 4.1-4.3 outlined briefly the synthetic pathway of these analogues. Ursolic acid **60** was oxidized with pyridinium chlorochromate (PCC) in mixture of dichloromethane acetone to give the 3-oxo compound **75** (Scheme 4.1). Compound **75** was further treated with hydroxylamine hydrochloride in pyridine to give the hydroxyimino compound **76**.

3-acetoxy ursolic acid **77** was obtained in a simple treatment with acetic anhydride in pyridine (Scheme 4.2). Compound **77** then was stirred with trimethylsilyl diazomethane (TMS) to give methyl ester compound **78**.

Treatment of ursolic acid **60** with trimethylsilyl diazomethane in methanol and toluene yielded methyl ester compound **79**. It was oxidized with pyridinium chlorochromate to give the 3-oxo methyl ester compound **80**. The compound **80** was further treated with hydroxylamine hydrochloride to obtaine 3-hydroxylamino methyl ester **81** (Scheme 4.3).

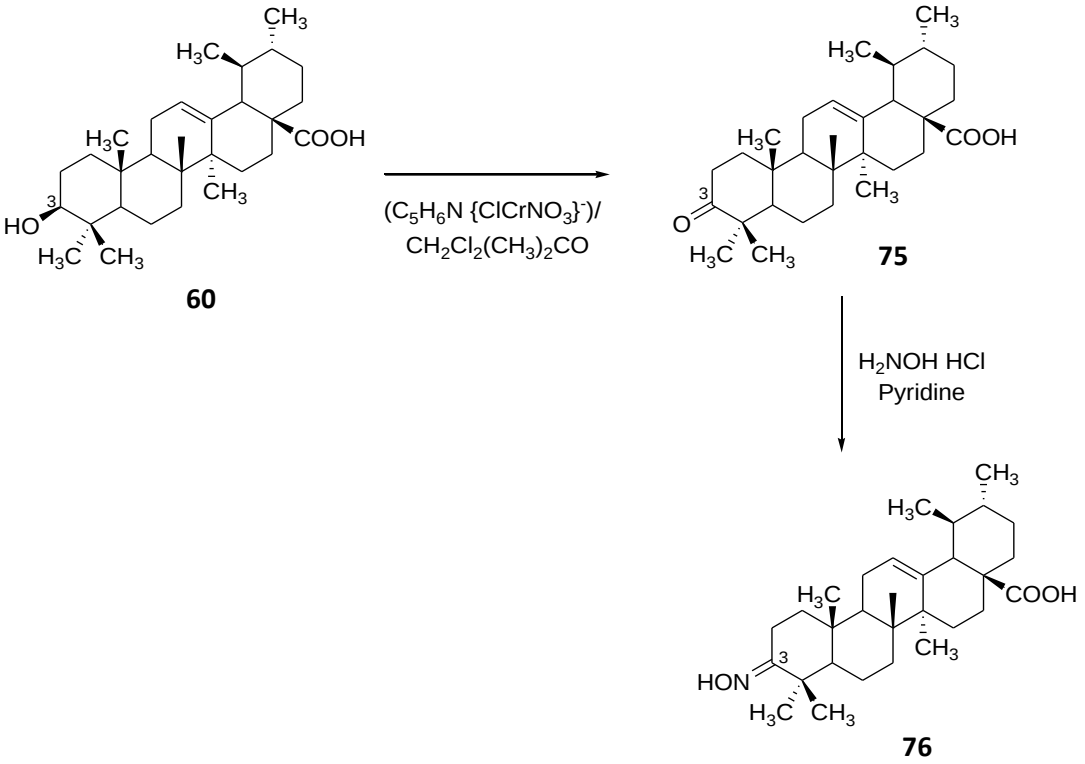

$(C_5H_6N)\{ClCrNO_3\}$ = PCC; CH_2Cl_2 = dichloromethane; $(CH_3)_2CO$ = acetone; H_2NOH HCl = hydroxylamine hydrochloride

Scheme 4.1: Synthesis of ursolic acid **60** derivatives **75**-**76**

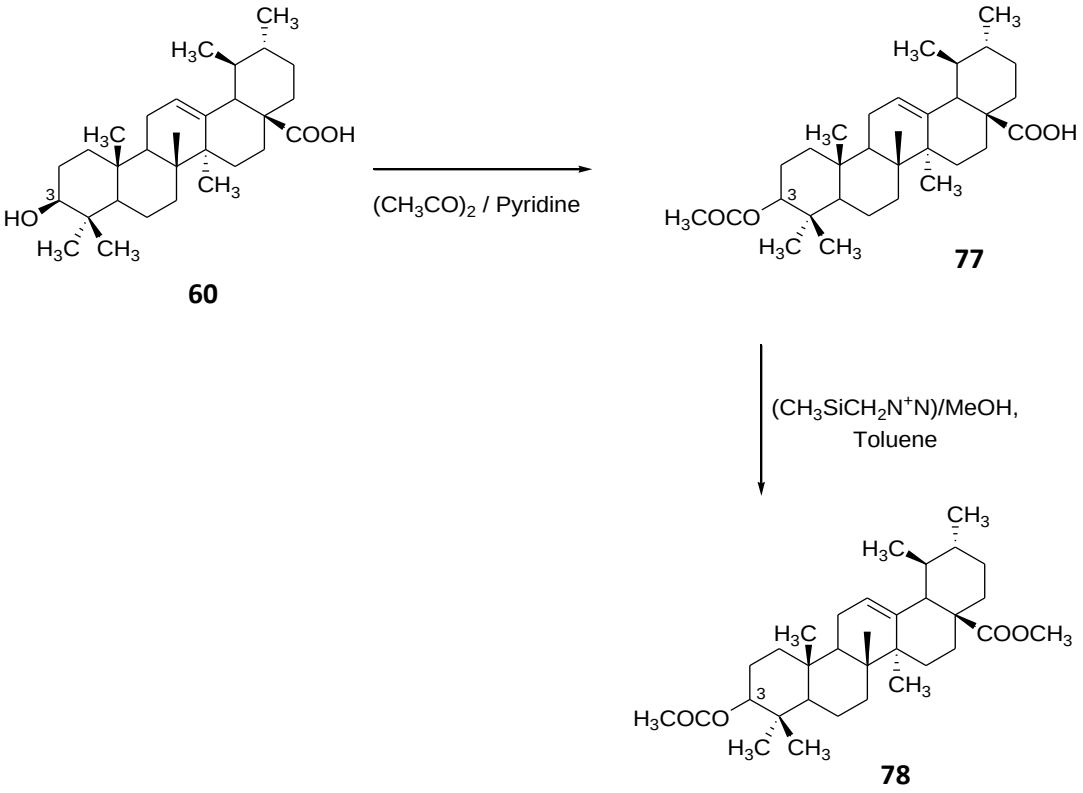

$(CH_3CO)_2$ = acetic anhydride; $(CH_3SiCH_2N^+N)$ = trimethylsilyl diazomethane (TMS)

Scheme 4.2: Synthesis of ursolic acid **60** derivatives **77**-**78**

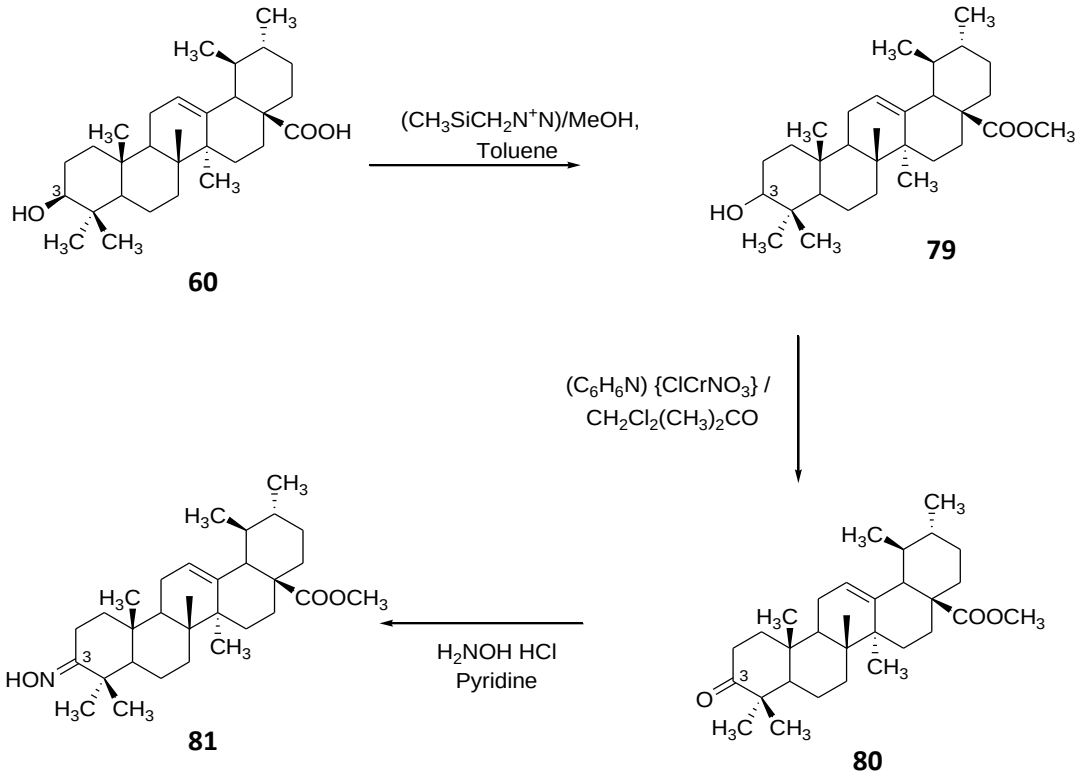

$(CH_3SiCH_2N^+N)$ = TMS; $(C_5H_6N)\{ClCrNO_3\}$ = PCC; H_2NOH HCl = hydroxylamine hydrochloride

Scheme 4.3: Synthesis of ursolic acid **60** derivatives **79**-**81**

4.1 Results and discussion

The following paragraphs described briefly the structure elucidation of the analogues (**75-81**). The HRESIMS of compound **75** shows a pseudo-molecular ion peak $[M-H]^-$ at m/z 453.33524 corresponding to the molecular formula of $C_{30}H_{46}O_3$. This observation was consistent with the removal of two hydrogen atoms from the compound **60**, the H-3 and C3-OH. This conclusion was supported by the absence of H-3 peak in the ^{1}H NMR spectrum (figure 4.1). A peak at very low field (218.0 ppm) suggested the presence of ketone group in **75** (figure 4.2). The C-2 and C-4 chemical shift were observed at 28.5 and 39.2 respectively, in **60**. The corresponding value for the same carbon in **75** were 33.5 and 47.5 demonstrated the high deshielding effect of CO at position C-3. The value of same carbons, C-2 and C-4, in **76** were 28.8 and 39.6 (figure 4.4) respectively, were almost similar to the initial compound **60**. Apart from that, the mass spectrum of **76** [ESI, $M+H]^+$ at m/z 470.35516 corresponding to molecular formula of $C_{30}H_{47}NO_3$ supported the incorporation of the hydroxyimino functional group, NOH.

The peak at 1.91 ppm in ^{1}H NMR spectrum (figure 4.5) (3H, *s*) and 20.7 and 169.9 ppm in ^{13}C NMR (figure 4.6) is consistence with the presence of acetyl group in **77**. The large coupling constant of H-3 in the ^{1}H NMR of **77** (4.68, 1H, *dd*, *J*= 5.1, 10.9) indicated that H-3 is α orientated (Ma et al., 2005). The mass spectrum of **77** showed value of m/z 497.36343 $[M-H]^-$ corresponding to molecular formula $C_{32}H_{50}O_4$. An additional peak could be observed in ^{1}H NMR of compound **78** at 3.74 (3H, *s*) (figure 4.7) and 51.6 in ^{13}C NMR (figure 4.8) indicated the presence of methoxy group. The values for most of the carbons were almost similar to the compound **78**. Apart from that, the mass spectrum [ESI, $(M-K)^-$] showed value of m/z 473.28149 which is corresponding to the molecular formula $C_{33}H_{52}O_4$.

The ^{1}H NMR (figure 4.11) of compound **80** indicated the absence of H-3 signal. The methoxy signal, however, was present at 5.10 ppm in ^{1}H NMR and 51.7 ppm in ^{13}C NMR (figure 4.12). The down field signal of C-3 at 216.3 ppm indicated the presence of ketone's carbonyl group. As in compound **75**, the C-4 chemical shifts were shifted downfield at 48.5 ppm, compared to ursolic acid **60**, due to the deshielding effect of the electrophilic characteristic of the C-3 ketone functional group. The mass spectrum value m/z 491.34198 [ESI, $(M+Na)^{+}$] is consistent with the molecular formula $C_{31}H_{48}O_3$ of compound **80**.

The presence of free hydroxyl group at the extreme downfield region of 12.36 ppm (1H, *s*) indicated the presence of hydroxyimino group, NOH, into the compound **81** (figure 4.13). It was further supported by the signal for oximes (R_2CNOH) at 164.3 ppm (figure 4.14). The H-2 was shifted to 3.49 ppm (*dd*, *J*= 3.3, 5.2) due to the deshielding effect of the hydroxyimino group at C-3. The mass spectral data supported the molecular formula $C_{31}H_{49}NO_3$ with m/z 506.35175 [ESI, $(M + Na)^{+}$].

Table 4.1 and 4.2 summarised the value of ^{1}H NMR and ^{13}C NMR of each compound **75-81**.

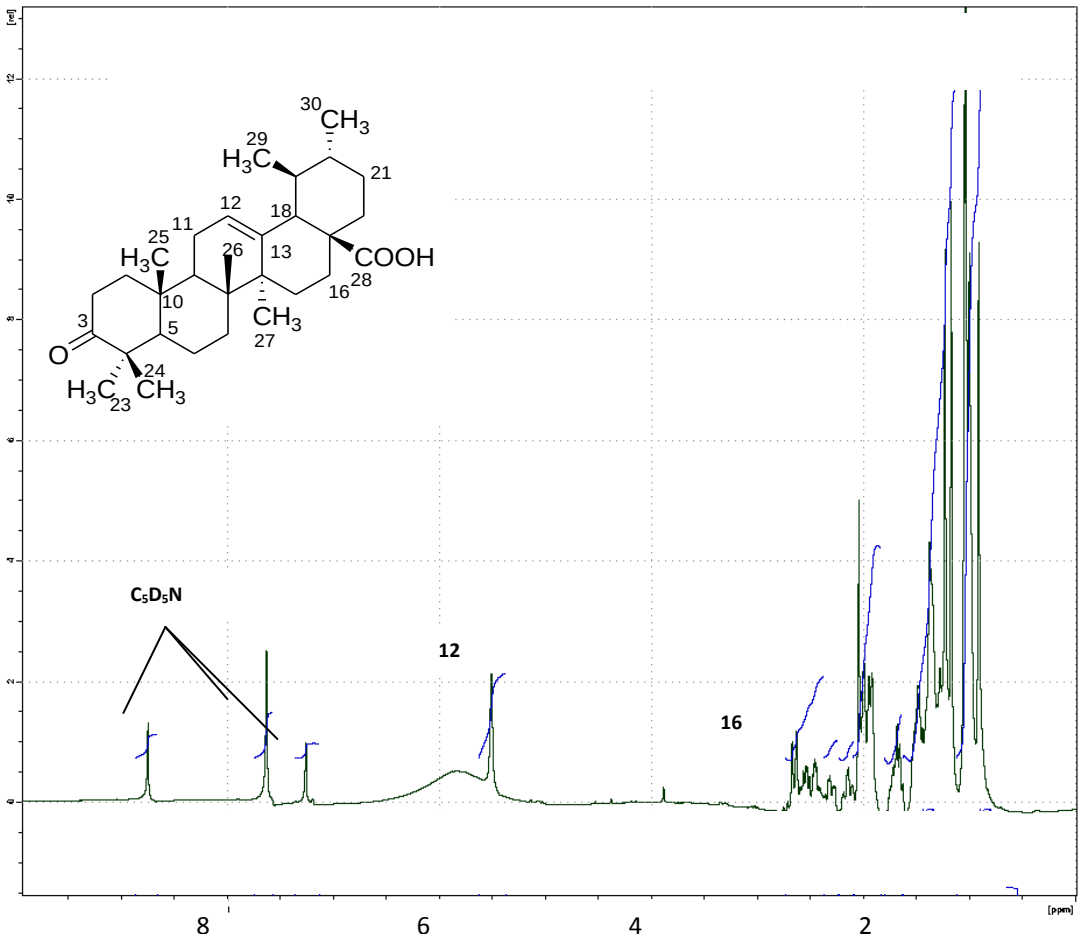

Figure 4.1: ^{1}H NMR spectrum of 3-oxo-urs-12-en-28-oic acid **75**

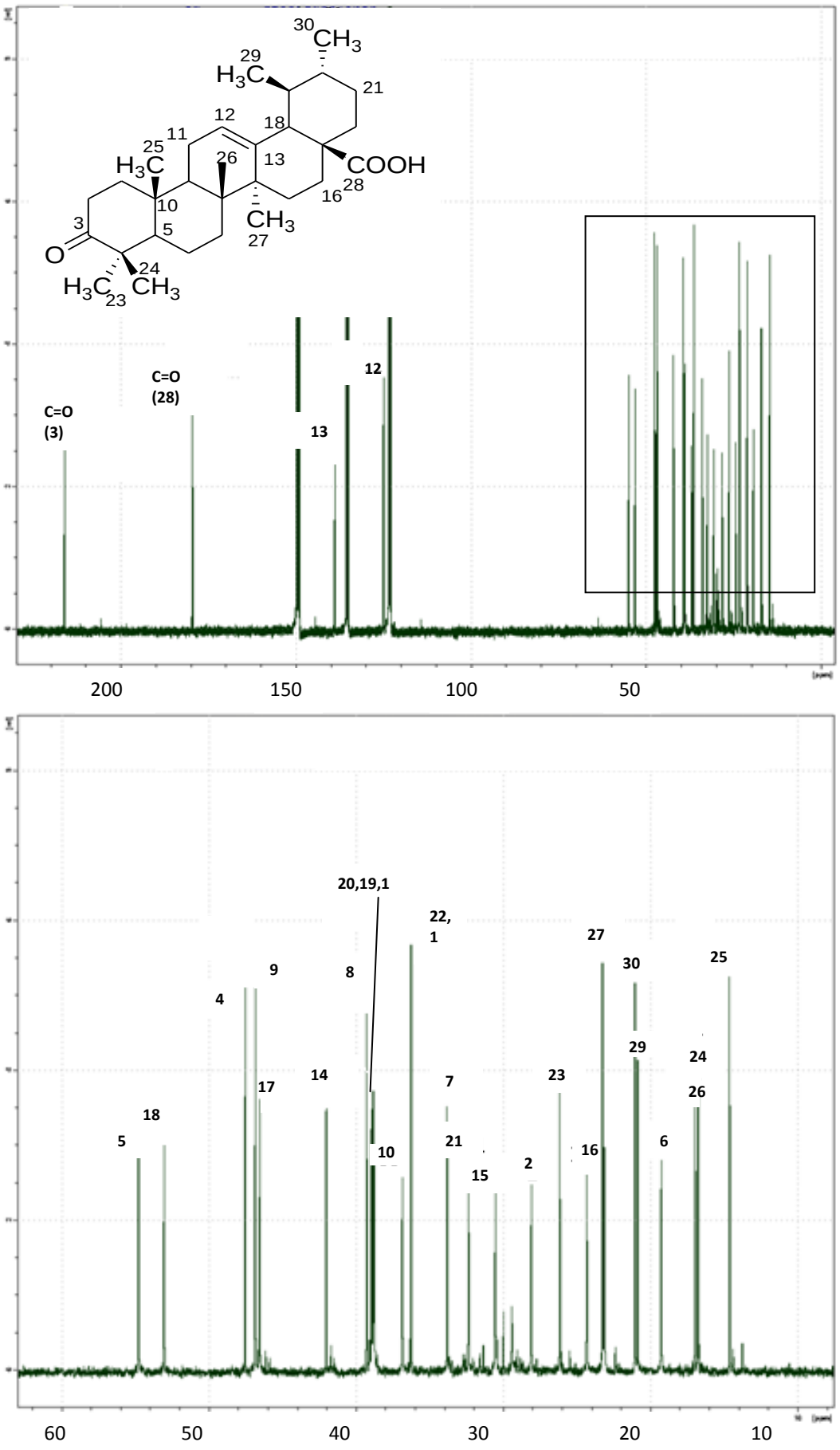

Figure 4.2: ^{13}C NMR spectrum of 3-oxo-urs-12-en-28-oic acid **75**

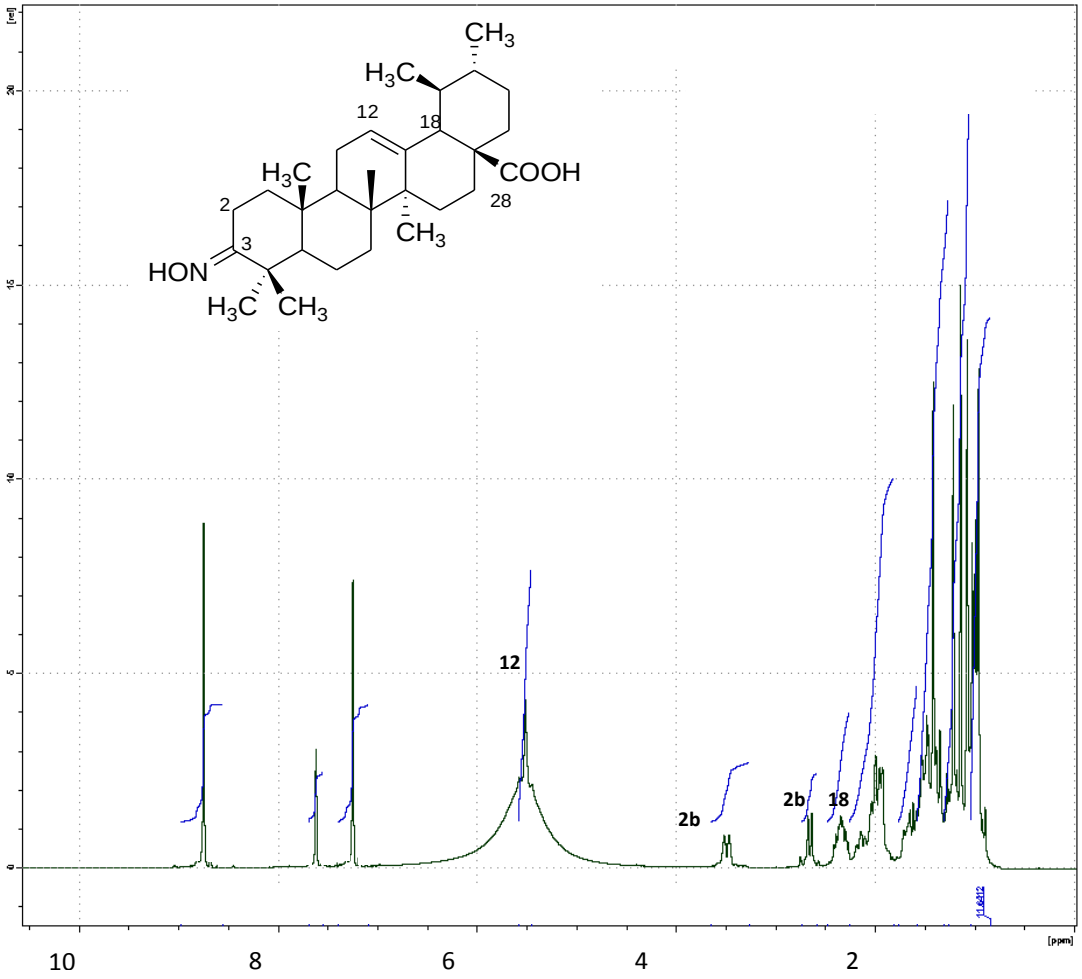

Figure 4.3: ^{1}H NMR spectrum of 3-hydroxyimino-urs-12-en-28-oic acid **76**

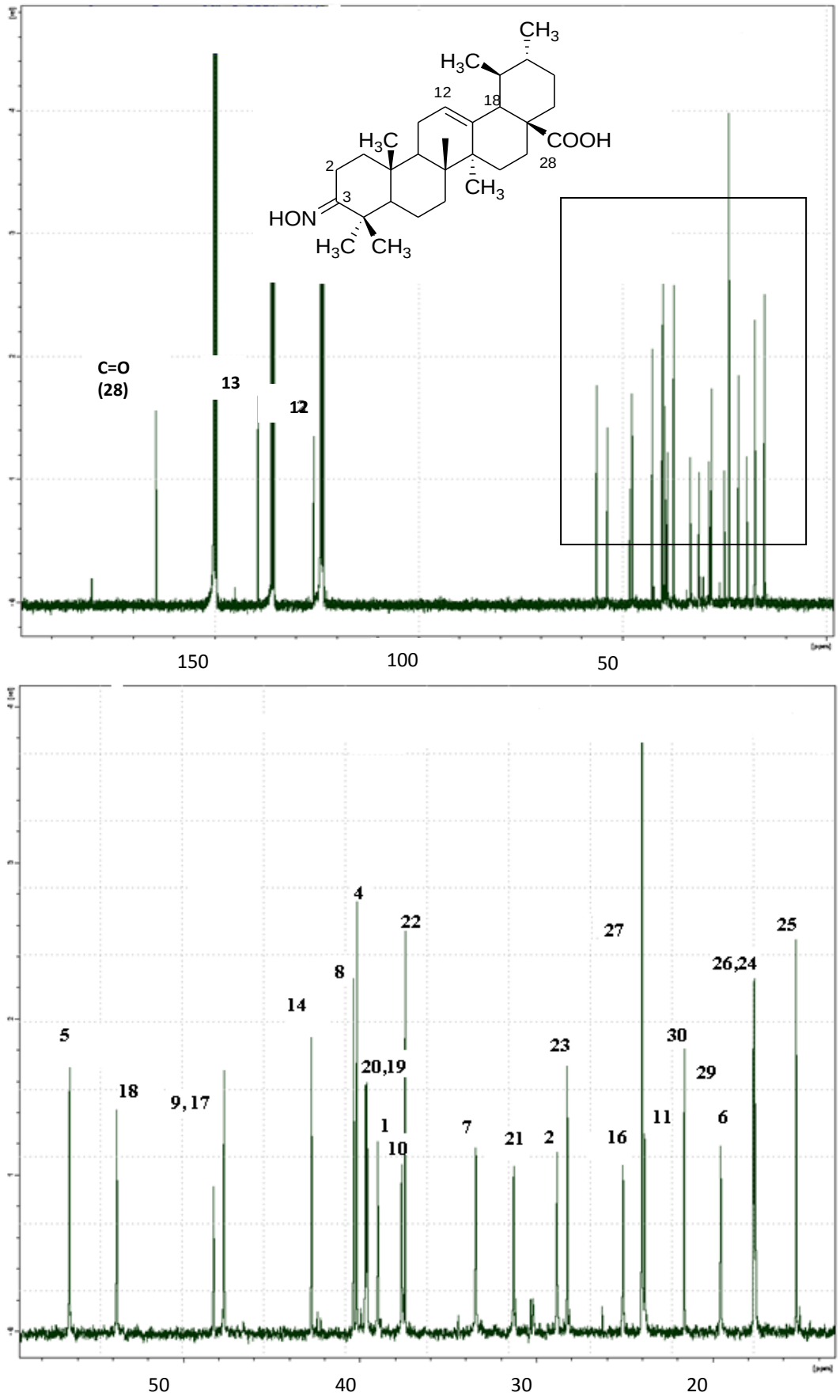

Figure 4.4: ^{13}C NMR spectrum of 3-hydroxyimino-urs-12-en-28-oic acid **76**

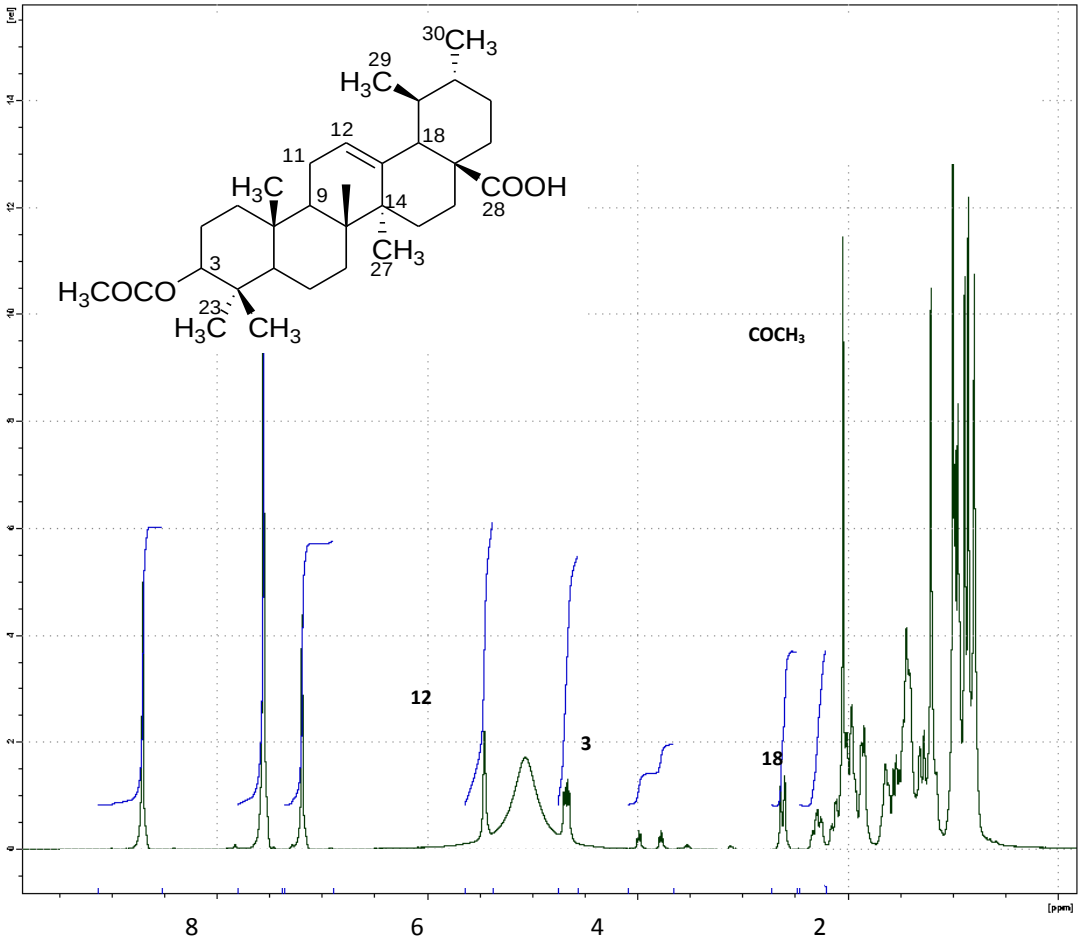

Figure 4.5: ^{1}H NMR spectrum of 3-acetyl-urs-12-en-28-oic acid **77**

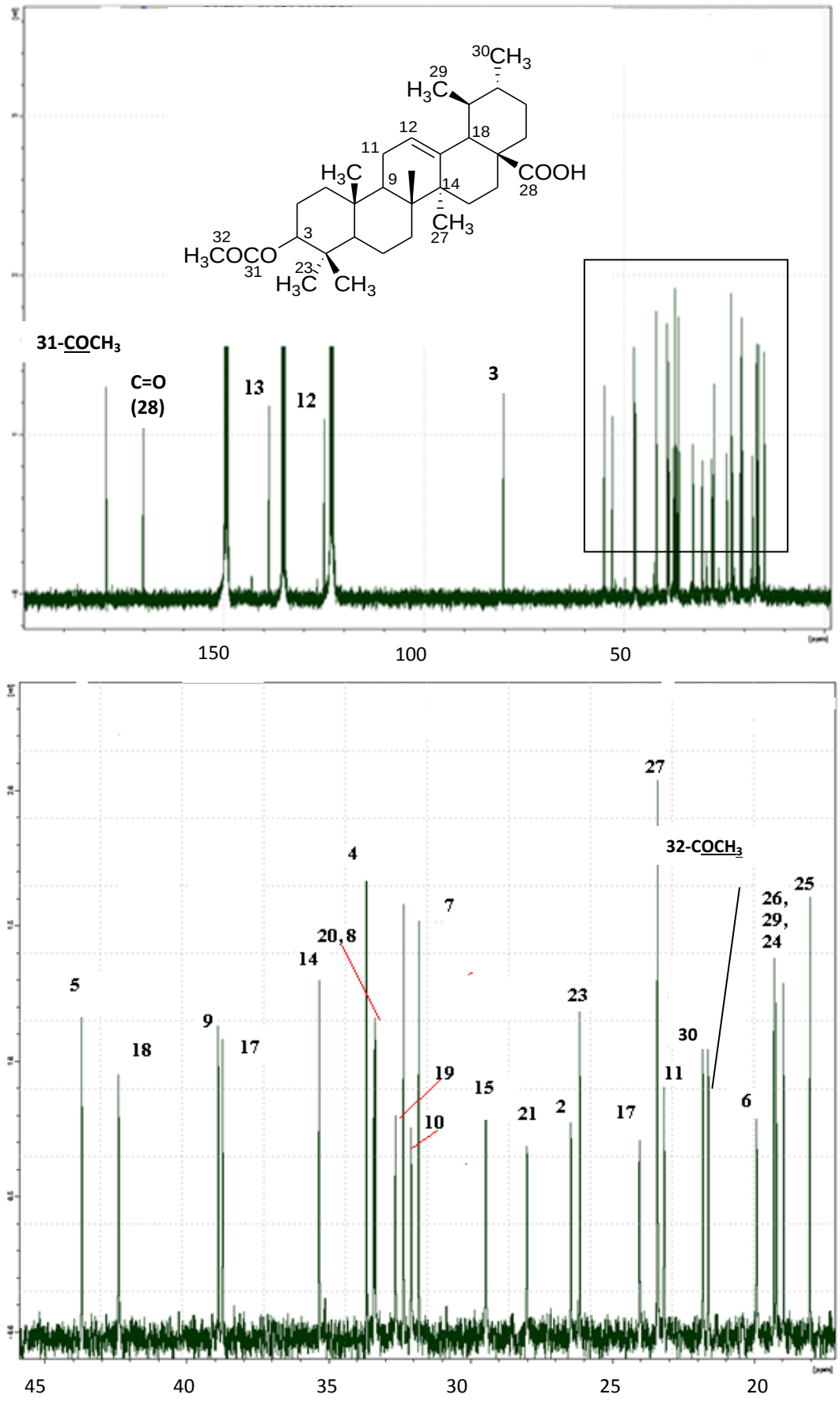

Figure 4.6: ^{13}C NMR spectrum of 3-acetyl-urs-12-en-28-oic acid **77**

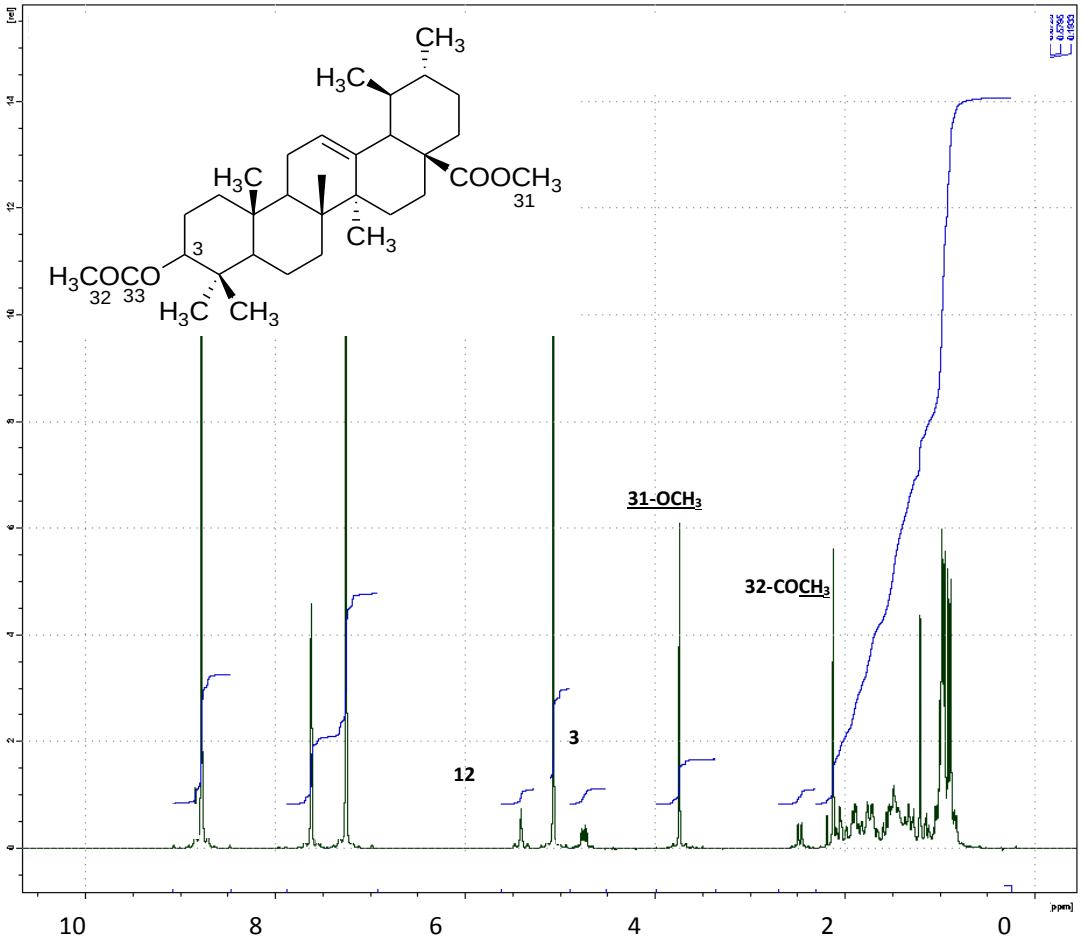

Figure 4.7: ^{1}H NMR spectrum of 3-acetyl-urs-12-en-28-oic acid methyl ester **78**

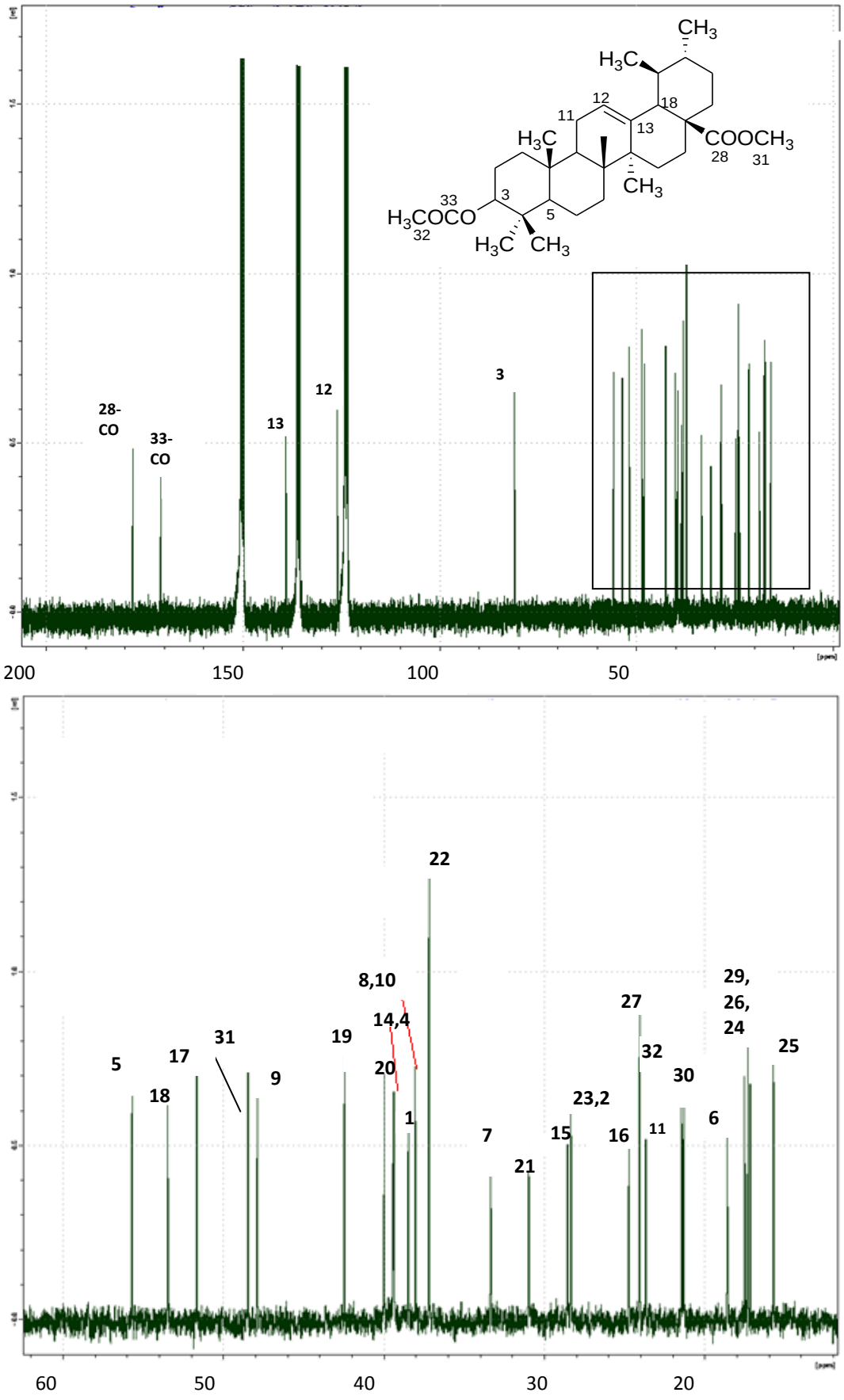

Figure 4.8: ^{13}C NMR spectrum of 3-acetyl-urs-12-en-28-oic acid methyl ester **78**

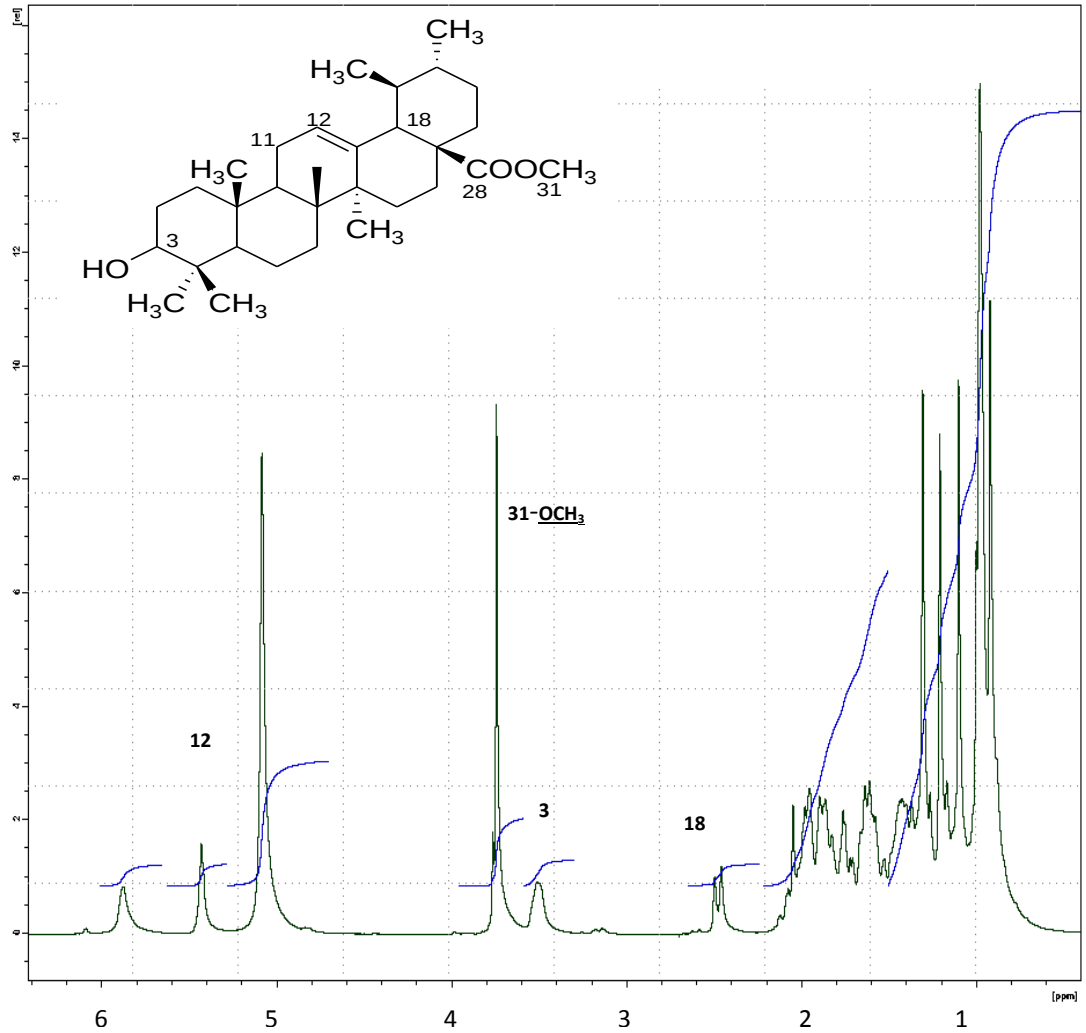

Figure 4.9: ^{1}H NMR spectrum of 3-hydroxy-urs-12-en-28-oic acid methyl ester **79**

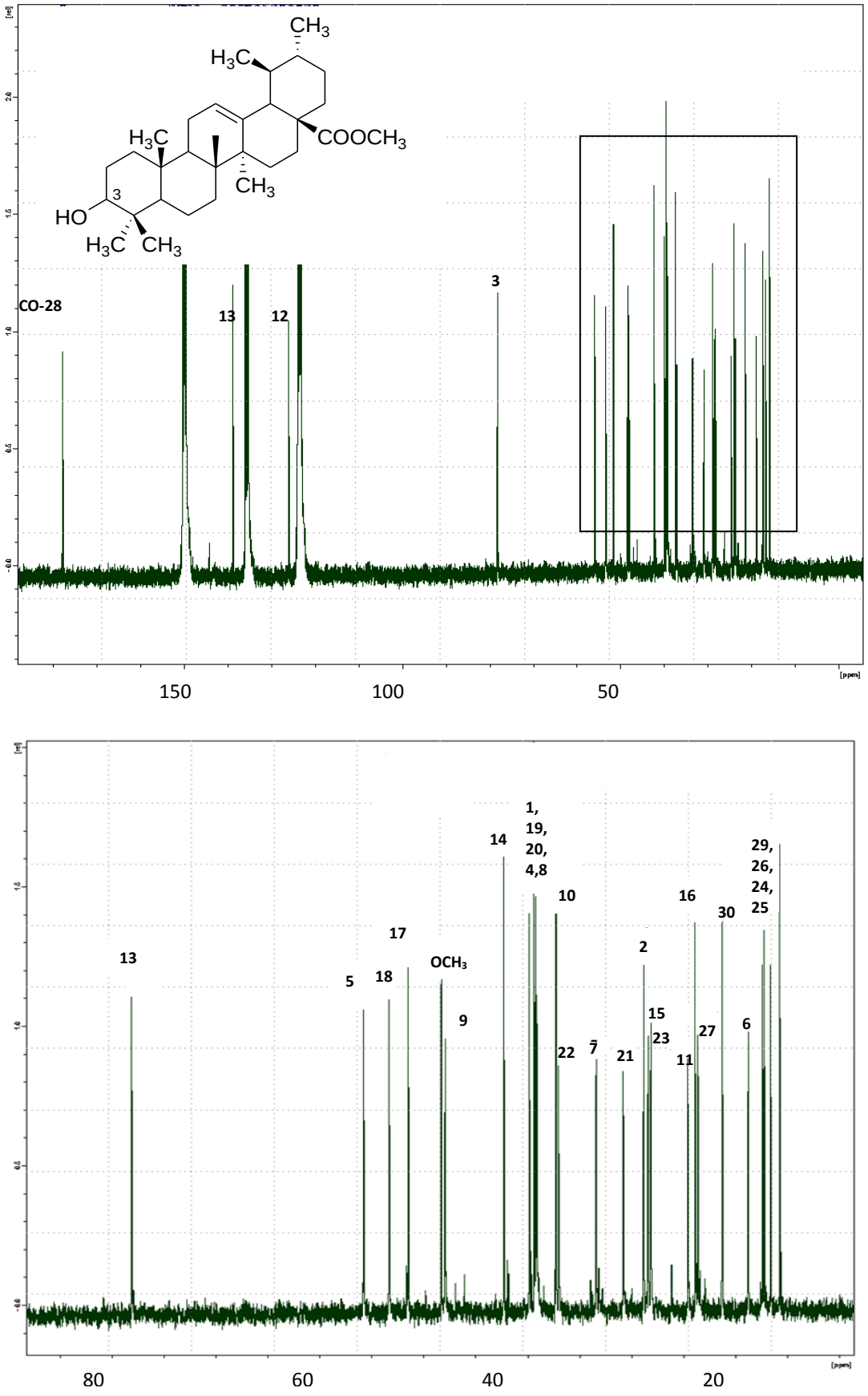

Figure 4.10: ^{13}C NMR spectrum of 3-hydroxy-urs-12-en-28-oic acid methyl ester **79**

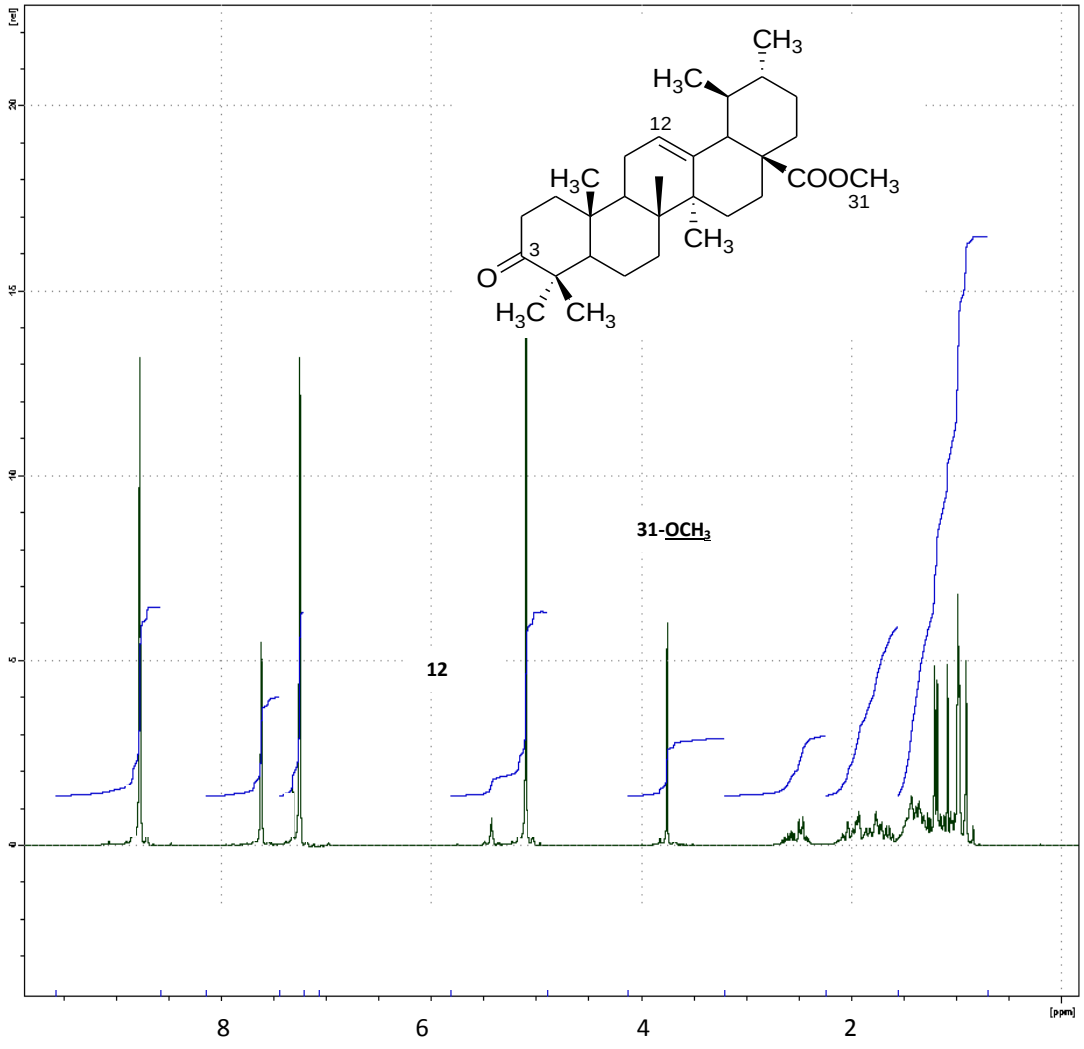

Figure 4.11: ^{1}H NMR spectrum of 3-oxo-urs-12-en-28-oic acid methyl ester **80**

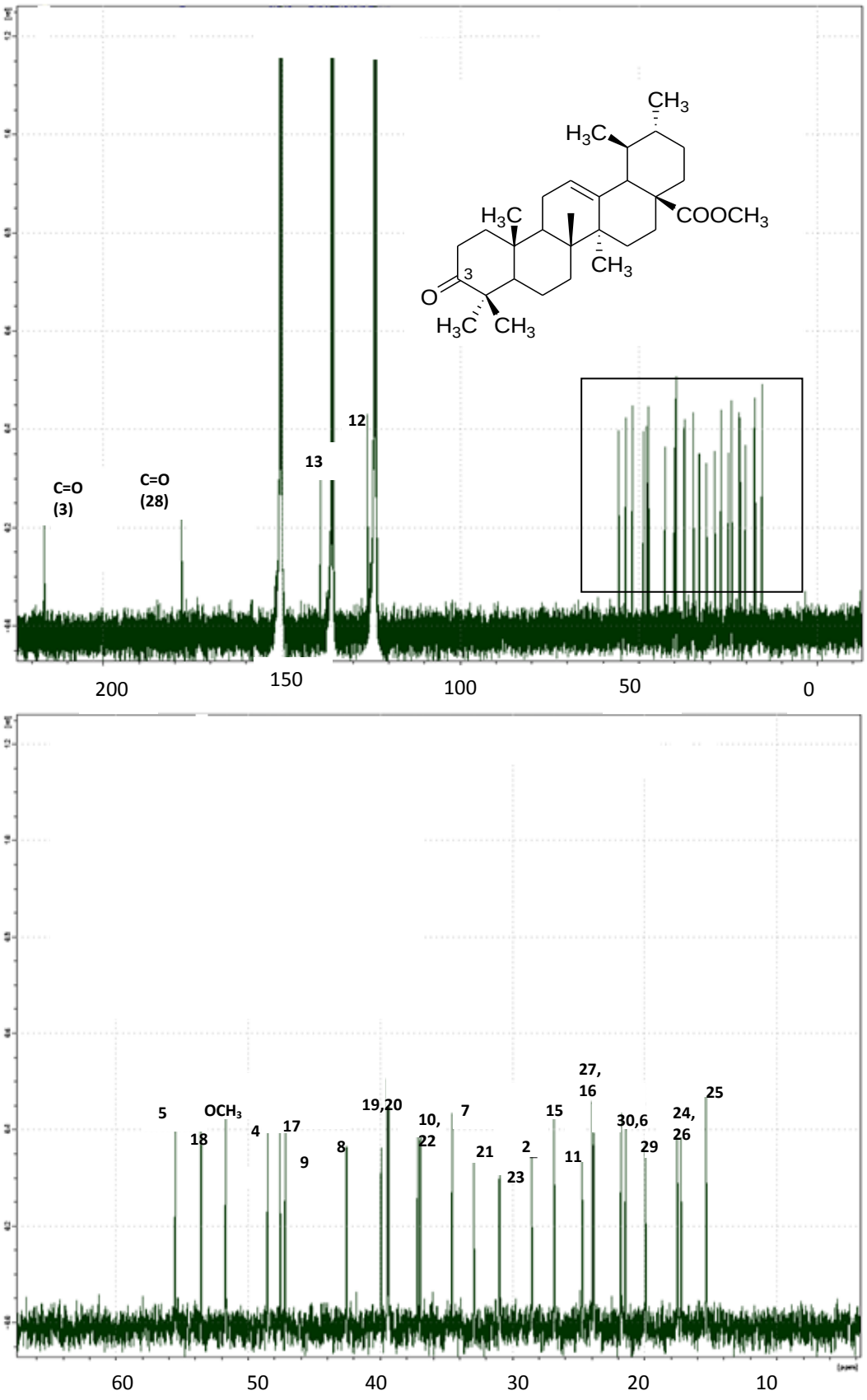

Figure 4.12: ^{13}C NMR spectrum of 3-oxo-urs-12-en-28-oic acid methyl ester **80**

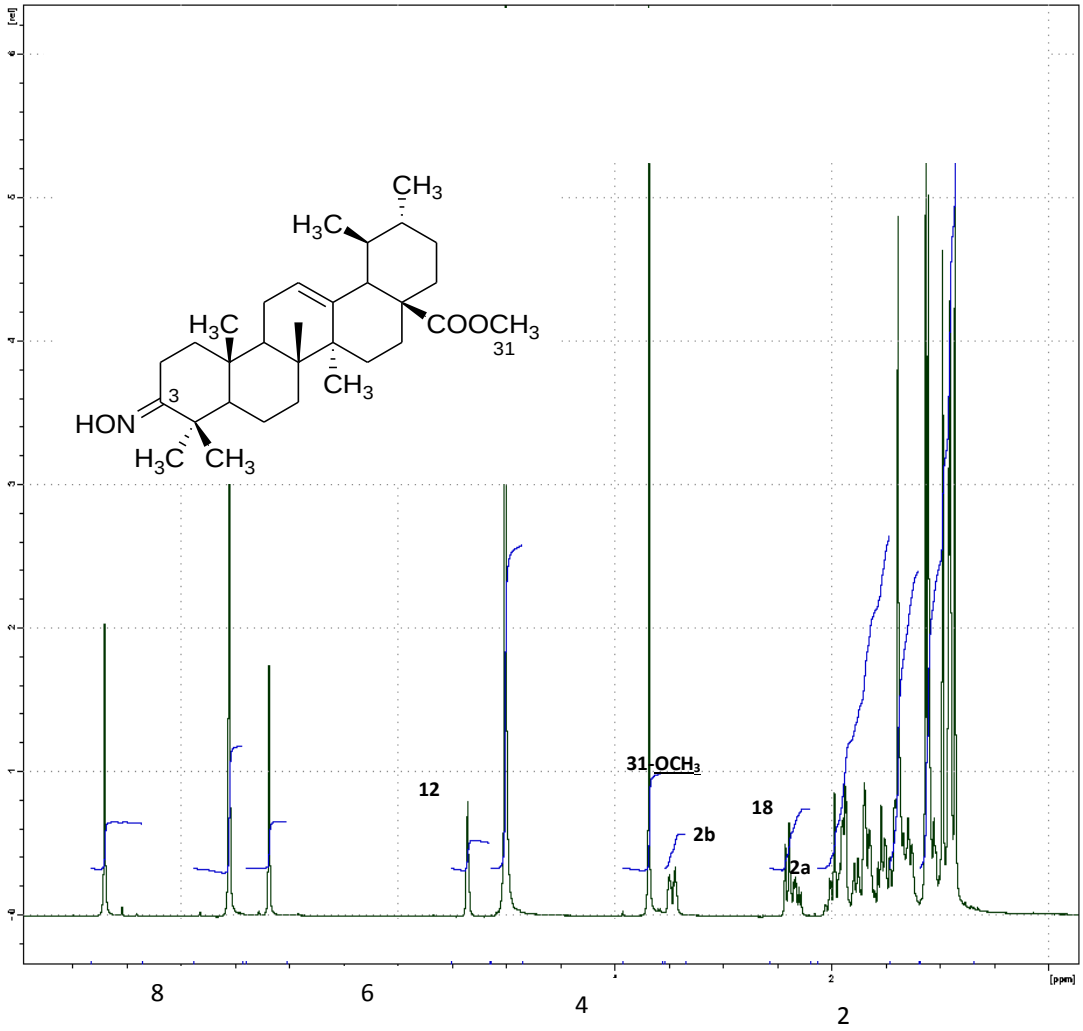

Figure 4.13: ^{1}H NMR spectrum of 3-hydroxyimino-urs-12-en-28-oic acid methyl este**r**

81

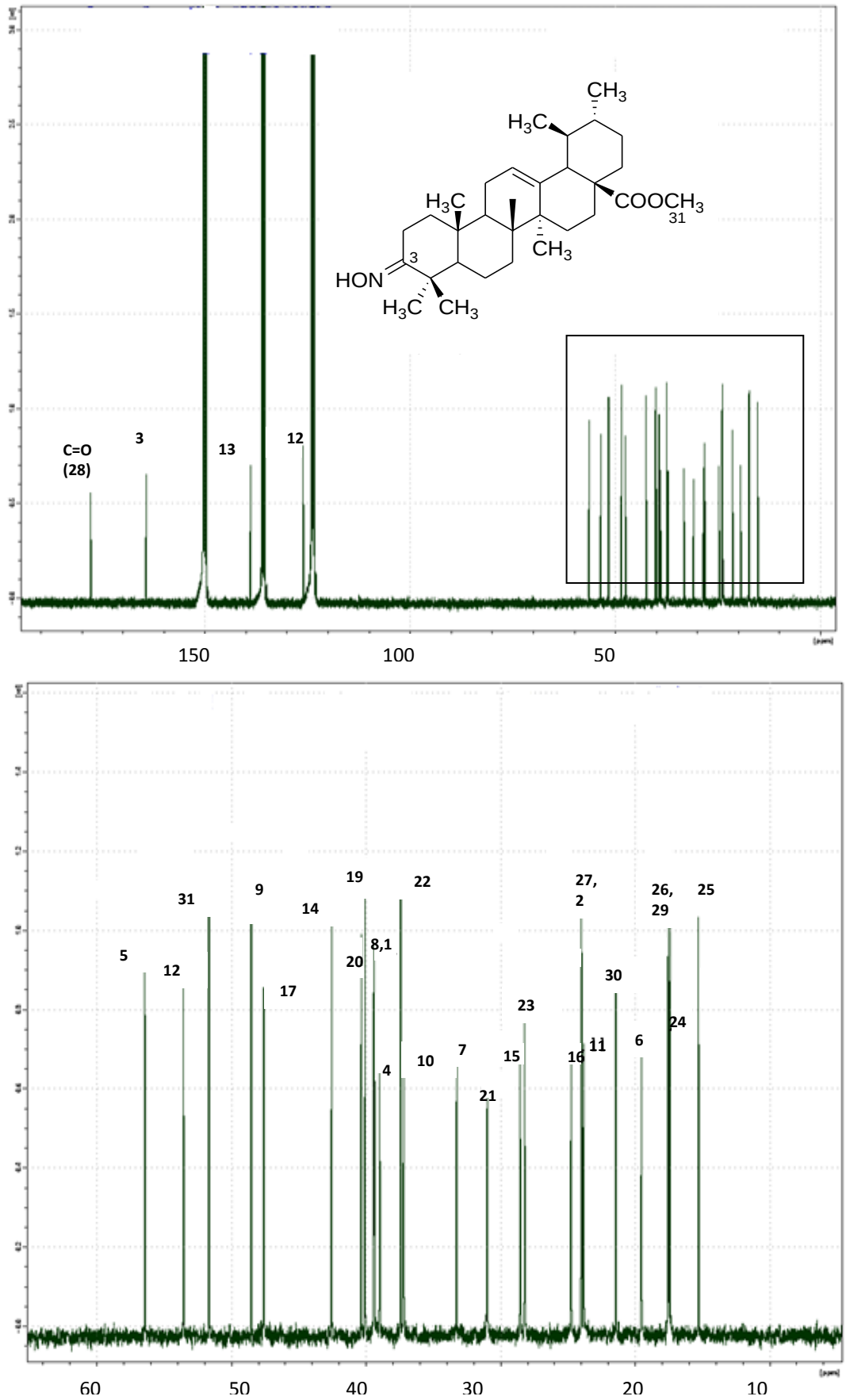

Figure 4.14: ^{13}CNMR spectrum of 3-hydroxyimino-urs-12-en-28-oic acid methyl ester

81

Table 4.1: ^{13}C NMR [70MHz, δ_C] of **75-81** in C_5D_5N

Position	***60***	***75***	***76***	***77***	***78***	***79***	***80***	***81***
1	38.9	38.7	38.9	38.8	38.4	39.8	39.9	39.3
2	28.4	28.0	28.8	28.0	28.5	28.8	28.5	24.7
3	77.9	218.0	164.4	79.1	80.8	78.0	216.3	164.2
4	39.3	47.5	40.1	41.8	39.3	39.0	48.4	38.9
5	55.6	54.7	56.4	54.9	55.6	55.7	55.4	56.4
6	18.5	19.2	19.5	17.9	18.5	18.7	21.3	19.4
7	33.4	33.7	33.4	36.5	33.3	33.3	34.5	33.2
8	39.7	39.2	40.3	38.9	38.0	39.6	42.5	39.4
9	47.8	46.5	47.6	47.4	47.8	47.9	47.1	47.5
10	37.2	36.8	37.6	36.8	38.0	37.3	37.1	37.1
11	23.4	23.3	23.8	22.9	23.0	24.5	24.6	23.7
12	125.4	126.0	125.7	124.8	125.8	125.9	125.8	126.0
13	139.0	140.0	139.4	138.6	138.8	138.7	138.9	138.9
14	42.3	41.9	42.7	41. 9	39.3	42.2	42.5	42.5
15	27.8	30.4	-	32.7	28.5	28.7	26.8	28.5
16	24.7	24.2	25.0	24.3	24.7	23.3	23.7	24.7
17	47.8	46.1	48.2	47.2	51.6	51.4	47.5	48.4
18	53.3	53.0	53.7	52.9	53.4	53.3	53.5	53.5
19	39.1	38.9	37.4	37.8	42.4	39.3	39.4	40.0
20	39.1	38.8	39.6	39.3	39.9	39.2	39.3	40.3
21	30.8	32.3	31.2	30.5	30.9	30.7	32.8	30.9
22	37.0	36.2	37.4	37.3	37.1	36.9	36.9	37.3
23	28.6	26.1	28.2	27.6	28.3	28.1	30.9	28.1
24	16.4	16.9	17.7	16.4	17.1	16.5	17.2	17.4
25	15.4	14.5	15.2	15.0	15.6	15.6	15.3	15.2
26	17.2	16.7	17.5	16.9	17.2	17.2	17.4	17.5
27	23.7	23.3	23.9	23.3	24.0	22.9	23.9	23.9
28	179.8	182.0	180.2	179.3	177.8	177.7	177.8	177.8
29	17.3	20.8	21.6	16.8	17.4	17.3	19.9	17.3
30	21.2	21.0	21.6	20.6	21.2	21.2	21.7	21.4
$\underline{CO}CH_3$	-	-	-	169.9	170.7	-	-	-
$CO\underline{CH_3}$	-	-	-	20.9	21.4	-	-	-
$COO\underline{CH_3}$	-	-	-	-	48.43	48.2	48.7	51.6

Table 4.2: ^{1}H NMR [300 MHz, δ_H (*J*,Hz)] of **75-81** in C_5D_5N

Position	***60***	***75***	***76***	***77***
1	-	-	-	-
2	-	-	3.5*bd*, *J*=15.5 2.6*bd*, *J*=11.25	-
3	β 3.39,*btr*	NIL	NIL	α,4.68*dd* *J*=5.06, 10.9
4	-	-	-	-
5	-	-	-	-
6	-	-	-	-
7	-	-	-	-
8	-	-	-	-
9	-	-	-	-
10	-	-	-	-
11	-	-	-	-
12	5.40*s*	5.60*bs*	5.50*bs*	5.45*bs*
13	-	-	-	-
14	-	-	-	-
15	-	-	-	-
16	2.17dt	2.15*dt*	-	2.24*m*
17				
18	2.65*d* *J*=11.8	2.75*d* *J*=11.8	2.30*m*	2.65*d* *J*=11.1
19	-	-	-	-
20	-	-	-	-
21	-	-	-	-
22	-	-	-	-
23	1.07	1.04	1.08	1.06
24	0.10	0.99	0.92	0.91
25	0.94	0.90	0.91	0.88
26	1.04	1.02	0.98	0.99
27	1.06	1.16	1.20	1.08
28	-	-	-	-
29	1.30	1.22	1.40	1.23
30	1.08	1.00	0.96	0.95
CO$\underline{CH_3}$	-	-	-	2.09*s*
CO$\underline{OCH_3}$	-	-	-	-
NOH	-	-	-	-

Table 4.2: ^{1}H NMR [300 MHz, δ_H (*J*,Hz)] of **75-81** in C_5D_5N(*continue*)

Position	***78***	***79***	***80***	***81***
1	-	-	-	-
2	-	-	-	3.50*d* *J*=15.58 2.25*m*
3	α4.75*dd* *J*=5.4, 10.8	3.51*brt*	NIL	NIL
		-	-	-
4	-	-	-	-
5	-	-	-	-
6	-	-	-	-
7	-	-	-	-
8	-	-	-	-
9	-	-	-	-
10	-	-	-	-
11	-	-	-	-
12	5.41		5.42*s*	5.35*s*
13	-	-	-	-
14	-	-	-	-
15	-	-	-	-
16	-	-	-	2.30*m*
17				
18	2.49*d* *J*=11.1	2.62 *J*=13.11	2.49*d* *J*=10.8	2.42*d* *J*=10.8
19	-	-	-	-
20	-	-	-	-
21	-	-	-	-
22	-	-	-	-
23	1.02	1.10	0.98	0.97
24	0.98	0.99	0.97	0.90
25	0.94	0.92	0.90	0.85
26	1.00	0.98	1.13	1.12
27	1.04	1.00	1.24	1.10
28	-	-	-	-
29	1.20	1.30	1.26	1.41
30	0.96	1.20	0.96	0.92
$COCH_3$	2.09*s*	-	-	-
	-	-	-	-
$COOCH_3$	3.74*s*	3.75$_S$	3.75*s*	3.68
NOH	-	-	-	12.36*s*

CHAPTER 5:

ANTI-INFLAMMATORY ACTIVITY

5.1 Introduction

Inflammation is a process by which the body's white blood cells release chemicals to protect body from infection and foreign substances, such as bacteria and viruses. This process is often associated with the release of prostaglandins which, through chemotaxis, attract leucocytes at the point of invasion, create local pain and, after transport in the blood to the brain, raise the body temperature by displacing the balance of the centre of thermal regulation (Havsteen, 1983). It can be classified as either acute or chronic. The manifestations of an acute inflammation are redness, edema, heat, pain and disturbed tissue function. These manifestations are the results of complex pathophysiological processes that include increased blood flow and vascular permeability, activation of humoral and cellular defence mechanisms, sensibilisation and activation of nociceptors (Safayahi, 1997). These processes are mediated by a variety of signaling molecules produced by mast cells, macrophages, granulocytes, platelets, lymphocytes, nerve endings, endothelial cells, as well as by the activation of complement factors.

In general, the inflammatory response involves three key processes (www.hcc.bcu.ac.uk/physiology/inflammation.htm):

i. Vasodilation resulting in increased blood flow to the damaged area
ii. Increase vascular permeability-plasma leaks from blood vessels into the damaged area.
iii. Emigration of neutrophils from blood into the damaged area

Prolonged inflammation, known as *chronic inflammation*, leads to a progressive shift in the type of cells present at the site of inflammation and is characterized by simultaneous destruction and healing of the tissue from the inflammatory process (en. wikipedia. org/ wiki /Inflammation).

Figure 5.1 illustrates the general event during inflammation. When antigen exposure occurs repeatedly, inflammatory cells such as mast cells and eusinophils will participate to activate the immunological mechanism (Hiroichi, 2005). The activated mast cells will produce many mediators of different chemical classes such as amines (histamine, serotonin), proteins and peptides (hydrolytic enzymes, cytokines, growth factors, colony stimulating factors, complement factors, antibodies, kinines), activated oxygen species (superoxide anion, hydroperoxide, hydroxyl radicals) and lipids (platelet activating factor, prostanoids, leukotrienes) (Safayahi, 1997) which cause dilation of capillaries and changes in the endothelial cell membranes that increase microvascular permeability and enhance the trapping of circulating leukocytes such as neutrophils, at the site of injury (Robert, 1998). The matured neutrophils will phagocyte the microorganism or antigen such as bacteria (www.hcc.bcu.ac.uk/physiology/inflammation.htm).

Therefore theoretically, anti-inflammatory compounds might be able to interfere with the pathophysiological processes by blocking the biosynthesis of pro-inflammatory mediators via direct interaction with a key enzyme, inhibiting the release of preformed and stored mediators, blocking mediator receptor interaction on target cells, or by acting as immune stimulation that could result in a less aggressive inflammatory response to allergen challenge.

5.2 Mediators of inflammation

Inflammatory mediators are soluble and diffusible molecules that either act locally at the site of tissue damage and infection or at more distant sites. They can be divided into exogenous and endogenous mediator (John & Regina, 1987).

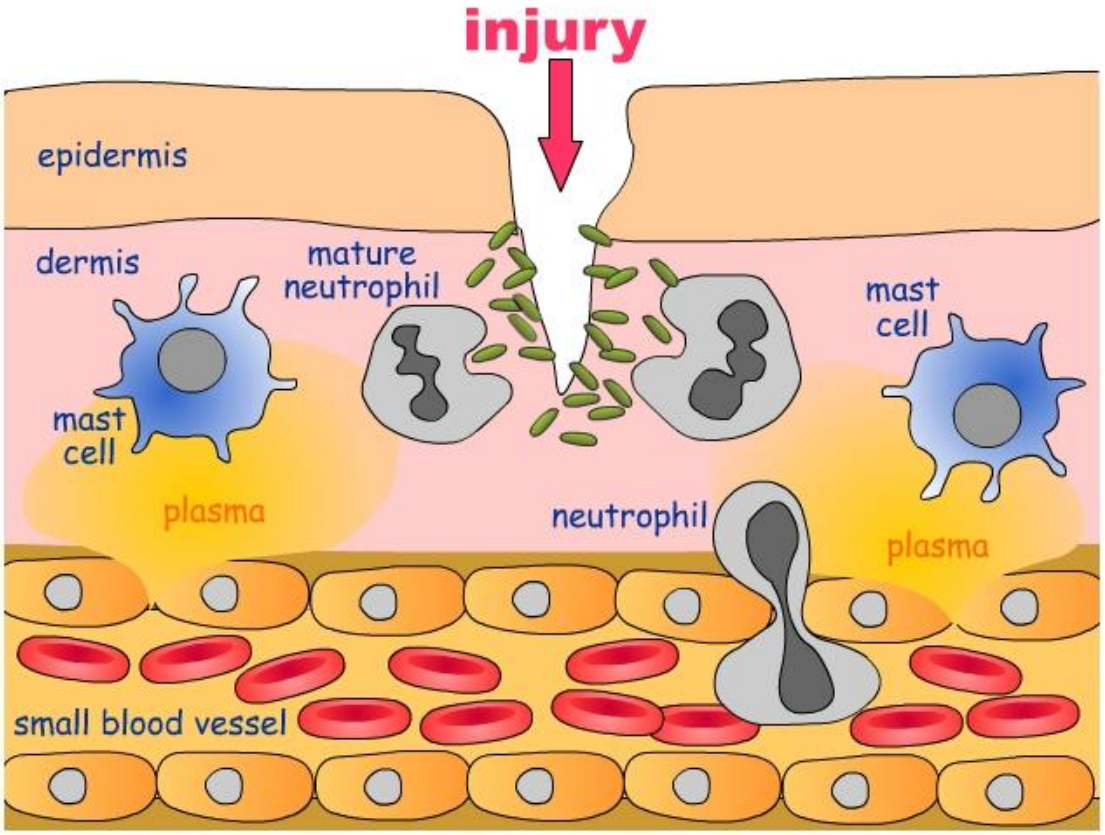

Figure 5.1: Principal events in the inflammatory response

(www.hcc.bcu.ac.uk/physiology/inflammation.htm)

Bacterial products and toxins can act as exogenous mediators of inflammation whereas the endogenous mediators of inflammation are produced from within the innate and adaptive immune system itself.

Histamine, an amine mediator, is released from mast cells during antigen-antibody reactions (John & Regina, 1987). This mediator is involved in inflammatory response due to skin injury. It could also be found in the rheumatoid synovium and asthmatic lung (Holgate, 1986) but not a major player in arthritis and asthma (John & Regina, 1987).

Peptides such as bradykinin, tachykinins, endothelins (ETs) and complement are involved in the occurrence of asthma (Peter et al., 1998). Kinins reported to be present in rat pleural inflammatory exudates and nasal secretions. They are vasoactive peptides that are formed from the high molecular weight (HMW) α-globulins and low molecular weight (LMW) kininogens via kininogenases (Bhoola, 1992). Bradykinin is metabolized by several peptidases known as kininases (Peter et al., 1998). It could be degraded by angiotensin converting enzyme (ACE) (Dusser et al., 1988), NEP (EC 3.4.24.11) (Frossard et al., 1990) and carboxypeptidase-N. Small amounts of bradykinin will cause pain, vasodilation and edema, all contributing to inflammation (John & Regina, 1987).

The structurally lipid mediators i.e. prostaglandins, thromboxane A2, prostacyclin and leukotrines are families of eucasanoids (http://en.wikipedia.org/wiki/Eicosanoid). Eucasanoids are signaling molecules made by oxidation of twenty-carbon essential fatty acids, (EFAs). They are synthesised from arachidonic acid (AA) that is released upon cell stimulation from membrane phospholipids via activation of lipid-cleaving enzymes, such as phosphoplipase A2 and three different pathways (Scheme 6.2) (Rowley et al., 1998). The pathways are cyclooxygenase (COX) pathway, lipoxygenase (LOX) and cytochrome P-450. In 1936, Euler discovered that prostaglandins (PGE) could cause contraction of smooth muscle cells in seminal fluid

and in prostate (Rowley et al., 1998). Moncada in 1976 discovered another prostaglandins, namely as prostacylin which could relaxes the blood vessels and inhibits aggregation of platelets (John a& Regina, 1987). Thromboxane, however showed opposite activity. It could induce vasoconstriction, cell adhesion to the vessel wall and platelet aggregation. The leukotrienes (LTB4, LTC4 and LTD6) cause transient wheal and flare reactions in human skin (John & Regina, 1987). Morley in 1986 reported that the phospholipids platelet-activating factor (PAF)-acether is released by the action of phospholipase A_2 from most pro-inflammatory cells, as well as by vascular endothelial cells and platelets (John & Regina, 1987). It induces inflammatory reactions in human skin (Chung, 1987). It is particularly effective in producing hyper reactivity and accumulation of eusinophils in lung tissue.

Interleukins-1 (IL-I) is a polypeptide produce by activated macrophages that mimics the symptoms of chronic inflammation (Dinarello, 1984). It has been detected in synovial fluids from patients with rheumatoids arthritis (Nouri et al., 1984.). Its action include activation of lymphocytes and production of fever that being mediated by release of PGE_2.

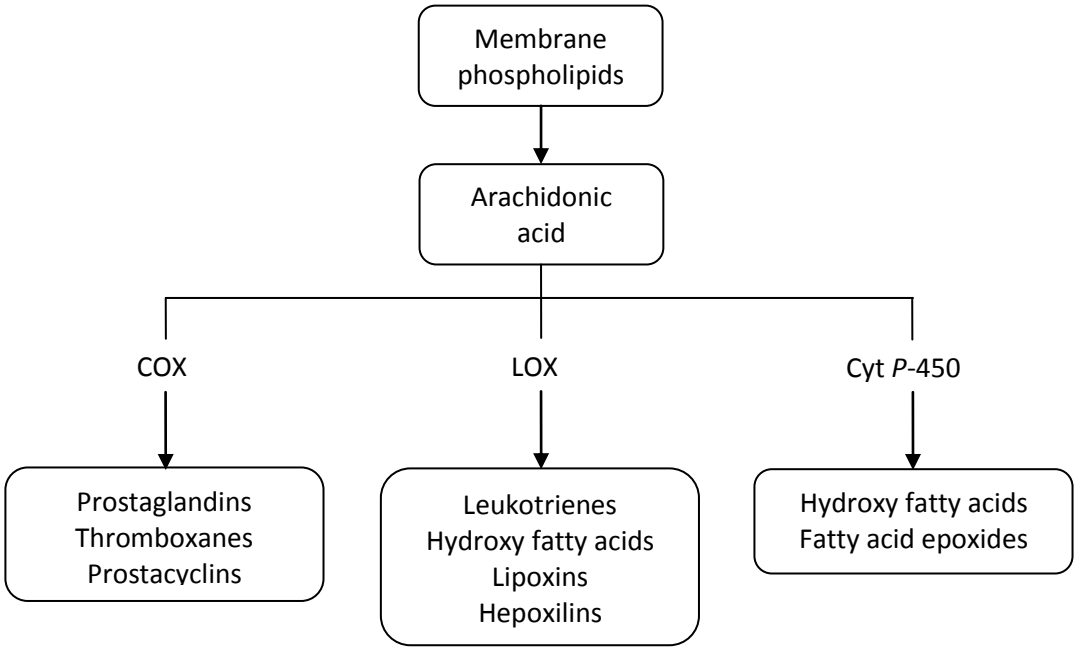

Scheme 5.2: Arachidonic acid cascade

5.3 Hyaluronidase vs hyaluronic acid

Hyaluronic acid **82** (hyaluronan or hyaluronate, HA) is a linear high molar mass polysaccharide composed of D-glucuronic acid-β(1,3)-N-acetyl-D-glucosamine disaccharide units linked together through β(1,4) glycosidic bonds (Jean-claude, 2009). It is a major constituent of the extracellular matrix (ECM) of vertebrates and is involved in many biological processes, such as cellular adhesion, mobility and differentiation processes (Catterall, 1995). The functions of HA **82** derived from its physicochemical properties. It acts as a lubricant responsible for the viscoelastic properties of tissue fluids. It also acts as a stabilizing and hydrating component of soft connective tissue due to its water balance and osmotic pressure regulatory properties and besides acting as structure forming molecule in the vitreous humor of the eye, in

Wharton's jelly and in joint fluids (Nermeen et al., 2010). From its physicochemical properties as polymer, HA **82** also exerts biological effects via specific interactions with hyaluronan-binding proteins called hyaladherins (El Maradny et al., 1997).

The chemical structure of HA **82** of repeating disaccharide units linked by β-1,4 glycosidic bonds has been elucidated in which each disaccharide unit consists of D-glucuronic acid (GlcUAc) and N-acetyl-D-glucosamine (GlcNAc) connected by a β-1,3 glycosidic bond (Nermeen et al, 2010). This polymer usually consists of 2000-2500 disaccharides to increase the molecular masses ranging from 10^6 to 10^7Da with extended lengths of 2-25 μm.

Hyaluronidase, a glycosidase (Nermeen et al., 2010) is popularly known as "spreading factor" referring to its activity in degrading HA **82** (Deepa et al., 2006). These enzymes also degrade chondroitin and chondroitin sulphates with limited ability (Nermeen et al., 2010). This inactive enzyme could be activated *in vivo* by metal ions such as calcium ions and HA **82** as the substrate (Yang et al., 2000). The interaction between hyaluronidase and HA **82** result a disruption of basement membrane integrity and followed by an angionic response (Takuya et al., 2003). This enzyme was reported to play a key role in the development of inflammatory diseases, since the destruction of the connective extracellular matrix promotes the spreading of chemotactic factors of inflammation (Facino et al., 1993). It is also involved in other fundamental biological phenomena such as fertilization and cancer (Stern, 2008) as well as tumor invasiveness and metastasis (Takuya et al., 2003).

According to amino acid sequence homology, hyaluronidase could be grouped into two main families; from eukaryotes and prokaryotes (Csoka et al., 1997). First

classification however is based on substrate specificity and on biochemical analysis of the hyaluronidase and their reaction products (Nermeen et al., 2010).

The first group is hyaluronate-4-glycanohydrolases, mammalian hyaluronidase (EC 3.2.1.35) (Nermeen et al., 2010). It degrades HA **82** by cleavage of the β-1,4-glycosidic bond furnishing tetrasaccharide molecule as the main product. These enzymes are glycosidases with both hydrolytic and transglycosidase activity and degrade HA **82**, chondroitin, chondroitin-4,6-sulphate to a small extent, dermatan sulphate. Examples from this class are testicular, lysosomal and bee venom hyaluronidase. The second group is hyaluronate 3-glycanohydrolases from leech (EC 3.2.1.36). It degrades HA **82** by cleavage of the β-1,3-glycosidic bond to yield sugar fragments with glucuronic acid at the reducing end. This hyaluronidase generates tetra- and hexasaccharide end products. The last group is microbial hyaluronidases (EC 4.2.2.1) called hyaluronate lyases. They degrade HA **82** by a β-elimination reaction to yield unsaturated disaccharide 2-acetamido-2-deoxy-3-*O*-(β-D-gluco-4-enepyranosyluronic acid)-D-glucose as the main product.

Hyaluronidase is present in substantial quantities in mast cells (Sasai & Tohoku., 1975). It demonstrated a variety of activity in different mamalian tissues (Bollet, Bonner & Nance, 1963) such as testes (Senn et al., 1992) and in various somatic tissues, e.g. liver, kidney, lymphatic system and skin as well as animal venom. It was also reported that hyaluronidase was expressed by metastatic human melanoma, colon carcinoma and glioblastoma cell lines (Liu et al., 1996).

Hyaluronic acid **82** existing as a polyanion as the carboxyl groups of the glucuronic acid causes the polymer highly negative charge (Nermeen et al., 2010). The

hydrophobic interactions and hydrogen bonds can be formed between HA **82** chains. It counteracted by electrostatic repulsion of the carboxyl groups (Scott et al, 1984). The positive charges of hyaluronidase interact with the negative charges of HA **82** to form non-specific electrostatic HA-Hyaluronidase complexes in which it is no more catalytically active (Jean-claude, 2009). This formation phenomenon is maximum at low ionic strength and pH 4 which is the optimal pH for hyaluronidase (Jean-claude, 2009). It also exists at higher ionic strength including 150 mM and higher pH values including pH 7. The small fragments of HA **82** are highly angiogenic and potent inducers of inflammatory cytokines (Nermeen et al, 2010) while the high molecular weight HA **82** polymers prevent angiogenesis. For example, HA oligosaccharides (4-25 disaccharides), the product of hyaluronidase in extracellular matrix, have an angiogenic action (Rooney et al., 1995, West et al., 1985, West et al., 1989) which favor the production of new blood vessels facilitating the development of cancer tumors. It also induced expression of inflammatory mediators in alveolar macrophages (Horton et al., 1999), inhibit tumor growth *in vivo* (Zeng et al., 1998).

Since these enzymes have been implicated in many biological functions, such as allergy, inflammation, migration of cancer cells and permeability of the vascular system, the modulation of hyaluronidases by suitable inhibitors will be useful for normal homeostasis in the body. Hyaluronidase is related to histamine release from mast cells (Masateru et al., 2001) which related to type I allergy as well as as the degranulation of mast cells (Hisao et al., 1985). Therefore, potent hyaluronidase inhibitors are assumed to suppress the degranulation of mast cells and possess anti-allergic activity (Toshihiro et al., 2010). The anti-allergic agents such as disodium cromoglycate (DSCG) and tranilast (N-3',4'-dimethoxycinnamoyl anthranilic acid) is presumed to be involved in inhibition of the degranulation of mast cells caused by the

antigen IgE antibody reaction (Hisao et al., 1985). Anti-inflammatory drugs such as salicylates, dexamethasone and indomethacin have been reported to possess hyaluronidase inhibitory activity (Deepa et al., 2006). These drugs may exert a portion of their anti-inflammatory activity by preventing generation of small hyaluronic acid fragments. For example, compounds that have been used to treat snake bites or to promote wound healing have been subsequently demonstrated to possess anti hyaluronidase activity and thus delay / stop the diffusion of toxins after the envenomation (Deepa et al., 2006). Therefore, the search for new agents with potential regulating hyaluronidase activity is a possible approach for finding treatment for hyaluronidase mediated ailments or diseases.

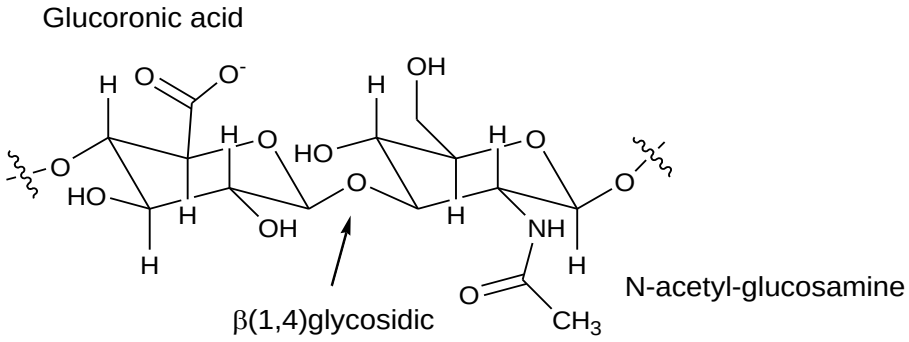

82

5.4 Results and discussion

A preliminary bioactivity screening programme for plants with potential therapeutic application in FRIM (Forest Research Institute Malaysia) has indicated that the crude extracts of *Prismatomeris malayana* exhibited strong anti-inflammatory properties (2004, not reported). In the study, it was found that the MeOH leaf extract inhibited TPA induced ear oedema at 96.03 ± 1.0 % at 2 mg/ear as compare with indomethacin (93.00 ± 0.20)% and platelet activating factor (PAF) receptor binding inhibitory activity at 76.9 ± 2.1 % at 18.2 µg/ml as compared to cedrol (74.4 ± 1.0 %) , respectively. In the light of the above finding, a bioassay guided study was performed on the most active extract ($CHCl_3$) to find the compound(s) responsible for the anti inflammation. In addition, hyaluronidase inhibitory activity was also performed on other selected isolated PTCs and the synthesized analogues.

5.4.1 Bioassay-guided study of the MeOH extracts of *Prismatomeris malayana* Ridley

The dried leaves, roots and stems of *Prismatomeris malayana* Ridley were extracted with MeOH by soaking at room temperature repetitively and yielded 9.85%, 4.54% and 2.47% MeOH crude extract respectively. The extracts were then subjected to screening for hyaluronidase, lipoxygenase inhibitory and TPA induce mouse ear oedema activity.

The leaf extract (PML) exhibited the highest inhibory activity of more than 70% in hyaluronidase (table 5.4.1.1) and TPA mouse ear oedema inhibitory assays (table 5.4.1.2). It was found to exhibit profound hyaluronidase activity (70.51 ± 4.34) % at

100 µg/ml as compare with that of positive control, apigenin (88.97 ± 7.93) % and TPA mouse ear oedema (73.00 ± 31) % at 2 mg/ear as compare with indomethacin (92.80 ± 0.21)%. These results suggest that the constituents in the leaf extract might be responsible for the inhibitory role in the hyaluronidase system (*in vitro*) and *in vivo* (TPA mouse ear oedema). Therefore the methanol leaf extract was further fractionated into four fractions; petroleum ether, chloroform, ethyl acetate and water fractions. Table 5.4.1.3 showed the inhibitory activity of the fractions from the methanol leaf extract.

Further bioassay guided fractionation and isolation based on the hyaluronidase inhibitory assays resulted in the isolation of ursolic acid **60** (14.25 % yield of the chloroform fraction) which gave the highest inhibition in hyaluronidase and TPA mouse ear oedema inhibitory activity at 79.67 ± 6.42 % and 73.00 ± 31% respectively (Table 5.4.1.3) (Please refer to scheme 8.1.6.1). By using the NMR 1D and 2D spectroscopic analysis method and by comparing the data with literature (Chien and Gow, 2001), compound **60** was identified as ursolic acid.

Dose response study on ursolic acid **60** using hyaluronidase and TPA mouse ear oedema inhibitory assays gave the IC_{50} value of 103.18 µM and 0.42 mg/ear respectively, as compare with the positive controls; apigenin (214.74 µM) and indomethacin (0.38 mg/ear). These findings showed that ursolic acid **60** exhibited strong inhibitory effects on hyaluronidase and ear oedema induced by TPA.

Topical application of TPA offers a model of skin inflammation appropriate for evaluating anti inflammatory agents (Arulmozhi et al., 2005). TPA produces inflammation by activating phospholipase A2 (PLA2) which subsequently activates the

release and metabolism of AA. The COX and 5-LO inhibitors are very effective in suppressing TPA-induced ear inflammation indicating the role of prostaglandins and leukotrienes respectively (Recio et al., 2000). Thus topical application of *Prismatomeris malayana* extracts that mildly inhibited TPA-induced ear inflammation could be due to its combined inhibition towards lipoxygenase.

Table 5.4.1.1: Hyaluronidase and lipoxygenase inhibitory activity of the methanol extracts from different parts of *Prismatomeris malayana*.

Samples	Hyaluronidase Percentage inhibition [a]	lipoxygenase percentage inhibition[b]
Stem	**64.31 ± 9.41[c]**	**61.04 ± 0.05[d]**
Leaf	**70.51 ± 4.34[c]**	**60.76 ± 0.16[d]**
Root	59.40 ± 6.91[c]	55.53 ± 0.36[d]
Apigenin	88.97 ± 7.93	
NDGA		97.15 ± 0.01

[a,b] Data represent the mean ± S.D of three independent experiments performed in triplicates. % inhibition at 100 µg/ml concentration.
[c,d] Means for percentage inhibition were significantly different (one- way analysis of variance, $p < 0.05$)

Table 5.4.1.2: Inhibitory activity of the extracts of *Prismatomeris malayana* on TPA – induced inflammation in mice

Samples	Inhibition of inflammation, I.R,[a] (%)
Stem	37.00 ± 11[b]
Leaves	**73.00[b] ± 31[b]**
Root	25.00[b] ± 10[b]
Indomethacin	72.00 ± 6

[a] I.R.: inhibitory ratio at 2.0 mg/ear for extracts and fractions, 0.5 mg for compound **97** (n=7)
[b] Means for percentage inhibition were not significantly different (Duncan's multiple range test, p=0.05)

Table 5.4.1.3: Hyaluronidase inhibitory activity of the fractions and sub-fractions from the leaves of *Prismatomeris malayana*.

Samples	Percentage inhibition[a]
Petroleum ether	60.47 ±0.12[b]
Chloroform	**72.19 ± 1.25[b]**
Ethyl acetate	48.19 ± 2.41[b]
Aqueous	60.19 ± 1.85[b]
*C1	61.26 ± 3.57[c]
*C2	67.99 ± 10.23[c]
*C3	74.26 ± 3.79[c]
Ursolic acid **60**	79.67 ±6.42[c]
Apigenin	88.97 ± 7.93

[a] Data represent the mean ± S.D of three independent experiments performed in triplicates. % inhibition at 100 µg/ml concentration.
[b,c] Means for percentage inhibition were significantly different (one- way analysisof variance, $p < 0.05$
*C1,C2,C3-subfractions of chloroform fraction

5.4.2 Structure activity relationship (SAR) of ursolic acid 60 and its analogues.

A total of thirty analogues of ursolic acid **60** were evaluated for their inhibitory activity on hyaluronidase. Three analogues were isolated from *Prismatomeris malayana*, *i.e* compound **60**, **61** and **64**. Seven analogues were prepared from the modification on the functional groups at OH-3 and COOH-28 of ursolic acid **60** (Refer to chapter 4). These analogues were compounds **75**, **76**, **77**, **78**, **79**, **80** and **81**. The remaining nineteen analogues i.e., compound **83-104** were commercially available. They were purchased from CHROMADEX and SIGMA. Table 5.4.2 gives the IC_{50} value for each analogue.

Basically, the analogues are under two basic pentacyclic triterpenes (PTC) skeleton; ursane (**60**, **61**, **75**, **76**, **77**, **78**, **79**, **80**, **81**, **84, 86, 91, 98, 99, 102**) and oleanane (**64**, **85**, **87**, **88**, **89**, **90**, **92**, **95**, **96**, **97, 101**, **104)**. The result in table 5.4.2 showed that ursolic acid **60** (103.18±1.70 µM) is more active than oleanolic acid **92** (227.97±2.81 µM). However, comparison on the analogues or derivatives of both skeleton that are similar to each other such as **84** (227.00 ±5.99 µM) and **85** (206.21 ± 2.32 µM), **86** (211.00 ± 3.16 µM) and **90** (215.00 ± 4.27 µM) does not revealed big difference in their activity. Thus it shows that the germinal or vicinal arrangement of methyl-29 and 30 would not give big effect on the activity but with some exceptional. The discussion will be divided into the ursane and oleanane skeleton.

In the PTC oleanane skeleton, the activity was reduced slightly when the methylhydroxyl was introduced at C-23 (**92** [227.97 ± 2.81 µM] vs. **96** [230.0 ± 2.17 µM]). The activity would however increased slightly when the methyl group was

introduced at C-17 (**90** [215.66 ± 4.27 µM] **vs 92** [227.97 ± 2.81 µM]). The 16-OH derivatives increased the activity (**87** [140.91 ± 6.71 µM] vs. **92** [227.97 ± 2.81 µM]) or with introduction of carboxyl at C-23 (**95 [**1482.56± 0.7 µM]). The C-30 ester derivatives resulted in activity loss greatly (**83** [1750.91 ± 2.38 µM] **vs 93** [146.18 ± 2.67 µM]). Carboxylation at the same carbon (C-30) increased the activity greatly (**93** [146.18 ± 2.67 µM]). Acetylation on 3-OH would decreased the inhibitory ability, greatly (**64**, [1466.5 ± 2.37 µM]). Introduction of sugar moiety with glycosidic bond to 3-OH or 28-COOH could either reduced the acitivity drastically (**89** [842.54 ± 0.11 µM]) or become not active whereas additional oxo group at C-11 did not improve the activity or will reduce it slightly (**92** [146.18 ± 2.67] µM vs. **94** [56.33 ± 0.01 µM] vs. **83** [1750.91 ± 2.38 µM]). Too many methyl group (**104**) or hydroxyl group (**101**) also resulted in loss of activity. Significant improvement in the activity was observed when the functional group methylester was introduced at C-17 (**88 [**84.52 ± 0.01 µM] vs. **92** [227.97 ± 2.81 µM], **90** [215.66 ± 4.27 µM]**)** or when carboxypropanoyloxy, **S2** was introduced at C-3 (**94** [56.33 ± 0.01 µM]**)**.

The inhibitory activity of PTC ursane skeleton will slightly decreased on the 3-oxo, 3-hydroxyimino and 3-acetylate derivatives (**75** [162.83 ± 6.37 µM], **76** [190.94 ± 0.01 µM], **77** [136.92 ± 0.04 µM]) compared to ursolic acid **60**. The same phenomenon could also observable if the 28-OH substituted with methyl of (**76** [190.94 ± 0.01 µM] vs **81** [275.68 ± 1.42 µM], **60** [103.18 ± 1.70] vs **79** [182.511 ± 0.84 µM], **77** [**136.92** ± 0.04**]** vs **78** [812.93 ± 10.29]). This situation suggested that the hydroxyl group of C-3 and C-28 is essential for the hyaluronidase inhibitory activity. The substitution of methyl with the carboxyl group of C-23 would decrease the inhibitory activity (**86** [211.44 ± 3.16 µM] vs. **98**, NA). The introduction of hydroxymethylene at C-23 and additional hydroxyl at C-1 did not affect the activity very much (**91 [**115.96 ± 0.47

µM] vs. **98**, NA), however additional hydroxyl at C-19 decreased the activity more (**61** [286.95 ± 10.28 µM]). The position of hydroxyl group also affect the activity as it decreased the activity more in **61** (C-19) compared to **91** (C-2), 115.96 ± 0.47 µM. The sugar moiety as usual, would be resulted in loss of activity (**99, 102)**.

It could be concluded that 3-OH is important for the activity in both ursane and oleanane skeleton. The methyl ester introduction at C-17 to replace the carboxylic functional group gives different effect on the hyaluronidase inhibition ability of both type of skeleton. Replacement on 3-OH such as hydroxyimino, acetyl, methyl also would make the activity become lower. Additional hydroxyl at C-2, 1 and 19 or oxo at C-11 and 3, or methyl group, however, would either give no effect or decreased the activity. The introduction of sugar moiety at any position would result in loss of activity. This is probably due to the bulkiness of the structure that make the respected compound could not reach the active site in the target, which is in the hyaluronidase enzyme. However, carboxypropionylox, **S2** that replace the 3-OH make the activity become very high. Figure 5.4.2 summarized the structure activity relationship on PTC compound from the observation on the activities of compound **60, 61, 64, 75-104**.

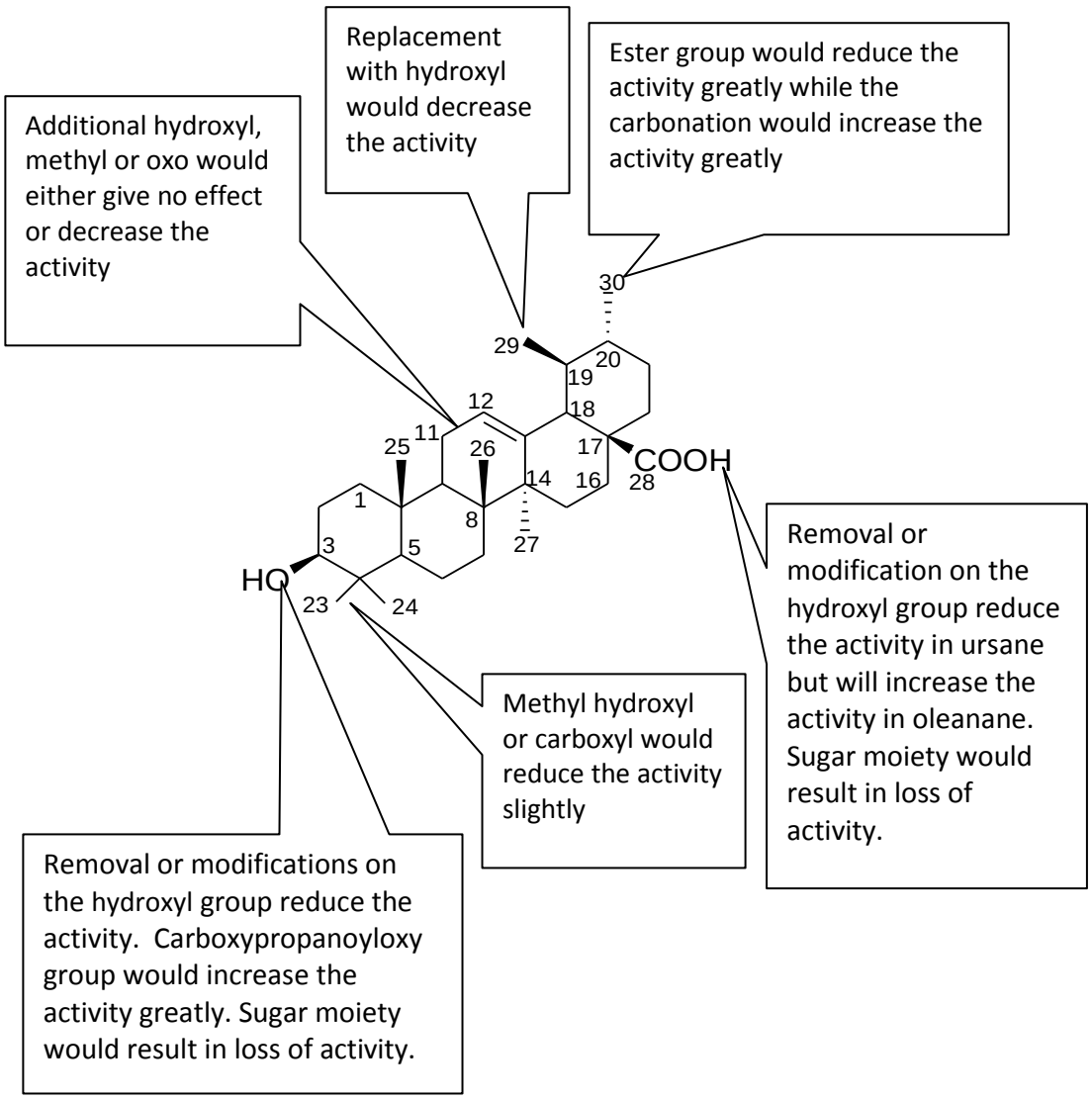

Figure 5.4.2: Structure activity relationship of pentacylic triterpenes

Table 5.4.2: Hyaluronidase inhibitory activity of the ursolic acid **60** and analogues at the concentration of 100-2000 µM

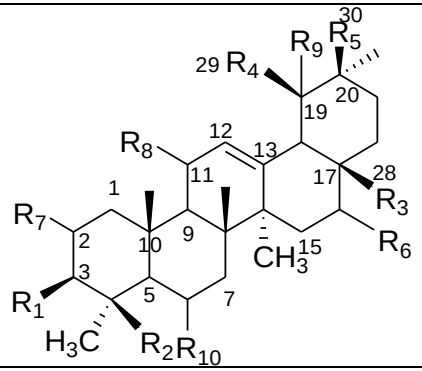

Compound	***Substitutional pattern***										*[a]IC50*
	R1	**R3**	**R2**	**R4**	**R5**	**R6**	**R7**	**R8**	**R9**	**R10**	
60	OH	COOH	CH_3	CH_3	H	H	H	H	H	H	103.18 ±1.70**
61	OH	COOH	CH_2OH	CH_3	H	H	H	H	OH	H	286.95 ± 10.28
75	=O	COOH	CH_3	CH_3	H	H	H	H	H	H	162.83 ± 6.37*
76	NOH	COOH	CH_3	CH_3	H	H	H	H	H	H	190.94±0.01*
77	OAc	COOH	CH_3	CH_3	H	H	H	H	H	H	136.92±0.04*
80	=O	$COOCH_3$	CH_3	CH_3	H	H	H	H	H	H	1184.15±6.63
81	NOH	$COOCH_3$	CH_3	CH_3	H	H	H	H	H	H	275.68±1.42
79	OH	$COOCH_3$	CH_3	CH_3	H	H	H	H	H	H	182.51±0.84*
78	OAc	$COOCH_3$	CH_3	CH_3	H	H	H	H	H	H	812.93±10.29
84	OH	CH_3	CH_2OH	CH_3	H	H	H	H	H	H	227.97±5.99
86	OH	CH_3	CH_3	CH_3	H	H	H	H	H	H	211.44±3.16*
91	OH	COOH	CH_2OH	CH_3	H	H	OH	H	H	H	115.96±0.47*
98	OH	CH_3	COOH	CH_3	H	H	H	H	H	H	NA
99	OH	CH_2OH	***S3***	CH_3	H	H	OH	H	H	H	NA
102	OH	COO***S4***	CH_2OH	CH_3	H	H	OH	H	H	OH	**NA**

[a] NA-inhibitory activity ,20% at concentration up to 5000µM; positive control-Apigenin. Values were presented as the mean ± S.D of three independent experiments performed in triplicates.

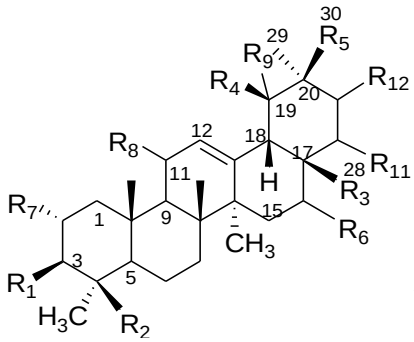

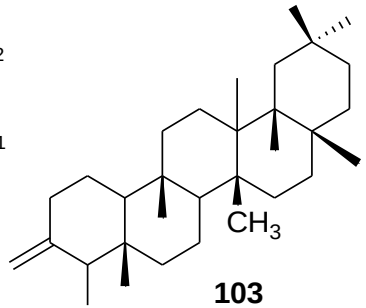

103

	R1	**R2**	**R3**	**R4**	**R5**	**R6**	**R7**	**R8**	**R9**	**R11**	**R12**	
64	OAc	CH_3	COOH	H	CH_3	H	H	H	H	H	H	1466.5±2.37
83	OH	CH_3	CH3	H	$COOCH_3$	H	H	=O	H	H	H	1750.91± 2.38
95	OH	COOH	CH3	H	CH_3	H	H	H	H	H	H	1482.56±0.70
85	OH	CH_3	CH_2OH	H	CH_3	H	H	H	H	H	H	206.21±2.32
87	OH	CH_3	COOH	H	CH_3	OH	H	H	H	H	H	140.91±6.71
88	OH	CH_3	$COOCH_3$	H	CH_3	H	H	H	H	H	H	84.52±0.01**
89	***S1***	CH_2OH	COOH	H	CH_3	H	H	H	H	H	H	842.54±0.11
90	OH	CH_3	CH_3	H	CH_3	H	H	H	H	H	H	215.66±4.27*
92	OH	CH_3	COOH	H	CH_3	H	H	H	H	H	H	227.97±2.81
93	OH	CH_3	CH_3	H	COOH	H	H	=O	H	H	H	146.18±2.67*
94	***S2***	CH_3	CH_3	H	COOH	H	H	=O	H	H	H	56.33±0.01**
96	OH	CH_2OH	COOH	H	CH_3	H	H	H	H	H	H	230.00±2.17
97	O-glucoside	CH_3	COOH	H	CH_3	OH	H	H	H	H	H	NA
101	OH	CH_2OH	CH_2OH	H	CH_3	OH	H	H	H	OH	OH	NA
104												NA
Apigenin												214.74

[a] NA-inhibitory activity <20% at concentration up to 5000μM; positive control-Apigenin. Values were presented as the mean. of three independent experiments performed in triplicates.

* p <0.05, ** p<0.01 compared with apigenin (Student's t-test).

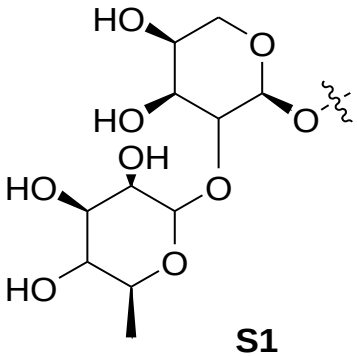
HO
O
HO
O
OH
HO
O
HO
O

S1

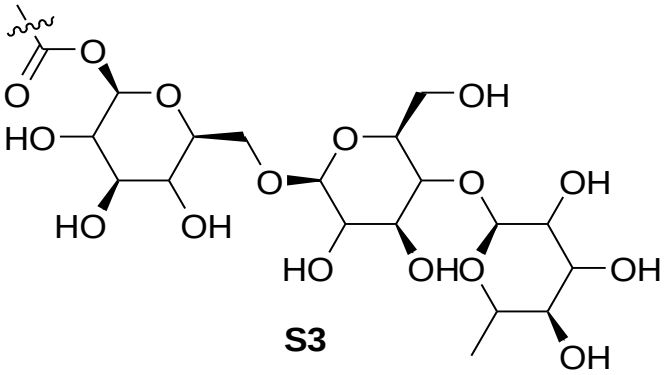
O
O
O
HO
O
OH
HO
OH
O
O
OH
HO
OH
HO
OH
OH

S3

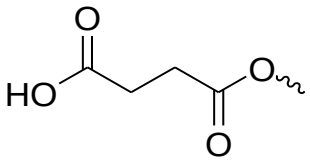
O
HO
O
O

S2

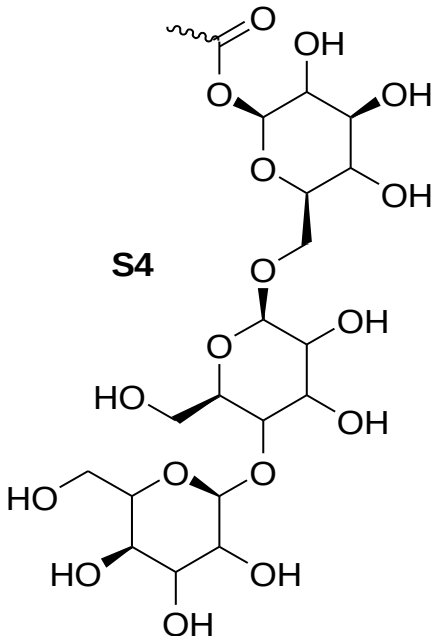
O
OH
O
OH
O
OH
O
O
OH
HO
OH
O
O
HO
O
HO
OH
OH

S4

CHAPTER 6:
QUANTITATIVE STRUCTURE ACTIVITY RELATIONSHIP (QSAR)

6.1 Introduction

In search for a new drug, a number of strategies can be followed. Some research methodologies may be based on random synthesis of new compounds, utilizing combinatorial chemistry techniques, followed by a biological test to select active substances. Similarly, various natural materials such as plants, tissues or body fluids can be screened for biologically active substances. However, a systematic optimization of a lead structure is needed in order to develop it into a better drug.

Structure activity relationship study (SAR) comes from the idea that biological response to a drug exposition depends on the drug's molecular structure. Therefore, if the structure activity relationship is known, the effect of a molecule can, in principle, be predicted from its structure. The strategies involve was a change in functional groups or substituent such that the drug's pharmacokinetics or binding site interactions will be improved. These strategies often involved the synthesis of analogues containing a range of substituents on aromatic or heteroaromatic rings or accessible functional groups. The problem is the number of possible analogues that could be made is infinite.

A quantitative structure activity relationship (QSAR) was developed from several works, especially those by Hansch, Fujita, Free and Wilson (Rainer, 2003). QSAR development requires three basic elements;

(1) an activity or property data set, measured experimentally,

(2) molecular descriptors / physicochemical properties, which are the quantitative descriptions of structural properties, and

(3) statistical techniques to establish the relationship between molecular descriptors and activities (Jarai et al., 2006).

QSAR describes the biological activity of the molecules mathematically in terms of molecular descriptors properties. This approach attempts to identify and quantify the physichochemical properties of a drug to see if any of these properties has the effect on the drug's biological activity. By quantifying these properties, it is possible to estimate the properties of new chemical compound without the need to synthesize and test them.

The first step in a QSAR study is the selection of a group of compounds for which experimental data are available. This group of compounds should cover the whole range of compounds whose activities or properties are to be modeled (Hall et al., 2002b). The QSAR analysis is further based on the measurement or calculation of appropriate physichochemical properties. Many different physichochemical properties are available for QSAR analysis, but only a few of them might be used as independent variables in a QSAR model. Appropriate descriptors are selected from previous knowledge of interaction processes or by statistical techniques, i.e. by choosing descriptors that are highly correlated to the experimental parameters of interest.

The most common physicochemical properties used in QSAR studies are hydrophobic (P or Π), electronic (σ) and steric properties (E_s). Other properties including dipole moments, hydrogen bonding, conformations and interatomic distances have also been used.

6.2 Statistical concepts in QSAR

Hansch equation relates biological activity to the most commonly used physichochemical properties (Graham, 2005). The basic assumption of Hansch analysis is that log BR (biological response) can be described by a weighted linear combination of the x_i (molecule parameters or physichochemical properties (Rainer & Andreas, 2003);

$$\text{Log } BR = a_o + a_1 x_1^{n1} + \ldots. + a_r x_i^{ni} + \ldots + a_{ir} x_n^{nn} \qquad (6.2)$$

The exponents n*i* can be 1 (linear) or 2 (quadratic). The regression coefficients a_i and are computed by multiple regression analysis. The reliability and significance of the regression equation could be determined by several statistical criteria:

i. **The correlation coefficient *R***, which is a relative measure of the quality of fit (R=0, no correlation; R=1, perfect correlation). Its squared value (R^2) measures the percentage of variance of the dependent variable (log *BR*) explained by the equation i.e. how well the model fits the experimental data. The R value should be more than 0.8 ($R \geq 0.8$) for the regression model to be accepted. R^2 can be expressed as below (Kartisky et al., 2005):

$$R^2 = 1 - \frac{SS_{Error}}{SS_{Total}}$$

Where SS_{Error} is the sum of squared residual values while SS_{Total} is the total sum of squared residual values of the dependant variables

ii. **The standard deviations, *S,*** is an another measure for the quality of fit. Its value should be as small as possible but never smaller than the error of the biological experiment (over prediction). It indicates how far the activity values are spread concerning their average. S^2 can be described as (Kartisky et al., 2005):

$$S^2 = \frac{SS_{Error}}{n-k-1}$$

where *n* and *k* is the number of variables

iii. **Fisher's *F* value (*F-test*)** , which is a measure of the statistical significance of the regression model (Kartisky et al., 2005). In other words, it can be interpreted as a ratio of the variance explained by the model. Thus larger values of the F-test mean better models, while values below 1 mean that the model is completely useless. The overall significance should be 95% for the regression model to be accepted. It depends on the number of parameters involved in the model. If an absolutely insignificant parameter is added to the models, then the coefficient of determination remain the same and the *F*-value becomes smaller. However, the highest *F*-values do not necessarily mean the best model, if the number of parameters in the model is increased.

$$F(k, n-k-1) = \frac{SS_{model}}{ks^2}$$

where *k* is the number of variables

iv. **Confidence intervals** for the regression coefficients at a statistical level of significance of 95% (Kartisky et al., 2005). These intervals overlap the true values of the regression coefficients at a statistical probability of 95%. The confidence intervals should be smaller than the regression coefficient for the regression model to be accepted.

In most of the QSAR work, the equations developed have been used for the prediction of property values for compounds not employed in the development of those equations (Kartisky et al., 2005). Several statistical criteria can be proposed to estimate the reliability of predictions made by a multiple regression equation. Cross validation is the most common method used. It is the most common way to solve problem of over-fitting.

The simplest and a commonly used method of cross validation in chemometrics is the "leave one out" method. In this technique, each compound is left out once from the analysis and the model is then derived from the remaining objects. The model is then used to predict the activity values of left out compounds.

For evaluation, predicted values can be used for prediction error sum of squares (*PRESS*), root mean squares prediction error (*RMSPE*) and squared cross-validated correlation coefficient (R^2_{cv}).

PRESS can be defined as (Kartisky et al., 2005):

$$PRESS = \sum_i \left(y_{e,i} - y_{p,i}\right)^2$$

where $y_{e,i}$ are experimental values of the property and $y_{p,i}$ are predicted values s for external validation test.

RMSPE can be defined as (Kartrisky et al., 2005):

$$RMSPE = \sqrt{\frac{PRESS}{n}}$$

It gives error on a per compound basis (Stone & Jonatahn, 1993)

R_{cv}^2 can be computed by comparing the predicted and the observed activity values. The R_{cv}^2 is usually smaller than R^2 and the value range from 1 to less than 0. A value of 1 indicated a good prediction value and a value of 0 indicates no modeling power. The value of R_{cv}^2 should be over 0.6 for the regression model to be accepted.

R_{cv}^2 can be defined as:

$$R_{cv}^2 = \frac{SD - PRESS}{SD}$$

Where SD is the Sum-of-Squares deviation for each activity from the mean.

The dataset could also divide into two parts by means of series design method (Jorgen, 2004). One part is taken as a training series to derive the QSAR model while the other as test set which biological potencies are calculated from the QSAR derived from the training set. Good correlation between the predicted and observed value indicated the high predictive power of the developed QSAR. However, this approach is only applicable into a big data set probably more than thirty compounds or activity.

6.3 Quantum chemical method

The development of QSAR model requires several physicochemical properties to be measured or calculated, in addition to the activity measurements. However these physicochemical properties are intrinsically related to the molecular structural properties. Hence a quantitative description of the structural and electronic properties of the molecules will provide the information similar to the physicochemical properties required for QSAR model.

The use of quantum chemical and molecular properties descriptors has been widely accepted to account for the various types of activities of the molecule and they were found useful in predicting the activities of other derivatives hitherto unknown (Hansch & Leo, 1979). Quantum chemistry can provide more accurate and detailed description of electronic distribution than empirical methods (Karelson, 2000). This method represents an attractive source of new molecular descriptors which can express almost any electronic and geometric property of molecules and the characteristics of intermolecular interactions. It enables the definition of a large number of molecular and local quantities characterizing reactivity, shape and binding properties of the whole molecule or its fragments (Karelson, 2000). Unlike the empirical molecular descriptors, there is no experimental error in quantum chemically derived descriptors. Its molecular wave function could calculate the electrical moments of a molecule.

Quantum chemical descriptors are related to atomic charges, the highest occupied molecular orbital (HOMO), the lowest unoccupied molecular orbital (LUMO), orbital electron density and molecular polarizability (Kartizky et al., 1994, Hu et al., 2009). Therefore, the descriptors can be classified into three main categories: (i) charge distribution-related descriptors; (ii) valency related descriptors; (iii) quantum mechanical energy-related descriptors.

Compared to other *ab initio* methods that are extremely time consuming and require large storage memories, finally, the semiemprical quantum chemical methods are relatively inexpensive and can be used for the calculation of molecular descriptors for very large sets of molecules within very short computational time. There are a variety of semiempirical quantum chemical methods including Austin model (AM1) (Karelson, 2000) and Recife model (RM1).

6.4 Recife model (RM1)

Semi empirical quantum chemical method supplies realistic quantum chemical molecular quantities in a reasonable computational time frame (Karelson et al.,1996). The Austin model 1 (AM1) was developed 20 years ago. This semi empirical method was introduced for the quantum calculations of molecular electronic structure. AM1 provides good descriptions even for anions and hydrogen bonded system. Re-optimization of AM1 parameters both in quality and quantity (Rocha et al., 2006) and better numerical methods resulted in more precise method of Recife model 1 (RM1). RM1 is expected to be very competitive. Theoretically it is identical with AM1 as well as the methodology, but with much newer and better parameters. It is capable of modeling most molecular systems in biological system.

6.5 Results and discussion

In order to ensure the validity of the predictive power of the QSAR model which will be developed from the set of chemical structure and their bioactivity, the structure of the molecule must be validated first. The experimentally obtained values for the chemical structures such as bond length, bond angle and dihedral angle should not be much different from the values calculated using the optimized structure. The dihedral angles of the optimized structure of the compound **80** are compared with the data obtained from the crystal structure of the same compound. The selected dihedral angle data was summarized in table 6.5. The data of both structures showed not much different between each other and thus could be concluded that the geometry optimization did not affect the configuration of the compound.

Figure 6.5.1 showed the optimized structure while the figure 6.5.2 showed the experimental structure of compound **80.**

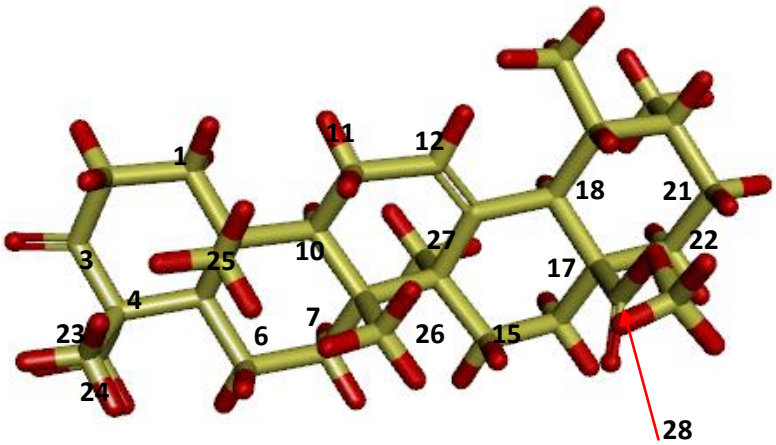

Figure 6.5.1: The optimized geometry of compound **80**

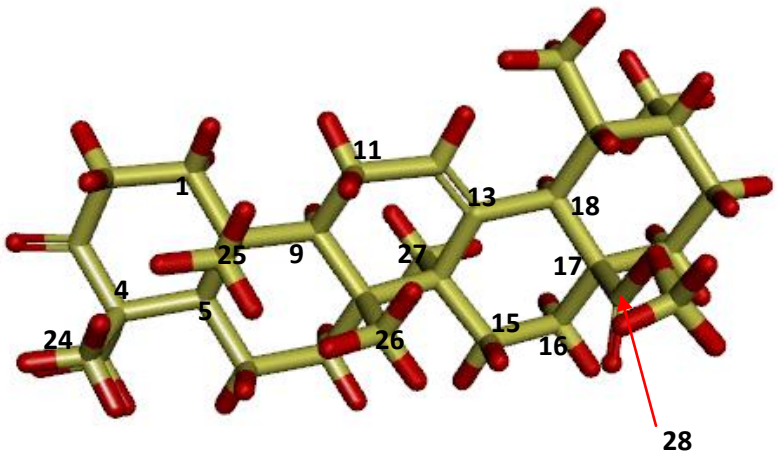

Figure 6.5.2: The absolute geometry of compound **80** from the crystallography experiment

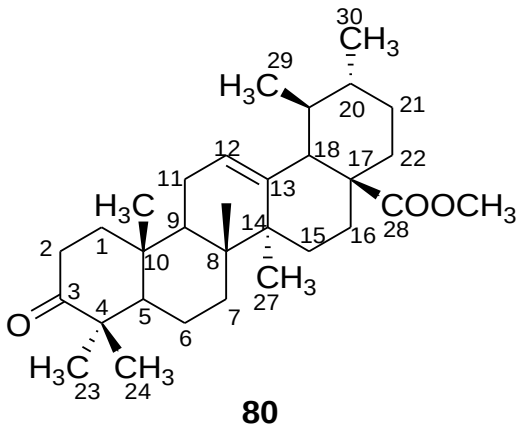

80

Table 6.5: The selected dihedral angle value of the optimized and the experimental geometry of compound **80**.

Dihedral angle	Optimised	Experimental	Dihedral angle	Optimised	Experimental
O1-C4-C5-C12	158.133	159.651	H63-C20-C26-C28	-51.865	-52.723
C4-C5-C12-C10	165.266	163.996	H63-C20-C21-C23	-68.444	-69.088
C6-C5-C17-H57	51.312	52.542	C21-C20-C26-C25	-54.152	-53.181
C12-C5-C17-C16	-61.854	-62.666	C21-C20-C26-C27	72.059	72.714
C5-C6-C7-H40	-64.323	-64.482	C14-C21-C23-C24	-166.691	-166.283
H38-C6-C7-H40	173.237	174.3	C14-C21-C23-H67	71.165	72.307
C6-C7-C8-C10	-59.123	-58.801	C14-C21-C23-H68	-43.545	-44.762
C7-C8-C10-C11	177.631	178.355	C20-C21-C23-C24	-48.469	-47.66
C15-C14-C21-C23	58.132	58.443	C20-C21-C23-H67	-170.616	-169.07
C16-C14-C21-C20	-179	-179.684	C20-C21-C23-H68	74.674	73.863
C16-C14-C21-C23	-59.992	-59.955	C22-C21-C23-C24	74.479	73.611
H55-C16-C17-H58	169.111	169.459	C22-C21-C23-H67	-47.667	-47.798
C18-C19-C20-C26	-167.325	167.109	C21-C23-C24-C25	58.014	57.866
C19-C20-C21-C14	-63.618	-62.185	C21-C23-C24-H70	179.292	178.481
C19-C20-C21-C22	56.367	57.78	C23-C24-C25-C26	-64.5	-65.061
H63-C20-C21-C14	51.517	50.47	C24-C25-C26-C20	60.587	60.73
H63-C20-C21-C22	171.506	170.436	C24-C25-C26-C27	-64.313	-65.596
C21-C20-C26-C28	-169.345	-168.684	C24-C25-C26-C28	176.517	175.412
H63-C20-C26-C25	63.332	62.781	H76-C28-C29-C30	65.098	66.904
H63-C20-C26-C27	-170.457	-168.684	H78-C29-C30-C31	172.613	173.715

6.6 Quantum chemical QSAR models to predict hyaluronidase inhibitory activity of ursolic acid 60 and its analogues

In this study, thirty compounds were evaluated for their IC_{50} values on the hyaluronidase inhibitory activity. The structures are shown in table 5.4.2. In this assay, the inhibitory effects of the thirty compounds on the activation of bovine testis hyaluronidase were examined using a spectrophotometric assay, which measure the turbidity of the complex formed between the undigested hyaluronic acid and albumin at 600nm (Ling et al., 2003). The percentage inhibition for each compound was determined with respect to the reference values in control experiments, which was run simultaneously. The results were expressed in terms of IC_{50} values. Compounds showing inhibitory activities of less than 20% at 50 x 10^2 μM are considered as not active. Therefore, only 24 compounds were considered to be into the data set. The IC_{50} value was converted into molar log IC_{50}. The experimental data was summarized in Table 5.4.2.

6.7 Heuristic method

The heuristic method was carried out in this study. The first set which consists of twenty four analogues gives seventeen correlations with three, four and five descriptors (Table 6.7.1). Correlation 1 was selected as it gives highest R^2 value of 0.6347. Figure 6.7 showed several outliers. To improve the correlation, the outliers such as compound **88**, **93** and **64** were eliminated either alone of in combination with each other. However, the R^2 values did not reach the 0.9 values. The result for compound **88** elimination was shown in table 6.7.2.

Even though several outliers were eliminated from the data set, the R^2 values did not improve very much by using this method. Therefore, another method was applied to generate better correlation.

Table 6.7.1: The best three to five descriptor correlation using Heuristic method for 24 PTC analogues

Correlation no.	***Number of descriptors***	***Correlation coefficient (R^2)***	***Fisher criteria (F)***	***Standard deviation (s^2)***
1	3	0.4855	6.2906	0.1039
2	4	0.5568	5.967	0.0942
3	4	0.5575	5.9843	0.094
4	4	0.5634	6.1288	0.0928
5	4	0.5644	6.1553	0.0926
6	4	0.5656	6.1834	0.0923
7	4	0.5781	6.5098	0.0896
8	4	0.5957	6.9992	0.0859
9	5	0.6006	5.4139	0.0896
10	5	0.6008	5.419	0.0895
11	5	0.6012	5.4262	0.0895
12	5	0.6039	5.4888	0.0888
13	5	0.6086	5.5982	0.0878

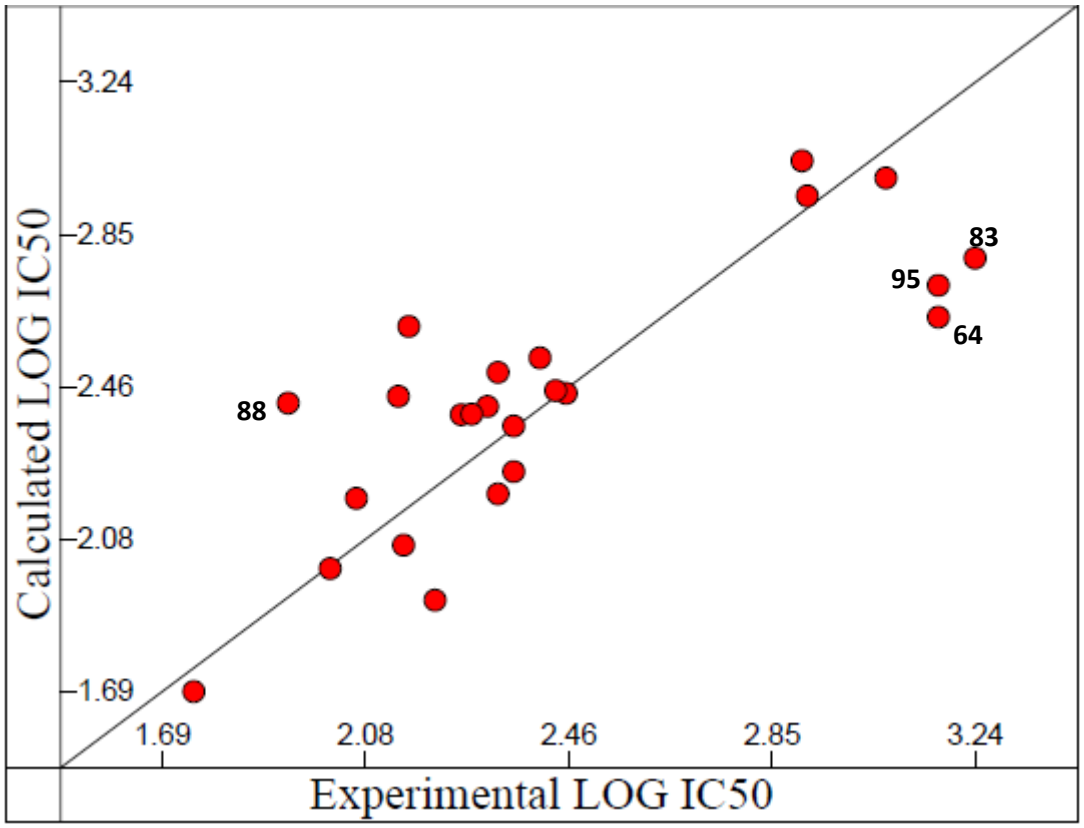

Figure 6.7: Calculated versus experimental activity according to Heuristic method for 24 PTC analogues (R^2=0.6347, F=6.25, s^2=0.0819; 5 descriptors)

Table 6.7.2: The best two to five descriptor correlation using Heuristic method after elimination of compound **88.**

Correlation no.	***Descriptor number***	***Correlation coefficient (R^2)***	***Fisher criteria (F)***	***Standard deviation (s^2)***
1	2	0.433	7.6358	0.1069
2	3	0.5409	7.4605	0.0911
3	3	0.541	7.4652	0.0911
4	3	0.5446	7.5725	0.0904
5	3	0.5497	7.7312	0.0894
6	3	0.5633	8.1687	0.0867
7	4	0.6201	7.3439	0.0796
8	4	0.6299	7.6582	0.0776
9	4	0.6345	7.8112	0.0766
10	4	0.6351	7.8312	0.0765
11	5	0.6783	7.1678	0.0714
12	5	0.6627	6.6796	0.0748
13	5	0.6632	6.696	0.0747

6.8 Multi linear method

Another method applied in this study was the best multi linear regression algorithm (BMLR). Calculation using BMLR method on the first data set which consists of 24 compounds (**60**, **61**,**64**,**75**,**76**,**77**,**78**, **79**, **80**, **81**, **82**, **83**, **84**, **85**, **86**, **87**, **88**, **89**, **90**, **91**, **92**, **93**, **94, 95**) was carried out to give best QSAR equation. Table 6.8.1 showed the number of descriptor and statistical parameters. The R^2 value given is very low (0.3620). The correlation plots are shown in figure 6.8.1. Compound labeled as **95** (boswellic alpha) and **88** (oleanolic acid methyl ester) were found as outliers and therefore were eliminated in order to improve the regression model. The two compounds display largest different between experimental and predicted log IC_{50} values. Compound **88** presents the second lowest value of log IC_{50} and among the most the active compound in the whole series of hyaluronidase inhibitors. Compound **95** however represent the lowest activity in hyaluronidase inhibition with high log IC_{50} value. Therefore from the second data set which consists of twenty two compounds,

eleven models obtained which consist of two to thirteen descriptors as listed in table 6.8.2. The R^2 values also improved (close to 1) as well as the other statistical values.

This method managed to avoid over fitting of the regression equations by monitoring the increase of R^2 in the equations with successive number of descriptors involved. The procedure is called the break point technique as illustrated in figure 6.8.2 that shows the change in slope in the plot of R^2 versus the number of descriptors added (Kartrizky et al., 2006). It could select the optimum multi regression model as shown in figure 6.8.2. The procedure was stopped when the difference between R^2 of the two consequent regression equations was less than or equal 0.02 (Kartrizky et al., 2006). From the second data set, this procedure showed that the optimum descriptors number was seven.

Table 6.8.1: The best two descriptor correlation using BML method for 24 PTC analogues

Number of descriptor	***Correlation coefficient (R^2)***	***Fisher criteria (F)***	***Standard deviation (s^2)***
2	0.3620	5.9569	0.1227

Table 6.8.2: The best two to thirteen descriptor correlation using BML method after elimination of compound **88** and **95** of PTC analogues

Descriptor number	***Correlation coefficient (R^2)***	***Fisher criteria (F)***	***Standard deviation (s^2)***
2	0.6285	16.07	0.0633
3	0.7926	22.9313	0.0373
4	0.8635	26.8767	0.026
5	0.9177	35.7046	0.0167
6	0.9431	41.41	0.0123
7	0.9717	68.77	0.0065
8	0.9851	107.4421	0.0037
9	0.9922	169.5916	0.0021
10	0.9965	310.7043	0.001
11	0.9984	579.3852	0.0005
12	0.9996	1723.6849	0.0002
13	0.9998	2904.9854	0.0001

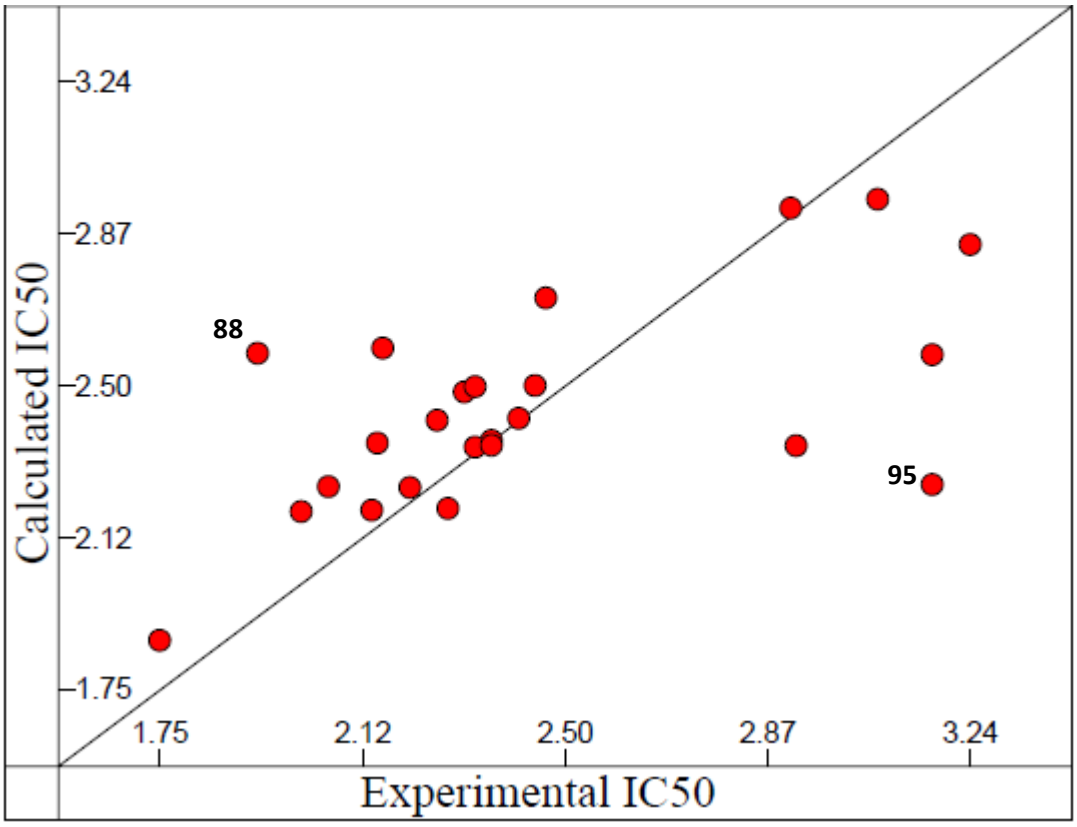

Figure 6.8.1: Calculated versus experimental activity according to BML method for 24 PTC analogues (R^2=0.3620,F= 5.96, s^2=0.1227; 2 descriptors)

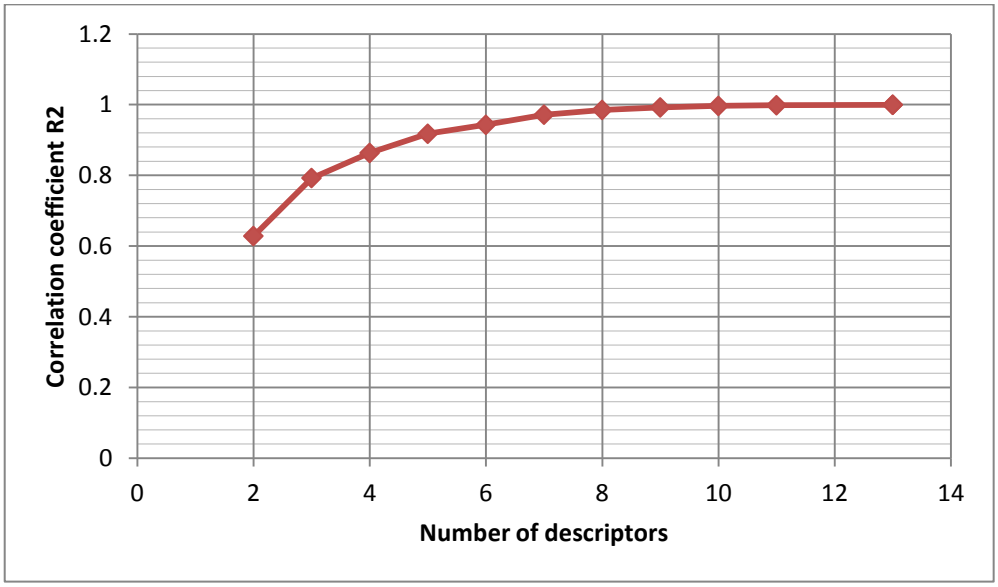

Figure 6.8.2: Correlation coefficient R^2 versus number of descriptors from BML method.

6.9 QSAR equation

A total of thirty analogues were evaluated for their IC_{50} towards hyaluronidase inhibitory activity (table 5.4.1). Six compounds were found to be inactive and thus could not contribute into the model development study. After making a comparison between the two methods on the data set, the QSAR model from the BML method are more effective than the Heuristic method. This is because the improvement in R^2 is more than 0.02. Thus, the best QSAR model was develop using the statistical data from table 6.8.2 which corresponding to seven descriptors. These descriptors were selected due to the break even point showed by figure 6.8.2. The multilinear equation, regression coefficients, their errors and t-test values is given in table 6.9.1. The geometry optimization and the values obtained from the semi empirical calculations are shown in table 6.9.2. If all the predicted parameters were taken for the generation of the model, the following equation was obtained using the BML method for the data set:

$$\text{Log}(1/IC_{50}) = 4.72 \times 10^{2}\, Q_i + 6.55 \times 10^{-1}\, E_{na} + 4.84 \times 10^{-3} PPSA1 + 1.00 \times 10^{-1} E_{nn} - 4.20 S_k + 1.95 \times 10^{2} V_H - 8.77 \times 10^{-1} E_{ee} - 1.722 \times 10^{2} \quad \textbf{(6.9)}$$

$F = 68.77$ $s^2 = 0.0065$ $R^2 = 0.971$ $R^2_{cv} = 0.9506$

From the equation 6.9, the descriptors involved in the model was of charge distribution-related or electronic descriptor (Q_i,$PPSA1$), quantum chemical descriptor (E_{na}, E_{nn}, V_H,E_{ee}) and geometrical descriptor (S_K). From the t-test value which show the statistical significance of the selected descriptors in the QSAR model, the order of significance of the descriptors are: $E_{na} > Q_i > PPSA1 > E_{nn} > S_K > V_H > E_{ee}$. The plotted

graph from the model is shown in figure 9.5. The calculated predicted logIC_{50} value from equation 6.9, experimental value and the difference were listed in table 6.9.2. The geometrical descriptor YZ Shadow YZS (S_k) is the area of the shadows of the molecule as projected on the YZ planes by the orientation of the molecule in the space along the axes of inertia (Liu et al., 2003). It could be define as (Karelson, 2000):

$$S_K = \frac{1}{2}\oint_{(c)}(v\,dp - p\,dv)$$

Where

C – contour of the projection of the molecule on the plane defined by two principle axes of the molecule ($k = XY, XZ, ORYZ$)

$v - x$ or y

p - y or z

The normalized shadow areas are calculated as the ratios S2 / (Y*max*Z*max*), where Y*max* and Z*max* are the maximum dimensions of the molecule along the YZ axes (Karelson, 2000). The shadow area are calculated by applying 2D square grid on the molecular projection and by summation of the areas of the squares overlapped with a projection. Those indices thus reflect the size (natural shadow indices), and geometrical shape (normalized shadow indices) of the molecule. The higher values of the YZ shadow thus increase the inhibitory activity.

It is known that the local electron densities or charges determine the mechanism and rate of most chemical reactions and physico-chemical properties of compounds. The valence electrons in molecules are not fixed to any particular atom but can move around the molecule. The electrons will be more at electronegative atoms compared to

electropositive one, thus results in the molecules partially negative and the others positive (Graham, 2005). In the equation 6.9, two electronic descriptors involved.

First descriptor was the partial positive surface area (PPSA1) is defined as the sum of the positively charged solvent-accessible atomic surface areas, S_A, in the molecule (Karelson, 2000):

$$PPSA1 = \sum_A S_A \qquad A \in \{\delta_A > 0\}$$

Where S_A is the respective atomic solvent-accessible surface area.

Positive regression coefficient of PPSA1 shows that the surface area of positive charge is a good physical-chemical parameter for hyaluronidase inhibitory activity. PPSA1 indicate that the positive charge and the atomic surface area can increase the inhibition towards the hyaluronidase activity.

Another electronic descriptor was min partial charge for a *C* atom (Zelfirov's PC) (Q_i). It could be defined as (Zefirov et al., 1987):

$$Qi = f(Xi)$$

Where Xi - atomic electronegativities

$$Xi = \left(X_i^0 \prod_{k=1}^{n} X_k \right)^{1/(n+1)}$$

Where X_i^0 - electronegativities of isolated atoms

n - atoms in the first coordination sphere of a given atom *i.e* C

Partial charges are important for the ionic interactions between the drugs and its binding site on the receptors. The positive regression in the model in the equation 6.9

showed that the bigger the partial charges in the molecule, the bigger the inhibition on hyaluronidase activity.

Four chemical descriptors involved in the selected model. First descriptor was min electron-nuclear attraction for a H atom (E_{na}). The definition of the descriptor is (Karelson, 2000):

$$E_{ne}(AB) = \sum_{B} \sum_{\mu,\nu \in A} P_{\mu\nu} \langle \mu \left| \frac{Z_B}{R_{iB}} \right| \nu \rangle$$

Where

A- given atomic species (in this case, H)

B- other atoms

$P_{\mu\nu}$ - density matrix elements over atomic basis $\{\mu\nu\}$

Z_B - charge of atomic nucleus B

R_{iB} – distance between the electron and atomic nucleus, B

$\langle \mu \left| \frac{Z_B}{R_{iB}} \right| \nu \rangle$ - electron-nuclear attraction integrals on atomic basis $\{\mu\nu\}$

The first summation is performed over all atomic nuclei in the molecule (B) whereas the second summation is carried out over all atomic orbitals at a given atom (A). The terms $\langle \mu \left| \frac{Z_B}{R_{iB}} \right| \nu \rangle$ denote the nuclear-electron attraction integrals on the given atomic basis. This energy describes the nuclear-electron attraction-driven processes in the molecule and could be related to the conformational (rotational, inversional) changes or atomic reactivity of the H atom. Thus the positive regression in the equation 6.9 indicated that the stronger the H electron-nuclear attraction, the higher the inhibition towards the hyaluronidase activity.

The second quantum chemical descriptor is min nuclear-nuclear repulsion for a C-O bond (E_{nn}) which can be calculated as (Clementi, 1980);

$$E_{nn}(AB) = \frac{Z_A Z_B}{R_{AB}}$$

Where

A-given atomic species

B-another atomic species

Z_A – charge of atomic nucleus, *A*

Z_B – charge of atomic nucleus, *B*

R_{iB} – distance between the atomic nuclei, *A* and *B*

This energy describes the strength of the nuclear repulsion at particular atom (C,O) and it might related to the conformational changes or atomic reactivity in the molecule (Karelson, 2000). This energy is considered as the global characteristics of a compound. Positive regression in the equation 6.9 showed that this energy contributed to increase the inhibition towards the hyluronidase activity. Thus, the lower the strength of C-O nuclear repulsion, the lower the inhibition will be.

The third quantum chemical descriptor is max valency of a H atom (V_H); V_A where *A* is the given atom. The atomic valence states energies for the given atomic (H) species in the molecule and its fragments (Karelson, 2000). It characterized the magnitude of the perturbation experienced by an atom in the molecular environment as compared to the isolated atom.

The final quantum chemical descriptor is max electron-electron repulsion for a C-H bond (E_{ee}). It could be defined as (Clementi, 1980):

$$E_{ee}(AB) = \sum_{\mu,\nu \in A} \sum_{\lambda,\sigma \in B} P_{\mu\nu} P_{\lambda\sigma} \langle \mu\nu | \lambda\sigma \rangle$$

Where:-

$P_{\mu\nu}$, $P_{\lambda\sigma}$ - density matrix elements over atomic basis $\{\mu\nu\lambda\sigma\}$

$\langle \mu\nu | \lambda\sigma \rangle$ - electron repulsion integrals on atomic basis $\{\mu\nu\lambda\sigma\}$

The energy characterize the electrostatic interactions between the chemical bond of C,H in a molecule (Karelson, 2000). Thus, the negative regression in the equation 6.9 indicated that high repulsion energy between C-H contributed to decrease the inhibition towards the hyaluronidase activity.

Table 6.9.2 showed the pIC_{50} values from the experimental and converted to logarithm of molar units and the predicted log IC_{50} values for all the twenty four compounds which were obtained from QSAR model; the equation 6.9. From the values of predicted log IC_{50}, it is clear that the QSAR equation generated through quantum chemical method predicted the pIC_{50} values very close to experimental values. Table 6.9.3 summarized the seven descriptors values for each compounds.

Table 6.9.1: The best nonlinear seven descriptors selected using BML method for 22 PTC analogues set

Descriptor	**symbol**	**t-test**	**X**	**ΔX**
Min partial charge for a C atom (Zelfirov's PC)	Q_i	12.6150	4.7198E+02	3.7414E+01
Min e-n attraction for a H atom	E_{na}	14.9564	6.5471E-01	4.3775E-02
PPSA-1 partial positive surface area (Zelfirov's PC)	$PPSA1$	11.1724	4.8406E-03	4.3326E-04
Min n-n repulsion for a C-O bond	E_{nn}	7.9805	1.0042E-01	1.2583E-02
YZ shadow	S_k	-6.0610	-4.2035E+00	6.9354E-01
Max valency of a H atom	V_H	5.2010	1.9541E+02	3.7572E+01
Max e-e repulsion for a C-H bond	E_{ee}	-4.0086	-8.7670E-01	2.1871E-01
Intercept		-4.4921	-1.7229E+02	3.8353+01

Table 6.9.2: The calculated and experimental values of the best correlation for 22 PTC analogues set (second set).

Compound	**Experimental log IC_{50}**	**Predicted log IC_{50}**	**Differences**
60	2.0100	1.9792	0.0308
61	2.4600	2.5909	0.1309
64	3.1700	3.1793	0.0093
75	2.2100	2.1746	-0.0354
76	2.2800	2.2988	0.0188
77	2.1400	2.1573	0.0173
80	3.0700	3.0697	-0.0003
81	2.4400	2.4073	-0.0327
79	2.2600	2.2502	-0.0098
78	2.9100	2.9120	0.0020
83	3.2400	3.1135	-0.1265
95	3.1700	3.1793	0.0093
84	2.3600	2.4008	0.0408
85	2.3100	2.2383	0.0717
86	2.3300	2.3264	-0.0036
87	2.1500	2.0864	-0.0636
88	1.9300	2.9307	1.0007
89	2.9200	2.9247	0.0047
90	2.3300	2.3264	-0.0036
91	2.0600	2.2502	-0.0098
92	2.3600	2.2832	-0.0768
93	2.1600	2.2143	0.0543
94	1.7500	1.7862	0.0362
96	2.4100	2.3959	-0.0141

Table 6.9.3: Quantum chemical descriptor for each PTC analogues

	E_{ee}	F_H	S_k	E_{nn}	$PPSAI$	E_{na}	Qi_l
60	36.6742	0.9975	56.2409	204.3285	555.0946	9.3014	-0.0301
61	36.6227	0.9979	58.461	203.1068	614.576	9.6601	-0.0302
64	36.4354	0.9967	58.961	203.0384	608.9415	10.6594	-0.0315
75	36.7109	0.9972	59.021	202.7228	648.3613	10.6196	-0.0315
76	36.5866	0.9987	51.3408	203.8475	612.1571	9.6232	-0.0317
77	36.5799	0.9977	61.681	204.213	571.1239	9.1528	-0.0315
78	36.7072	0.9975	58.781	204.1242	597.2751	9.5378	-0.0312
79	36.5468	0.998	51.3008	204.2344	618.3597	9.6505	-0.0318
80	36.7038	0.9974	63.161	204.1346	575.3271	9.1104	-0.0309
81	36.7489	0.9981	62.9211	203.1493	653.3146	9.6533	-0.0311
82	36.4912	0.9967	84.9215	202.9983	765.997	9.1568	-0.031
83	36.5851	0.9977	59.641	204.1928	603.0916	9.6231	-0.0313
84	36.3918	0.9971	56.6809	204.2373	543.0753	9.2816	-0.0315
86	36.5456	0.9976	58.341	203.1455	643.8741	9.6211	-0.0315
87	36.5788	0.9971	52.1808	209.0011	545.268	9.2768	-0.15
89	36.6251	0.9968	63.1011	203.1738	618.0181	9.7915	-0.0315
90	36.5435	0.9976	56.8809	204.2068	594.6963	9.1587	-0.031
91	36.6216	0.9968	57.7809	209.5274	561.1042	9.169	-0.0315
95	36.5903	0.9982	69.7412	204.3086	649.1003	9.6347	-0.031
88	36.4572	0.9969	60.861	202.0786	633.923	9.1607	-0.0315
94	36.6651	0.9973	54.4609	204.1924	555.4807	9.1298	-0.0302
96	36.4739	0.997	57.8409	202.0863	649.9969	9.0889	-0.0324
60	36.5033	0.996	54.5209	204.1782	594.6964	9.1252	-0.0313
61	36.419	0.9981	56.6409	204.2075	559.7748	9.2979	-0.031

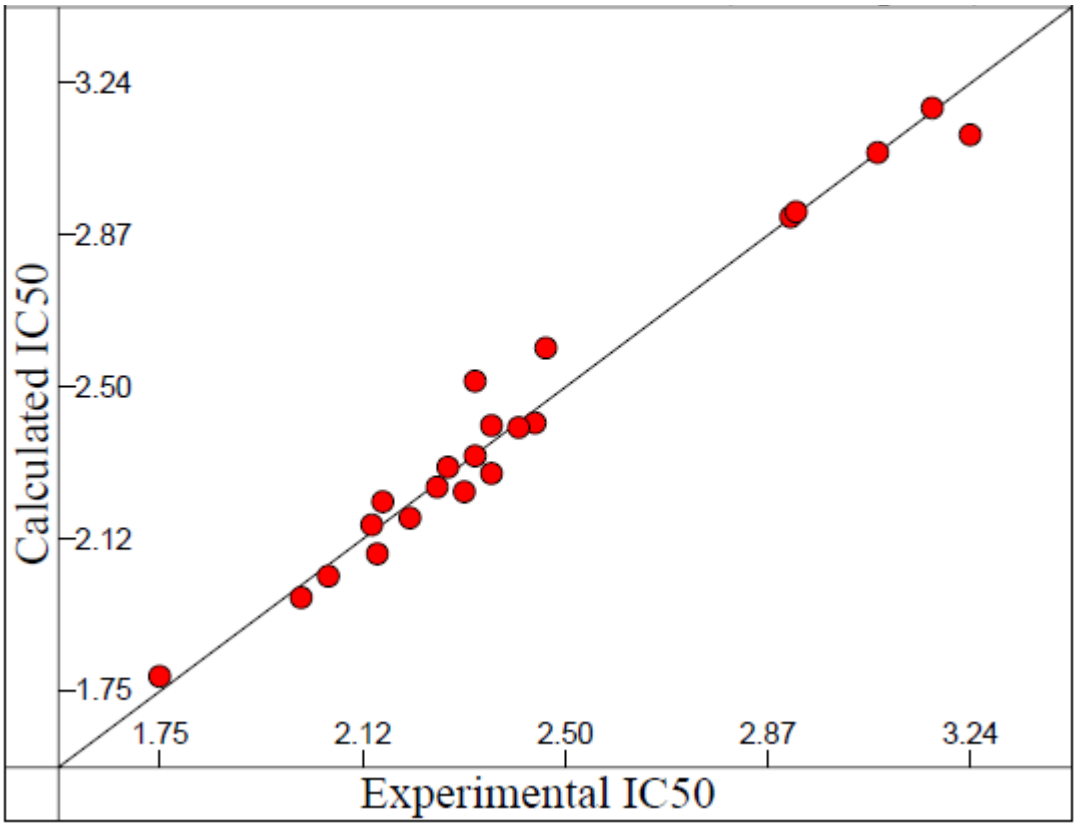

Figure 6.9: Calculated versus experimental activity according to BML method after elimination of compounds **95**, **88** for PTC analogues set (second set) (R^2=0.9717, F=68.77, s^2=0.0065).

6.10 Method validation [leave-one-out method]

The most important test of the model is its ability to correctly predict the properties of other or new compounds that were not included in the QSAR model. The leave-one-out method technique is based on the difference between the squared cross-validated correlation coefficient (R^2_{cv}) and correlation coefficient (R^2). The corresponding R^2_{cv} for all selected models will be calculated automatically by the validation module which implemented in CODESSA 2.6 package. From the calculation, the value of R^2_{cv} (0.9506) is very close to the R^2 (0.9717) since the difference is very small (0.9717-0.9506 = 0.0211). This finding suggests a good predictive ability of the selected best multi linear model.

CHAPTER 7:
CONCLUSIONS

CONCLUSIONS

The first part of the study was aimed at an investigation of the alkaloid contents of a plant species from the Rubiaceae family namely as *Prismatomeris malayana* Ridley. From the bioassay guided isolation on the methanol extracts of roots, stems and leaves of *Prismatomeris malayana* Ridley (FRI 50080) based on the hyaluronidase inhibitory activity, a pentacylic triterpenoid, ursolic acid **60**, was isolated and identified as the most active component. Apart from that, another sixteen compounds were isolated from the three parts and the structures were confirmed from the spectroscopic data of the NMR, IR, UV and Mass spectrum. Five of them are pentacyclic triterpenoids (**61**, **62**, **63**, **64**, **65**), seven are anthraquinones (**71**, **11**, **72**, **10**, **73**, **74, 21**) and four of them are iridoids (**66, 68**, **69, 70**).

The second part involved the modification on the functional group 3-OH and 28-COOH of ursolic acid **60** either by oxidation, acetylation, methylation or substituted with hydroxyimino group. A total of seven derivatives or analogues were successfully synthesized and strucutures were identified from the NMR and mass spectroscopic data. The compounds are 3-oxo-urs-12-en-28-oic acid **75**, 3-hydroxyimino-urs-12-en-28-oic acid **76**, 3-acetyl-urs-12-en-28-oic acid **77**, 3-acetyl-urs-12-en-28-oic acid methyl ester **78,** 3-hydroxy-urs-12-en-28-oic acid methyl ester **79,** 3-oxo-urs-12-en-28-oic acid methyl ester **80** and 3-hydroxyimino-urs-12-en-28-oic acid methyl ester **81**.

The study on the inflammation properties of *P. malayana* was also involved in this part. Three bioassays were applied on the investigation of the methanol extracts of different parts *i.e.* hyaluronidase and lipoxygenase inhibitory assay and TPA induced mouse ear oedema assay. The methanol extract of the leaves showed highest inhibitory on all three

assays, thus was selected for further bioassay guided fractionation and isolation study base on the the hyaluronidase inhibitory assay. Although the TPA induced mouse ear oedema assay showed good inhibition result of the methanol leaves extract, it was not applied for further study due to large quantity of sample required, specifically at the compound level. The structure activity relationship study on thirty analogues of pentacylic triterpenes towards the hyaluronidase inhibition showed that compound (3β)-3-[(3-carboxypropanoyl)oxy]-11-oxolean-12-en-30-oic acid **94** and oleanolic acid methyl ester **88** showed higher inhibition compared to ursolic acid **60** and positive control, apigenin (Table 5.5). It could be concluded that 3-OH and 28-COOH might play an important role in the activity and the presence of sugar moiety could make the compound lost their activity. However, note that glycosides would be lower in activity than aglycones, but in vivo they may well be converted into the aglycone and thus exert activity.

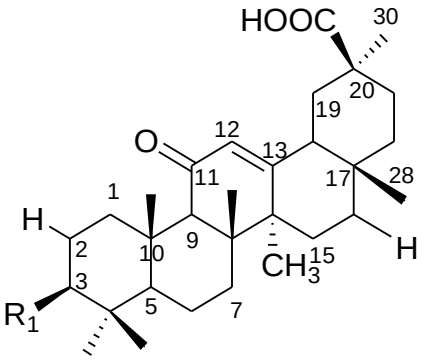

94

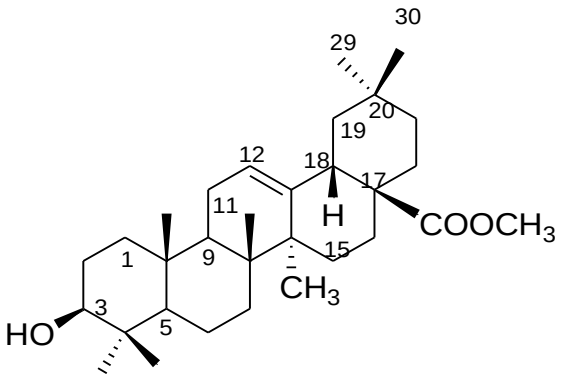

88

R_1=S2

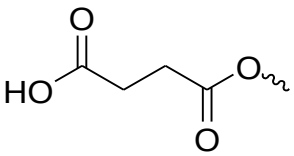

S2

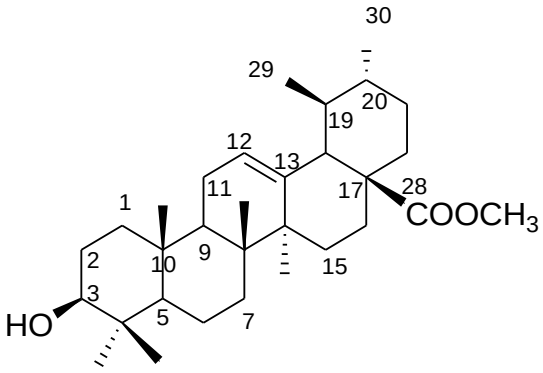

60

The computational approach was carried out successfully to quantitatively correlate the three dimensional structures of bioactive pentacyclic triterpenes and the hyaluronidase inhibitory activity. A data set which consisted of twenty four pentacylic triterpenoids derivatives with hyaluronidase inhibitory properties was investigated to relate their log IC_{50} values to the molecular structure. Two compounds labeled as **95** and **88** were eliminated and registered as outliers as they display large difference between experimental and predicted logIC_{50} values. Compound **88** presents the lowest value of logIC_{50} and is the most active compound in the data set. A QSAR modeling was carried out using CODESSA V 2.6 software.

The QSAR model was developed by using the BMLR method. Seven descriptors in the model were the descriptors involved in the model was of charge distribution-related or electronic descriptor (Q_i,$PPSA1$), quantum chemical descriptor (E_{na}, E_{nn}, V_H,E_{ee}) and geometrical descriptor (S_K). The two electrostatic descriptors playing role in determining the chemical properties of compounds involved in the QSAR model. The multi linear regression equation is good in terms of stability and predictive ability with a lower difference in R^2-R^2_{cv}.

To the author's knowledge, until present, no QSAR works have been previously published for the inhibition of hyaluronidase activity for pentacylic triterpenoids. Therefore, the present work contributes towards hyaluronidase inhibitory activity prediction with the developed QSAR model and could be very useful in future research on anti-inflammatory drug development of such type of compounds. In the future, mechanistic studies on the active anti-inflammatory compounds can be pursued and further studies on anti-inflammatory drug development of pentacylic triterpenes (PTC) can be further investigated.

CHAPTER 8:
MATERIALS AND METHODS

8.1 Phytochemical study

An intensive phytochemical investigation on *Prismatomeris malayana* Ridley was carried out starting from plant identification, phytochemical analysis, extraction, isolation and structure identification of the isolated chemical entities from this species.

8.1.1 Plant material

P. malayana in this study was collected from Setiu, Terengganu on 29th January 2006 and deposited in the herbarium of Forest Research Institute Malaysia (FRIM) with herbarium specimen number FRI 50080**.** The plant sample was identified by FRIM botanist. The plant sample was dried in an oven at 40^{o} C, divided into different parts and ground.

8.1.2 Instrumentation

Melting points were measured on Biocote SMP10 melting point apparatus. The infrared spectra were obtained on Spectrum 100 Fourier transform Infrared (FT-IR) spectrometer Perkin Elmer equipped with a mid-infrared deuterated triglycine sulphate (DTGS) detector. NMR analysis were carried out on a Bruker DRX 300 NMR spectrometer (300 MHz for ^{1}H NMR and 75 MHz for ^{13}C NMR) system with deuterated solvents such as chloroform ($CDCl_3$), demethyl sulphoxide (DMSO), methanol (MeOD) and phyridine (C_5D_5N). The mass spectra were obtained on LTQ Orbitrap mass spectrometer (Thermo Fisher Scientific, Bremen, Germany) equipped with an electrospray ionisation probe by employing either negative or positive ion mode, which ever could afforded the best limits of detection for the compounds.

8.1.3 Chromatography

Chromatography separation and isolation was performed using various techniques such as column chromatography (CC) and thin layer chromatography (TLC).

Several packing materials were used for column chromatography i.e MCI gel CHP 20P, Sephadex LH-20, Chromatorex ODS, silica gel 60 (70-230 Mesh ASTM or equivalent to silica gel of size 0.063-0.200 mm). The ratio of silica gel to sample is approximately 30:1 while for the other packing material is 10:1. The gel was made into slurry with a suitable solvent before packing into the glass column with various dimension and height depending on the quantity of the sample.

Aluminium supported silica gel F254 plates were used for thin layer chromatography (tlc). TLC spots were visualized under ultra-violet light (254 nm and 365 nm). The plates were then sprayed with 10% sulphuric acid followed by heating using heating mantel to detect the presence of phenolics and terpenes which indicated by the presence of colourful spots. The iodine vapour was also used for the detection purpose.

8.1.4 Visualising reagents

a) Iodine vapour

The TLC plate was placed in a container or tank containing iodine/iodine vapour. Brown spots on a yellow background indicated the presence of unsaturated compounds.

b) 10% sulphuric acid solution

The 10% acid sulphuric solution was sprayed on the TLC plate. The plate was then heated at 100^{o}C-150^{o}C until full development of colours had occurred. The occurrence

of pink, red, brown, purple, grey, dark green and black colours indicated the presence of phenyl propenes and simple terpenes.

8.1.5 Extraction, fractionation and isolation

8.1.5.1 Bioassay-Guided Fractionation Process

The crude methanol extracts were evaluated for anti inflammatory activity using three assays; lipoxygenase inhibitory hyaluronidase inhibitory and 12-*O*-tetradecanoylphorbol-13-acetate (TPA) induced mouse ear oedema assays (refer chapter 5.2.1, 5.2.2). The results for the extracts, fractions from the active extracts followed by the sub fractions and active component were listed in table 5.2.3. Scheme 8.1.5.1 outlines the bioassay guided fractionation and isolation of the bioactive compound from *Prismatomeris malayana* Ridley. Table 8.1.5.1 showed the percentage yield of each fraction, while table 8.1.5.2 – 8.1.5.4 showed the percentage yield of pure compounds.

8.1.5.2 Isolation of chemical constituents

Leaves: Oven-dried leaves (2.041 kg) were ground and extracted with MeOH by soaking for three times at room temperature. The concentrated extract (20.1g) was suspended in H_2O and partitioned with petroleum ether, followed by $CHCl_3$ and finally with EtOAc (Table 8.1.5.1). The $CHCl_3$ layer obtained was concentrated and chromatographed over Diaion HP-20SS column using 100% MeOH to afford three fractions. Fraction 1 and 2 was purified by using silica gel column eluting with $CHCl_3$-MeOH (CM) system, to afford four pentacylic triterpenoids; **60**, **61**, **62** and **65**. The EtOAc and H_2O layer was chromatographed over Sephadex LH-20 column eluted with 100% MeOH while the H_2O layer was chromatographed over MCI gel CHP20P column

using H_2O with increasing proportion of MeOH. The resulting fraction obtained were further purified by a combination of column chromatography employing silica gel with CM system, MCI gel with water- methanol (WM) system and MCI gel CHP20P. The EtOAc layer afforded one saponins, **63** and one iridoids **66** while the H_2O layer gave two iridoids; **68** and **70**. Table 8.1.5.2 listed all the isolated compounds from the leaves while scheme 8.1.5.2 summarized the isolation and purification procedures taken in a flow diagram.

Roots: Cut and oven-dried roots (2.2 kg) were ground and extracted with MeOH by soaking for three times at room temperature. The concentrated extract (100g) was suspended in H_2O and successively partitioned with EtOAc. The EtOAc layer after drying under reduced pressure (15.6 g) was chromatographed over silica gel and eluted using petroleum ether with increasing amounts of acetone to give 8 fractions. Each of these fractions was further fractionated and purified by a silica gel column and eluted with hexane-$CHCl_3$ systems to afforded six anthraquinones; **11**, **72**, **10**, **73**, **74** and **21**) and one triterpenoid **64.** The H_2O layer was fractionated and purified using MCI gel CHP20P column to give one iridoids **68** (Table 8.1.5.3 Scheme 8.1.5.3).

Stems: Oven-dried and ground stems (4.2 kg) was extracted with MeOH at room temperature for three times. The extract was concentrated under reduced pressure (103.68 g) and was partitioned between H_2O and $CHCl_3$. The resulting $CHCl_3$ layer (13.5 g) was chromatographed over Sephadex LH-20. The resulting fractions were further purified using silica gel column with petroleum ether-acetone followed by 100% hexane to afforded one anthraquinone **21**. The H_2O layer was chromatographed over MCI gel CHP20P to give one iridoids **68** (Table 8.1.5.4, Scheme 8.1.5.4).

Table 8.1.5.1: Percentage yield of extracts and fractions from leaves (PML), roots (PMR) and stem (PMS).

Code	Dry sample Weight (Kg)	Percentage yield (w/w %)				
		MeOH extract	Petroleum ether fraction	$CHCl_3$ fraction	EtOAC fraction	H_2O fraction
PML	2.04	9.85	11.14	17.46	5.81	24.58
PMS	4.20	2.47	-	13.02	-	35.50
PMR	2.20	4.55	-	-	15.60	35.0

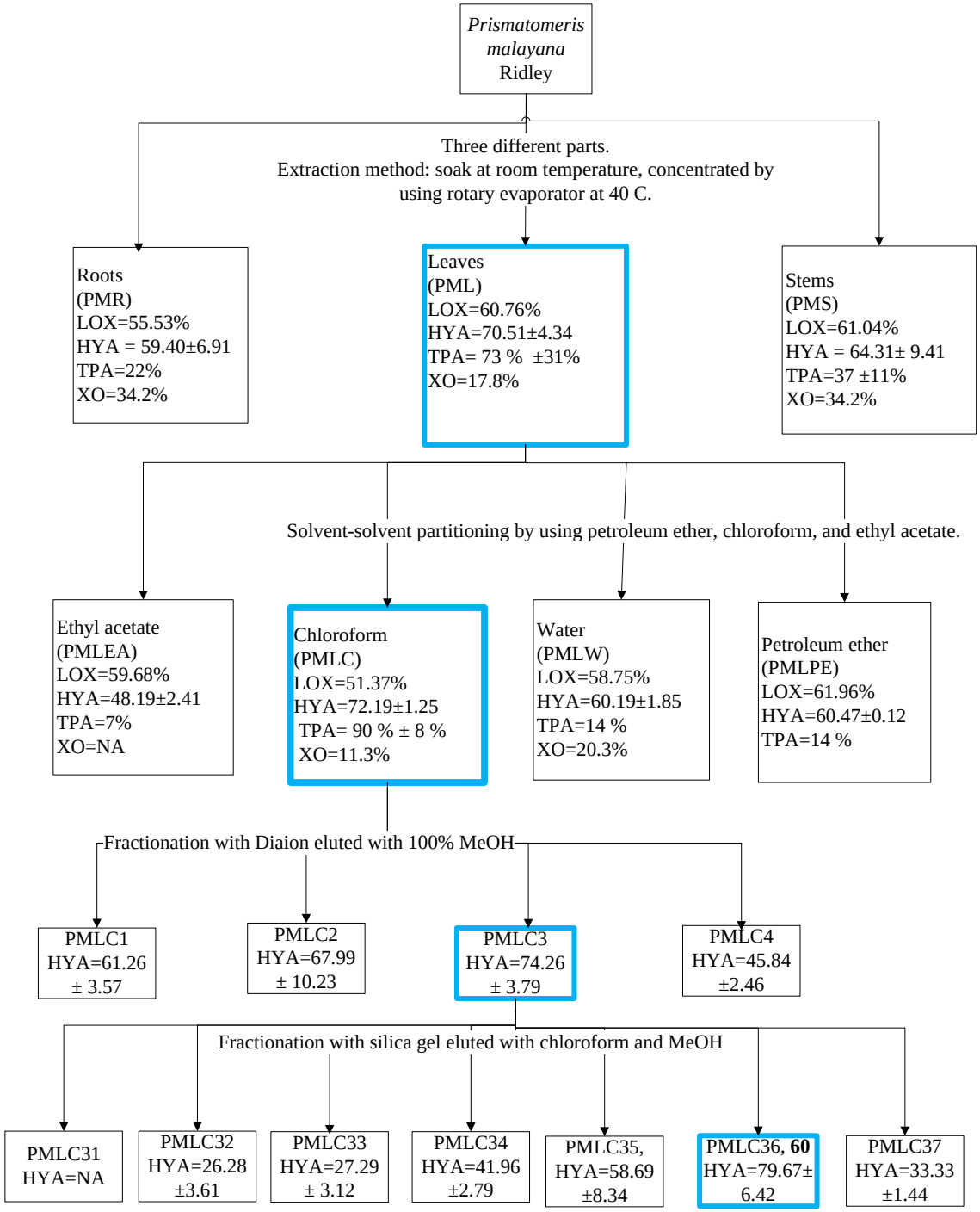

Scheme 8.1.5.1: Bioassay guided isolation and purification of active anti inflammatory compound from *Prismatomeris malayana*

Table 8.1.5.2: Isolated compounds from the leaves of *Prismatomeris malayana* Ridley

Crude extract	**Name of compound**	**% Yield of compounds from crude extract**
Petroleum ether	-	-
$CHCl_3$	3β-urs-12-en-28-oic acid (urolic acid), **60**	4.5900
	3β,19,23-trihydroxyurs-12-en-28-oic acid, **61**	0.0087
	3β,23-dihydroxyurs-12-en-28-oic acid, **62**	0.0020
	3β-hydroxyurs-11,12-epoxy-ursane-28, 13-olide, **65**	0.0015
EtOAC	28-*O*-glucopyranosyl-3α,19α,24-trihydroxyurs-12-en-28 oic acid, **62**	0.0110
	Prismalayanoside, **66**	0.0054
H_2O	Asperulosidic acid, **68**	0.1116
	Scandoside, **70**	0.4975

Table 8.1.5.3: Isolated compounds from the roots of *Prismatomeris malayana* Ridley.

Crude extract	**Name of compound**	**% Yield of compounds from crude extract**
EtOAC	1-hydroxy-2-hydroxymethyl-3-methoxy-9,10-anthraquinone, **74**	0.500
	Rubiadin-1-methyl ether, **11**	0.1300, 0.0110
	Damnacanthol, **72**	0.0923, 0.0058
	Rubiadin, **10**	0.200
	2-ethyl-3-hydroxymethyl-4-hydroxy-9,10-anthraquinone, **73**	0.0030
	Lucidin-ω-methyl ether, **21**	0.0580
	1-hydroxy-2-hydroxymethyl-3-methoxy-9,10-anthraquinone, **74**	0.005
	3β-acetylolean-12-en-28-oic acid, **64**	0.0220
H_2O	Asperulosidic acid, **68**	1.40

Table 8.1.5.4: Isolated compounds from the stem of *Prismatomeris malayana* Ridley.

Crude extract	**Name of compound**	**% Yield of compounds from crude extract**
$CHCl_3$	Lucidin-3-methyl ether, **71**	0.0230
H_2O	Asperuloside, **69**	0.3300

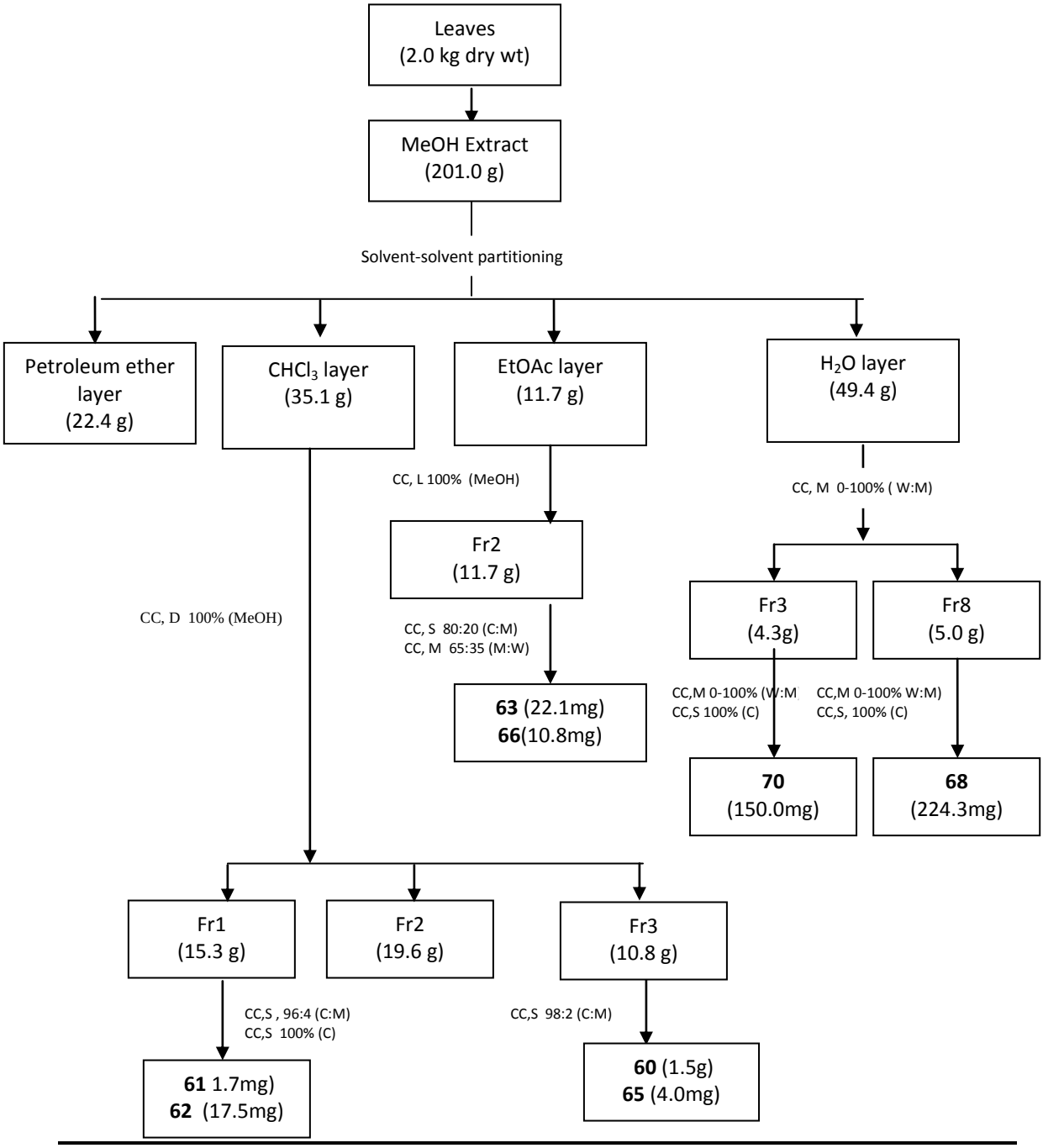

CC-Column chromatography; S-Silica gel: C:M-Chloroform methanol; W:M- Water methanol; M-MCI gel CHP 20P; L-Sephadex LH-20; D-Diaio

Scheme 8.1.5.2 Isolation of leaf components of *Prismatomeris malayana*

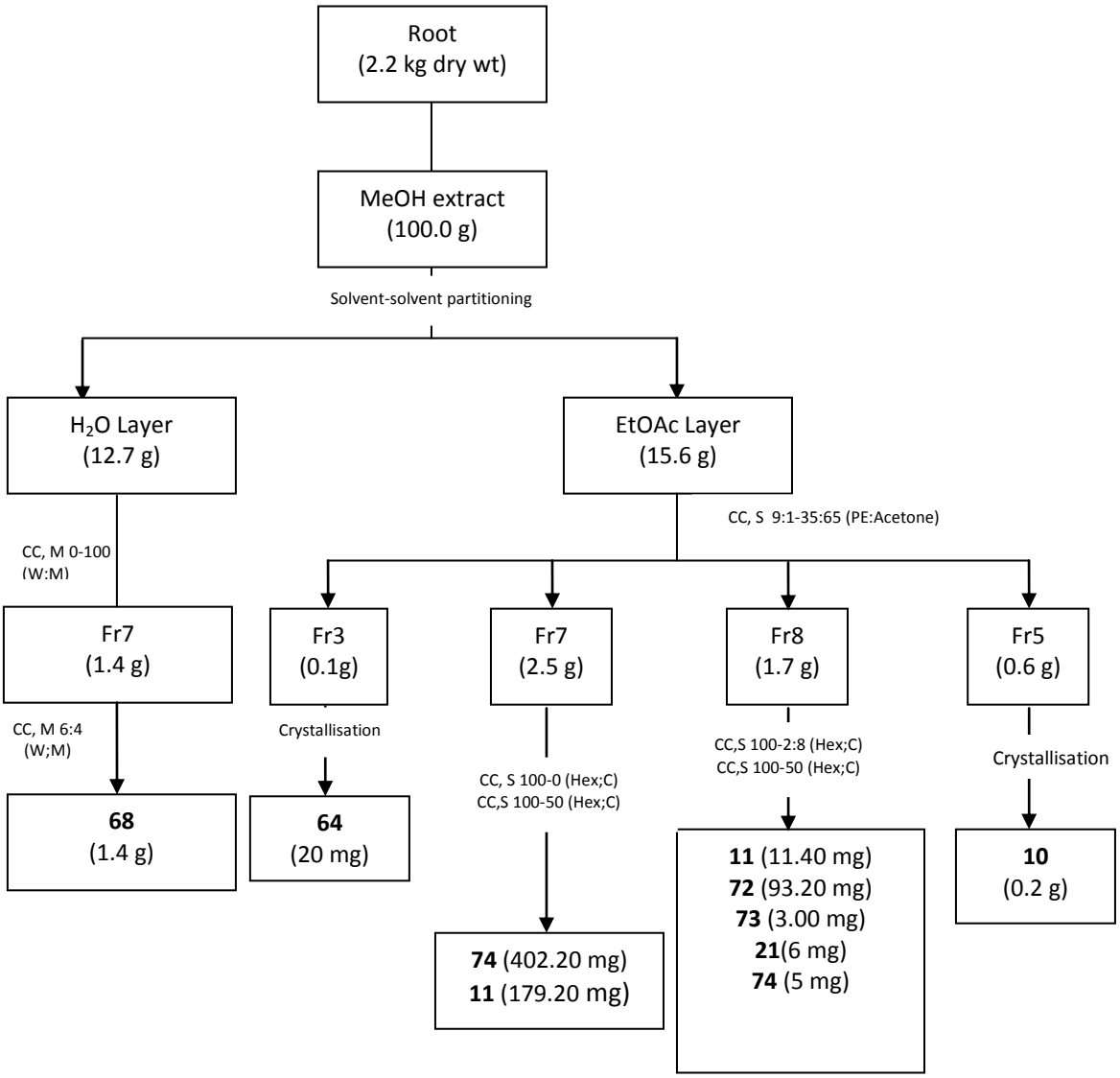

CC-Column chromatography; S-Silica gel: C:M-Chloroform methanol; W:M- Water methanol; M-MCI gel CHP 20P; L-Sephadex LH-20; D-Diaion; PE-Petroleum ether

Scheme 8.1.5.3: Isolation of root components of *Prismatomeris malayana*

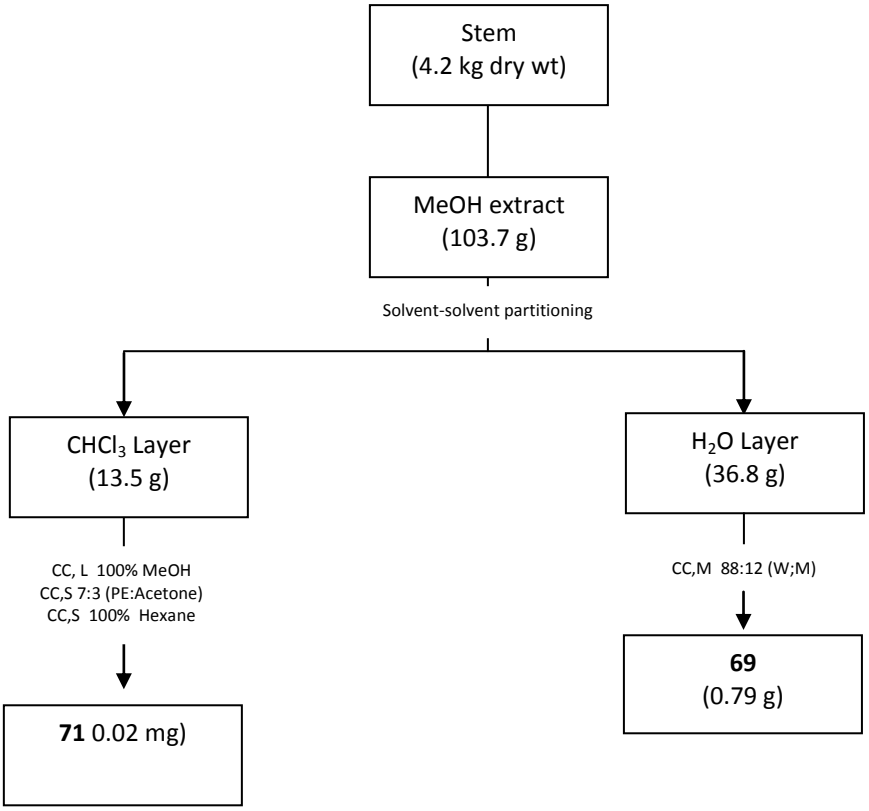

CC-Column chromatography; S-Silica gel: C:M-Chloroform methanol; W:M- Water methanol; M-MCI gel CHP 20P; L-Sephadex LH-20; D-Diaion; PE-Petroleum ether

Scheme 8.1.5.4: Isolation of stem components of *Prismatomeris malayana*

8.1.6 Physical and spectral data of isolated compounds 60-66 and 68-74

3β - urs-12-en-28-oic acid (Ursolic acid) **60**

: white amorphous powder
: $C_{30}H_{48}O_3$
UV λ_{max} (MeOH), nm : Not tested
IR ν_{max} ($CHCl_3$), cm^{-1} :1686$cm^{-1,}$ 3866 – 3188 cm^{-1}, 2860 cm^{-1}
Mass $(M+Na)^+$ m/z : 479.35059
^{1}H NMR (300MHz, C_5d_5N) δ : See Table 3.2.1
^{13}C NMR (75MHz, C_5D_5N) δ : See Table 3.2.1

3α, 19α, 24-trihydroxyurs-12-en-28-oic acid **61**

: white amorphous powder
: $C_{30}H_{48}O_5$
UV λ_{max} (MeOH) nm : Not tested
IR ν_{max} ($CHCl_3$) cm^{-1} : 1688$cm^{-1,}$ 3691 -3208 cm^{-1}, 2937 cm^{-1}
Mass $(M+Na)^+$ m/z : 511.34012
^{1}H NMR (300MHz, C_5d_5N) δ : See Table 3.2.2
^{13}C NMR (75MHz, C_5D_5N) δ : See Table 3.2.2

3β, 23-dihydroxyurs-12-en-28-oic acid **62**

: white amorphous powder
: $C_{30}H_{48}O_4$
UV λ_{max} (MeOH) nm : Not tested
IR ν_{max} ($CHCl_3$) cm^{-1} : 1689cm^{-1}, 3736 - 3066 cm^{-1}, 2933 cm^{-1}
Mass $(M+Na)^+$ m/z : 495.34546
^{1}H NMR (300MHz, C_5d_5N) δ : See Table 3.2.3
^{13}C NMR (75MHz, C_5D_5N) δ : See Table 3.2.3

28-*O*-glucopyranosyl-3α,19α,24-trihydroxyurs-12-en-28 oic acid **63**.

: brown solid
: $C_{36}H_{58}O_{10}$
UV λ_{max} (MeOH) nm : Not tested
IR ν_{max} ($CHCl_3$) cm^{-1} : 1724 cm^{-1}, 3716 and 3018 cm^{-1}
Mass $(M+Na)^+$ m/z : 673.39362
^{1}H NMR (300MHz, C_5d_5N) δ : See Table 3.2.4
^{13}C NMR (75MHz, C_5D_5N) δ : See Table 3.2.4

3β-acetylolean-12-en-28-oic acid **64**

: colorless crystal
: $C_{32}H_{50}O_4$.
UV λ_{max} (MeOH) nm : Not tested
IR ν_{max} ($CHCl_3$) cm^{-1} : 1722 cm^{-1}, 2947cm^{-1} , 1694
Mass $(M+Na)^+$ m/z : 497.36142
^{1}H NMR (300MHz, C_5d_5N) δ : See Table 3.2.5
^{13}C NMR (75MHz, C_5D_5N) δ : See Table 3.2.5

3β-hydroxyurs-11-en-ursane-13,28-olide **65**

: white amorphous powder
: $C_{30}H_{46}O_3$.

UV λ_{max} (MeOH) nm : Not tested
IR ν_{max} ($CHCl_3$) cm^{-1} : 2884 cm^{-1} , 1687 cm^{-1}
Mass $(M+Na)^+$ m/z : 477.33621
^1H NMR (300MHz, C_5d_5N) δ : See Table 3.2.6
^{13}C NMR (75MHz, C_5D_5N) δ : See Table 3.2.6

prismalayanoside **66**

: yellowish amorphous solid
: $C_{31}H_{36}O_{17}$
: $[\alpha]_D$ -0.31 (c=0.22, MeOH)
UV λ_{max} (MeOH) nm : 234, 292 and 314 nm
IR ν_{max} ($CHCl_3$) cm^{-1} : 2929 cm^{-1}, 1686 cm^{-1}
Mass $(M-H)^-$ m/z : 679.41669
^1H NMR (300MHz, CD_3OD) δ : See Table 3.2.10
^{13}C NMR (75MHz, CD_3OD) δ : See Table 3.2.10

asperulosidic acid **68**

: brown amorphous powder
: $C_{18}H_{24}O_{12}$
UV λ_{max} (MeOH) nm : Not tested
IR ν_{max} ($CHCl_3$) cm^{-1} : 3365 cm^{-1}, 1688 cm^{-1} and 1636 cm^{-1}
Mass $(M-H)^-$ m/z : 431.11816
^1H NMR (300MHz, CD_3OD) δ : See Table 3.2.8
^{13}C NMR (75MHz, CD_3OD) δ : See Table 3.2.8

asperuloside **69**.

: white amorphous powder
: $C_{18}H_{22}O_{11}$
UV λ_{max} (MeOH) nm : Not tested
IR ν_{max} ($CHCl_3$) cm^{-1} : 3360cm^{-1}, 1689 cm^{-1} and 1635cm^{-1}
Mass $(M+K)^+$ m/z : 453.11
^1H NMR (300MHz, CD_3OD) δ : See Table 3.2.9
^{13}C NMR (75MHz, CD_3OD) δ : See Table 3.2.9

scandoside **70**

: brown amorphous powder
: $C_{16}H_{22}O_{11}$.
UV λ_{max} (MeOH) nm : Not tested
IR ν_{max} ($CHCl_3$) cm^{-1} : 3369 cm^{-1}, 1635 cm^{-1}
Mass $(M-H)^-$ m/z : 389.10745
^1H NMR (300MHz, CD_3OD) δ : See Table 3.2.7
^{13}C NMR (75MHz, CD_3OD) δ : See Table 3.2.7

Lucidin-3-methyl ether **71**

: yellow amorphous powder
: $C_{16}H_{12}O_5$
UV λ_{max} (MeOH) nm : 283, 247, 203 nm
IR ν_{max} ($CHCl_3$) cm^{-1} : 3306 cm^1, 1647 cm^{-1}
Mass $(M-H)^-$ m/z : 283.05963
^{1}H NMR (300MHz, DMSO-d_6) δ : See Table 3.2.11
^{13}C NMR (75MHz, DMSO-d_6) δ : See Table 3.2.11

Rubiadin-1-methyl ether **11**

: yellow amorphous powder
: $C_{16}H_{12}O_4$
UV λ_{max} (MeOH) nm : 280, 238 and 204 nm
IR ν_{max} ($CHCl_3$) cm^{-1} :3306 cm^{-1} cm^1, 1650 cm^{-1}
Mass $(M-H)^-$ m/z : 267.06534
^{1}H NMR (300MHz, DMSO-d_6) δ : See Table 3.2.12
^{13}C NMR (75MHz, DMSO-d_6) δ : See Table 3.2.12

Damnacanthol **72**

: yellow amorphous powder
: $C_{16}H_{12}O_5$
UV λ_{max} (MeOH) nm : 278, 239, 203 nm
IR ν_{max} ($CHCl_3$) cm^{-1} : 3300 cm^{-1}, 1647 cm^{-1}, 1672 cm^{-1}
Mass $(M-H)^-$ m/z : 283.05991
^{1}H NMR (300MHz, DMSO-d_6) δ : See Table 3.2.13
^{13}C NMR (75MHz, DMSO-d_6) δ : See Table 3.2.13

Rubiadin **10**

: yellowish orange crystal
: $C_{15}H_{10}O_4$
UV λ_{max} (MeOH) nm : 409, 279, 245 and 206 nm
IR ν_{max} ($CHCl_3$) cm^{-1} : 3391 cm^{-1}, 1621 cm^{-1}
Mass $(M-H)^-$ m/z : 253.04933
^{1}H NMR (300MHz, DMSO-d_6) δ : See Table 3.2.14
^{13}C NMR (75MHz, DMSO-d_6) δ : See Table 3.2.14

1-ethyl-3-hydroxymethyl-4-hydroxy-9,10-anthraquinone **73**.

: yellowish orange powder
: $C_{16}H_{12}O_5$
UV λ_{max} (MeOH) nm : 277, 239 and 204 nm
IR ν_{max} ($CHCl_3$) cm^{-1} : 3395 cm^{-1}, 1700 cm^{-1}
Mass $(M-H)^-$ m/z : 283.26373
^{1}H NMR (300MHz, DMSO-d_6) δ : See Table 3.2.15
^{13}C NMR (75MHz, DMSO-d_6) δ : See Table 3.2.15

2-oxyhydroxymethyl-3-methoxy-9,10-anthraquinone **74**.

: yellowish powder
: $C_{16}H_{12}O_5$
UV λ_{max} (MeOH) nm : 279, 239 and 203 nm
IR ν_{max} ($CHCl_3$) cm^{-1} :1724 cm^{-1}, 1672 cm^{-1}, 3309 m^1
Mass $(M+Na)^+$ m/z : 307.05450
^1H NMR (300MHz, DMSO-d_6) δ : See Table 3.2.17
^{13}C NMR (75MHz, DMSO-d_6) δ : See Table 3.2.17

lucidin-ω-methyl ether **21**

: yellowish powder
: $C_{16}H_{12}O_5$
UV λ_{max} (MeOH) nm : 410, 280, 245, 205 nm
IR ν_{max} ($CHCl_3$) cm^{-1} :2929 cm^{-1}, 1623cm^{-1}, 1730 cm^{-1},1674 cm^1
Mass $(M-H)^-$ m/z : 283.05991
^1H NMR (300MHz, DMSO-d_6) δ : See Table 3.2.18
^{13}C NMR (75MHz, DMSO-d_6) δ : See Table 3.2.18

8.1.7 Physical and spectral data of compounds 83-99

3β-hydroxy-11-oxoolean-18α-12-en-28-methyl-29-oate
(18-α-glycyrrethinic acid methyl ester) **83**

:White amorphous powder
: $C_{31}H_{48}O_4$
Mass $(M+H)^+$ m/z : 485.54

^1H NMR (300MHz, C_5D_5N) δ: 5.72(1H,s,H-12), 3.68(3H,s,OCH_3), 3.54(1H, dd, *J*=4.74, 10.26, H-3), 3.11(1H,d,*J*=13.2), 2.4(1H, S,H-9), 2.28(1H,d,*J*=12.0, H-18 α), 1.40(3H,s,H-28), 1.27(3H,s,H-23), 1.21(3H,s,H-26), 1.13(3H,s,H-29), 1.09(3H,s,H-24), 0.64 (3H,s,H-25).

^{13}C NMR (75MHz, C_5D_5N) δ: 37.6 (C-1), 27.05(C-2), 78.06(C-3), 52.06(C-4), 61.2(C-5) 18.2(C-6), 32.3 (C-7) ,37.7(C-8), 55.5(C-9), 40.5(C-10), 199.4(C-11), 124.5(C-12), 165.5(C-13), 43.01(C-14), 28.3(C-15), 27.05 (C-16), 45.3(C-17), 44.2 (C-18), 39.9(C-19), 36.1(C-20), 35.7(C-21), 34.2(C-22), 20.9(C-23), 16.8(C-24), 16.1(C-25), 17.2(C-26), 20.7(C-27), 20.7(C-28), 28.9(C-29), 179 (C-30):

3β-urs-12-en-3-28-diol
(uvaol) **84**:

:White amorphous powder
: $C_{30}H_{50}O_2$
Mass $(M-H)^-$ m/z : 441.34

^1H NMR (300MHz, C_5D_5N) δ:5.27(1H,bt,H-12), 3.93(1H,dd,*J*=5.4,10.47) 3.48(1H,dd,*J*=5.34,10.5,H-28), 1.24(3H,s,H-27), 1.2(3H,s,H-23), 1.04(3H,s,H-29), 1.0(3H,s,H-26), 0.9(3H,s,H-30), 0.88(3H,s,H-24), 0.86(3H,s,H-24).

^{13}C NMR (75MHz, C_5D_5N) δ: 38.7(C-1), 8.1(C-2), 78.0(C-3), 39.7(C-4), 55.7(C-5), 18.7(C-6), 33.2(C-7), 40.3(C-8), 48.0(C-9), 37.1(C-10), 23.8(C-11), 25.01(C-12),

139.6(C-13), 42.3 (C-14), 28.8(C-15), 25.5(C-16), 39.2(C-17), 54.6(C-18), 39.8(C-19), 39.4(C-20), 31.2(C-21), 36.2(C-22), 28.8(C-23), 16.6(C-24), 15.9(C-25), 16.9 (C-26), 23.6(C-27), 69.1(C-28),17.8(C-29), 21.6(C-30):

3β-olean-12-en-3,28-diol
(erithrodiol) **85**

:White amorphous powder
$C_{30}H_{50}O_2$
Mass $(M-H)^-$ m/z : 441.33

^{1}H NMR (300MHz, C_5D_5N):5.5(1H, bs, H-12), 3.91(1H, d, *J*=10, H-28a), 3.38(2H, m, H-3, H-28b), 1.34(3H, s, H-27), 1.15(3H, s, H-24), 1.09(3H,s,H-30), 1.09(3H, s, H-26), 1.0(3H,s,H-25), 0.98(3H, s, H-29).

^{13}C NMR (75MHz, C_5D_5N) δ: 39.3(C-1),26.5 (C-2),81.3 (C-3),43.8 (C-4), 47.9(C-5), 18.4(C-6),33.2 (C-7), 40(C-8),48.5 (C-9),37.2 (C-10), 24(C-11), 122(C-12),145.5 (C-13), 42.4(C-14), 28.7(C-15), 24(C-16), 46.9(C-17), 42.4(C-18), 47(C-19), 31.2(C-20), 34.6(C-21), 33.6(C-22), 27.9(C-23), 14.4(C-24), 16.4(C-25), 17.9(C-26), 26.4(C-27), 64.4(C-28), 33.1(C-29), 23.9(C-30):

3β-hydroxyurs-12-en-28-methyl
(amyrin alpha) **86**

:White amorphous powder
: $C_{30}H_{50}O$
Mass $(M-H)^-$ m/z : 425.34

^{1}H NMR (300MHz, C_5D_5N) δ: 5.27(1H,t,*J*=3.12,H-12), 3.56(1H,dd,*J*=5.55, 10.86, H-3), 1.31(3H,s,H-28), 1.2(3H,s,H-23), 1.12(3H,s, H-26), 1.09(3H, s, H-27), 1.02(3H, s, H-24), 0.97(3H, s, H-30), 0.96(3H, s,H-29), 0.94(3H,s,H-25).

^{13}C NMR (75MHz, C_5D_5N) δ: 39.2(C-1), 28.2(C-2), 78.1(C-3), 41.7(C-4), 55.7(C-5), 18.8(C-6), 33.26(C-7), 39.9(C-8), 48.1(C-9), 37.1(C-10), 23.6(C-11), 124.9(C-12), 139.9(C-13), 48.1(C-14), 28.2(C-15), 26.9(C-16), 33.9(C-17), 59.2(C-18), 39.8(C-19), 39.4(C-20), 31.4(C-21), 41.7(C-22), 28.8(C-23), 15.9(C-24), 16.6(C-25), 17.08(C-26), 23.5(C-27), 28.9(C-28), 17.8(C-29), 21.5(C-30):

Echinocystic acid **87**

:White amorphous powder
: $C_{30}H_{48}O_4$
Mass $(M-H)^-$ m/z : 471.35

^{1}H NMR (300MHz, C_5D_5N) δ: 5.63 (1H, bs, H-12), 5.23 (1H,bs,H-16), 3.65 (1H, bd, *J*=11.91, H-18), 3.41(1H, bd, *J*=7.68), 2.87(1H, t, *J*=13.17, H-19), 2.87(1H, m, H-15), 1.85(3H, s, H-27), 1.36(3H, s, H-23), 1.16(3H, s, H-30), 1.04(3H, s, H-29), 1.00(3H,s,H-26), 0.97(3H,s, H-24), 0.82(3H,s,H-25).

^{13}C NMR (75MHz, C_5D_5N) δ: 39.0 (C-1), 74.7(C-2), 78.05(C-3), 39.4(C-4), 55.8 (C-5), 18.8(C-6), 33.3(C-7), 38.9 (C-8), 47.2(C-9), 39.4(C-10), 23.8(C-11), 41.4(C-14), 36.1(C-15), 23.8(C-16), 47.2(C-17), 42.1(C-18), 49.8(C-19), 31.04(C-20), 37.4(C-21),

32.9(C-22), 28.7(C-23), 16.6(C-24), 15.6 (C-25), 18.8(C-26), 27.2(C-27), 33.5(C-29), 24.6(C-30):

Oleanolic acid methyl ester **88**

:White amorphous powder
: $C_{31}H_{50}O_3$
Mass $(M-H)^-$ m/z : 469.50

^{1}H NMR (300MHz, C_5D_5N) δ: 5.44 (1H,bt,H-12), 3.75(3H,s,OCH_3), 3.52(1H,dd,*J*= 5.1,10.5), 3.16(1H,bd,*J*=10.5), 1.35(3H,s,H-27), 1.25(3H,s,H-23), 1.08(3H,s,H-26), 1.02(3H,s,H-24,30), 0.97(3H,s,H-29), 0.9(3H,s,H-25) .

^{13}C NMR (75MHz, C_5D_5N) δ: 43.3(C-1), 32.3(C-2), 79.5(C-3), 41.1(C-4), 57.2(C-5), 26.2(C-6), 38.8(C-7), 43.3(C-8), 53.1(C-9), 39.9(C-10), 24.9(C-11), 132.1(C-13), 47.4(C-14), 32.3(C-15), 25.1(C-16), 49.5(C-17), 43.4(C-18), 48.4(C-19), 29.6(C-20), 34.6(C-21), 21.1(C-22), 18.05(C-24), 17.04(C-25), 18.7(C-26), 17.04(C-27), 21.1(C-28), 21.1(C-29), 21.1(C-30), 11.7 (CH_3CO):

3β-(2-*O*-(6-deoxy-alpha-L-mannopyranosyl)-alpha-L-arabinopyranosyl) oxy)-23-hydroxyolean-12-en-28-oic acid
(hederin alpha) **89**

:White amorphous powder
: $C_{41}H_{66}O_{12}$
Mass $(M-H)^-$ m/z : 749.45

^{1}H NMR (300MHz, C_5D_5N) δ: 6.42(1H,s,H-1”), 5.69(1H,s,H-12), 5.17(1H,d, 6.3,H-1’), 4.77-4.56(3H,m,H-2”, 2’, 3”), 4.38-4.15(5H,m,H-3’, 4’,5a’, 4”, 23a, 3), 3.80(2H, m, H-5b’, 23b), 3.35(1H, bd, *J*=10.38, H18), 1.69(1H, d, *J*=6.03, H-6”), 1.26(3H,s,H-27), 1.12(3H, s, H-24), 1.06(3H,s,H-26), 1.04(3H,s, H-30), 0.97(3H X 2, s, H-25, 29).

^{13}C NMR (75MHz, C_5D_5N) δ: 38.0(C-1), 26.0(C-2), 80.9 (C-3), 41.9(C-4), 48.1(C-5), 18(C-6), 33.2(C-7), 39.7(C-8), 47.7(C-9), 36.8(C-10), 23.6(C-11), 122.8(C-12), 144.8(C-13), 43.5(C-14), 28.3(C-15), 23.6(C-16), 46.3(C-17), 42.1(C-18), 46.6(C-19), 30.9(C-20), 34.0(C-21), 32.8(C-22), 26.1(C-23), 16.02(C-24), 14.0(C-25), 17.4(C-26), 23.7(C-27), 180.0(C-28), 33.2(C-29), 18.5(C-30), 104.5(C-1’), 101.7(C-1”), 75.7(C-2’), 72.5(C-2”), 74.1(C-3’), 72.4(C-3”), 69.5(C-4’),74.9(C-4”), 63.4(C-5’), 69.7(C-5”):

3β-olean-12-*en*-28-methyl
(amyrin beta) **90**

: White amorphous powder
: $C_{30}H_{50}O$
Mass $(M-H)^-$ m/z : 425.45

^{1}H NMR (300MHz, C_5D_5N) δ:5.29(1H, bs,H-12), 3.53(3H,dd, *J*=5.46, 10.71), 1.30(3H,s,H-28), 1.26(3H,s,H-27), 1.16(3H,s,H-26), 1.05(3H,s,H-30), 1.01(3H,s,H-25), 0.97(1H,bd, H-23,24,29).

^{13}C NMR (75MHz, C_5D_5N) δ: 39.1 (C-1), 28.1 (C-2), 78.03 (C-3), 40.1 (C-4), 55.1 (C-5), 18.7(C-6), 39.1 (C-7), 48.0 (C-8), 37.4 (C-9), (C-10), 23.3 (C-11), 122.3(c-12), 145.2 (C-13), 41.3 (C-14), 26.4 (C-15), 27.1 (C-16), 33.4 (C-17), 47.5 (C-18), 47.03

(C-19), 33.44 (C-20), 34.3 (C-21), 37.2 (C-22), 28.6 (C-23), 15.7 (C-24), 16.6 (C-25), 17.01 (C-26), 26.1 (C-27) 28.7 (C-28), 32.7 (C-29), 23.8 (C-30):

2α,3β,23-Trihydroxyurs-12-en-28-oic acid
(asiatic acid) **91**

:White amorphous powder
: $C_{30}H_{48}O_5$
Mass $(M-H)^-$ m/z : 487.34

^{1}H NMR (300MHz, C_5D_5N) δ: 5.51(1H,s,H-12), 4.35-4.22(3H,m,H-3,H-23a,H-3), 3.76(1H,d,*J*=10.5,H-23b), 2.68(1H,d,J=11.4,H-18), 1.186 (3H,s,H-27), 1.11(3H,s,H-26,H-29), 1.01(3H,s,H-30), 0.99(3H,s,H-25), 0.97(3H,s,H-24).

^{13}C NMR (75MHz, C_5D_5N) δ: 47.8 (C-1), 68.6 (C-2), 77.9 (C-3), 43.4 (C-4), 44.8 (C-5), 21.1 (C-6), 27.9 (C-7), 39.8 (C-8), 47.8 (C-9), 38.05 (C-10), 23.5 (C-11), (C-12), (C-13), 42.3 (C-14), 28.4 (C-15), 24.6 (C-16), 47.6 (C-17), 53.3 (C-18), 39.8 (C-19), 39.1 (C-20), 30.8 (C-21), 37.2 (C-22), 14.2 (C-23), 17.2 (C-24), 17.2(C-25), 17.2 (C-26), 23.6 (C-27), (C-28), 17.3 (C-29), 21.1 (C-30):

3 β-hydroxy-olean-12-en-28-oic acid
(oleanolic acid) **92**

:White amorphous powder
: $C_{30}H_{48}O_3$
Mass $(M+Na)^+$ m/z : 479.35

^{1}H NMR (300MHz, C_5D_5N) δ: 5.88(1H,bs,H-12), 3.54(1H,t,*J*=6.33, 15.66), 3.41(1H,dd,*J*=4.08, 9.78,H-18), 1.35(3H,s,H-27), 1.31,s,H-23), 1.097(3H, s,H-24,30), 1.07(3H,s,H-26). 1.02(3H,s,H-29), 0.96(3H,s,H-25).

^{13}C NMR (75MHz, C_5D_5N) δ: 38.7(C-1), 28.05 (C-2), 77.8 (C-3), 39.1 (C-4), 55.5 (C-5), 18.5 (C-6), 33.9 (C-7), 39.5 (C-8), 46.4 (C-9), 37.1 (C-10), 23.6 (C-11),122.5(C-12), 144.6 (C-13), 41.7 (C-14), 27.8 (C-15), 23.4 (C-16), 47.8 (C-17), 41.9 (C-18), 46.2 (C-19), 30.7 (C-20), 32.9 (C-21), 33 (C-22), 28.5 (C-23), 16.3 (C-24), 15.3 (C-25), 18.5 (C-26), 25.9 (C-27), 179.9 (C-28), 33 (C-29), 23.5 (C-30):

3α-hydroxy-11-oxo-12-en-30-noroleane-20β-oic acid
(18α-glycyrrhetinic acid) **93**

:White amorphous powder
: $C_{31}H_{48}O_4$
Mass $(M-H)^-$ m/z : 469.33

^{1}H NMR (300MHz, C_5D_5N) δ: 5.88 (1H,s,H-12), 3.58(1H,bd, *J*=7.32,H-3), 3.17(1H, bd,*J*=13.2, H-8), 2.46(1H,s, H-9), 1.52(3H,s,H-28), 1.46(3H,s,H-30), 1.32(3Hx 2,s,H-23, 26), 1.19 (3H,s,H-29), 1.15(3H,s,H-24), 0.77(3H,s,H-25).

^{13}C NMR (75MHz, C_5D_5N) δ: 37.6 (C-1), 27.1(C-2), 78.1(C-3), 52.1(C-4), 61.2(C-5) 18.2(C-6), 32.3 (C-7) ,37.7(C-8), 55.5 (C-9), 40.5(C-10), 199.4(C-11), 124.5(C-12), 165.5(C-13), 43.01(C-14), 28.3(C-15), 27.05 (C-16), 45.3(C-17), 44.2(C-18), 39.9(C-19), 36.1(C-20), 35.7(C-21), 34.2(C-22), 20.9(C-23), 16.8 (C-24), 16.1 (C-25), 17.2(C-26), 20.7(C-27), 20.7(C-28), 28.9(C-29), 179 (C-30).

3β-3-[(3-carboxypropanoyl) oxy]-11-oxoolean-12-en-30-oic acid (carbenoxolone) **94**

:White amorphous powder
: $C_{34}H_{50}O_7$
Mass $(M-H)^-$ m/z : 569.54

^{1}H NMR (300MHz, C_5D_5N) δ: 5.58(1H,s,H-12), 4.38(1H,dd, *J*=4.65, 11.61, H-3), 2.64(1H, bd,*J*=13.56, H-18), 1.29 (3H,s,H-28), 1.03 (3H,s,H-27), 1.01 (3H,s,H-26), 0.89 (3H,s,H30), 0.78 (3H X 2, d, J=3.3, H-23, 24), 0.57 (3H,s,H-25).

^{13}C NMR (75MHz, C_5D_5N) δ: 39.8(C-1), 32.4 (C-2), 81.9 (C-3), 46.7 (C-4), 62.9 (C-5), 18.4 (C-6), 33.7 (C-7), 38.2 (C-8), 56.2 (C-9), 39.1 (C-10), 202.6 (C-11), 128.8 (C-12), 174.02 (C-13), 46.4 (C-14), 27.7 (C-15), 27.6 (C-16), 44.6 (C-17), 46.4 (C-18), 43.8 (C-19), 33.05 (C-20), 33.0 (C-21), 39.8 (C-22), 29.6 (C-23), 18.4 (C-24), 16.9 (C-25), 19.3 (C-26), 28.6 (C-27), 29.4 (C-28), 184.8 (C-29), 23.8 (C-30), COOH(180.4), COO (175.1):

3α-hydroxy-olean-12-en-24-oic-acid (boswellic alpha) **95**

:White amorphous powder
: $C_{30}H_{48}O_3$
Mass $(M-H)^-$ m/z : 455.45

^{1}H NMR (300MHz, C_5D_5N) δ:5.33(1H, bs, H-12), 4.79(1H,bs,H-3), 1.86(3H,s,H-30), 1.33(3H,s,H-26), 1.21(3H,s,H-25), 1.17(3H, s,H-29), 0.93(3H, s,H-28), 0.93(3H,s,H-27).

^{13}C NMR (75MHz, C_5D_5N) δ: 36.1 (C-1), 27.7 (C-2), 72.5 (C-3), 49.6 (C-4), 50.8 (C-5), 22.02 (C-6), 34.7 (C-7), 41.6 (C-8), 48.6 (C-9), 38.7 (C-10), 25.1 (C-11), 123.9 (C-12), 146.4 (C-13), 43.4 (C-14), 28.5 (C-15), 28.9 (C-16), 32.5 (C-17), 48.9 (C-18), 48.3 (C-19), 34.1 (C-20), 34.7 (C-21), 38.7 (C-22), 25.1 (C-23), 181.3 (C-24), 15.2 (C-25), 18.4 (C-26), 27.1 (C-27), 26.7 (C-28), 29.9 (C-29), 25.1 (C-30):

3β, 23-dihydroxy-olean-12-en-28-oic acid (hederagenin) **96**

:White amorphous powder
: $C_{30}H_{48}O_4$
Mass $(M-H)^-$ m/z : 471.34299

^{1}H NMR (300MHz, C_5D_5N) δ: 5.52(1H,s,H-12), 4.26-4.2(2H, m, H-23a, H-3), 3.76(1H,d,*J*=10.29, H-23b), 3.35(1H,bd, *J*=10.38, H-18), 1.25(3H,s,H-27), 1.07(3H,s,H-24), 1.05 (3H,s,H-26), 1.02(3H,s,H-30), 0.98(3H,s,H-25), 0.94(3H,s,H-29).

^{13}C NMR (75MHz, C_5D_5N) δ: 38.9 (C-1), 33.4 (C-2), 73.4 (C-3), 39.05 (C-4), 48.6 (C-5), 18.7 (C-6), 33.4 (C-7), 37.3 (C-8), 42.1 (C-9), 39.05 (C-10), 23.6 (C-11), 128 (C-12), 146 (C-13), 42.3 (C-14), 27.8 (C-15), 23.6 (C-16), 43.01 (C-17), 48.3 (C-18), 46 (C-19), 31.06 (C-20), 28.4 (C-21), 35.0 (C-22), 67.9 (C-24), 13.3 (C-25), 18.6 (C-26), 26.2 (C-27), 16.07 (C-28), 23.8 (C-30):

3α-hydroxy-urs-12-en-24-oic-acid
(Boswellic beta) **98**

:White amorphous powder
: $C_{30}H_{48}O_3$
Mass $(M-H)^-$ m/z : 455.53

^{1}H NMR (300MHz, C_5D_5N) δ:5.33(1H,bs,H-12), 4.78(1H,bs,H-3), 1.82(3H,s,H-23), 1.22(3H,s,H-27), 0.85(3H,s,H-29,30).

^{13}C NMR (75MHz, C_5D_5N) δ: ^{13}C-NMR (75MHz, C_5D_5N) δ: 36.7 (C-1), 28.5 (C-2), 72.2 (C-3), 49.9 (C-4), 51.1 (C-5), 22.4 (C-6), 35.7 (C-7), 39.8 (C-8), 49.05 (C-9), 42.1 (C-10), 25.5 (C-11), 126.8 (C-12), 141.5 (C-13), 44.5 (C-14), 29.9 (C-15), 29.3 (C-16), 35.7 (C-17), 61.05 (C-18), 41.6 (C-19), 41.5 (C-20), 33.1 (C-21), 43.4 (C-22), 25.5 (C-23), 182.4 (C-24), 15.8 (C-25), 18.9 (C-26), 23.2 (C-27), 27.06 (C-28), 19.4 (C-29), 30. 7 (C-30):

Friedelin **99**

:White amorphous powder
: $C_{30}H_{50}O$
Mass $(M-H)^-$ m/z :425.56

^{1}H NMR (300MHz, C_5D_5N) δ:2,51(1H, m,H-2a), 2.42(1H, m, H-2b), 2.28 (1H,q,H-4), 1.89 (1H, m, H-1a), 1.22(3H, s, H-1.22), 1.11(3H, s, H-27), 1.08(3H, s, H-26), 1.05 (3H, s, H-29), 1.03(3H,d, *J*=6.69,H-23),0.98(3H,s,H-25), 0.73(3H,s,H-24).

^{13}C NMR (75MHz, C_5D_5N) δ: 2.6 (C-1), 41.7 (C-2), 212 (C-3), 58.1 (C-4), 42.2 (C-5), 41.3 (C-6), 18.6 (C-7), 53.2 (C-8), 36.4(C-9), 59.3 (C-10), 35.8 (C-11), 30.8 (C-12), 40.02 (C-13), 38.5 (C-14), 32.7 (C-15), 36.4 (C-16), 30.3 (C-17), 43.2 (C-18), 35.7 (C-19), 28.5 (C-20), 33.2(C-21), 39.6 (C-22), 7.4 (C-23), 14.8 (C-24), 18.1 (C-25), 20.5 (C-26), 19 (C-27), 32.7 (C-28), 32.1 (C-29), 35.2 (C-30):

8.2 Preparation of ursolic acid derivatives

8.2.1 3-Oxo-urs-12-en-28-oic acid (75)

To a solution of ursolic acid **60** (112.3 mg, 0.25 mmol) in acetone-dicholoromethane (10 ml) was added pyridinium chlochromate (PCC) (161.3 mg, 0.75 mmol). After being stirred at room temperature until the reaction almost complete (TLC monitoring), the mixture was concentrated and partitioned with H_2O and CH_2Cl_2. The CH_2Cl_2 was concentrated and purified by silica gel column chromatography eluted with hexane acetone (95:5) to give **75**. Yield 79.34%, white amorphous powder.

8.2.2 3-hydroxyimino-urs-12-en-28-oic acid (76)

A solution of **75** (26.2 mg, 0.34 mmol) and hydroxylamine hydrocholoride (27.6 mg, 0.40 mmol) in pyridine (5 ml) was heated for four hour at 50 ^{o}C. After coolling to room temperature, the reaction mixture was concentrated under vacuum to dryness. It was then purified using silica gel and eluted with petroleum ether $CHCl_3$ to obtain **76**. Yield 90%: colorless crystal.

8.2.3 3-acetyl-urs-12-en-28-oic acid (77)

Ursolic acid **60** (120.0 mg, 0.26 mmol) was treated with acetic anhydride (534.0 mg, 5.32 mmol) and pyridine at room temperature overnight and worked up with 10% HCl, $NaHCO_3$, followed by separation using separating funnel to get the dicholoromethane layer. $MgSO_4$ was added to absorb water from it and rinse using dichloromethane. It was purified using silica gel and eluted using chloroform petroleum ether (90:10) to give **76**. Yield 50%, white amorphous powder.

8.2.4 3-Oxo-urs-12-en-28-oic acid methyl ester (80)

Methyl ursolate **79** was treated with PCC same fashion as in **75** to get compound **80**. It was purified using silica gel column chromatography and eluted using chloroform petroleum ether (90:10). Yield 90%, colorless crystal.

8.2.5 3-hydroxyimino-urs-12-en-28-oic acid methyl ester (81)

A solution of **80** (80.0 mg, 0.17 mmol) and hydroxylamine hydrochloride (108.0 mg, 1.56 mmol) in pyridine was heated for 2hrs at 50 ^{o} C. It was then cooled to room temperature and diluted after that with CH_2Cl_2 followed by washing with 10% HCl for three times. It was then dried over anhydrous Na_2SO_4 and concentrated under reduced pressure. It was purified with silica gel column chromatography using $CHCl_3$ hexane (40:60) to give **81** Yield 95%.

8.2.6 3-hydroxy-urs-12-en-28-oic acid methyl ester (79)

To a stirred solution of ursolic acid **60** (10.0 mg, 0.02 mmol) in approximately 10 ml of toluene: MeOH (3:2) and solution of $TMSCHN_2$ (trimethylsilane diazomethane) in hexane was added drop wise until the yellow color persisted. The mixture was stirred at room temperature and concentrated. It was purified using silica gel column chromatography with hexane $CHCl_3$ (70:30) to give **79**. Yield 95 %, white amorphous powder.

8.2.7 3-acetyl-urs-12-en-28-oic acid methyl ester (78)

Compound **77** was treated with $TMSCHN_2$ in the fashion as in preparation of **79** to give **78**. Yield 95%, colorless crystal.

8.2.8 Physical and spectral data of compounds 75-81

3-oxo-urs-12-en-28-oic acid **(75)**

: white amorphous powder
: $C_{30}H_{46}O_3$.
UV λ_{max} (MeOH), nm : Not tested
Mass $(M-H)^-$ m/z : 453.33524
^1H NMR (300MHz, C_5d_5N) δ : See Table 4.1
^{13}C NMR (75MHz, C_5D_5N) δ : See Table 4.2

3-hydroxyimino-urs-12-en-28-oic acid **(76)**

: white amorphous powder
: $C_{30}H_{47}NO_3$.
UV λ_{max} (MeOH), nm : Not tested
Mass $(M+H)^+$ m/z : 470.35516
^1H NMR (300MHz, C_5d_5N) δ : See Table 4.1
^{13}C NMR (75MHz, C_5D_5N) δ : See Table 4.2

3-acetyl-urs-12-en-28-oic acid **(77)**

: white amorphous powder
: $C_{32}H_{50}O_4$
UV λ_{max} (MeOH), nm : Not tested
Mass $(M-H)^-$ m/z : 497.36343
^1H NMR (300MHz, C_5d_5N) δ : See Table 4.1
^{13}C NMR (75MHz, C_5D_5N) δ : See Table 4.2

3-acetyl-urs-12-en-28-oic acid methyl ester **(78)**

: white amorphous powder
: $C_{32}H_{50}O_4$
UV λ_{max} (MeOH), nm : Not tested
Mass $(M-K)^-$ m/z : 473.28149
^1H NMR (300MHz, C_5d_5N) δ : See Table 4.1
^{13}C NMR (75MHz, C_5D_5N) δ : See Table 4.2

3-hydroxy-urs-12-en-28-oic acid methyl ester **(79)**

: white amorphous powder
: $C_{31}H_{50}O_3$
UV λ_{max} (MeOH), nm : Not tested
Mass $(M-K)^-$ m/z : 493.35556
^1H NMR (300MHz, C_5d_5N) δ : See Table 4.1
^{13}C NMR (75MHz, C_5D_5N) δ : See Table 4.2

3-oxo-urs-12-en-28-oic acid methyl ester **(80)**

	: white amorphous powder
	: $C_{31}H_{48}O_3$
UV λ_{max} (MeOH), nm	: Not tested
Mass $(M+Na)^+$ m/z	: 491.34198
^{1}H NMR (300MHz, C_5d_5N) δ	: See Table 4.1
^{13}C NMR (75MHz, C_5D_5N) δ	: See Table 4.2

3-hydroxyimino-urs-12-en-28-oic acid methyl ester **(81)**

	: white amorphous powder
	: $C_{31}H_{49}NO_3$
UV λ_{max} (MeOH), nm	: Not tested
Mass $(M+Na)^+$ m/z	: 506.35175
^{1}H NMR (300MHz, C_5d_5N) δ	: See Table 4.1
^{13}C NMR (75MHz, C_5D_5N) δ	: See Table 4.2

8.3 Biological assays

The biological evaluations were performed on inflammatory related bioassays. The assays were hyaluronidase and lipoxygenase inhibitory and TPA induced mouse ear oedema.

8.3.1 Hyaluronidase inhibitory assay

The assay was performed according to the Sigma protocol with slight modifications (Ling et al., 2003). The assay medium consisting of 1.00-1.67 U hyaluronidase in 100 µl 20 mM sodium phosphate buffer pH 7.0 with 77 mM sodium chloride and 0.01% Bovine Serum Albumin (BSA) was preincubated with 5 µl of the test compound in DMSO (dimethyl sulphoxide) for 10 min at 37^{o}C. Then the assay was commenced by adding 100 µl hyaluronic acid **82** (0.03% in 300 mM sodium phosphate, pH 5.35) to the incubation mixture and incubated for a further 45 min at 37 ^{o}C. The undigested

hyaluronic acid **82** was precipitated with 1 ml acid albumin solution made up of 0.1% bovine serum albumin in 24 mM sodium acetate and 79 mM acetic acid, pH 3.75. After standing at room temperature for 10 min, the absorbance of the reaction mixture was measured at 600 nm. The absorbance in the absence of enzyme was used as the reference value for maximum inhibition. The inhibitory activity of test compound was calculated as the percentage ratio of the absorbance in the presence of test compound vs. absorbance in the absence of enzyme.

$$\% \text{ Inhibition} = \frac{A_t}{A_c} \times 100\%$$

Where: A_t = absorbance in the presence of test compound; and

A_c = absorbance in the absence of enzyme

The enzyme activity was determine by control experiment that run simultaneously, in which the enzyme was pre incubated with 5µl DMSO, followed by the assay procedures described above. In this case, the percentage ratio of the absorbance in the presence of enzyme vs. that in the absence of enzyme was in the range of 15-20%. The performance of the assay was verified using apigenin as a reference under exactly the same experimental conditions. The extract was tested at concentration of 100 µg/ml in the final reaction mixture. The compounds however were tested at several concentration from 100-2000 uM in the final reaction mixture. The results were expressed as mean of the inhibitory values ± S.D of three separate experiments measured in triplicates.

8.3.2 TPA induced mouse ear oedema assay

The assay was performed according to Hirota (1990). The 12-*O*-tetradecanoylphorbol-13-acetate, TPA (1 µg) dissolved in acetone (20 µl) was applied to the ear of male strain albino mice (25-30g) by means of a micropipette. The plant extracts were applied topically to the inner surface of the right ear at 2 mg/ear about 30 min before each TPA treatment. The other ear which acted as a control was applied with sample vehicle. After eight hours of TPA treatment, the mouse was sacrified and the ears were cut off. The ears were weight to investigate the resulting oedema. The results were expressed as percentage inhibition (IE%), taken to mean the complete suppression of erythema in the test animals. Each value used was the mean of individual determinations from seven mice. Indomethacin, a known inflammatory inhibitor was used as a positive control for this study.

The inhibitory effects (IE%) of each extract was calculated as the ratio of the weight increase of the ear sections, according to the following formula:

Inhibitory effect (IE%) = [(L-R)/(L-C*)] x 100

= [(L-R)/(L-(L/2.41))]x 100

Where: L = weight of leaf ear which treated with TPA only

R = weight of right ear which is treated with TPA plus tested extract

*C = weight of normal ear (untreated ear)

*C is calculated weight. It has been found that treating a normal ear with 1 µg TPA resulted in a 2.41 times increase in weight.

8.3.3 Lipoxygenase inhibitory assay

Lipoxygenase inhibiting activity was measured using a spectrophotometric method (Riaz et al., 2004). The reaction mixture consisted of Sodium phosphate buffer 160 µl, 10 µl of test sample solution and 20 µl of soybean lipoxygenase solution was initiated by the addition of 10 µl of the substrate in the form of sodium linoleic acid solution. The enzymatic conversion of linoleic acid was measured at 234 nm over a period of 6 min. Test compounds and reference standards were dissolved in MeOH. All reactions were performed in triplicates in a 96-well microplate.

$$\text{Inhibition \%} = \frac{E-S}{E} \times 100$$

Where: E= Optical density of control

S= Optical density of sample (test compounds)

8.3.4 Statistical analysis

Data obtained were expressed as mean standard error (± S.D.). The data were analyzed for statistical significance using Student's *t*-test (for hyaluronidase and lipoxygenase) and Duncan's multiple range tests for TPA mouse ear oedema inhibitory activity. *P*-values less than 0.05 were considered to be significant [$*p<0.05$; $**p<0.01$; $***p<0.001$]. The IC_{50} value was calculated using Probit analysis program version 1987.

8.4 QSAR model preparation using quantum chemical method

The self consistent field (SCF) calculation and frequency calculation using RM1 semi empirical quantum chemical method were performed followed by QSAR analysis using CODESSA 2.6 to come out with QSAR model.

8.4.1 Data collection from the biological and chemical aspect

A number of ursolic acid **60** derivatives or analogues were prepared either from the structure modification process **75-81**, isolated from *Prismatomeris malayana;* **60, 61, 64** together with the commercially available compounds **83-103** which were purchased from Chromadex. The structure of each compound **60**, **61**, **64**, **75-81**, **83-103** was confirmed from the spectroscopic data of NMR and LCMS/MS and compared with the literature values. The spectral properties of compounds **60, 61, 64** and **75-81** were discussed in chapter 3 and 4 respectively while for compounds **83-103** were listed in 8.1.8 section.

Two compounds **78** and **80** were isolated as crystal and the crystal data were collected using Bruker SMART APEX diffractometer. The crystallographic data allowed to determines the absolute configuration of the two compounds. The crystal structure file was converted into molecular structure files using Chem3D Ultra 7.0 software package. All the analogues are listed in the table 5.4.2 (Please refer to chapter 5).

All analogues were evaluated for their inflammatory activity on the hyaluronidase enzyme and the data was calculated as IC_{50} values. The data however were converted into log IC_{50} value units which were used instead of IC_{50} to improve the normal

distribution of the experimental data points (Kartizky, 2006). The data were presented in table 6.9.2.

8.4.2 Conversion into 3D structure and mopac file

The crystal structure of compound **80** was used to determine the relative configuration of the other analogues. Starting from this structure, other structures were drawn using Chem 3D Ultra software. These structures were optimized using the MOPAC software package available in the Chem3D Ultra 7.0.

8.4.3 Structure optimization using quantum chemical method

The optimized 3D structures then are used for self consistent field (SCF) calculation. The SCF method was also known as the Hartree-FOCK method. The SCF calculation will provide quantum chemical molecular properties. The main idea of SCF theory is to replace all interactions to any one body with an effective interaction and thus reduce any multi-body problem into an effective one-body problem. The geometry optimization was done at RM1 semi empirical quantum chemical level which implemented in the MOPAC 6.0. The output files from scf calculation provide structural information on the basis of wave function of the molecular system.

8.4.4 Force calculation using quantum chemical method

The optimized 3D structures were subjected to frequency calculation using RM1 semi empirical quantum chemical method. The force constants are first calculated from the second derivatives of the energy with respect to displacements of all pairs of atoms. The force constants and the isotopic masses are then used to calculate the vibrational

frequencies. The force calculation will also give the thermodynamic characteristics of compounds. The output file provided the structural information on the basis of the potential energy surface of the molecular system.

8.4.5 QSAR analysis using CODESSA

An input file was prepared which contained the data obtained from scf, thermodynamics, force and molecular structure calculations for each structure together with the activity value (log IC_{50}). All the data files were loaded into the CODESSA 2.6 (Kartizky et al., 1994) for further calculation.

8.4.5.1 Calculation of descriptors

The first step in developing a QSAR model is the descriptors calculation. Descriptors are defined as numerical characteristics associated with chemical structures (Kartisky, 2005). They are derived on the basis of the structures chemical constitution, topology, geometry, and inherent wave function and potential energy surface. The molecular descriptors calculated in CODESSA are divided into six groups; constitutional, topological, geometrical, electrostatic, quantum chemical and thermodynamic. In the CODESSA program, over 450 descriptors could be calculated on the basis of the geometrical or electronic structures of the molecules. New descriptors also could be constructed using descriptors already calculated and standard mathematical operations.

8.4.5.2 Developing a QSAR model

The exceedingly large number of descriptors creates difficulties in the generation of the best multi linear model for a given property. The consequences are:

i. The number of all possible multi-parameter correlation is enormous to calculate all of them.
ii. Many of the theoretical descriptor scales are statistically interrelated which results in a critical loss of information if applied simultaneously in the same correlation.

This phenomenon is called overfitting and it could be avoided by selecting only several descriptors (Jurgen, 2004). Thus, for the optimal number of descriptors in a QSAR model, the rule-of-thumb should be applied which describe that the number of descriptors should be equal one-sixth or one-third the number of molecules in the data set.

Therefore, the good statistical methods that could select appropriate descriptors and best quality correlation are essential in developing QSAR/QSPR models. The two most advanced procedures for systematic development of the multi-linear QSAR/QSPR equations are the *Heuristic* method and the *Best Multi-Linear Regression* method.

In QSAR models, the correlation represents the results of the (multi)linear regression between the property (a set of experimental values of a physical or chemical property, biological activity or performance under the study), y

$$y = a_o + \sum a_i x_i$$

and selected descriptors *xi*. This object is therefore composed of regression coefficients *ai*, correlation coefficient R^2, standard error s^2, and Fisher criterion *F* value for the set of structures used to derive the correlation. By default each correlation is characterised by its correlation coefficient, R^2, and Fisher criterion *F* value. These values could be used to determine the quality of the derived model (section test of methods).

a. Heuristic method

The Heuristic method could demonstrate which descriptors are insignificant from the standpoint of a single-parameter correlation and highly inter-correlated. All descriptors are checked to ensure that values of each descriptor are available for each structure and there is a variation in these values. Descriptors for which values are not available for every structure in the data in question are discarded. Descriptors having a constant value for all structure in the dataset are also discarded. This information will be helpful in reducing the number of descriptors involved in the search for the best QSAR model.

In Heuristic method, a descriptor is eliminated if:

i. the *F*-test's value for the one-parameter correlation with the descriptor is below 1.0.

ii. the squared correlation coefficient of the one parameter equation is less than $R^2_{min} = 0.1$.

iii. The parameter's *t*-value is less than $t_1 = 1.5$

iv. The descriptor is highly inter-correlated which is above $r_{full} = 0.99$

b. Best multi linear method

The Best Multi-Linear Regression (BMLR) method is a more thorough procedure as it builds a single correlation using all selected descriptors in order to find the best regression model. Therefore, it will take longer time to complete compared to the Heuristic method. This method could processes 300 descriptors and 150 structures simultaneously. To achieve the maximum effectiveness, this method should fulfill the following criteria:

i. The upper limit of the square of the linear correlation coefficient R^2min for two descriptors scales to be considered orthogonal. Is set to $R^2_{min} = 0.1$.

ii. The lower limit of the square of the linear correlation coefficient for two descriptor scales to be considered non-collinear. Default value R^2nc = 0.65

iii. The maximum number of best correlations to be considered in the search of the best correlations with one descriptor scale added, is set to $N_c = 400$.

iv. The probability level for the Fisher criterion *F* is taken as 95%.

8.4.6 Method validation

The good, robust and predictive QSAR model is its capability of making accurate and reliable predictions of the modeled response of new analogues. Validation is the process that established the reliability and relevance of a procedure for a specific purpose. The model could either validated using internal or external method. The internal method are

such as least square fit (R^2), cross-validation (R_{cv}^2), chi (χ), root-mean-squared error (RMSE) and scrambling (Jorgen, 2004). External validation will use compounds test set that not included in the model development or so called training set.

The internal validation was applied in this study due to considerably small data set. In least square method, linear regression, R^2 shows the comparison between the experimental and predicted values. Thus, any outlier s from the data set will be removed in order to optimize the QSAR model. Leave-one-out-cross validation was also applied in this study again to measure the model predictive ability and any possibility if the model has been over fitted. The R^2 should be larger than the R_{cv}^2. The model will be suspected to be over fitting if the R^2 value significantly larger (25%) than the R_{cv}^2 (Jorgen, 2004).

REFERENCES

REFERENCES

Abe, I., Rohmer, M. & Prestwich, G.C. (1993). Enzymatic cyclization of squalene and oxidosqualene to sterols and triterpenes. *Chem. Rev*., **93**, 2189-2206.

Andersson, L.& Rova, J. H. (1999). *The* rps16 intron and the phylogeny of the Rubioideae (Rubiaceae). *Plant Syst. Evol.,* **214**, 161-186.

Arulmozhi, D.K., Veeranjaneyulu, A., Bodhankar S.L. & Arora S.K. (2005). Pharmacological investigations of *Sapindus trifoliatus* in various *in vitro* and *in vivo* models of inflammation. *Indian J. Pharmaco.l*, **37 (2)**, 96-102.

Atsuko, I., Takao, T., Naotaka, N. & Toyoyuki, N. (2003). Two triterpenoid saponins from *Neonauclea sessilifolia*. *Chem. Pharm. Bull.*, **51 (11)**, 1335-1337.

Bauch, H.J.& Leistner, E. (1978). Aromatic metabolites in cell suspension cultures of *Galium mollugo. Planta Med.,* **33**,105-123.

Bhoola, K,D**.**, Figueroa, C.D**.** & Worthy, K. (1992). Bioregulation of kinins: kallikreins, kininogens, and kininases. *Pharmacol. Rev.,* **44** (1),1-80.

Biswanath, D., Sudhan, D. & Yoshihiro, H. (2007). Natural occurring iridoids. A review, part 1. *Chem. Pharm. Bull.,* **55 (2)**, 159-222.

Bollet, A.J., Bonner, W.M. & Nance, J.L. (1963). The present of hyaluronidase in various mammalian tissues. *J. Biol. Chem.*, **238**, 3522-3572.

Bremer, B. & Manen, J.F. (2000). Phylogeny and classification of the subfamily Rubioideae (Rubiaceae). *Plant Syst. Evol.,* **225**, 43-72.

Briggs, L.H., Cain, B.F., Le Quesne, P.W. & Shoolery, J.N. (1963). The structure of asperuloside. *Tett. Lett.*, 69-74.

Burkill, I.H. (1966). *A dictionary of the economic products of the Malay Peninsula.* Kuala Lumpur, Malaysia: Ministry of Agriculture and co-operatives.

Catterall, J.B. (1995). Hyaluronic acid, cell adhesion and metastasis. *Cancer J*., **8**, 320-324.

Chan, K.Y., Zhang, J., Chang, C.W. (2011). Mode of action investigation for the anti-bacterial cationic anthraquinones analogs. *Bioorg. Med. Chem. Lett*., **21**, 6353-6356.

Chao-Mei, M., Shao-Qing, C., Jing-Rong, C., Rui-Qing, W., Peng-Fei, T., Masao &, H., Mohsen, D. (2005). The cytotoxic activity of ursolic acid derivatives. *Eur. J. Med. Chem.,* **40**, 582–589.

Chen, G., Xue, J., Xu, S.–X, & Zhang, R.–Q. (2007). Chemical constituents of the leaves of *Diospyros kaki* and their cytotoxic effects. *Journal of Asian Natural Products Research*, 9(**4**) 347-353.

Chung, K.F., Dent, G., McCusker, M., Guinot, P., Page, C.P. & Barnes, P.J. (1987). Effect of ginkgolide mixture (BN 52063) in antagonizing skin and platelet responses to platelet activating factor in man. *Lancet,* **1**, 248-251.

Clementi, E. (1980). *Computational aspects of large chemical systems*, New York: Springer Verlag.

CODESSA PRO User's manual (2005). Florida: University of Florida.
Retrieved from
http://www.codessa-pro.com.

Corner, E.J.H. (1940). *Wayside trees of Malaya,* vol. 2. Singapore: Government printing office.

Csoka, A.B., Frost, G.I., Wong, T. & Stern, R. (1997). Purification and microsequencing of hyaluronidase isozymes from human urine. *FEBS Lett.*, **417**, 307-310.

De las Heras, B., Rodriguez, B., Bosca, L. & Villar, A.M. (2003). Terpenoids: sources, structure elucidation and therapeutic potential in inflammation. *Curr. Top. Med. Chem.,* **3,** 171-185.

De Padua, L.S., Bunyapraphatsara, N. & Lemmens, R.H.M.J. (1999). *Plants resources of South-East Asia, Medicinal and poisonous plants 1*. Bogor: Prosea foundation, **12 (1)**, 24.

Deepa, K.M., Girish, K.S. & Veerabasappa, G. T. (2006). A glycoprotein from a folk medicinal plant, *Withania somnifera*, inhibits hyaluronidase activity of snake venom. *Comp. Biochem. Physicol.-C.*, **143,** 158-161.

Derek, V.B. & John, J.W. (1995). Novel anthraquinones from undifferentiated cell cultures of *Galium verum. Phytochem.*, **38 (1)**, 107-111.

Dey, S. K., Islam, S., Mostafa, M., Nahar, N. & Mosihuzzaman, M. (2003). Some secondary metabolites from cytotoxic extract of *Prismatomeris tetrandra. J. Bangladesh Chem. Soc.,* **6,** 22-27.

Dinarello, C.A. (1984). Interleukin-1. *Rev. Infect. Dis.*, **6**, .51-95.

Dong-Hyun, K., Kyung-Min, H., In-Sik, C., Dae-Keun, K., Sung-Hoon, K., Byoung-Mog, K., Tae-Sook, J., Mi-Hyun, P., Eun-Mi, A. & Nam-In, B. (2005). Triterpenoids from the flower of *Campsis grandifolia K. Schum*. as human acyl-CoA: Cholesterol acyltransferase inhibitors. *Arch Pharm Res*, **5**, 550-556.

Dudley, H.W. & Ian, F. (1989). *Spectroscopic methods in organic chemistry* 4th ed. England. McGraw-Hill Book company Europe.

Dusser, D.J., Nadel, J.A., Sekizawa, K., Graf, P.D.& Borson, D.B. (1988). Neutral endopeptidase and angiotensin converting enzyme inhibitors potentiate kinin-induced contraction of ferret trachea. *J. Pharmacol. Exp. Ther*., **244**, 531-536.

El Maradny, E., Kanayama, N., Kobayasi, H., Hossain, B., Khatun, S. & She, L.P. (1997). The role of hyaluronic acid as a mediator and regulator of cervical ripening. *Human Reproduction*, **12**, 1080-1088.

en.wikipedia.org/wiki/Inflammation
Retrieved on 14 April 2014.

Facino, R.M., Carini, M., Aldini, G., Marnelio, C., Arlandini, E., Franzoi, L., Colombo, M., Pietta & P., Mauri, P. (1993). Direct characterization of caffeol esters with antihyaluronidase activity in crude extracts from *Echinacea augustifolia* roots by fast atom bombardment tandem mass spectrometry II. *Farmaco*., **48,** 1447-1461.

Floss, H.G. (1979). Biochemistry of plant phenolics, recent advances in phytochemistry. *Proceedings of the joint symposium of the phytochemical society of Europe and the Phytochemical Society of North America*, **12,** 59-89.

Frossard, N., Stretton, C.D. &Barnes, P.J. (1990). Modulation of bradykinin responses in airway smooth muscle by epithelial enzymes. *Agents Actions*, **31(3-4),** 204-209.

Goh, S.H. (1995). *Malaysian medicinal plants for the treatment of cardiovascular diseases*, Kuala Lumpur: Pelanduk Publication (M) Sdn. Bhd.

Graham, L.P. (2005). *An introduction to medicinal chemistry* (3rd ed.). Oxford: Oxford university press.

Grisehach, H. (1965). *Biosynthetic pathways in higher plants*. London: Academic Press, London.

Hall, L.H., Kellog, G.E, Haney, D.N. & Molconn-Z. (2002a). *4.00 user's guide*. Edusoft.Ic, Inc, Ashland , VA.

Hall, L.H., Kier, L.B. & Hall, L.M. (2002b). *The guide for development of QSAR with MDL QSAR*. San Leandro: MDL information system.
Retrieved on 20 December 2012 from
http://www.edosoft-lc.com/molcomm/manuals/400/chaptwo.html

Hansch, C. & Leo, P. (1979). *Substituent constants for correlation analysis in chemistry and biology*. New York: Wiley and sons.

Haralampidis, K., Trojanowska, M. & Osbourn, A., E. (2002). Biosynthesis of triterpenoid saponins in plants. *Adv. Biochem. Eng*., **75**, .31-49.

Harborne, J.B. & Simmons, N.W. (1964). *Biochemistry of phenolic compounds*. New York: Academic Press.

Havsteen, B. (1983). Flavonoids, a class of natural products of high pharmacological potency, *Biochem Pharmacol*., **32 (7),** 1141-1148.

Hiroichi, N. (2005). Immunopharmacological approach to elucidating the mechanism of allergic inflammation. *Allergology International*., **54**, 251-261.

Hirota, M., Mori, T., Yoshida, M. & Iriye, R. (1990). Suppression of tumor promoter-induced inflammation of mouse ear by ursolic acid and 4,4-dimethylcholestane derivatives. *Agric. Biol. Chem*., **54 (4),** 1073-1075.

Hisao, K., Hitoshi, M. & Toshio, S. (1985). Activation of hyaluronidase by metallic salts and compound 48/80, and inhibitory effect of anti-allergic agents on hyaluronidase. *Chem Pharm. Bull*., **32 (2),** 642-646.

Holgate, S.T. (1986). The pathophysiology of bronchial asthma and targets for its drug treatment. *Agents action*, **18,** 281-287.

Holstein, S.A. & Hohl, R.J. (2004). Isoprenoids: remarkable diversity of form and function. *Lipids*, **39,** 293-309.

Horton, M.R., Shapiro, S., Bao, C., Lowenstein, C.I. & Noble, P.W. (1999). Induction and regulation of macrophage metalloelastase by hyaluronan fragments in mouse macrophages. *J. Immunol.*, **162,** 4171-4176.

http://en.wikipedia.org/wiki/Eicosanoid Retrieved on 28 July 2012

http://iphy10.org/~rpage/theplantlist/A/rubiaceae/Prismatomeris Retrieved on 15 January 2012

http://www.edosoft-lc.com/molcomm/manuals/400/chaptwo.html Retrieved on 2 August 2012

Hu, R., Jean-Pierre, D., Michel, D. & Ruisheng, Z. (2009). QSAR models for 2-amino-6-arylsulfonylbenzonitriles and congeners HIV-1 reverse transcriptase inhibitors based on linear and nonlinear regression methods. *Eur. J. Med. Chem.*, **44,** 2158-2171.

Imbimbo, B.P. (2009). An update on the efficacy of non-steroidal anti-inflammatory drugs in Alzheimer's disease. *Expert Opin. Investig. Drugs*, **18**, 1147-1168.

In-Ah, L., Jin, H.L., Nam-In, B. & Dong-Hyun, K. (2005). Antihyperlipidemic effect of crocin isolated from the fructus of *Gardenia jasminoides* and its metabolite crocetin. *Bio. Pharm. Bull*., **28 (11)**, 2106-2110.

Inger, L.M., Mart, A.F.J. & van de laar Harald, E.V.(2010). Non-steroidal anti-inflammatory drugs: an overview of cardiovascular risks, *Pharmaceuticals*, **3**, 2146-2162.

Inoue, K., Shiobara, Y., Nayeshiro, H., Inouye, H., Wilson, G. & Zenk, M.H. (1984). Biosynthesis of anthraquinones and related compounds in *Gallium mollugo* cell suspension cultures. *Phytochemistry*, **23,** 307–311.

Inouye, H., Inouye, S., Shimokawa, N. & Okigawa, M. (1968). Die iridoid glucoside aus *Paederia scandens (lour.) merrill var. mairei (léveillé) hara*. *Tet. Let.*, **9(6)**, 683-688.

Inouye, H., Inouye, S., Shimokawa, N. & Okigawa, M. (1969). Studies on monoterpene glucosides. VII. Iridoid glucosides of *Paederia scandens*. *Chem Pharm Bull.,* **17**, 1942 – 1948

Inouye, H., Yoshida ,T., Tobita, S. & Okigawa, M. (1970). Studies on monoterpene glucosides–IX: Chemical correlation between asperuloside and loganin. *Tetrahedron*, **26(16)**, 3905-3915.

Jarai, M., Markus, F. & James, H. (2006). A quantitative structure-activity relationship (QSAR) analysis of triarylmethane dye tracers. *Jounal of Hydrology*, **316**, 84-97.

Jean, B. (1995). *Pharmacognosy, phytochemistry, medicinal plants*. Lavoisier: Technique and Documentation-Lavoisier.

Jean-claude, V. (2009). How hyaluronan-protein complexes modulate the hyaluronidase activity: The model. *Biophysical Chemistry*, **145**, 126-134.

Jiang, J.s, Feng, Z.M. & Zhang, P.C. (2005). Chemical constituents from the root of *Prismatomeris tetrandra. Zhongguo Zhong Yao Za Zi,* **30(22)**, 1751-1753.

Jie-Ping, F. & Chao-Hong, H. (2006). Single step preparative separation of barbinervic acid and its epimer (rotungenic acid), along with two other pentacyclic triterpene acids from the leaves of *Diospyros kaki* using HSCCC. *Journal of Liquid Chromatography and Related Technologies*, **(29)**, 1-13.

John, V. & Regina, B. (1987). Inflammation and the mechanism of action of anti-inflammatory drugs. *The FASEB journal*, **11**, 89-86.

Jurge, B. (2004). *Chemoinformatics: Concepts, methods and tools for Drug Discovery*. United State: Springer International publisher science, technology, medicine.

Kanchanapoom, T., Kasai, R., Yamasaki, K. (2002). Iridoid and phenolic glycosides from *Morinda corei*. *Phytochemistry,* **59**, 551-556.

Karelson M. & Lobanov, V. S. (1996). Quantum chemical descriptors in QSAR/QSPR studies. *Chem. Rev*., **96**, 141-354.

Karelson, M. (2000). *Molecular descriptors in QSAR/QSPR*. New York: John Wiley and sons, Inc., Publication.

Kartisky, A.R., Svetoslav, H.S., Dimitar, A.D. & Karelson, M. (2008). QSAR modeling of the antifungal activity against *Candida albicans* for a diverse set of organic compounds. *Bioorg. Med. Chem.,* **16**, 7055-7069.

Kartizky, A.R., Liliana, M.P., Svetoslav, S., Dimitar, A.B. & Karelson, M. (2006). QSAR study of antiplatelet agents. *Bioorg. Med. Chem*, **14,** 7490-7500.

Kartizky, A.R., Lobanov, V.S. & Karelson M. (1994). Comprehensive descriptors for structural and statistical analysis. *Reference Manual, Version 2.0*.,

Kartizky, A.R., Ruslan, P., Subbu, P., Karelson, M., Indra, P. & Nitin, D. (2002). A QSPR study of sweetness potency using the CODESSA program. *Croatia Chemical Acta*, **75**, 475-502.

Kartsen, K., Dietmar, G., Sujit, K.D., Nilufar, N., Mohammad, M., Nasim, S. M., Hossain, S, Philip, J.S. & Jian-Jung, P.F.S. (2007). Prismatomerin, a new iridoid from *Prismatomeris terandra*. Structure elucidation, determination of absolute configuration and cytotoxicity. *J. Nat. Prod.*, **70 (8)**, 1339-1343.

Keng, H. (1969). *Orders and families of Malayan seed plants*. Kuala Lumpur: Singapore University of Malaya Press.

Kim, I.H., Uchiyama, N., Kawahara, N., Goda, Y. (2006). Iridoid glycosides and cucurbitacin glycoside from *Neopicrorhiza scrophulariiflora. Phytochemistry*, **67**, 2691-2696.

Kittisak, L., Sukanya, D.A., Vichien, J. & Jerapan, K. (1999). Anti-malarials from *Stephania venosa*, *Prismatomeris sessiliflora*, *Diospyros Montana* and *Murraya siamensis. Planta Medica*, **65**, 754-756.

Klaus, M. H. (1995). The shikimate pathway as an entry to aromatic secondary metabolism. *Plant Physiology*, **107**), 7-12.

Kohei, K., Wakako, H., Shogo, T., Ken, H., Toshiko, S., Yuko, K., Hiromi, Y. & Yoshiyuki, M. (2010). Inhibitory effect of anthraquinones isolated from the Noni *(Morinda citrifolia)* root on animal A-, B- and Y-families of DNA polymerases and human cancer cell proliferation. *Food Chem.*, **118**, 725-730.

Kohej, K., Yohei, T., Hanani, E., Mansur, U. & Toshiko, S. (2005). New anthraquinone and iridoid from the fruits of *Morinda citrifolia. Chem. Pharm. Bull.*, **53 (12)**,1597-1599.

Kotaro, T. & Masako T. (1978). Studies on the const. of the medicinal plants. XXL. Const. of the leaves of *Clethra barbinervis Sieb. Et Zucc* and the ^{13}C-Nuclear Magnetic Resonance spectra of 19α-hydroxyurs-12-en-28-oic acid type of triterpenoids. *Chem. Pharm Bull*, **26 (9),** 689-2693.

Koyama, J., Nisino, Y. (2008). Correlation between reduction potentials and inhibitorns of Epstein-Barr virus activation by anthraquinone derivatives. *Bioorg. Med. Che. Lett.*, **18**, 4106-4109.

Krohn, K., Gehle, D., Dey, S.K., Nahar, N., Mosihuzzaman, M., Sultana, N., Sohrab, M.H., Stephens, P.J., Pan, J.J., Sasse, F. (2007). Prismatomerin a new iridoid from *Prismatomeris tetrandra*. Structure elucidation, determination of absolute configuration and cytotoxicity. *J. Nat. Prod*., **70**, 1339-1343.

Kuigoua, G.M., Kouam, S.F., Ngadjui, B. t., Schulz, B., Green, I.R., Choudhary, M.I., Krohn, K. (2010). Secondary metabolic products from the stem bark of *Plumeria rubra* Linn. displaying anti-microbial activities. *Planta Med*, **76**, 620-625.

Kwanjai, K., Somdej, K. & Ruchanee, P. (2005). Biological activity of anthraquinones and triterpenoids from *Prismatomeris fragrans.* *Journal of Ethnopharmacology*, **100**, 284-288.

Lee, H.H. (1968). Colouring matters from *Prismatomeris malayana*. *Phytochem.*, **8**, 501-503.

Leistener, E. (1981). Biosynthesis of plant quinones. *In: Conn, E.E.(Ed), The biochemistry of plants* (pp. 403-423). vol **7**. London: Academic Press.

Leistener, E. (1985). Biosynthesis of chorismate-derives quinones in plant cell cultures. *In: Primary and secondary metabolism of plant cell cultures* (pp.215-224). Berlin: Springer Berlin,.

Leistner, E. (1967). Incorporation of shikimic acid into 1,2-dihydroxy-anthraquinone (alizarin) by *Rubia tinctorum L.*, *Tet. Lett.*, 475-476.

Lemmens, R.H.M.J. & Bunyapraphatsara, N. (2003). *Plant resources of South-East Asia, Medicinal and poisonous plants 3* **12 (3)**. *Bogor, Indonesia:* Prosea Foundation.

Ling, S.K. (2003). *Chemical and biological studies of four selected medicinal plants of Malaysia, PhD Thesis. Nagasaki:* Nagasaki University, Japan.

Ling, S.K., Takashi, T. & Isao, K. (2003). Effects of iridoids on lipoxygenase and hyaluronidase activities and their activation by β-glucosidase in the presence of amino acids. *Biol. Pharm. Bull.* **26,** 352-356.

Lipinski, C.A., Lombardo, F., Dominy, B.W. & Feeney, P.J. (2001). Experimental and computational approaches to estimate solubility and permeability in drug discovery and development sttings. *Adv. Drug Deliv. Rev*., **46**, 3-26.

Liu, D., Pearlman, E., Diaconu, E., Guo, K., Mori, H. T. & Markowitz, S., (1996). Expression of hyaluronidase by tumor cells induces angiogenesis in vivo. *Proc. Natl. Acad. Sci. U.S.A*., **93**, 7832-7837.

Liu, H.X., Zhang, R.S., Yao, X.J., Liu, M.C., Hu, Z.D. & Fan, B.T. (2003). QSAR study of ethyl 2-[(3-methyl-2.5-dioxy(3-pyrrolinyl) amino-4-(trifluoromethyl) pyrimidine-5-carboxylate: An inhibitor of AP-1 and NF-κB mediated gene expression based on support vector machines. *J. Chem. Inf. Comput. Sci.*. **43**, 1288-1296.

Maria, A.A., Antonietta B., Anita, G. & Luisa, M. (2010). Non-steroidal anti-inflammatory drugs and brain inflammation: Effects on microglial functions. *Pharmaceuticals*, **3**, 1949-1964.

Masaaki, K., Tadamasa, T & Haruo, M. (1983). Triterpenoid,s of the bark of *Jieris japonica D.Don* II., ^{13}C nuclear Magnetic Resonance of the ϒ-lactones of ursane- and oleanane-type triterpenes. *Chem. Pharm. Bull*., **31 (5)**, 1567-1571.

Mariko, K., Ute, F., Mio, N., Mika, O., Masahiro, U. (1998). Anthraquinones from Ophiorriza pumila tissue and cell culture. *Phytochemistry*, **48**, 107-111.

Masateru, O., Chikako, M., Takemi, T., Yasuyuki, I. & Toshihiro, N. (2001). Anti-oxidantive and anti-hyaluronidase activities of some constituents from the aerial part of *Daucus carota. Food sci. technol. Res.,* **7 (4)**, 307-310.

Maurya, A., Feroz, K., Bawankule, D.U. & Yadav, D.K. (2012). QSAR, docking and *in vivo* studies for immunomodulatory activity of isolated triterpenoids from *Eucalyptus tereticornis* and *Gentiana kurroo*. *European Journal of Pharmaceutical Sciences*, **47**, 152-161.

Miyako, Y., Masahiro, F., Tsuneatsu, N., Hikaru, O., Kazuhisamat S., Jiro T., Yoshiharu, K., Ryota, T, Junei K., Kunihide, M. & Tushihiro, F. (2005). Anti-proliferative constituents from *Umbeliferae* plants VII. Active triterpenes and rosmarinic acid from *Centella asiatica. Biol. Pharm. Bull*., **28 (1)**, 173-175.

Milkyas, E., Annabel, E., John, P.A., Hoseah, M.A., Albert, N. (2013). Anthraquinones of the roots of *Pentas micrantha*. *Molecules,* **18,** 311-321.

Moncada, S., Gryglewski, R., Bunting, S. & Vane, J.R. (1976). An enzyme isolated from arteries transforms prostaglandind endoperoxides to an unstable substance that inhibits platelet aggregation. *Nature* (London) **(263)**, 663-665.

Morley, J. (1986). Platelet activating factor and asthma. *Agents Actions*, **19**, 100-108.

Mulholland, D.A., Mohammed, A.M., Coombes, P.H, Haque, S., Pohjala, L.L., Tammela, P.S. & Crouch, N.R. (2011). Triterpenoid acids and lactones from the leaves of *Fadogia tetraquetra var. tetraquetra* (Rubiaceae). *Nat. Prod. Commun*., **6(11)**, 1573-6.

Nakanishi, K., Goto, T., Itồ, S., Natori, S. & Nozoe, S. (1974). *Natural Products Chemistry*, **1**, 1-10.

Nermeen, S. El-Safory, Ahmed E. F. & Cheng-Kang, L. (2010). Hyaluronidases, a group of glycosidases: Current and future perspectives. *Carbohydrate polymers,* **81**, 165-181.

Newman, D. J., Gordon M. C. & Kenneth M. S. (2003). Natural Products as Sources of New Drugs over the Period 1981-2002. *J. Nat. Prod., **66**,* 1022-1037.

Ng, F.S.P.(1940). *Tree flora of Malaya*, vol.4. Kuala Lumpur: Longman Malaysia.

Nouri, A.M. E., Panayi, G.S. & Goodman, S.M. (1984). Cytokines and the chronic inflammation of rheumatic disease.1. The presence of interleukin-1 in synovial fluids. *Clin. Exp. Immunol. ,* **55**, 295-302.

O'Neil, M.J. & Lewis, J.A. (1993). *The renaissance of plant research in the pharmaceutical industry*. Washington: American Chemical Society.

Ogihara, K., Iraha, R., Higa, M.E. & Yogi, S. (1997). Studies on const. from the twigs of *Messerschmidia argentea* 2. *Bulletin of the college of Science University of the Ryukyus*, **64,** 53-59.

Peter, J.B., Chung, K.F. & Clive, P.P. (1988). Inflammatory mediators of asthma: An update, *Pharmacological Reviews*, **50(4)**, 517-572.

Pimm, S.L., Russell, G.j., Gittleman, J.L. & Brooks, T.M. (1995). The future of biodiversity. *Science*, **269**, 347-350.

Pittaya, T., Yuttapon, B., Piyanut, S., Uma, P. & Walter, C. T. (2008). Anthraquinones from the roots of *Prismatomeris malayana. Nat. Prod. Res.,* **22 (11)**, 962-968.

Rainer, F. & Andreas, G. (2003). General introduction to QSAR Chapter 1. In*: Quantitative strucuture activity relationship (QSAR) models of mutagens and carcinogens*. New York: CRC Press.

Recio, M.C., Giner, R.M., Uriburu, L., Manez, S., Cerda, M. & De La Fuenta J.R. (2000). In vivo activity of pseudoguaianolide sesquiterpene lactones in acute and chronic inflammation. *Life Sci*, **66**, 2509-18.

Riaz, N,. Malik, M., Rehman, A., Ahmed Z., Muhammad, P., Nawaz, S.A., Siddiqui, J. & Choudhary, M.I. (2004). Lipoxygenase inhibiting and antioxidant oligostilbene and monoterpene galactoside from *Paeonia emodi*. *Phytochemistry*, **65**, 1129-1135.

Ridley, H. N. (1967). *The Flora of the Malay Peninsula*. Kuala Lumpur: L. Reeve & Co., LTD.

Rocha, G.B., Freire, R.O., Simas, A.M. & Stewart, J.J.P. (2006). RM1: A reparameterisation of AM1 for H,C,N,O,P,S,F,Cl, Br and I. *J. Computational Chemistry*, **27**, 1101-1111.

Rohmer, M. (1999). The discovery of a mevalonate-independent pathway for isoprenoid biosynthesis in bacteria, algae and higher plants. *Nat. Prod. Rep*., **16**, 565-574.

Rooney, P., Kumar, S., Ponting, J. & Wang, M. (1995). The role of hyaluronan in tumour neovascularisation. *Int J. Cancer,* **60**, 632-636.

Rowley A.F., Kuhn H. & Schewe T. (1998). *Eicosanoids and related compounds in plants and animals*. Portland: Portland Press.

Ruzicka, L, (1953). The isoprene rule and the biogenesis of terpenic compounds. *Experientia,* **9**, 357.

Ruzicka, L. & Trebler, H. (1921). Zur Kenntnis des Pinens III Konstitution des Nitrosopinens und seiner Umwandlungsprodukte. *Helv. Chim. Acta,* **4**, 505.

Safayahi, H. (1997). Anti-inflammatory actions of pentacyclic triterpenes. *Planta Med*, **63**, 487-493.

Sasai, Y. & Ishibashi, M. (1975). Histochemical demonstration of hyaluronic acid in human dermal mast cells. *Tohoku J. Exp. Med*., **116**, 285-293.

Scott, J.E, Heatley, F. & Hull, W.E. (1984). Secondary structure of hyaluronate in solution. A ^{1}H NMR investigation at 300 and 500 MHz in dimethyl sulphoxide solution. *Biochemical Journal*, **220**, 197-205.

Senn, A., Germond, M. & De Grandi, P. (1992). Immunofluorescence study of actin, acrosin, dynein, tubulin and hyaluronidase and their impact on in-vitro fertilization. *Human Reproduction*, **6**, 841-849.

Silverstein, R.M., Bassler, G.C., Morrill, T.C. (1991). *Spectrometric identification of organic compounds*. Singapore: John Wiley and Sons, Inc.

Simone, C.B.G, Alexandra, D-K, Sophie, Da N., Philippe, G., Karim, B., Grace, G., Pascal, S. & Safa, M. (2008). Evaluation of ursolic acid isolated from Ilex paraguariensis and derivatives on aromatase inhibition. *Eur. J. Med. Chem.*, **43**, 1865-1877.

Simpson, H. (1998). *Biotechnology and the economics of discovery in the pharmaceutical industry*. London: BSC Print Ltd.

Singh, D.N., Verma, N., Raghuwanshi, S. (2006). Anti-fungal anthraquinones from *Saprosma fragrans*. *Bioorg. Med. Chem. Lett*., **16**, 4512-4514.

Stern. R. (2008). Hyaluronidases in cancer biology. *Semin. Cancer Biol.,* **18**, 275-280.
Stone, M. & Jonatan, P. (1993). Statistical Thinking and technique for QSAR and related studies. 1. General Theory. *J. Chemometrics*, **7**, 455-475.

Su-Ching, K., Pey-Rin, C. (1995). Constituents of roots of Rubia lanceolata Hayata. *Journal of the Chinese Chemical Society*, **42**, 869-891.

Suzuki, A., Hasegawa. M., Ishii, M. (2005). Anthraquinone derivatives as a new family of protein photocleaVERS. *Bioorg. Med. Chem. Lett*., **15**, 4624-4627.

Takuya, K., Yukikazu, Y., Masatoshi, I. & Syuichi, O.(2003). Hyaluronidase-inhibiting polysaccharide isolated and purified from hot water extract of sporophyll of *Undaria pinnatifida*. *Food Science Technology Research*, **9 (1)**, 25-29.

Tingting, Z, Weiquan, Z., Guorong, F., Yifeng, C. & Yutian, W. (2007). Isolation and purification of iridoid glycosides from *Gardenia jasminoides Ellis* by isocratic reversed-phase two dimensional preparative high-performance liquid chromatography with column switch technology. *Journal of Chromatography B*, **858**, 296-301.

Toshihiro, M., Mai, W., Yu, T., Toshio, M. & Fumihiko, Y. (2010). Hyaluronidase inhibitors from *Takuran, Lycopus lucidus. Chem Pharm Bull*., **58 (3)**, 394-397.

Umezawa, T. (2003). Diversity in lignan biosynthesis. *Phytochem. Rev.,* **2**, 371-390.
Van den Berg, A.J.J. & Labadie, R.P. (1989). Quinones. *In: Methods in Plant biochemistry,* vol 1 (pp. 451-491). London: Academic Press London.

Venketeshwer, R. (2012). *Phytochemicals as Nutraceuticals - Global Approaches to Their Role in Nutrition and Health*. Rijeka, Croatia: InTech Published.

Verpoorte R. (1999). Chemodiversity and the biological role of secondary metabolites, some thoughts for selecting plant material for drug development. In Lars B. & Jan G. B. (eds.), *Bioassay methods in natural product research and drug development. Proceedings of the phytochemical society of Europe*. Kluwer: Academic Publishers.

Vierhuis, E., York, W.S., Kolli, V.S.K., Vincken, J.P., Schols, H.A., Van Alebeek, G.-J.W.M., Voragen, A.G.J. (2001). Structural analyses of two arabinose containing oligosaccharides derived from olive fruit xyloglucan: XXSG and XLSG. *Carbohyd. Res.*, **332**, 285-297.

Vincken, J.P., Lynn, H., Aede de, G. & Harry, G. (2007). Saponins, classification and occurrence in the plant kingdom. *Phytochem.*, **68**, 275-297.

Von Euler, U.S. (1936). On the specific vaso-dilating and plain muscle stimulating substances from accessory genital glands in man and certain animals (prostaglandin and vesiglandin). *J. Physiol.* **88**(2), 213–234.

Wang, S., Wang, Q., Wang, Y. (2008). Novel anthraquinone derivatives: Synthesis via click chemistry approach and their induction of apoptosis in BGC gastric cancer cells via reactive oxygen species (ROS)-dependent mitochondrial pathway. *Bioorg. Med. Che. Lett.*, **18**, 6505-6508.

Weiss, U. & Edwards, J.M. (1980). *Biosynthesis of aromatic compounds from acetic acid-The biosynthesis of aromatic compounds*, New York: A Wiley-Interscience.

Werner, S., Nebojsa S., Robert W., Robert, S. & Olaf, K. (2003). Complete assignments of ^{1}H and ^{13}C NMR resonance of oleanolic acid, 18α-oleanolic acid, ursolic acid and their 11-oxo derivatives. *Magnetic Resonance in Chemistry*, **41**, 636-638.

West, D.C., Hampson, I.N., Arnold, F. & Kumar S. (1985). Angiogenesis induced by degradation products of hyaluronic acid. *Science*, **228**, 1324-1326.

West, D.C., Kumar, S. (1989). Hyaluronan and angiogenesis, In: *The Biology of hyaluronan*, Vol 143 (pp. 187-207). New York: John Wiley and Sons.

Wiliam, D.W. (1998). The nervous system. In Robert, M.B.(ed.). *Physiology (4th ed.*) (pp. 113) St. Louise: Mosby Inc.

Winter, R.W., Cornell, K.A., Johnson, L.L. (1995). Hydrozy anthraquinones as anti-malarial agents. *Bioorg. Med. Chem. Lett.*, **5**, 1927-1932.

Wu, M., Wu, P., Liu, M., Xie, H., Jiang, Y. & Wei, X. (2009). Iridoids from *Gentiana loureirii*. *Phytochemistry*, **70**, 746-750.

www.colby.edu/chemistry/PChem/notes/MOPACinst.pdf Retrieved on 22 Mac 2012

www.madsci.org/post/archives/2001-04/986571103.Bc.r.html Retrieved on 29 September 2011.

Ying-Shan, H., Robert van der Heijden, Alfons, W.M. Lafeber, C.E. & Robert, V. (2002). Biosynthesis of anthraquinones in cell cultures of *Cinchona robusta* proceeds via the methylerythritol 4-phosphate pathway. *Phytochem.*, **59**, 45-55.

Zefirov, N.S., Kirpichenok, M.A., Izmailov, F.F. & Trofimoz, M.I. (1987). *Dokl Akad. Nauk SSSR*, **296**, 883.

Zeng, C., Toole, B.P., Kinney, S.D., Kuo, J.W. & Stamenkovic, I. (1998). Inhibition of tumor growth *in vivo* by hyaluronan oligomers. *International journal of cancer,* **77**, 396-401.

Zi –Ming, F., Jian-Shuang, J., Ying-Hong, W. & Pei-Cheng, Z. (2005). Anthraquinones from the roots of *Prismatomeris tetrandra. Chem. Pharm. Bull.,* **53(10)**, 1330-1332.

APPENDIX

APPENDIX
Journals, Articles in Seminar, Proceeding and Conferences

1. Khalijah Awang, Nor Hayati Abdullah, Noel F. Thomas and Sek Weng Ng. Methyl 3-Dehydroxy-3-Oxoursolate. Acta Crytallographica (2009). E65, 02113 [Doi: 10.1107/S1600536809030669]

2. Nor Hayati Abdullah,Khalijah Awang, Noel F. Thomas and Sek Weng Ng. Methyl 3-Acetoxy-3-Dehydroxyursolate. Acta Crytallographica (2009). E65, 02114 [[Doi: 10.1107/S1600536809030657]

3. Nor Hayati Abdullah, Ling Sui Kiong, Khalijah Awang, Mohd. Faisal Iskandar Sukhari. Effect of Extraction Parameters on Total Triterpenoid Saponins from *Prismatomeris malayana*. Malaysian Journal Of Science, Vol 28, November 2008

4. Nor Hayati A., Ibrahim A.N., Noel F. Thomas, Khalijah A., Fadzureena J., Mazura Mp. *Pentacylic Triterpenoids Inhibition towards Hyaluronidase Activity: Synthesis and Qsar Study,* 15th Project Evaluation and Monitoring (PEM), 31Oktober-2 November 2012, Hotel Heritage, Cameron Highland Pahang.

5. Nor Hayati Abdullah, Khalijah Awang, Noel F. Thomas. Anti Inflammatory Activity of Ursolic Acid and Derivatives. International Conference on Natural Product (ICNP), 13-16 November 2011.

6. Nor Hayati Abdullah, Ling Sui Kiong, Khalijah Awang, Mohd. Faisal Iskandar Sukhari. Effect of Extraction Parameters on Total Triterpenoid Saponins from *Prismatomeris Malayana*. International Conference on Molecular Chemistry 2008 - Current Trends in Molecular Chemistry. 25-26 November 2008, University Malaya.

7. Nor Hayati Abdullah, Ling Sui Kiong, Mazura Md. Pisar. Chemical Analysis of *Prismatomeris malayana* and Its Anti-Inflammatory Activity. Malaysian Science and Technology Congress 2008, 16-17 December 2008, Kuala Lumpur Convention Centre, Kuala Lumpur.

8. Structure Activity Relationship Study on Isolated Compounds and Standardised Extract Preparation from *Prismatomeris malayana*. Norhayati, S.K. Ling, M.A. Nor Azah, M.P. Mazura, S. Saidatul Husni, J. Fadzureena, B.K. Ong, Ihsan Safwan, Zainon Abu Samah, S. Mohd. Faisal Iskandar, A. Khalijah, N. Ibrahim Ali. National Biotechnology Conference, PWTC Kuala Lumpur, May 2010.

9. Isolation And Structure Modification on the Anti Inflammatory Compound from *Prismatomeris malayana*. Nor Hayati Abdullah, Mazura Md. Pisar, Fadzureena Jamaludin, Khalijah Awang, Ibrahim Ali Noorbatcha. FRIM Project Evaluation Meeting, FRIM, Selangor, April 2010.
10. Prismalayanoside, a Novel Iridoid Glycoside from *Prismatomeris malayana* Ridley. Nor Hayati Abdullah, Yasodha Sivasothy, Nurhanan Murni Yunos, Siti Syrifah Mohd Mutalip, Khalijah Awang. (Submitted to Journal of Biooorganic and Medicinal Chemistry)